Reliability and Optimization of Structural Systems

Assessment, Design and Life-Cycle Performance

Dan M. Frangopol, Mitsuo Kawatani and Chul-Woo Kim

EDITORS

Taylor & Francis
Taylor & Francis Group

RELIABILITY AND OPTIMIZATION OF STRUCTURAL SYSTEMS:
Assessment, Design and Life-Cycle Performance

BALKEMA – Proceedings and Monographs
in Engineering, Water and Earth Sciences

PROCEEDINGS OF THE THIRTEENTH IFIP WG 7.5 WORKING CONFERENCE ON RELIABILITY AND OPTIMIZATION OF STRUCTURAL SYSTEMS, KOBE, JAPAN, OCTOBER 11–14, 2006

Reliability and Optimization of Structural Systems: *Assessment, Design and Life-Cycle Performance*

Editors

Dan M. Frangopol
Lehigh University, Bethlehem, Pennsylvania, USA

Mitsuo Kawatani & Chul-Woo Kim
Kobe University, Kobe, Japan

Taylor & Francis
Taylor & Francis Group
LONDON / LEIDEN / NEW YORK / PHILADELPHIA / SINGAPORE

Cover Photo: Akashi Kaikyo Bridge, Courtesy of Studio NOB

This edition published in the Taylor & Francis e-Library, 2007.

"To purchase your own copy of this or any of Taylor & Francis or Routledge's collection of thousands of eBooks please go to www.eBookstore.tandf.co.uk."

Taylor & Francis is an imprint of the Taylor & Francis Group, an informa business

Published by: Taylor & Francis/Balkema
P.O. Box 447, 2300 AK Leiden, The Netherlands
e-mail: Pub.NL@tandf.co.uk
www.balkema.nl, www.taylorandfrancis.co.uk, www.crcpress.com

ISBN 0-203-93221-8 Master e-book ISBN

ISBN 13: 978-0-415-40655-0 (hbk)

Reliability and Optimization of Structural Systems: Assessment, Design and Life-Cycle Performance – Frangopol, Kawatani & Kim (eds)
© 2007 Taylor & Francis Group, London, ISBN 978-0-415-40655-0

Table of contents

Reliability and Optimization of Structural Systems: Assessment, Design and Life-Cycle Performance – Frangopol, Kawatani & Kim (eds)
© 2007 Taylor & Francis Group, London, ISBN 978-0-415-40655-0

Preface

This volume contains the Proceedings of the thirteenth scientific meeting of the International Federation for Information Processing (IFIP) Working Group 7.5 on Reliability and Optimization of Structural Systems that took place in Kobe, Japan, October 11-14, 2006. This volume contains all papers including three keynote papers presented at the 13th IFIP WG7.5 working conference on Reliability and Optimization of Structural Systems.

The papers presented in this volume are distributed among Asia, Europe, and North America. The Conference was organized by IFIP TC-7, IFIP's Technical Committee on System Modeling and Optimization. It was co-sponsored by Kobe University, the International Association for Bridge Maintenance and Safety (IABMAS), and the Civil Engineering Risk and Reliability Association (CERRA).

The purpose of the Working Group is to promote modern structural system reliability and optimization theory and its applications, to stimulate research, development and application of structural system reliability and optimization theory, to assist and advance research and development in these fields, to further the dissemination and exchange of information in reliability and optimization of structural systems, and to encourage education in structural system reliability and optimization theory.

The main themes of the conference were structural reliability methods, reliability-based optimization, structural system reliability and risk analysis, lifetime performance and various applications in civil engineering.

IFIP Working Group 7.5 had the following membership as of the 13th IFIP WG 7.5 Working Conference. Many of the researchers and practitioners listed below played an active role in the scientific program of the conference.

A. H.-S. Ang., USA
G. Augusti, Italy
F. Biondini, Italy
A. Borri, Italy
C. Bucher, Germany
J. Casas, Spain
H.N. Cho, Korea
M. Ciampoli, Italy
C.A. Cornell, USA
R.B. Corotis, USA
A. Der Kiureghian, USA
O. Ditlevsen, Denmark
M. Dogaki, Japan
H. Ellis, USA
L. Esteva, Mexico
M.H. Faber, Swizerland
D.M. Frangopol, USA (Chair)
G. Fu, USA
H. Furuta, Japan
P. Geyskens, USA
M. Gioffre, Italy
C. Guedes-Soares, Portugal
M. Grigoriu, USA
H. Ishikawa, Japan
R. Iwankiewicz, South Africa
S. Jendo, Poland
M. Kawatani, Japan
N. Kogiso, Japan
M. Lemaire, France
M. A. Maes, Canada
K. Marti, Germany
R. Melchers, Australia
Y. Murotsu, Japan
A.S. Nowak, USA
M.D. Pandey, Canada
R. Rackwitz, Germany
J.O. Royset, USA
M. Sakano, Japan
T. Sato, Japan
N. Shetty, United Kingdom
W. Shiraki, Japan
P. Sniady, Poland

J.D. Sørensen, Denmark (Vice-Chair)
B. Sudret, France
M. M. Szerszen, USA
W. Tang, Hong Kong
N.J. Tarp-Johansen, Denmark
P. Thoft-Christensen, Denmark
J. van Noortwik, The Netherlands
P. Waarts, The Netherlands
Y.-K. Wen, USA
Z. Zembaty, Poland

Participants of the 13th IFIP WG 7.5 Conference

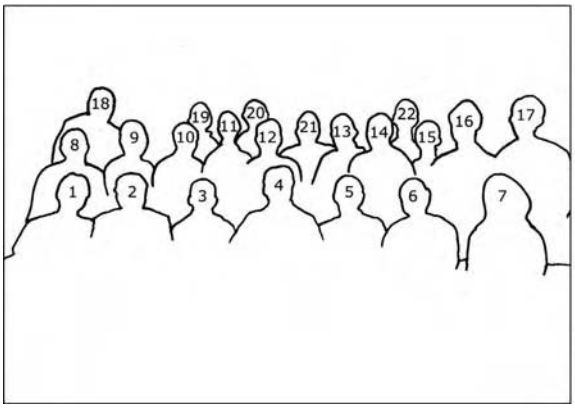

1. M. Kawatani
2. H. Furuta
3. L. Esteva
4. D.M. Frangopol
5. P. Thoft-Christensen
6. A. H-S. Ang
7. Y. Kawakami
8. M.R. Moarefzadeh
9. M. Dogaki
10. K. Nishijima
11. S. Maes
12. W. Shiraki
13. F. Biondini
14. Z. Zembaty
15. W.C. Pu
16. C.W. Kim
17. M. Sakano
18. N. Kogiso
19. M.H. Faber
20. M.A. Maes
21. J.D. Sorensen
22. Y. Geng

Members of the Technical Committee were:

Armen Der Kiureghian, USA
Dan M. Frangopol, USA (Chair)
Hitoshi Furuta, Japan
Mitsuo Kawatani, Japan (Co-Chair)
Marc A. Maes, Canada
Andrzej Nowak, USA
Rudiger Rackwitz, Germany
John Dalsgaard Sørensen, Denmark
Palle Thoft-Christensen, Denmark

Members of the Local Organizing Committee were:

Masahiro Dogaki
Hitoshi Furuta
Mitsuo Kawatani (Chair)
Chul-Woo Kim (Secretary)
Nozomu Kogiso
Masahiro Sakano
Tadanobu Sato
Wataru Shiraki

Results from previous conferences have been published in the following proceedings:

Reliability and Optimization of Structural Systems. Proceedings of the first IFIP WG 7.5 Working Conference, Aalborg, Denmark, May 6-8, 1987 (Ed. P. Thoft-Christensen). Lecture Notes in Engineering, Vol.33, Springer-Verlag Berlin Heidelberg New York.

Reliability and Optimization of Structural Systems. Proceedings of the second IFIP WG 7.5 Working Conference, London, UK, Sept. 26-28, 1988 (Ed. P. Thoft-Christensen). Lecture Notes in Engineering, Vol.48, Springer-Verlag Berlin Heidelberg New York.

Reliability and Optimization of Structural Systems. Proceedings of the third IFIP WG 7.5 Working Conference, Berkeley, California, USA, Mar. 26-27, 1990 (Eds. A. Der Kiureghian & P. Thoft-Christensen). Lecture Notes in Engineering, Vol.61, Springer-Verlag Berlin Heidelberg New York.

Reliability and Optimization of Structural Systems. Proceedings of the fourth IFIP WG 7.5 Working Conference, Munich, Germany, Sept. 11-13, 1991 (Eds. R. Rackwitz & P. Thoft-Christensen). Lecture Notes in Engineering, Vol.76, Springer-Verlag Berlin Heidelberg New York.

Reliability and Optimization of Structural Systems. Proceedings of the fifth IFIP WG 7.5 Working Conference, Takamatsu, Kagawa, Japan, Mar. 22-26, 1993 (Eds. P. Thoft-Christensen & H. Ishikawa). IFIP Transactions B-12, Applications in Technology, Elsevier Science Publishers B.V., Amsterdam.

Reliability and Optimization of Structural Systems. Proceedings of the sixth IFIP WG 7.5 Working Conference, Assisi, Italy, Sept. 7-9, 1994 (Eds. R. Rackwitz , G. Augusti & A. Borri), 1995 Chapman & Hall, London.

Reliability and Optimization of Structural Systems. Proceedings of the seventh IFIP WG 7.5 Working Conference, Boulder, CO, USA, April 2-4, 1996 (Eds. D.M. Frangopol, R.B. Corotis & R. Rackwitz), Pergamon, Elsevier.

Reliability and Optimization of Structural Systems. Proceedings of the eighth IFIP WG 7.5 Working Conference, Krakow, Poland, May 11-13, 1998 (Eds. A.S. Nowak & M.M. Szerszen), Univ. of Michigan, Ann Arbor, MI, USA.

Reliability and Optimization of Structural Systems. Proceedings of the ninth IFIP WG 7.5 Working Conference, Univ. of Michigan, Ann Arbor, Sept. 25-27, 2000 (Eds. A.S. Nowak & M.M. Szerszen), Univ. of Michigan, Ann Arbor, MI, USA.

Reliability and Optimization of Structural Systems. Proceedings of the tenth IFIP WG 7.5 Working Conference, Kansai University, Osaka, Japan, Mar. 25-27, 2002 (Eds. H. Furuta, M. Dogaki & M. Sakano), A.A. Balkema publishers.

Reliability and Optimization of Structural Systems. Proceedings of the eleventh IFIP WG 7.5 Working Conference, Banff, Canada, Nov. 2-5, 2003 (Eds. M.A. Maes & L. Huyse), A.A. Balkema publishers.

Advances in Reliability and Optimization of Structural Systems. Proceedings of the twelfth IFIP WG 7.5 Working Conference, Aalborg, Denmark, May 22-25, 2005 (Eds. J.D. Sørensen & D.M. Frangopol), Taylor & Francis/Balkema publishers.

The editors wish to express their sincere gratitude to the work by all members of the Organizing Committee. Thanks are due to the authors of the various papers for the excellent contributions they made to the conference. Without each of them, the working conference would not have been so successful.

The Editors,

Dan M. Frangopol
Lehigh University, Bethlehem, PA, USA

Mitsuo Kawatani and Chul-Woo Kim
Kobe University, Kobe, Japan

Keynote papers

Reliability and Optimization of Structural Systems: Assessment, Design and Life-Cycle Performance – Frangopol, Kawatani & Kim (eds)
© 2007 Taylor & Francis Group, London, ISBN 978-0-415-40655-0

Optimization and reliability problems in structural design of wind turbines

J.D. Sørensen
Aalborg University & Risø National Laboratory, Denmark

ABSTRACT: Reliability-based cost-benefit optimization formulations for wind turbines are presented. Some of the important aspects for stochastic modeling of loads, strengths and models uncertainties for wind turbines are described. Single wind turbines and wind turbines in wind farms with wake effects are discussed. Limit state equations are presented for fatigue limit states and for ultimate limit states with extreme wind load, and illustrated by bending failure. Illustrative examples are presented, and as a part of the results optimal reliability levels are obtained which corresponds to an annual reliability index equal to 3. An example with fatigue failure indicates that the reliability level is almost the same for single wind turbines and for wind turbines in wind farms if the wake effects are modeled equivalently in the design equation and in the limit state equation.

1 INTRODUCTION

Reliability analysis and optimization of wind turbines require that the special conditions for wind turbine operation are taken into account. Wind turbines for electricity production have increased significantly the last years both in production capability and in size. This development is expected to continue also in the coming years. Offshore wind turbines with an electricity production of 5–10 MW are planned. Typically, these large wind turbines are placed in offshore wind parks with 50–100 wind turbines.

The optimal design of wind turbines can be obtained using a life-cycle approach where all relevant benefits and costs are included. The associated general reliability-based optimization problem with a maximum acceptable probability of failure constraint is formulated. Offshore wind turbines are characterized by a low risk of human injury in case of failure when compared to onshore wind turbines, and to civil engineering structures in general. It is then relevant to assess the minimum reliability level for the structural design on the basis of reliability-based cost optimization considering the whole life-cycle of the turbines without a reliability constraint. Especially for offshore wind turbines costs related to operation and maintenance can be significant and have to be included. One reason is that maintenance can only be performed under certain weather conditions.

Behind a wind turbine a wake is formed where the mean wind speed decreases and the turbulence intensity increases. The distance between the turbines is among other things dependent on the recovery of wind energy behind the neighboring turbines and the increased wind load. This paper describes the basic relationships of mean wind speed and turbulence intensity in wind turbine parks with emphasis on modeling the wind load. For offshore wind turbines also environmental loads from waves, ice and current can also be significant.

The basic structural failure modes for wind turbines are:

- Fatigue failure in
  - Tower – typically in welded steel connections

  - Blade – made of glass fiber, composites, …
  - Nacelle – made of cast steel
- Ultimate failure (e.g. bending failure) due to extreme load in
  - Tower – made of steel
  - Blade – made of glass fiber, composites, …
  - Nacelle – made of cast steel
  - Foundation

The wind load effects depend highly on the chosen type of control (stall or pitch) in the operational mode, i.e. for mean wind speeds at hub height below 25 m/s.

Non-structural failure modes include failure of electrical components and machine components as e.g. gear boxes. Generally the following design situations have to be considered: normal operation, start/stop operations, and abnormal/accidental loads – often related to errors in control system, grid, ...

Representative probabilistic models are presented and representative limit state equations for ultimate structural failure of wind turbine towers and fatigue failure are formulated. Illustrative examples are presented for fatigue failure using both linear and bilinear SN-curves and for single as well as wind farms, and for ULS failure for an offshore wind turbine.

2 LIFE-CYCLE AND COST-BENEFIT MODELS FOR WIND TURBINES

For single wind turbines and for wind turbine parks, the optimal design generally can be obtained using a life-cycle approach where all relevant benefits and costs are included. However, these can differ depending on who is the decision maker. The producer of the wind turbine, the owner of the wind turbine obtaining the income from production of electricity and the society will in general have different utility (benefits & costs) functions. These differences are not treated in this paper.

Basically the optimal design of wind turbines in a wind turbine park can be obtained from the optimization problem:

$$\begin{aligned} &\max_{z} \quad B(z) - \left\{C_I(z) + C_{\text{grid+transmission}}(z) + C_{\text{operation+maintenance}}(z) + C_F(z)\right\} \\ &\text{s.t.} \quad \Delta P_F(z) \le \Delta P_F^{\max} \end{aligned} \tag{1}$$

where z are the design variables including dimensions of the wind turbines (height, cross sectional dimensions, rotor diameter, . . . , wind farm layout, . . .). B is the expected benefit from electricity production, C_I is the production cost of the wind turbines (material, foundation, transportation and installation costs), $C_{\text{grid+transmission}}$ is the cost of grid and electricity transmission system, $C_{\text{operation+maintenance}}$ is the expected cost of operation and maintenance, C_F is the expected costs of eventual failure of wind turbines, ΔP_F is the annual probability of failure and $\Delta P_F^{\max}$ is the maximum acceptable annual probability of failure. For offshore wind turbines the probability of loss of human lives is often negligible. In these cases it can be relevant not to include the constraint and thus a purely monetary optimization is obtained.

The expected cost of failure, C_F of a wind farm with m wind turbines can be estimated by:

$$C_F = \sum_{i=1}^{m} C_{F_i} P(\text{failure of } i \text{ wind turbines}) \tag{2}$$

where C_{F_i} is the costs of failure of i wind turbines. Due to correlation of failure modes in different wind turbines, the probability of more than one wind turbine in a storm can be high. Further, the consequences of failure of m wind turbines can be higher than failure of m single wind turbines placed at different locations since a wind park with several MW wind turbines can be considered as a wind power plant.

Next, the situation is considered where it can be assumed that the wind turbines are systematically reconstructed in case of failure. It is assumed that one wind turbine is considered. The direct failure costs is denoted C_F, the benefits per year are b, and the real rate of interest is r. Failure events are modeled by a Poisson process with rate λ. The optimal design is determined from the following optimization problem (Rackwitz, 2001):

$$\max_{z} \quad W(z) = \frac{b}{r\,C_0} - \frac{C_I(z)}{C_0} - \left(\frac{C_I(z)}{C_0} + \frac{C_F}{C_0}\right)\frac{\lambda \Delta P_F(z)}{r + \lambda \Delta P_F(z)} \tag{3}$$
$$\text{s.t.} \quad \lambda \cdot \Delta P_F(z) \le \Delta P_F^{\max}$$

where C_0 is the reference initial cost corresponding to a reference design z_0. The optimal design z^* is determined by the solution to (3). If the constraint on the maximum acceptable probability of failure is omitted, then the corresponding value $\Delta P_F(z^*)$ can be considered the optimal annual probability of failure related to the failure event and the actual cost-benefit ratios.

The failure rate λ and probability of failure can be estimated for the considered failure event, if a limit state equation, $g(X_1, \ldots, X_n, z)$, and a stochastic model for the stochastic variables, $(X_1, \ldots, X_n)$, are established. If more than one failure event is critical, then a series-parallel system model of the relevant failure modes can be used.

3 WIND LOAD

As mentioned in the introduction, the operational mode of a wind turbine is important when modeling the wind load:

- *Standstill*: if the 10-minutes mean wind speed at hub height exceeds 25 m/s then the wind turbine is parked, and the wind load corresponds to the annual extreme wind load.
- *Operation*: the wind turbine is in operation and produces electricity. The wind velocity is maximum 25 m/s. The maximum wind load is dependent on the control system (stall or pitch) of the wind turbine and the maximum turbulence intensity. Since the number of 10-minutes periods

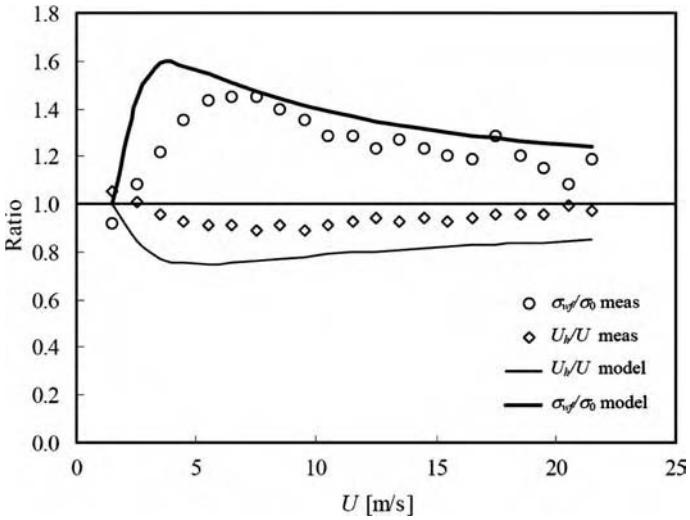

Figure 1. Illustrative ratios of wind velocity U at hub height and turbulence σ_u inside (U_h and σ_{wf}) and outside (U and σ_0) a wind farm, as function of wind velocity. The full lines are model predictions – from (Frandsen, 2005).

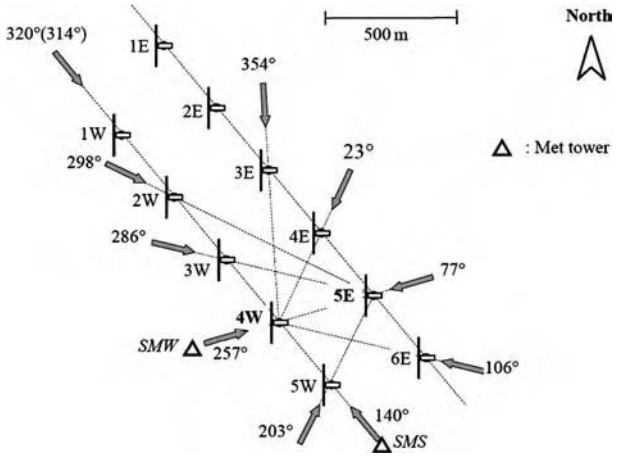

Figure 2. Layout of the Vindeby offshore wind farm – from (Frandsen, 2005).

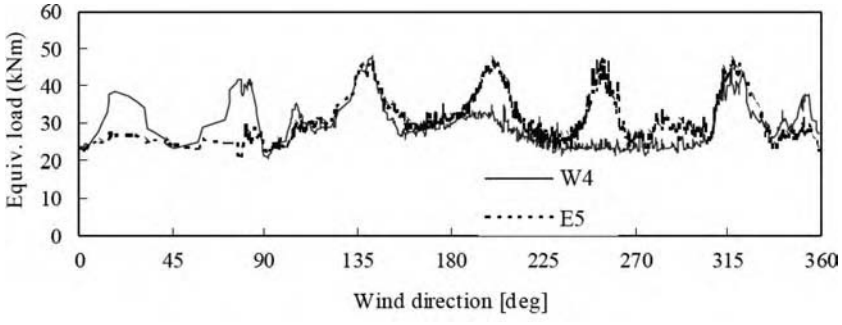

Figure 3. Equivalent load effect (flap-wise bending) for two wind turbines, 4W and 5E in figure 4, as function of wind direction, in the Vindeby wind farm, $8 < U < 9$ m/s – from (Frandsen, 2005).

with wind velocity at the critical velocity smaller than or equal to the 25 m/s is in general large, the maximum wind load during operation is obtained from simulations of the wind velocity field in front of the wind turbine and the actual control system of the wind turbine. A distribution function is determined for the maximum wind load over the expected number of 10-minutes periods with wind velocity from approximately 10 m/s to 25 m/s.

For wind turbines in a wind turbine park the turbulence is increased significantly behind other wind turbines, and the wind velocity is decreased slightly. In figure 1 from (Frandsen, 2005) the change in turbulence intensity I (standard deviation of turbulence divided by mean 10-minutes wind speed) and mean 10-minutes wind speed U is illustrated.

In figure 3 from (Frandsen, 2005) data are shown, obtained from the Vindeby wind park (south of Denmark), see figure 2. It is seen that the wind load effect (flapwise blade bending moment) proportional to the standard deviation of the turbulence increase significantly behind other wind turbines. For wind turbine W4 the directions 23°, 77°, 106°, 140°, 320° and 354°, and for wind turbine E5 the directions 140°, 203°, 257°, 286°, 298° and 320°.

4 LIMIT STATE EQUATIONS

4.1 *Probabilistic model for ULS failure*

For the failure mode 'bending failure of the tower' the limit state equation for a single wind turbine in standstill mode can be written, see (Tarp-Johansen et al. 2003) and (Sørensen and Tarp-Johansen 2005):

$$g_S(z_S, \mathbf{X}) = R(z_S) - Qh \tag{4}$$

where h is the hub height and the bending moment resistance is

$$R = z_S X_R F_y \tag{5}$$

z_S is the design variable in standstill (e.g. section modulus), F_y is the yield strength and X_R is the model uncertainty. The load effect is

$$Q = P C_T A\left(1 + 2k_p Ic_{amp} X_{dyn}\right) X_{aero} X_{\exp} X_{st} X_{str} X_{sim} \tag{6}$$

$P = 0.5\rho V^2$ is the extreme mean wind pressure, U is the extreme annual mean wind velocity at hub height, $I = \sigma_u / V$ is the turbulence intensity at hub height, σ_u is the standard deviation of turbulence at hub height, modeled as a stochastic variable with standard deviation $\sigma[\sigma_u] = 2I_{15}$ and expected value $E[\sigma_u] = \hat{\sigma} - \sigma[\sigma_u]$, (Tarp-Johansen et al. 2003). I_{15} is the turbulence intensity corresponding to a mean wind speed equal to 15 m/s. The characteristic value $\hat{\sigma} = I_{15}(15 + aV)/(1 + a)$ is assumed to be a 90% quantile. All parameters are described in table 1.

In operational mode, the wind turbine is operating at a wind velocity which is maximum equal to 25 m/s. The limit state equation is written:

$$g_O(z_O, \mathbf{X}) = R(z_O) - Qh \tag{7}$$

where the bending moment resistance is $R = z_O X_R F_y$ and the load effect is

$$Q = P C_T A\left(\eta + (1-\eta) T \frac{\sigma_u}{E[\sigma_u]} X_{dyn} X_{St} X_{ext} X_{sim}\right) X_{aero} X_{\exp} X_{str} \tag{8}$$

where z_O is the design variable operation (section modulus), η is a parameter modeling the mean response relative to the expected extreme response, $P = 0.5\rho V^2$ is the mean wind pressure at maximum operational wind velocity $V = 25$ m/s, T is the normalized annual extreme load during operation, which is assumed to be Gumbel distributed, see (Tarp-Johansen et al. 2002) and (Tarp-Johansen et al. 2003), with expected value $E[T] = k_p + \ln N / k_p$ and coefficient of variation $COV[T] \approx \pi / (\sqrt{6}(k_p^2 + \ln N)) = 8\%$. It is assumed that the characteristic value is a 98% quantile and $k_p = 3.3$, which implies that $N = 171$ and $E[T] = 4.86$. All parameters are described in table 1.

For a wind turbine park the limit state equation for a wind turbine in standstill is the same as for a single wind turbine. In operation mode wakes behind wind turbines change the wind flow, see above. In the following it is assumed conservatively that the wind velocity is unchanged, and that the standard deviation of the turbulence is increased basically following the models recommended in (IEC 61400 2005). The limit state equation is written:

$$g_O(z_O, \mathbf{X}) = R(z_O) - Qh \tag{9}$$

Table 1. Example stochastic variables for local buckling failure mode. Variables denoted X model model-uncertainty. N: Normal, LN: Lognormal, G: Gumbel.

Variable		Distribution type	Mean value	*COV*	Characteristic value
h	Rotor height		70 m		
P	Annual maximum mean wind pressure – Standstill	G	538 kPa	0.23	98%
P	Operation mean wind pressure – Operation		$0.5\rho(25\text{m/s})^2$		
T	Annual maximum normalized operational wind load – Operation	G	$E[T]$	$COV[T]$	98%
σ_u	Standard deviation of turbulence – Standstill	LN			90%
σ_u	Standard deviation of turbulence – Operation	LN			90%
X_{wake}	Model uncertainty	LN	1	0.15	1
$C_T A$	Thrust coefficient × rotor disk area				
c_{amp}	Factor		1.35		
k_p	Peak factor		3.3		
X_{exp}	Exposure (terrain)	LN	1	0.10	
X_{st}	Climate statistics	LN	1	0.05	1
X_{dyn}	Structural dynamics	LN	1	0.05	1
X_{aero}	Shape factor / model scale	G	1	0.10	1
X_{sim}	Simulation statistics – Standstill	N	1	0.05	1
X_{sim}	Simulation statistics – Operation	N	1	0.05	1
X_{ext}	Extrapolation – Operation	LN	1	0.05	1
X_{str}	Stress evaluation	LN	1	0.03	1
F_y	Yield stress	LN	240 MPa	0.05	5%
X_M	Resistance – model uncertainty	LN	1	0.03	1

where the resistance is $R = z_O X_R F_y$ and the load effect is

$$Q = P\,C_T A\left(\eta + (1-\eta)T\frac{\sigma_u}{E[\sigma_u]}X_{dyn}X_{St}X_{ext}X_{sim}\right)X_{aero}X_{\text{exp}}X_{str} \tag{10}$$

with $\hat{\sigma}_P = \sqrt{\hat{\sigma}^2 + X_{wake}0.9V^2/(1.5+0.3d\sqrt{\frac{V}{c}})^2}$ is the characteristic value of σ_u, equal to the 90% quantile and $c = 1$ m/s is a parameter. $V[\sigma_{u,P}] = V[\sigma_u]$ is the coefficient of variation of standard deviation of turbulence, assumed to be the same as for one wind turbine in operation, X_W is a model uncertainty related to turbulence model in park conditions, modeled as a stochastic variable. The other parameters are described in table 1, based on (Tarp-Johansen et al. 2003) and (Sørensen and Tarp-Johansen 2005).

4.2 *Probabilistic models for fatigue failure*

Design and analysis for fatigue are assumed to be performed using linear and bilinear SN-curves, eventually with lower cut-off limit as e.g. used in (Eurocode 3, 2003). It is assumed that Miner's rule with linear damage accumulation can be used. Further it is assumed that fatigue contributions from events as start and stop of the wind turbine can be neglected.

A bilinear SN-curve is considered, see figure 4 with slope change at $N_D = 5 \cdot 10^6$:

$$N = K_1 S^{-m_1} \quad \text{for} \quad S \geq \Delta\sigma_D \tag{11}$$

$$N = K_2 S^{-m_2} \quad \text{for} \quad S < \Delta\sigma_D \tag{12}$$

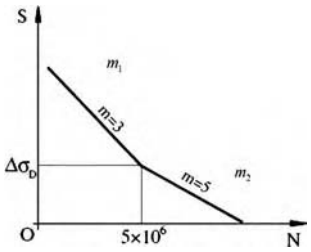

Figure 4. Bi-linear SN-curve.

where N is the number of cycles to failure with constant stress range S, K_1, m_1 are material parameters for $S \geq \Delta\sigma_D$ and K_2, m_2 are material parameters for $S < \Delta\sigma_D$.

$$\Delta\sigma_D = \left(\frac{K_1}{5\cdot 10^6}\right)^{1/m_1} \tag{13}$$

For a wind turbine in free wind flow the limit state equation is written, see also (Sørensen et al. 2007):

$$g(t) = \Delta - \int_{U_{in}}^{U_{out}} \nu \cdot t \cdot D(m_1, m_2, \Delta\sigma_D; \sigma_{\Delta\sigma}, U) f_U(U) dU \tag{14}$$

where Δ is a stochastic variable modeling the model uncertainty related to the Miner's rule for linear damage accumulation, t is time in years and ν is the total number of fatigue load cycles per year (determined by e.g. Rainflow counting).

$$D(m_1, m_2, \Delta\sigma_D; \sigma_{\Delta\sigma}, U) = \int_0^{\Delta\sigma_D} \frac{(X_W X_{SCF} s)^{m_2}}{K_2} f_{\Delta\sigma}(s|\sigma_{\Delta\sigma}(U)) ds + \int_{\Delta\sigma_D}^{\infty} \frac{(X_W X_{SCF} s)^{m_1}}{K_1} f_{\Delta\sigma}(s|\sigma_{\Delta\sigma}(U)) ds \tag{15}$$

is the expected damage rate given standard deviation of stress ranges, $\sigma_{\Delta\sigma}$ and mean wind speed U. X_W is the model uncertainty related to wind load effects (exposure, assessment of lift and drag coefficients, dynamic response calculations) and X_{SCF} is the model uncertainty related to local stress analysis.

U_{in} is the cut-in wind speed (typically 5 m/s) and U_{out} is the cut-out wind speed (typically 25 m/s). $f_{\Delta\sigma}(s|\sigma_{\Delta\sigma}(U))$ is the density function for stress ranges given standard deviation of $\sigma_{\Delta\sigma}(U)$ at mean wind speed U. This distribution function can be obtained by e.g. Rainflow counting of response, and can e.g. be assumed to be Weibull distributed. It is assumed that:

$$\sigma_{\Delta\sigma}(U) = \alpha_{\Delta\sigma}(U)\frac{\bar{\sigma}_u(U)}{z} \tag{16}$$

where $\alpha_{\Delta\sigma}(U)$ is an influence coefficient for stress ranges given mean wind speed U, $\bar{\sigma}_u(U)$is the mean value of the standard deviation of turbulence and z is a design parameter (e.g. proportional to cross sectional area) obtained from a design equation corresponding to (14).

For a wind turbine in a farm a limit state equation based on IEC 61400-1 (IEC 2005) can be written:

$$g(t) = \Delta - \int_{U_{in}}^{U_{out}} \nu \cdot t \cdot \left\{ \begin{array}{l} (1 - N_W \cdot p_W) D\left(m_1, m_2, \Delta\sigma_D; \alpha_{\Delta\sigma}(U)\overline{\sigma}_u(U)/z, U\right) \\ + p_W \sum_{j=1}^{N_W} D\left(m_1, m_2, \Delta\sigma_D; \alpha_{\Delta\sigma}(U)\overline{\sigma}_{u,j}(U)/z, U\right) \end{array} \right\} f_U(U)dU \qquad (17)$$

where N_W is the number of neighboring wind turbines and p_W is the probability of wake from a neighboring wind turbine (equal to 0.06). $\bar{\sigma}_{u,j}$ is the mean standard deviation of turbulence from neighboring wind turbine no j

$$\overline{\sigma}_{u,j}(U) = \sqrt{\overline{\sigma}_u^2 + X_{wake} \frac{0.9 \cdot U^2}{\left(1.5 + 0.3 d_j \sqrt{U/c}\right)^2}} \qquad (18)$$

d_j is the distance normalized by rotor diameter to neighboring wind turbine no j and c a constant equal to 1 m/s.

5 EXAMPLES

5.1 *Example 1 – Fatigue failure*

Fatigue failure is considered for wind turbines with a design life time $T_L = 20$ years and fatigue life time $T_F = 60$ years, corresponding to Fatigue Design Factor $FDF = 60/20 = 3$. The mean wind speed is assumed to be Weibull distributed with location parameter $A = 10.0$ m/s and shape parameter $k = 2.3$. It is assumed that the reference turbulence intensity is $I_{ref} = 0.14$, and that 5 wind turbines are close to the wind turbine considered with $d_i = 4$.

In figures 5 and 6 are shown typical examples of the ratio $\sigma_{\Delta\sigma}(U)/\sigma_u(U)$, see also (Sørensen et al. 2007). The ratio is seen to be highly non-linear – due to the control system.

In table 2 is shown a typical example of a stochastic model for a welded steel detail, based partly on (Faber et al. 2005) and (Tarp-Johansen et al. 2003).

Fatigue critical details with load effects proportional to the mudline bending moment and the blade flap moment in a pith controlled wind turbine is considered. It is noted that it could be relevant to use another stochastic model for the blade flap moment effect, but in order to

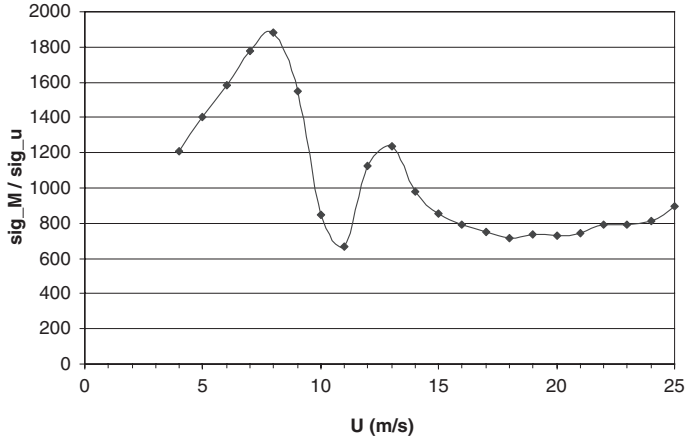

Figure 5. $\sigma_{\Delta\sigma}(U)/\sigma_u(U)$ for mudline bending moment – pitch controlled wind turbine.

compare the different influence coefficient models the same stochastic model is used. The stress range is assumed Weibull distributed with shape parameter $k = 0.8$, and the number of load cycles per year $\nu = 5 \cdot 10^7$. The results are shown in table 3 and 4 and in figures 7 and 8. α_1, α_2 are the parts of fatigue damage from SN-curve with slopes m_1 and m_2 ($\alpha_1 + \alpha_2 = 1$), $\Delta\beta(20)$ is the reliability index in year 20 with 1 year reference period, and $\beta(20)$ is the reliability index corresponding to accumulated probability of failure in 20 years.

It is seen that the reliability index β are smaller for the bi-linear SN-curve than for the linear SN-curve. The reliability decreases due to larger uncertainty on the lower part of the SN-curve and due to higher importance of the model uncertainties (X_W, X_{SCF}) at the lower part of the SN-curve (higher m value). The reliability level is seen to be slightly smaller for wind turbines in a wind

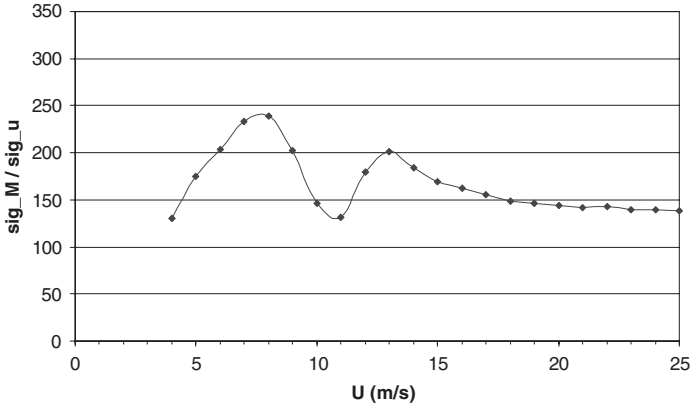

Figure 6. $\sigma_{\Delta\sigma}(U)/\sigma_u(U)$ for blade flap moment – pitch controlled wind turbine.

Table 2. Stochastic model for fatigue failure mode.

Variable	Distribution	Expected value	Standard deviation
Δ	N	1	0.10
X_W	LN	1	0.15
X_{SCF}	LN	1	0.10
X_{wake}	LN	1	0.15
m_1	D	3	
$\log K_1$	N	determined from $\Delta\sigma_D$	0.22
m_2	D	5	
$\log K_2$	N	determined from $\Delta\sigma_D$	0.29
$\Delta\sigma_D$	D	71 MPa	
$\log K_1$ and $\log K_2$ are fully correlated			

Table 3. Results – fatigue critical detail with mudline moment.

SN-curve	β	$\Delta\beta$	α_1
Linear	3.38	3.77	1
Linear – wind farm	3.24	3.65	1
Bi-linear	2.46	3.11	0.28
Bi-linear – wind farm	2.35	3.03	0.31

Table 4. Results – fatigue critical detail with blade flap moment.

SN-curve	β	$\Delta\beta$	α_1
Linear	3.34	3.74	1
Linear – wind farm	3.21	3.63	1
Bi-linear	2.40	3.06	0.26
Bi-linear – wind farm	2.31	3.00	0.31

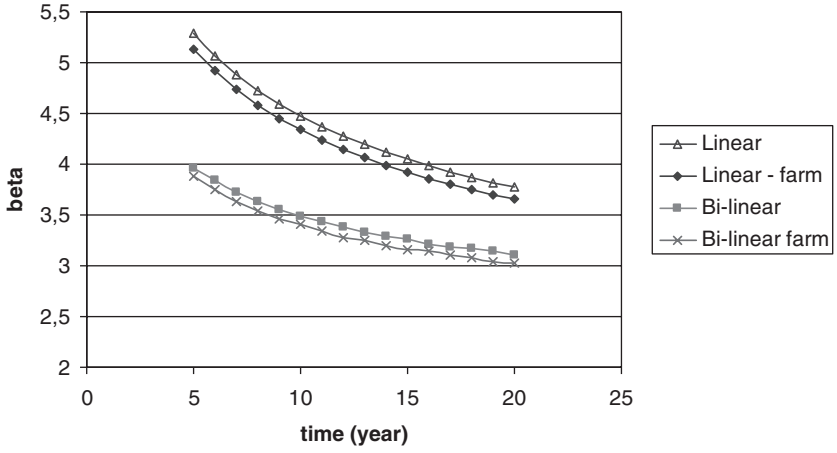

Figure 7. Annual reliability index as function of time for fatigue critical detail with mudline moment.

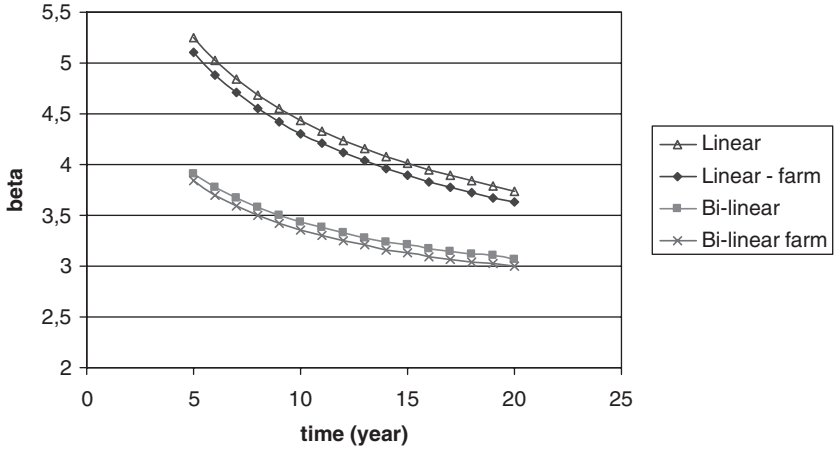

Figure 8. Annual reliability index as function of time for fatigue critical detail with blade flap moment.

farm than for single wind turbines. The two different influence coefficient functions are seen to give almost the same reliability levels.

5.2 *Example 2 – ULS extreme load failure*

The next example is based on simplified models for offshore wind-turbine support structures in shallow waters corresponding to wind turbines with 2.0 MW, 7-m hub height and an 80-m rotor

Table 5. Optimal values of R, t and D for different values of real rate of interest r.

r	R [m]	t [m]	D [m]	β	W^*
0.02	4.21	0.019	5.81	3.26	5.33
0.05	4.38	0.017	5.27	3.01	1.60
0.08	4.46	0.016	5.00	2.87	0.68

diameter. (Tarp-Johansen et al. 2002) describe the limit state functions and the economy model for the following example in more detail. Two failure modes are considered: local buckling of tower due to wind load, and sliding of foundation due to wind and wave loads. The following design variables are used: radius of foundation, R; diameter of tower, D and thickness of tower, t. Details are described in (Sørensen & Tarp-Johansen 2005).

The representative cost model consists of initial costs, failure costs, control system costs and benefits. The initial costs are modeled by:

$$\frac{C_I}{C_0} = C_{\text{foundation}} + C_{\text{turbine}} + C_{others} = \frac{1}{6}\frac{R}{R_0} + \frac{1}{6}\frac{Dt}{A_0} + \frac{1}{3} \tag{19}$$

where the reference values are $R_0 = 8.5\,\text{m}$ and $A_0 = 3/26\,\text{m}^2$. The failure costs are assumed to be $C_F/C_0 = 1/36$. The benefits per year are $b/C_0 = 1/8$ and the real rate of interest is assumed to be $r = 0.05$.

Table 5 shows the results for a single wind turbine with systematic rebuilding where the real rate of interest equal to 2%, 5% and 8%. It is seen that the reliability indices β is approximately 3, corresponding to a probability of failure per year equal to 10^{-3}. Further R increases, while t and D decrease with increasing real rate of interest, r. The reliability indices decrease with increasing real rate of interest, r.

6 CONCLUSIONS

Reliability-based cost-benefit optimization formulations for wind turbines are presented. Compared to onshore wind turbines offshore wind turbines are characterized by a very low risk of human injury in case of failure It is then relevant to assess the minimum reliability level for structural design on the basis of reliability-based cost optimization considering the whole life-cycle of the turbines without a reliability constraint.

Some of the important aspects for stochastic modeling of loads, strengths and models uncertainties for wind turbines are described. Single wind turbines and wind turbines in wind farms with wake effects are discussed. Limit state equations are presented for fatigue limit states and for ultimate limit states, and illustrated by bending failure.

Illustrative examples are presented, and as a part of the results optimal reliability levels are obtained. Example 1 with fatigue failure indicates that the reliability level is almost the same for single wind turbines and for wind turbines in wind farms if the wake effects are modeled equivalently in the design equation and in the limit state equation. Example 2 with ultimate limit states shows that the optimal reliability level for offshore wind turbines related to structural failure corresponds to annual probabilities of failure approximately equal to corresponding to reliability index equal to 3. This reliability level is significantly lower than for civil engineering structures in general.

7 ACKNOWLEDGEMENTS

The work presented in this paper is part of the project 'Probabilistic design of wind turbines' supported by the Danish Research Agency, grant no. 2104-05-0075. The financial support is greatly appreciated.

REFERENCES

Eurocode 3 (2001). Design of Steel Structures, prEN1993, CEN.

Faber, MH, Engelund, S, Sørensen, JD, and Bloch, A (2000). Simplified and Generic Risk-based Inspection Planning, Proc Int Conf Offshore Mech & Arct Eng, S&R paper 6143.

Frandsen, S. (2005). Turbulence and turbulence-generated structural loading in wind turbine clusters, Risø National Laboratory, Denmark, Report R1188.

IEC 61400-1 (2005). Wind turbine generator systems – Part 1: Safety requirements.

Rackwitz, R (2001). Risk Control and Optimization for Structural Facilities, *System Modelling and Optimization*, pp 143–167.

Sørensen, J.D. and Tarp-Johansen, N.J. (2005). Reliability-based optimization and optimal reliability level of offshore wind turbines. International Journal of Offshore and Polar Engineering (IJOPE), Vol. 15 (2), 1–6.

Sørensen, J.D., S. Frandsen and Tarp-Johansen, N.J. (2007). Fatigue Reliability and Effective Turbulence Models in Wind Farms. Submitted for ICASP10 conf., July 2007, Tokyo, Japan.

Tarp-Johansen, NJ, Sørensen, JD, and Madsen, PH (2002). Experience with Acceptance Criteria for Offshore Wind Turbines in Extreme Loading, Wksp on reliability-based code calibration, Zurich, CD-ROM, http://www.jcss.ethz.ch/.

Tarp-Johansen, N.J., Madsen, P.H., and Frandsen, S.T. (2003). Calibration of Partial Safety Factors for Extreme Loads on Wind Turbines. Proc CD-ROM. CD 2. European wind energy conference and exhibition 2003 (EWEC 2003), Madrid (ES), 16–19 June 2003.

Reliability and Optimization of Structural Systems: Assessment, Design and Life-Cycle Performance – Frangopol, Kawatani & Kim (eds)
© 2007 Taylor & Francis Group, London, ISBN 978-0-415-40655-0

Life-cycle performance and cost analysis of bridge network considering seismic risk

H. Furuta
Department of Informatics, Kansai University, Japan

K. Koyama
NTT Comware, Tokyo, Japan

Dan M. Frangopol
Department of Civil and Environmental Engineering, Lehigh University, USA

ABSTRACT: In this study, an attempt is made to develop an LCC analysis of bridge structures considering seismic risk. Using the probability of damage occurrence, LCC can be calculated for the bridge structure with earthquake excitations. Furthermore, it is intended to develop an optimal maintenance planning system and an optimal seismic design system of road network by using Multi Objective Genetic Algorithm.

1 INTRODUCTION

During the past decade, maintenance work on civil infrastructures is increasing in volume and importance. In Japan, the number of existing bridges requiring repair and replacement increased dramatically. In order to establish a rational maintenance program, it is necessary to develop a cost-effective decision-support system that can provide a practical and economical plan. Although low-cost maintenance plans are desirable for bridge owners interested in short-term investment, it is necessary to consider lifetime constraints when choosing an appropriate maintenance program.

Recently, Life-Cycle Cost (LCC) has been paid attention as a possible and promising method to achieve a rational maintenance program. In general, LCC consists of initial cost, maintenance cost, and renewal cost. However, when considering LCC in the region that often suffers from natural hazards such as typhoons and earthquakes, it is necessary to account for the effects of such natural hazards. In Japan, it is important to take into account the social and economical effects caused by the collapse of structures due to the earthquake as well as the minimization of maintenance cost. The loss by the collapse of structures due to the earthquake can be defined in terms of an expected cost and introduced into the calculation of LCC.

In this study, an attempt is made to develop an LCC analysis of bridge structures considering seismic risk. Using the probability of damage occurrence, LCC can be calculated for the bridge structure with earthquake excitations. Furthermore, it is intended to develop an optimal maintenance planning system and an optimal seismic design system of road network by using Multi Objective Genetic Algorithm (MOGA).

2 EARTHQUAKE OCCURRENCE PROBABILITY IN SERVICE TIME

In this study, the earthquake occurrence probability is evaluated by using seismic hazard curve. In the hazard curve, the annual occurrence probability of earthquake is calculated by considering the distribution of distance from epicenter, historical earthquake records, horizontal maximum acceleration and active fault. The hazard curve used here is shown in Figure 1.

3 REQUIRED YIELD STRENGTH SPECTRUM

In this study, a probability model of yield strength is developed by using the yield strength spectrum. The yield strength spectrum shows a nonlinear relation between natural period and yield strength. This spectrum can be obtained for various ductility factors and damage indices. Here, the values presented in Table 1 are used in the analysis for natural period, target ductility factor, earthquake level, type of soil and number of seismic wave. (Furuta et al., 2003b)

Figure 2 shows the calculated results of the yield strength spectrum. Because there are many data, only representative values are shown in Figure 3. Figure 3 shows the analysis results using the data presented in Figure 2. These results are obtained through the regression analysis for the earthquake level of 800 gal. In this study, the distribution of yield strength is obtained by using this spectrum.

When designing a structure, type of soil, ground maximum acceleration and target ductility factor should be given. The natural period of the structure is changed by the design. In order to make the design simple, it is not good that the probability model of the required yield strength changes depending on the design. In this study, a probability distribution model of yield strength is developed for various types of soil and target ductility factors. In this model the required yield strength can be constant regardless of the natural period. Here, the probability distribution model is assumed to be the lognormal distribution. The probability density function of the lognormal distribution is given in Equation 1.

$$f_{P_{my}}(x)=\frac{1}{\sigma_{\ln(x)}\sqrt{2\pi}}\frac{1}{x}\exp\left[-\frac{1}{2}\left(\frac{\ln(x)-\mu_{\ln(x)}}{\sigma_{\ln(x)}}\right)^2\right] \tag{1}$$

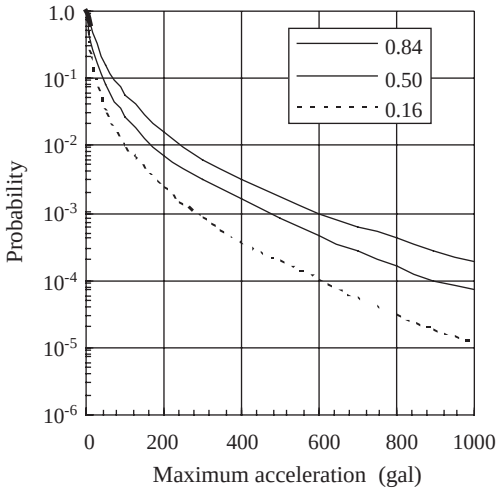

Figure 1. Seismic hazard curve.

Table 1. Analysis condition.

Natural period T	0.1∼5.0 (sec)
Taget ductility factor μ_T	1.0, 2.0
Earthquake level	400, 800 (gal)
Type of soil	1, 2, 3
Seismic wave	18

4 RELIABILITY ANALYSIS OF STEEL BRIDGE PIER

As an example, a steel bridge pier is employed, in which its failure probability and reliability index are calculated.

4.1 *Analysis model*

Figure 4 shows the detail of the steel bridge pier and its cross section. To simplify the design, it is assumed that the cross section is square without stiffening and the width of flange and web is equal. To avoid the local buckling, this pier is designed according to the "Japanese Specification of Highway Bridge".

Then, the minimum thickness is determined so as to satisfy the following requirement:

$$\frac{b_f}{b_w} = \frac{b_w}{t_w} \le 48 \tag{2}$$

where the steel material is SM490Y.

In this study, the residual stress and the initial deflection are considered for the initial imperfection of the steel pier. This pier is used for a three-spanned continuous steel girder bridge with 40 m span length. The bridge has two main girders and Reinforced Concrete (RC) slabs. For the design

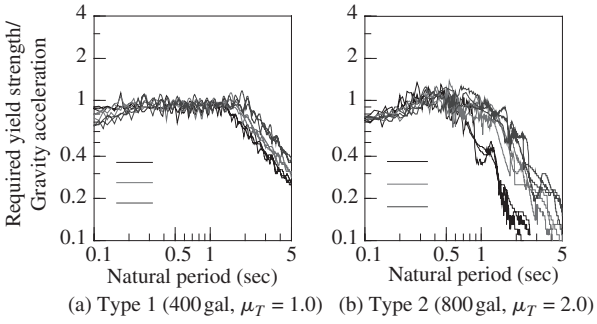

Figure 2. Required yield strength spectra.

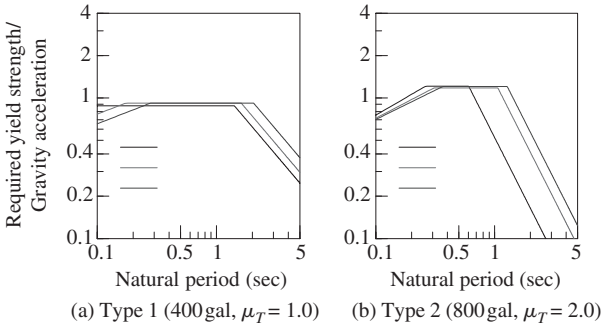

Figure 3. Standard required yield strength spectra.

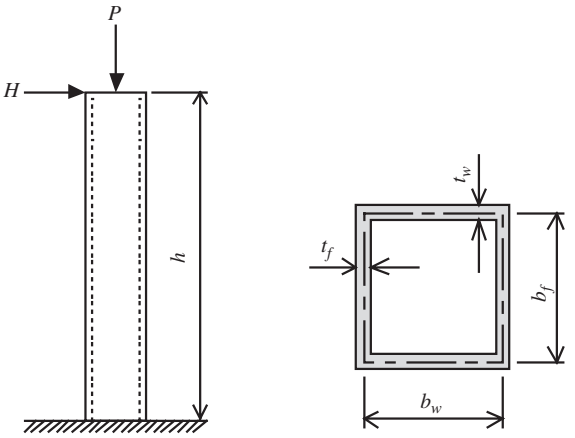

Figure 4. Analysis model.

Table 2. Results of analysis.

Ductility factor	Earthquake	Soil	Var_{in}	σ_{in}
1	I	I	0.0030	0.0551
		II	0.0029	0.0537
		III	0.0052	0.0722
	II	I	0.0049	0.0699
		II	0.0054	0.0736
		III	0.0044	0.0662
2	I	I	0.0222	0.1488
		II	0.0343	0.1852
		III	0.0287	0.1694
	II	I	0.0306	0.1749
		II	0.0361	0.1900
		III	0.0410	0.2025
3	I	I	0.0256	0.1599
		II	0.0287	0.1696
		III	0.0339	0.1842
	II	I	0.0372	0.1927
		II	0.0457	0.2140
		III	0.0576	0.2401
4	I	I	0.0286	0.1691
		II	0.0302	0.1736
		III	0.0388	0.1970
	II	I	0.0383	0.1956
		II	0.0413	0.2030
		III	0.0523	0.2287
5	I	I	0.0302	0.1739
		II	0.0337	0.1834
		III	0.0390	0.1974
	II	I	0.0372	0.1930
		II	0.0397	0.1990
		III	0.0498	0.2232

condition, the vertical load P is calculated to be 10.84 MN, which corresponds to the reaction force to the superstructure. The height of the steel pier is 10 m, and its width is 2,000 mm and its thickness is 42~60 mm.

4.2 *Limit state functions*

In this study, both the serviceability limit condition and the ultimate limit condition are taken into account as the limit state.

4.2.1 *Serviceability limit condition*

The elastic limit of the structure is employed for the serviceability limit condition. The limit state function is given as follows:

$$Z = P_a - P_{yn} \tag{3}$$

where P_a means the yield strength of the structure and P_{yn} means the required yield strength of ductility factor $\mu = 1.0$.

4.2.2 *Ultimate limit condition*

In this study, the ductility factor μ is taken as the parameter which decides the ultimate limit condition. Considering the difference of structural type and structural material, the reliability analysis is performed for the ductility factor $\mu = 1.0,\ 2.0,\ 3.0,\ 4.0,\ 5.0$. Then, the limit state function is given as

$$Z = P_a - P_{yn} \tag{4}$$

where P_{yn} is required yield strength of the ductility factor $\mu = 1.0, 2.0, 3.0, 4.0, 5.0$.

4.3 *Reliability analysis*

For the above ultimate and serviceability limit functions, the reliability analysis is performed, where the load combination is not considered. Because the distribution of earthquake force becomes a non-normal distribution, the safety margin Z also becomes a non-normal distribution. Therefore, it is necessary to transfer Z to a normal distribution.

Since it needs enormous task to analyze all the target ductility factor and type of soil, only type II soil is taken into consideration and the corresponding damage index to the earthquake is assumed as follow:

For type I earthquake, 400 gal is employed as the maximum acceleration. Type I earthquake is defined in the Japanese Specification of Highway Bridge. This type I earthquake is used to check the seismic design for middle earthquakes. Then, the damage index of the structure is assumed to be $\mu_T = 1.0$. On the contrary, Type II earthquake is used to check for strong earthquakes, in which the maximum acceleration is 800 gal. Then, the damage index of the structure is $\mu_T = 2.0$.

5 LIFE-CYCLE COST ANALYSIS CONSIDERING SEISMIC RISK

5.1 *Initial cost and loss cost*

As the initial cost, only pier is considered, because the sufficient data for the whole bridge is not prepared. Then, the initial cost consists of material cost, painting cost and transportation cost. (Table 3) It is also assumed that type I earthquake will lose 80% of the initial cost and type II earthquake will lose 110%.

Table 3. Initial cost (*Yen*).

Item		Unit	Cost
Fabrication cost	Material cost	*t*	97,585
	Painting cost	m^2	1700
Erection cost	Transport cost	*t*	9000

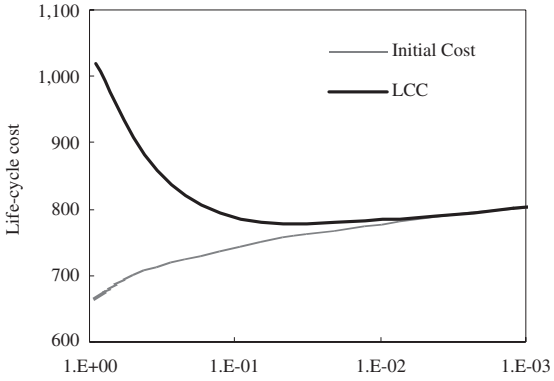

1. Type 1 earthquake $\mu_T = 1.0$

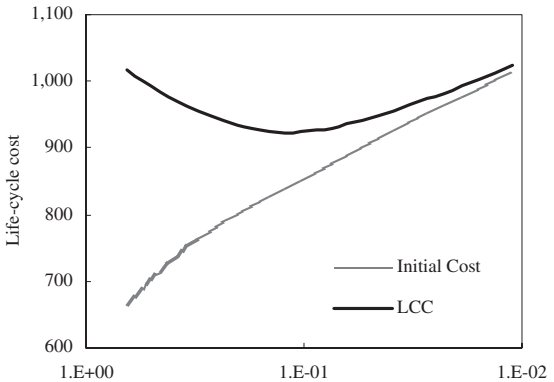

2. Type 2 earthquake $\mu_T = 2.0$

Figure 5. Relations between LCC and failure probability.

5.2 *Formulation of LCC considering seismic risk*

The failure probability of structure is calculated by Equation 5.

$$P_{f,t=L} = P(t) \times P_f \tag{5}$$

Then, LCC is formulated as

$$LCC = C_I + P_{f,t=L} \frac{C_F}{(1+i)^t} \tag{6}$$

where i is the discount rate and assumed to be 2%.

5.3 *Results of analysis*

The relation between LCC and failure probability is shown in Figure 5, in which LCC is calculated with the same assumption as those used in the reliability analysis.

5.3.1 *Case 1*

For the case shown in Figure 5-1, LCC is minimized when the thickness $t_f = t_w$ is 50(mm). Then, the failure probability P_f is 0.03 and the reliability index μ_T is 1.86.

5.3.2 *Case 2*

For the case shown in Figure 5-2, LCC is minimized when the thickness $t_f = t_w$ is 56(mm), in which P_f is 0.12 and reliability index *i*s 1.17. From these results, it is confirmed that it is possible to propose the optimal design plan in service time including the loss cost, which has the minimum LCC from the standpoint of reliability-based design, by introducing the loss of the structure due to the earthquake and the repairing cost.

5.4 *Multi-objective analysis*

Here, the following two objective functions are employed to grasp the relations between safety index and LCC.

$$\text{OBJ1:}\quad \beta = \sum \beta_i \rightarrow \max \tag{7}$$

$$\text{OBJ2:}\quad LCC = \sum LCC_i \rightarrow \min \tag{8}$$

The Pareto solutions are obtained by Multi-Objective Genetic Algorithm (MOGA) (Furuta et al., 2003a). For MOGA calculation, the following parameters are used; the number of generation is 500, the number of individuals is 200, the rate of crossover is 0.6, the rate of mutation is 0.02 and the uniform crossover is chosen.

As an example, a road network in Osaka city is considered, which covers 6 km by 90 km and has 20 bridges (Furuta et al., 2002). For the maximum acceleration, 800 gal is assumed according to the Kobe earthquake occurred in 1995. Then, the damage degree is defined as $\mu_T = 2.0$, for which the safety index should be larger than 2.0. LCC is evaluated as the sum of initial construction cost, failure cost and user cost. The failure cost is assumed to be 1.2 times of the initial construction cost. For this example, MOGA provides many Pareto optimal solutions. Paying attention to the solution with the minimum LCC, LCC becomes 99,094 (thousand yen) and the average value of β for 20 bridges is 3.25. Although all the bridges satisfy the constraint that β should be larger than 2.0, eight bridges have just 2.0 for β. Next, consider the solution with the maximum value for β whose average value becomes 4.08 and each bridge has β value larger than 3.0. Then, LCC is 108,701 (thousand yen). It is noted that the solution having $\beta = 2.0$ for all the bridge has the largest LCC that is 120,000 (thousand yen). This implies that if the safety of bridge is specified as a lower level such as $\beta = 2.0$, LCC becomes large, because the failure cost due to the earthquake becomes very large as a result. From the result it is confirmed that the proposed method can provide useful relations between LCC and the safety of bridge considering seismic risk.

6 LCC ANALYSIS FOR ROAD NETWORK

For road networks, three network models (Model 1, Model 2, and Model 3) are employed, which are presented in Figure 6. In these models, it is assumed that each network model includes a road passing over a river, and that traffics reach the destination through detours when some bridges can

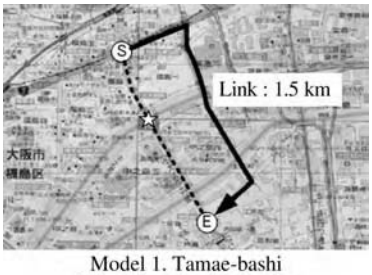

Model 1. Tamae-bashi
Fukushima-ku, Osaka city

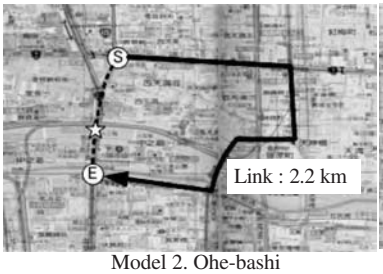

Model 2. Ohe-bashi
Kita-ku, Osaka city

Model 3. Sakuranomiya-bashi
Tyuo-ku, Osaka city

Figure 6. Three road network models.

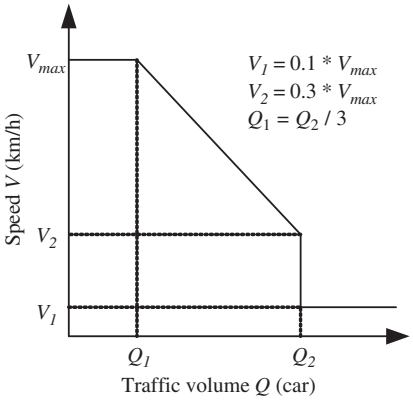

Figure 7. Relation between traffic volume and velocity.

not be passed. Moreover, it is assumed that the traffic volume and the velocity have relations shown in Figure 7.

Here, user cost is defined in terms of the sum of the time cost and energy consumption cost due to the detour or closure of road. The cost by increasing the driving time C_{UT} is calculated as the subtraction of the usual running cost and the running cost for the detour and closure.

$$UC_T = \alpha \cdot \{(Q \cdot T) - (Q_0 \cdot T_0)\} \tag{9}$$

$$UC_C = \beta \cdot \{(Q \cdot L) - (Q_0 \cdot L_0)\} \tag{10}$$

where UC_t: unit time cost, UC_r: unit running cost, Q, T, L: detour traffic volume, running time, and link length at the time of road closure, Q_0, T_0, L_0: initial traffic volume, running time, and link length.

Table 4. Unit requiring driving cost.

Speed V (km/h)	Unit Driving Cost (Yen/Car/km)
5	35
10	28
20	21
30	18
40	18

Table 5. Restoring method and cost.

Damage index	Restoring method	Repair cost	Repair time
As, A	Rebuild	120% of initial construction cost	2 months
B	Repair	73,000 Yen/1 m^2	1 month
C	Repair	35,000 Yen/1 m^2	2 weeks
D	No Repair		

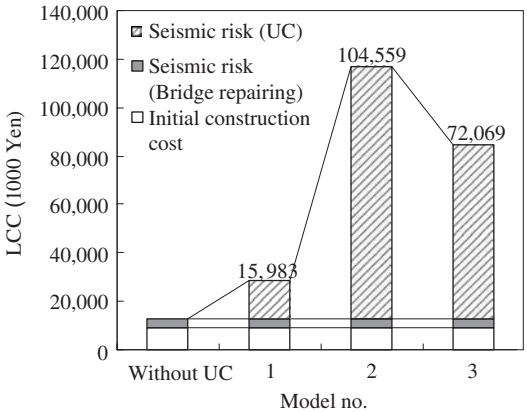

Figure 8. LCC of each model.

Using the data given in (Furuta et al., 2002) and assuming the ratio of small and medium trucks to be 10%, the unit time cost is estimated as 82 Yen/car/min., and β is assumed as shown in Table 4. The restoring periods are assumed to be two months and two weeks for the damage (As, A) and B, respectively.

Taking into account the discount rate, LCC is calculated as

$$LCC = C_i + \sum P_j(a) \cdot P(DI,a) \cdot \left\{ \frac{C_m(DI,a) + UC(DI,a)}{(1+i)^T} \right\} \tag{11}$$

where $C_m(DI,a)$: repair cost for each damage degree, $UC(DI,a)$: UC for each damage degree, i: discount rate, and T: service life.

For each damage degree, restoring method and cost are presented in Table 5.

For the three road networks, LCC is calculated by assuming that the fractile value in the hazard curve is 0.5, discount rate is 0, service life is 100 years. Figure 8 shows the calculated results, which indicate that there are big differences among the three networks, because of the differences

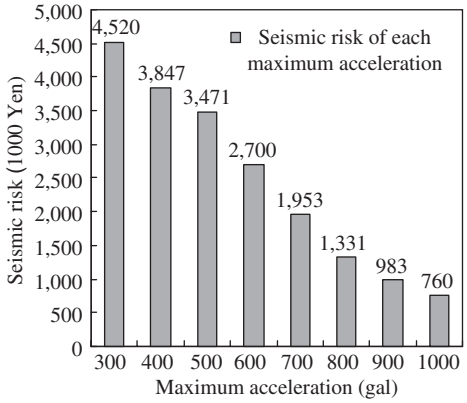

Figure 9. Seismic risk of each maximum acceleration.

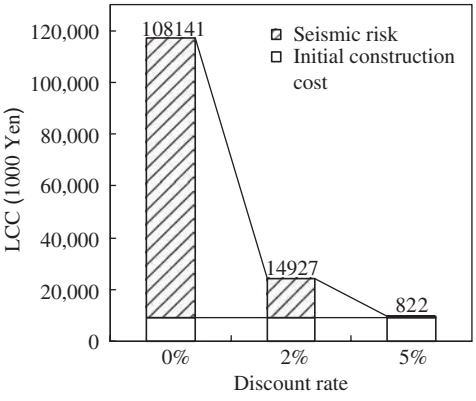

Figure 10. LCC for each discount rate.

in distances of detour and the initial traffic volumes. In the network with high traffics, seismic risk becomes 104,559,000 Yen that is 11 times of the initial construction cost and 30 times of the maintenance cost.

Comparing the case involving the user cost in the seismic risk and that without involving it, the seismic risk is only 1/3 of the initial cost when the user cost is not considered.

Paying attention to the damage curve given in Figure 3, it is evident that there is some difference in the damage probabilities according to the earthquake intensity. Figure 9 shows the relation between the seismic risk and the maximum acceleration. From this figure, it is obtained that the seismic risk decreases as the maximum acceleration increases. This is due to the facts that the bridge pier was designed to satisfy the requirement that the damage should be minor and the bridge function can be recovered in a short period. Therefore, the probabilities of damage B, C, and D become high.

Since it is difficult to determine an appropriate discount rate, only 2% and 5% discount rates are considered. Figure 10 shows the comparison among 0, 2 and 5 % discount rates, When the discount rate is considered to be 5%, the seismic risk becomes small such as 1/10 of the initial cost. It is concluded that the discount rate greatly affects the estimation of LCC.

7 CONCLUSIONS

In this study, an attempt was made to propose a calculation method of LCC considering seismic risk based on the reliability theory.

Through several numerical calculations, the following conclusions were derived:

(1) The proposed method can calculate LCC and failure probability for the structure that shows simple behavior by the earthquake.
(2) Introducing the expected failure cost of the structure due to the earthquake excitations, LCC could be evaluated for the case with seismic risk.
(3) Using the reliability-based design concept, it is possible to provide a design plan to make the reliability index maximum and LCC minimum.
(4) Applying the Multi-Objective Genetic Algorithm, it is possible to obtain the relations between LCC and the safety of bridge considering seismic risk.
(5) In the calculation of LCC, many factors are interrelated and include various uncertainties. Therefore, there still remain many issues to overcome in the future.
(6) Through the LCC calculation of several representative road networks, it is obtained that the difference of road network greatly influences on the seismic risk.
(7) Comparing the case with user cost and that without user cost, it is made clear that the effect of seismic risk is small unless user cost is considered, however, it becomes quite large if user cost is considered.
(8) Paying attention to the change of LCC according to the change of the maximum acceleration of earthquake, the seismic risk decreases, as the maximum acceleration increases.
(9) The effect of discount rate is examined by changing its value. As a result, it is obtained that the discount rate has a large influence on the estimation of LCC. This implies that it is very important to determine an appropriate discount rate in the calculation of LCC.
(10) Examining the effect of damage degree, the medium damage level shows a big ratio of 54 %, whereas the severe and rather severe damage levels show 28 % and 27 %, respectively.

REFERENCES

Furuta, H., Nose, Y., Dogaki, M., & Frangopol, D.M. 2002. Bridge maintenance system of road network using life-cycle cost and benefit, *Proc. of 1st IABMAS Conference, Barcelona, Spain.*

Furuta, H., Kameda, T., Fukuda, Y., & Frangopol, D.M. 2003a. Life-cycle cost analysis for infrastructure systems: Life-cycle cost vs. safety level vs. service life, *Proc. of 3rd Life-Cycle Cost Analysis and Design of Infrastructure Systems, Lausanne, Switzerland.*

Furuta, H. & Koyama, K. 2003b. Optimal maintenance planning of bridge structures considering earthquake effects, *Proc. of IFIP TC7 Conference, Antipolis, France.*

Reliability and Optimization of Structural Systems: Assessment, Design and Life-Cycle Performance – Frangopol, Kawatani & Kim (eds)
© 2007 Taylor & Francis Group, London, ISBN 978-0-415-40655-0

Exchangeable condition states and Bayesian reliability updating

Marc A. Maes
Civil Engineering Department, Schulich School of Engineering, University of Calgary, Canada

ABSTRACT: Inspection of deteriorating infrastructure often raises the issue of spatial differences and variations within similar structural elements or zones. A possible approach consists of modelling these "zones" using an unobservable condition state which can be either discrete (as in the case where indicators or state variables are used) or continuous (as in the case of a global degree of damage or exposure). Subsequently, inspection data or process outputs may be used to "update" these uncertain condition states. The challenge is to assimilate such data from different zones and sources so that the "shared" information as well as the "zone-specific" information can be used to update each individual condition state in an optimal way. In this paper Bayesian models based on exchangeable condition states are used to model the proper "mixing" of such observations and to allow flexible decision making. We investigate the merit and the effect of different mixing assumptions, including the effect of correlation between condition states. This type of modeling is linked to a key concept in Bayesian inference, namely that of exchangeability. The paper discusses some of the implications and challenges of working with exchangeable mixtures. Multi-stage Bayesian models have been used in structural inspection and maintenance planning, in the context of deteriorating R/C structures, pipelines, large industrial plants, and failure rate modeling in complex systems. The present paper shows how a multi-stage Bayesian approach with continuous condition states and both discrete and continuous hyper-parameters can be used to update time-dependent reliabilities for a system consisting of n exchangeable zones subject to deterioration, both in the case of section-specific limit states or limit states involving spatial extremes. An example application is given of an offshore gas pipeline subject to internal corrosion due to spatially variable CO_2 condensation. The pipeline is subject to planned inspections at certain points in time and this information can be used to update the condition states throughout the system as well as its long-term reliability.

1 INTRODUCTION

Tools for statistical inference in spatially distributed systems often involve challenging probabilistic models. Spatial characteristics play an important role in decision making with respect to safety and sustainability, including structural deterioration – most notably corrosion processes in steel and concrete infrastructure –, soil modeling, failures in geographically distributed systems, and occurrences of natural hazards in space and time.

Central to such models is the consideration of "condition states" that are may directly observable, but that can be subject to some form of Bayesian updating given other observable variables. The objective is to assimilate data from different sources such as different systems or different zones in a rational way in order to allow optimal decision making. This paper focuses on exchangeable (as opposed to independent) condition states which, based on de Finetti's theorem can always be written as Bayesian mixtures. The key concept of exchangeability and its implications on decision making are described. The various approaches are illustrated using an investigation of the role of dependence between condition states and an application involving spatial effects in pipeline corrosion and pipeline reliability-based inspection. This is followed by the conclusions.

2 EXCHANGEABILITY

Statistical inference for the multi-level Bayesian models described subsequently in this paper, rely on the concept of exchangeable random events, one of the foundations of subjective probability. This section reviews that concept.

In the eleventh chapter of his "Theory of Probability", Bruno de Finetti (1974) reviews the logical basis of inductive reasoning, and its influence upon formal statistical inference. He identifies Bayes' theorem as the vital element in the inductive process and "the key to every constructive activity of the human mind". The traditional assumption of independence is rejected because it conflicts with inductive reasoning, i.e. changing one's mind. Statistical inference that is based on the assumption of independent and identically distributed (iid) random quantities is, according to de Finetti, either incorrectly formulated or mistakenly interpreted.

This reasoning can easily be illustrated by the simple Bayesian net in Fig. 1. Bayesian nets are very effective in communicating inferential relationships between variables (Jensen, 2001) with circles denoting stochastic nodes, rectangles denoting constants, and simple and double directed links denoting stochastic and deterministic dependence, respectively. In Fig. 1(a) we show independent random variables (or, in the following, also random events): there is no stochastic relationship between the n variables. Equivalently, the probability distribution of each θ_i can be shown as parameterized on a constant α_i as shown in Fig. 1(b). In the case these distributions can be assumed to be identical, Fig. 1(c) shows that the different states θ_i are now iid (independent and identically distributed. But paradoxically, this Bayesian net shows that no information flow is possible from one state to another. For instance, if one of the random variables θ is observed, then none of the remaining ones will be affected. In classical probabilistic inference, the entire net must be erased and replaced with a similar one having a new, re-calculated, "fixed but unknown" value of α in the top rectangle.

Having thus abandoned independence, the simplest path forward is to continue to regard the order of occurrence of events as irrelevant, and this lies at the root of the principle of exchangeability.

The following definition applies equally to exchangeable events as well as to exchangeable random variables. For the latter, it is as follows: the random variables $\theta_1, \theta_2, \ldots, \theta_n$ are considered to be exchangeable if the joint pdf of $\theta_{i1}, \theta_{i2}, \ldots, \theta_{in}$ is identical to the joint pdf of $\theta_1, \theta_2, \ldots, \theta_n$, for all permutations $(i_1, \ldots, i_n)$ of the subscripts $(1, 2, \ldots n)$. Expressed differently, the order in which the θ_i are considered is of no importance to probability statements about the θ_i, or, the θ_i play a symmetrical role in relation to all problems of probability (de Finetti, 1937). This assumption is in fact critical to many models used in engineering inference.

The definition of exchangeability implies two straightforward facts:

(1) Any subset $\theta_1, \theta_2, \ldots, \theta_m$ of $\theta_1, \theta_2, \ldots, \theta_n$ $(2 < m < n)$ is also exchangeable. Note that the opposite is not necessarily valid; for example, two by two exchangeability of (θ_1, θ_2), (θ_2, θ_3) and (θ_1, θ_3) does not imply exchangeability of the triplet $(\theta_1, \theta_2, \theta_3)$.
(2) Any random mixtures of exchangeable variables are also exchangeable. An important class identified in de Finetti (1974) is the case of partial exchangeability (exchange within different classes), and the Markov form of changeability.
(3) iid random quantities are necessarily exchangeable.

An infinite string of random quantities is exchangeable, if all finite segments $\theta_1, \theta_2, \ldots, \theta_n$ $(2 < n)$ are exchangeable.

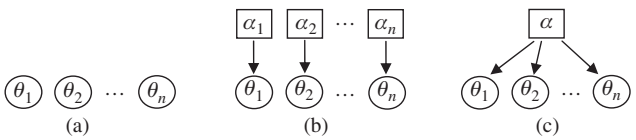

Figure 1. Independent random variables θ_i $(i = 1, \ldots, n)$.

The quintessential representation of exchangeable events is based on de Finetti's Theorem (1974): consider a set of exchangeable random quantities $\theta_1, \theta_2, \ldots, \theta_n$ ($n > 2$) and an event E_k, related to this set, for example:

$$E_a = \{\theta_1 < a_1, \theta_2 < a_2, ..., \theta_n < a_n\}, \tag{1}$$

or

$$E_b = \left\{Z = \max_n \theta_i < z\right\}, \tag{2}$$

then the joint probability density function (pdf) f of the exchangeable random variables can always be expressed as the mixture:

$$f(\theta_1, ..., \theta_n) = \int f(\theta_1, ..., \theta_n | V) dF(V) \tag{3}$$

and the related event as:

$$\Pr(E_k) = \int \Pr(E_k | V) dF(V), \tag{4}$$

where $\Pr(E_R|V)$ is the probability attributable to the event E_k, when the $\theta_i|V$ are considered to be independent and to have the same distribution function V. Thus, the probability of E_k, assuming exchangeable θ_i, is a linear combination of probabilities corresponding to the iid case, the integral (4) being extended over all possible distribution functions V, according to a weight functional $F(V)$.

de Finetti proves the validity of this "mixture theorem" in both directions: first, exchangeability holds as soon as the mixture form (4) is applicable; and, second, if exchangeability is assumed, then $\Pr(E_k)$ must necessarily be of the mixing type (4); the latter proof not being as straightforward. For discrete events and discrete random variables, the prototype example of exchangeability is related to drawing coloured balls from urns having unknown composition. It is intuitively obvious that this simple model can be expressed as a mixture.

The expressions (3) and (4) can also be parameterized in terms of a random variable α having a pdf $f(\alpha)$as follows:

$$f(\theta_1, \theta_2, \ldots, \theta_n) = \int_\alpha \prod_{i=1}^{n} f(\theta_i | \alpha) f(\alpha) d\alpha \tag{5}$$

which corresponds to the paradigm Bayesian net shown in Fig. 2 showing the θ_i to be conditionally iid with pdf $f(\theta|\alpha)$; and similarly:

$$\Pr(E_k) = \int_\alpha \Pr(E_k | \alpha) f_\alpha(\alpha) d\alpha \tag{6}$$

where $\Pr(E_k|\alpha)$ is the probability of event E_k assuming that the θ_i are iid with pdf $f(\theta|\alpha)$. In other words, the probability of E_k is a mixture of probabilities associated with a given state of belief (represented by α).

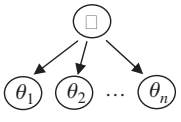

Figure 2. Exchangeable random variables θ_i ($i = 1, \ldots, n$).

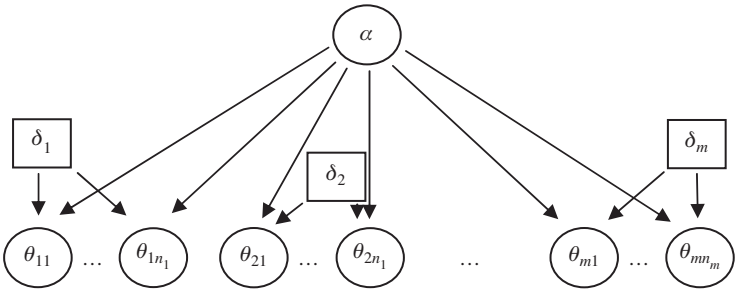

Figure 3. Exchangeability in *m* classes.

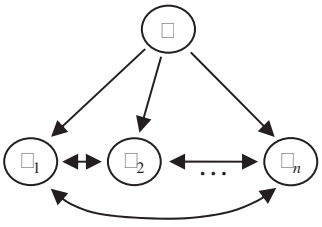

Figure 4. Conditionally dependent exchangeable random variables.

It can also be seen from (6) that statistical inference for exchangeable events, i.e. updating $\Pr(E_k)$ to $\Pr(E_k|E_l)$ when information about E_l becomes available, is equivalent to using a different mixing distribution in (5):

$$f_{\alpha|E_l}(\alpha|E_l) \propto f_\alpha(\alpha)\Pr(E_e|\alpha) \tag{7}$$

In other words, the mixing distribution is changed but exchangeability is neatly preserved:

$$\Pr(E_k|E_l) = \int \underbrace{\Pr(E_k|E_l,\alpha)}_{\text{based on indepedent } \theta_i} f(\alpha|E_l)d\alpha \tag{8}$$

where the Pr term within the integrand is based on independence; if for given α, E_k and E_l are independent as is often the case in sequential statistical inference, then this term simplifies to $\Pr(E_k|\alpha)$ and the "effect" of E_l is only felt in the updates of the mixing pdf $f_{\alpha|E_l}$.

Exchangeability can also be generalized to exchangeability within "exchangeability classes". This can be modeled using non-identically distributed conditional $\theta|\alpha$, an example of which is shown in the Bayesian net of Fig. 3. Another extension towards conditionally dependent random variables θ is shown in Fig. 4.

In the special case of event (1), it is clear from (8) that if the *n* exchangeable random variables $\theta_1, \ldots, \theta_n$ with pdf given by (5), benefit from the observation of *m* additional data $\theta^* = (\theta_{n+1}, \theta_{n+2}, \ldots, \theta_{n+m})$ then the joint pdf of the exchangeable random variables is the new mixture:

$$f(\theta_1,\theta_2,\ldots\theta_n|\theta^*) = \int \prod_{i=1}^{n} f(\theta|\alpha) f(\alpha|\theta^*)d\alpha \tag{9}$$

Exchangeable random variables θ have the following first and second moment structure:

$$E(\theta) = \int_{\theta} E(\theta|\alpha) f(\alpha) d\alpha \tag{10}$$

$$\text{covar}(\theta_i \theta_j) = \int_{\theta} \left[E(\theta|\alpha)^2 - E(\theta)^2 \right] f(\alpha) d\alpha \tag{11}$$

$$\text{var}(\theta) = \int_{\theta} \text{var}(\theta|\alpha) f(\alpha) d\alpha + \text{covar}(\theta_i \theta_j) \tag{12}$$

As in (9), these moments change if data θ* become available. For instance, if θ are exchangeable random variables having a conditional pdf $f(\theta|\alpha)$ which is normal with unknown mean α and fixed variance σ_θ^2, then, using a normal mixing pdf $f(\alpha)$ with mean α_0 and variance σ_α^2, the first two moments and the correlation coefficient ρ of the exchangeable random variable before and after the release of θ* are, using (7, 9, 10, 11, 12):

$$E(\theta) = \alpha_0 \qquad \text{var}(\theta) = \sigma_\theta^2 \left(1 + \frac{\sigma_\alpha^2}{\sigma_\theta^2}\right) \qquad \rho(\theta_i \theta_j) = \frac{1}{1 + \frac{\sigma_\theta^2}{\sigma_\alpha^2}} \tag{13}$$

$$E(\theta \mid \theta^*) = \alpha_0 \left(\frac{1}{1 + \frac{\sigma_\alpha^2}{\sigma_\theta^2}}\right) + \theta^* \left(\frac{1}{1 + \frac{\sigma_\theta^2}{\sigma_\alpha^2}}\right) \quad \text{var}(\theta \mid \theta^*) = \sigma_\theta^2 + \frac{1}{\frac{1}{\sigma_\theta^2} + \frac{1}{\sigma_\alpha^2}} \quad \rho(\theta_i \theta_j) = \frac{1}{2 + \frac{\sigma_\theta^2}{\sigma_\alpha^2}} \tag{14}$$

Note that "independence" is the limiting case of exchangeability with $\sigma_\alpha^2 \to 0$ as in Fig. 1(c) which translates into zero correlation and full lack of updating potential in (13) and (14). Also, the other extreme of total ignorance is achieved when $\sigma_\alpha^2 \to \infty$ corresponding to full correlation in (13), and strictly data-based moments in (14).

3 EXCHANGEABLE CONDITION STATES

Consider a set of related engineering "systems" each of which is, at a given point in time, characterized by a condition state (CS) denoted by the variable θ. A CS may characterize "quality" or measure "past and present performance" (e.g the tendency for a system not to suffer failures), or the speed and extent of a certain process (e.g. deterioration), or the amount of "exposure" in general. The CS θ can be either discrete (as in the case where indicators or state variables are used) or continuous (as in the case of a global degree of damage or exposure). They can be represented by one random variable or by a vector of random variables. But what they have in common is the fact that they cannot directly be "observed". Accordingly, in such models, statistical inference can be performed using data (obtained through inspection, from historical data, or on the basis of tests) associated with observable variables X that are related to each system and that are helpful in inferring what sort of CS a particular system finds itself in.

Essentially, the single variable θ in the paradigm exchangeable representation of Fig. 2 can be thought of as being replaced by the pair (θ, X) for each system. In other words we have exchangeable pairs of (θ, X) as shown in Fig. 5(a).

Alternatively, since the joint pdf of θ and X can also be expressed as the product of a marginal and a conditional pdf, the same situation can be depicted by the belief net shown in Fig. 5(b). This is the more traditional depiction of the so-called hierarchical Bayes or 2-level Bayes method with CS θ_i's that are conditionally iid with $f(\theta|\alpha)$ given the so-called hyper-parameter α, having pdf $f(\alpha)$. The random variables $X_1, \ldots, X_n$ represent an observable (physical) output of each system i. Each X_i has a conditional probability density function $f(x_i|\theta_i)$ where θ_i is the CS for each element.

In a nutshell, two stage Bayesian models are based on the following assumptions:

(1) X_i are observable random variable or vectors of observable random variables which are independent from system to system.
(2) The CS θ_i are exchangeable: given the hyper-parameter(s), the condition states $\theta_1, \ldots, \theta_n$ are n independent realizations of a random variable Θ with the conditional pdf $f(\theta|\alpha)$.
(3) The "hyper-parameter" α is a realization of a random variable A or a vector of random variables A with hyper-prior probability function $f(\alpha)$.
(4) In principle, the 2-stage model is fully characterized by a joint pdf of the form $f(x_1, \ldots, x_n, \theta_1, \ldots, \theta_n, \alpha)$.

The need for advanced models such as the two-stage Bayes model described below originated in the nuclear industry (Vaurio, 1987; Kaplan, 1983). The objective is to assimilate data from different sources in order to overcome either conflicting data, or a general paucity of data, as is typically the case for failure data in very reliable systems. Bunea et al. (2005) consider the case of n different nuclear facilities each having their own failure data sets with each facility trying to enhance its decision making by benefiting from the "lessons learned" at other facilities. Two-stage models, originally known as hierarchical Bayes models, are also used by Hofer (1999) to model initiating events in large industrial processes.

So-called empirical Bayes methods (Maritz and Lwin, 1989) which are essentially approaches based on "mixing" (and have little to do with Bayesian probability methods) have been used for similar purposes but they suffer from the lack of a valid rational framework for statistical inference. The use of fully Bayesian methods for inference in the context of spatial problems was advocated by Faber and Sorensen (2002) using discrete CS in structural inspection and maintenance planning, by Maes (2002) for continuous CS in R/C structural deterioration, and for CS associated with common cause failures in power plants.

Two-stage models can in fact also be viewed as a special case of the more general Bayesian state space models (Chatman, 1996) where stochastic observation variables X are broken down into a signal governed by state variables θ and a contaminating noise variable. Bayesian regression is a further application of such models.

Various "mixture"-based approaches in deterioration are studied in Maes (2003). A computational framework for discrete CS associated with deteriorating R/C structures is presented in Faber et al. (2006) with further applications in asset integrity management contained in Straub et al. (2006). In the area of deterioration, the above "systems" now become "zones" or "portions" of a larger structure or spatially distributed system subject to different exposure and deterioration regimes, each of which is characterized by discrete or continuous CS. The use of such methods has revealed itself to be particularly useful in life-cycle optimization, optimal inspection, maintenance planning and decision making in general. Applications to risk-based inspection for concrete structures and for pipelines can be found in Malioka and Faber (2003) and Maes et al. (2006), respectively.

Applications to decision making involving various individuals or organizations acting on the basis of different preferences and perceptions are given in Maes and Faber (2006). Here the "systems" are the different decision makers and the CS characterize their tastes and value systems.

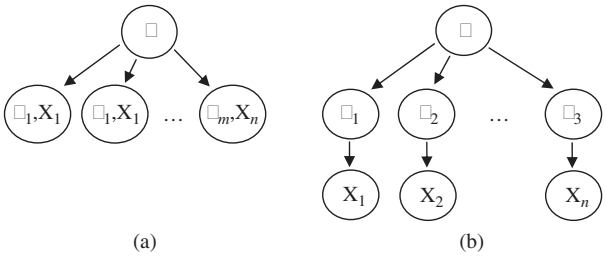

Figure 5. Exchangeable condition states θ_i with observable outputs X_i.

4 UPDATING OF CONDITION STATES

When performing statistical inference in this model, we need to distinguish between updating one of the n systems, Fig. 6(a), or updating an "arbitrary" system as shown in Fig. 6(b). In the first case, suppose the system of interest is the system with index 0 which is an arbitrary system belonging to the n possible systems. This system possesses observed response variables X_0 and a condition state θ_0. All other n-1 realizations of the observable parameters $X_1, \ldots, X_n$ for the remaining n-1 systems are now combined in X^*. The vector θ^* similarly contains the remaining CS $\theta_1, \ldots, \theta_n$ without the one specific θ_0. This amounts to the following partition, shown in the belief net of Fig. 6(a):

$$\begin{cases} \{X\} = \{X^*\} \bigcup \{X_0\} & \text{where } \{X^*\} = \{X_i\}_{\substack{i=1,\ldots,n \\ i \neq 0}} \\ \{\theta\} = \{\theta^*\} \bigcup \{\theta_0\} & \text{where } \{\theta^*\} = \{\theta_i\}_{\substack{i=1,\ldots,n \\ i \neq 0}} \end{cases} \tag{15}$$

When observed values $x = \{x_0, \ldots, x_n\}$ become available, the entire model is updated. The hyper-parameter α is updated first and then each of the CS θ_i. Using Bayes' theorem the hyper-posterior pdf $f(\alpha|x)$ can be found as:

$$f(\alpha|x) \propto L(\alpha|x) f(\alpha) \tag{16}$$

where $L(\alpha|x)$ is the likelihood function, $f(\alpha)$ is the hyper-prior pdf of α, and where normalization must be performed with respect to α. Since all X_i are conditionally independent, the likelihood function $L(\alpha|x)$ in (16) is the product of the conditional pdfs $f(x_i|\alpha)$, which may be found from the conditional pdfs $f(x_i|\theta_i)$ and $f(\theta_i|\alpha)$:

$$L(\alpha|x) = \prod_{i=0}^{n} f(x_i|\alpha) = \prod_{i=0}^{n} \int_{\theta_i} f(x_i|\theta_i) f(\theta_i|\alpha) \mathrm{d}\theta_i \tag{17}$$

Accordingly, the expression of the posterior hyper-pdf $f(\alpha|x)$ is:

$$f(\alpha|x) \propto \prod_{i=0}^{n} \int_{\theta_i} f(x_i|\theta_i) f(\theta_i|\alpha) \mathrm{d}\theta_i f(\alpha) \tag{18}$$

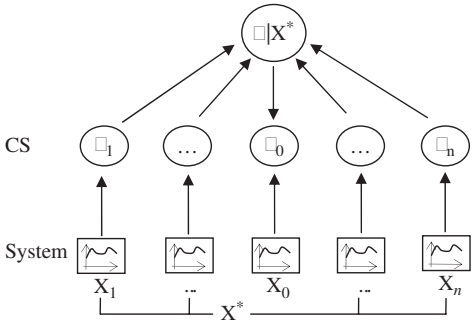

Figure 6a. Two-stage Bayesian model showing the updating process of a specific condition state θ_0.

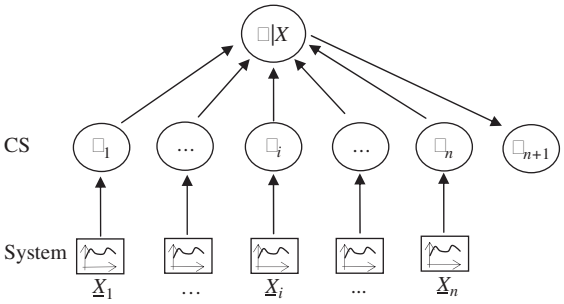

Figure 6b. Two-stage Bayesian model showing the updating process of an arbitrary (unspecified or new) system with unknown condition state θ_{i+1}.

Turning now to the updating of a specific CS, we can consider the "prior" pdf $f(\theta_0)$ of the CS of interest (before data x become available) to be given by:

$$f(\theta_0) = \int_{\alpha} f(\theta_0|\alpha) f(\alpha)\,\mathrm{d}\alpha \tag{19}$$

where $f(\theta_0|\alpha)$ is the conditional prior pdf of θ_0 and $f(\alpha)$ is the hyper-prior pdf of α. This "prior" is now updated to a "posterior" pdf $f(\theta_0|x)$ for every specific CS θ_0. As shown in the belief net of Fig. 6(a) the realization x_0 directly governs the condition "state" θ_0 without any influence on the hyper-parameter α. All other observed x_i's assembled in x^* influence the CS θ_0 indirectly through the updated hyper-parameter α. But, x_0 and x^* are independent and consequently the posterior pdf $f(\theta_0|x)$ is equal to $f(\theta_0|x^*, x_0)$. Applying Bayes' theorem we obtain for the posterior pdf $f(\theta_0|x)$:

$$f(\theta_0|x) \propto f(x_0|\theta_0, x^*) f(\theta_0|x^*) \tag{20}$$

Due to the independence of x_0 and x^* the conditional pdf $f(x_0|\theta_0, x^*)$ becomes $f(x_0|\theta_0)$.

$$f(\theta_0|x) \propto f(x_0|\theta_0) f(\theta_0|x^*) \tag{21}$$

The posterior pdf $f(\theta_0|x^*)$ for given x^* can be obtained from (19) by replacing $f(\alpha)$ by $f(\alpha|x^*)$.

$$f(\theta_0|x^*) = \int_{\alpha} f(\theta_0|\alpha) f(\alpha|x^*)\,\mathrm{d}\alpha \tag{22}$$

The final expression for posterior pdf of CS θ_0 is:

$$f(\theta_0|x) \propto f(x_0|\theta_0) \int_{\alpha} f(\theta_0|\alpha) f(\alpha|x^*)\,\mathrm{d}\alpha \tag{23}$$

where $f(x_0|\theta_0)$ is the conditional prior pdf of x_0. Note that equation (23) is written in a proportional way and $f(\theta_0|x)$ has to be normalized with respect to θ_0. It can be seen that the posterior pdf (23) for CS θ_0 is now a Bayesian average between (direct) system-specific observations x_0 and (indirect) non-system specific data x^*.

The previous method can be generalized to find the joint posterior pdf of two or more specific condition states. For instance, for two systems 0 and 0', the joint pdf is:

$$f(\theta_0, \theta_{0'}|x) \div f(x_0|\theta_0) f(x_{0'}|\theta_{0'}) \int_{\alpha} f(\theta_0|\alpha) f(\theta_{0'}|\alpha) f(\alpha|x^{**})\,dx \tag{24}$$

where $f(\alpha|x^{**})$ is updated according to (18) but with the data x_0 and x_0, removed. Similarly, the joint pdf of all n systems is:

$$f(\theta_0,...,\theta_n \mid x) \div \prod_{i=1}^{n} f(x_i \mid \theta_i) f(\theta_0,...,\theta_n) \tag{25}$$

here the joint pdf of θ in the last factor is given by (5). Note that this expression is not the same as the more familiar expression (27) below for arbitrary systems.

The case where a "new" system with unknown CS is being considered (either a system not previously included in the n existing systems, or an "arbitrary" unspecified system) can be represented by the belief net of Fig. 6(b) where we can now introduce an additional "descendant" $\theta = \theta_{n+1}$ with the result that its CS has the following "updated" pdf:

$$f(\theta \mid x) \propto \int_{\alpha} f(\theta \mid \alpha) f(\alpha \mid x) d\alpha \tag{26}$$

Similarly, the joint pdf of m arbitrary or new exchangeable condition states is given by

$$f(\theta_1,...,\theta_m \mid x) \div \int \prod_{i=1}^{m} f(\theta_i \mid \alpha) f(\alpha \mid x) dx \tag{27}$$

which must be compared with (25) as mentioned above.

The framework can also be extended to conditionally dependent condition states (Fig. 4) and the dis/advantages of such an approach are examined in Maes and Dann (2006).

5 RELIABILITY UPDATING USING EXCHANGEABLE CS

In this section, we refer to the n subsystems or zones as "components" of a larger system the state of which can be defined in terms of the states of the components. For instance, a 10 km long stretch of pipeline can be divided into n zones each often representing a separate pipeline joint. Limit states can be local (e.g. related to a cross-section of the pipeline) or global (e.g. related to the entire pipeline system). First consider a decision involving a specific (critical) component characterized by the CS θ_0 (e.g. a limit state at a specific pipeline cross-section). Defining the component failure probability $P_{F|\theta}$ conditional on a component having a CS θ, then the failure probability for the specific component 0 (or, cross-section) of interest given a set of component data $x = (x_0, x_1, \ldots, x_n)$ is equal to:

$$P_{F,0|x} = \int_{\theta} P_{F|\theta_0}(\theta_0) f(\theta_0 \mid x) d\theta_0 \tag{28}$$

where the required pdf is given by the component-specific expression (23).

This result is different from the following result (29) which applies to a decision involving an arbitrary component θ (or, any cross-section) following the acquisition of data $x = (x_0, x_1, \ldots, x_n)$:

$$P_{F|x} = \int_{\theta} P_{F|\theta}(\theta) f(\theta \mid x) d\theta \tag{29}$$

where the pdf in the integrand is given by (26) instead of (23).

For any system-wide decision (e.g. involving system limit states) such as a series system or a k-out-of-n system, the failure probability should be weighed over the posterior joint pdf of the

n component (sectional) condition states. As an example in a series system s such as a pipeline, we have:

$$P_{F,s|x} = \int_{\theta_1} \cdots \int_{\theta_n} \max_{i=1}^{n} P_{F|\theta_i} f(\theta_1, \ldots, \theta_n \mid x) d\theta_1, \ldots, d\theta_n \tag{30}$$

where the joint pdf in the integrand is given by (25). It should be noted that this expectation, typical for exchangeable CS θ_i, is quite different from the more traditional but incorrect updating scheme:

$$P_{F,s|x} \overset{?}{=} \max_{i=1}^{n} P_{F,i|x} \tag{31}$$

where $P_{F,i|x}$ is based on either (28) or (29).

6 EXAMPLE: RELIABILITY-BASED PIPELINE INSPECTION

Consider part of an offshore gas pipeline as shown in Fig. 7. Condensation of CO_2 in the gas causes interior corrosion in certain locations of the flow line such as in bends or low points. In the course of time, corrosion wears out the pipe wall thickness. We assume that an inspection with a pig is performed after the first five years and after the first ten years of operation. The pipe, which has a total length of 500 m, is subdivided into 10 equidistant segments (Fig. 7) each having its own "condition state" in order to allow for spatial variability. These CS are treated as exchangeable, and each CS is supported by corrosion depth data as described below.

Without the benefit of inspection data, the evolution of corrosion as a function of time can be estimated using (deWaard and Mailliams, 1975):

$$d(\tau, s) = 44.8 C_d \gamma p(s)^{0.67} \left[1 - \left(1 - \frac{\tau}{80}\right)^{1.67}\right] 10^{\left(1.78 - \frac{1710}{T(s)}\right)} \exp(0.67\theta) \tag{32}$$

where d is the estimated maximum corrosion depth at time τ at a cross-section with longitudinal co-ordinate s (Fig. 7), γ is the influence of the inhibitor added to the gas, p is the design operating pressure at a cross-section in MPa, T is the temperature in K, and θ is the condition state (CS) which can be interpreted as the tendency to corrode, or the "corrosivity" of the pipe. C_d is a model error which involves the uncertainty in predicting and measuring the corrosion depth d. C_d is log-normally distributed having a mean value 1.0 and a cov = 25%.

In (32) it is assumed that the internal design operating pressure $p(\tau, s)$ is a function of time τ and the longitudinal co-ordinate s is as shown in Fig. 8. A pressure difference between both ends of the pipeline is maintained at 5%. In (32) the factor for the temporal variability of p due to reservoir deflation is already included in the factor between square brackets and therefore the internal pressure is only a function of the co-ordinate s in (32). The temperature T is constant in time but is also a function of s as shown in Fig. 8.

Assuming that the pipeline stress-strain behavior can be described by the Ludwik Law (Stewart et al, 1994), and based on an incremental large strain plasticity analysis, the full burst pressure for the pipe without defects is given by (Maes et al, 2006):

$$p_b = 0.935\, C_2 \left(\frac{2}{\delta - 1}\right) \left[\frac{2}{3^{(1+h)/2}} \left(\frac{h}{e\varepsilon_Y}\right)^h \sigma_Y + \frac{2C_1}{\sqrt{3} \cdot e^h}\right] \tag{33}$$

where p_b is the full burst pressure, h is the strain hardening index, δ is the slenderness ratio D/t (D is the original outer diameter of the pipe and t is the original wall thickness) is the pipe slenderness ratio and σ_Y is the yield strength, $\varepsilon_Y = 0.5\%$ is the yield strain and e is the base of the natural

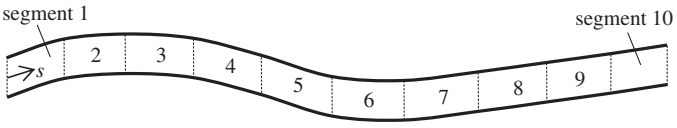

Figure 7. Offshore gas pipeline divided into 10 segments.

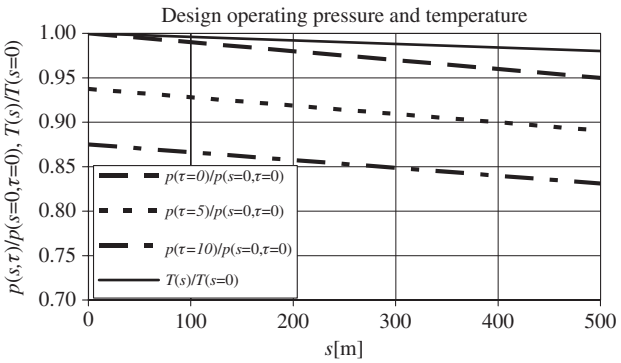

Figure 8. Design operating pressure p and temperature T as a function of the longitudinal coordinate s.

logarithm. The model scatter error C_1 is an additive error which represents the fact that stress data for given strain levels in the Ludwik stress-strain results are inherently scattered. The model uncertainty C_2 represents the overall burst model uncertainty.

The effect of corrosion in the pipe is modeled by a longitudinal groove in the wall of the pipeline with a depth $d(\tau, s)$ that increases over the years. When the groove would be infinitely long with a with uniform depth d and width w, such that;

$$\chi = \frac{d}{t} \tag{34}$$

and

$$\varphi = \frac{w}{\pi(D-t)} \tag{35}$$

where χ is the defect/wall thickness ratio, t is the original wall thickness and φ is the fraction of circumference which is corroded, then an analysis can be performed for one of two cases:

1. In the case of a shallow groove ($\chi < \chi^*$), the entire cross-section is able to mobilize its strain hardening capacity so that the resulting burst pressure p_∞ of the grooved section is based on plastic strains developing in the entire hoop direction. This is shown by part I of the broken line in Fig. 9 which represents the relative decrease in burst pressure as a function of groove depth. Part II in this Figure represents the fact that the burst pressure cannot be less than the burst pressure corresponding to a cylinder having a uniform thickness equal to $(t - d)$. For modeling purposes, Parts I and II are made continuous instead of bilinear.
2. In the case of deeper grooves ($\chi > \chi^*$), plasticity only occurs locally in or near the groove while the remainder of the cross-section remains elastic. Clearly, this "bulging" condition causes a steeper decline of burst pressure with defect depth as shown in Part III in Fig. 9.

In Maes et al. (2006) the equation for this critical transition defect depth ratio χ^* is given by:

$$\chi^* = \left[1 - \left[\frac{\sqrt{3}\mathrm{e}\varepsilon_Y(1+\varphi)}{2h}\exp\left(-\frac{\varphi}{1+\varphi}\right)\right]^h\right] \tag{36}$$

where h is the strain hardening index, φ is the fraction (35) of circumference which is corroded and $\varepsilon_Y = 0.5\%$ is the yield strain. Clearly, this transition value is dependent on steel grade.

For the two mentioned cases, the burst pressure p_∞ for an infinitely long groove (Maes et al, 2006) can be written as:

$$p_\infty = \begin{cases} \left[1 - \dfrac{1 - f(1-\chi^*)}{\chi^*}\chi\right] p_b & \text{for } \chi \le \chi^* \\ f(1-\chi)\, p_b & \text{for } \chi > \chi^* \end{cases} \tag{37}$$

where χ^* is the critical defect depth ratio given by (36), t the original wall thickness of the pipe and p_b is the full burst pressure without defects (33). The circumferential corrosion factor f is a function of the strain hardening index h and the fraction of the circumference φ (35) which is corroded:

$$f = \left(\frac{2}{1+\varphi}\right)^h \tag{38}$$

When the longitudinal groove of depth d has finite length L and width w, then the true burst pressure p_L will taken on a value that is greater than the burst pressure p_∞ for a pipe with infinitely long groove and less than the defect free burst pressure p_b:

$$p_\infty < p_L < p_b \tag{39}$$

The ultimate burst pressure p_L is linearly interpolated between the two above bounds using a defect-geometry factor g which varies between 0 and 100% (Cronin and Pick, 2002):

$$p_L = p_\infty (1-g) + p_b g \tag{40}$$

where p_L is the burst pressure for a pipe with groove length L and depth d, p_b (33)is the full burst pressure for defect free pipelines and p_∞ (37) is the burst pressure for a infinitely long groove with groove depth d.

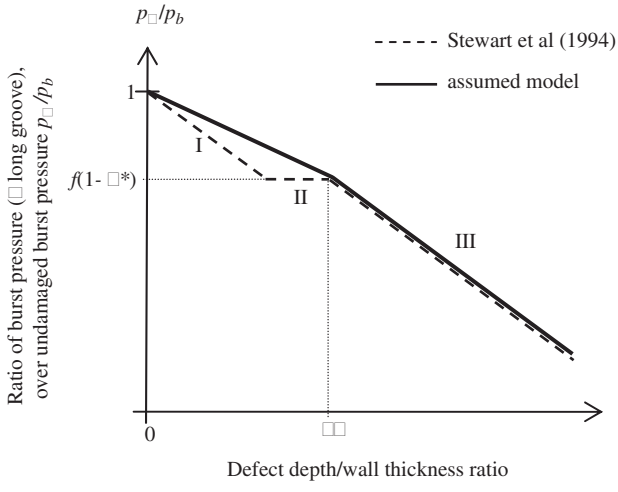

Figure 9. Assumed burst capacity for infinitely long groove.

The expression for g in (40) is purely geometric and independent of the fraction of circumference φ which is corroded. Maes et al. (2006) shows that the defect-geometry factor g in (40) for a finite parabolic groove of depth ratio χ [27], length L, and circumferential width φ, is equal to:

$$g = \frac{8\delta(1-\chi)}{\lambda^2} - 4\left[\frac{\sqrt{\delta(1-\chi)}}{\lambda} + \frac{2\delta(1-\chi)}{\lambda^2}\right]\exp\left(-\frac{\lambda}{2\sqrt{\delta(1-\chi)}}\right) \tag{41}$$

where δ is the pipe slenderness D/t, λ is the groove length ratio L/t and χ is the defect/wall thickness ratio (34).

For each of the 10 pipeline segments i with CS θ_i, the corrosion defect depth ratio $\chi_{i,obs}$ (34) is observed at time $\tau = \tau_{insp,1} = 5$ years and again at $\tau = \tau_{insp,2} = 10$ years. The CS θ in (25) can now be updated twice based on these two inspection outcomes.

We select a two-stage Bayesian model with exchangeable condition states (Fig. 5(b)). Each condition state θ_i is based on hyper-parameters α with a prior pdf $f(\alpha)$. We use 6 discretely distributed hyper-parameter which are given in Table 1 together with the prior probabilities.

Tables 2, 3 and 4 show the required input parameters, the random variables and the observed corrosion depth ratios χ_{obs} at inspection time $\tau = \tau_{insp,1} = 5$ years and $\tau = \tau_{insp,2} = 10$ years for this example. The conditional prior $f(\theta|\alpha)$ is a normal pdf with a mean of α and a standard deviation of 1.75 (Table 6).

Table 1. Hyper-parameters α with prior probabilities (pipeline example) and posterior probabilities after the first and second round of inspections.

Hyper-parameter α	5.0	5.5	6.0	6.5	7.0	7.5
Prior probability	0.167	0.167	0.167	0.167	0.167	0.167
1. Posterior probability	0.044	0.181	0.342	0.295	0.117	0.021
2. Posterior probability	0.000	0.008	0.133	0.465	0.341	0.052

Table 2. Parameters used in the pipeline example.

Parameters		Value
Pipe slenderness ratio	δ	30
Wall thickness	t	22 mm
Operating temperature	$T(s=0)$	303 K
Influence factor of the inhibitor	γ	0.5
Corrosion groove width factor	φ	0.17
Total length of the pipe	l	500 m

Table 3. Random variables used in the pipeline example.

Random variables		Pdf type	Mean	st. dev.	Cov
Strain hardening index	h	normal	0.106	0.0106	10%
Yield strength	σ_Y	lognormal	450 MPa	29.7 MPa	6.6%
Max. annual pressure ratio	$p/p_{oper}(\tau, s)$	Gumbel	1.07	0.0214	2%
Corrosivity	θ	normal	α	1.75	–
Groove length	L	normal	$20t$	$2t$	10%
Model error burst pressure	C_1	normal	0	6.9	–
Model error burst pressure	C_2	normal	1.0	0.05	5%
Model error corrosion rate	C_d	lognormal	1.0	0.25	25%

Table 4. Observed corrosion depth ratio χ_{obs} at $\tau = 5$ years and $\tau = 10$ years.

Segment	1	2	3	4	5	6	7	8	9	10
χ_{obs} at $\tau = 5$	0	0.10	0.10	0	0	0.20	0.05	0	0	0
χ_{obs} at $\tau = 10$	0.10	0.10	0.20	0	0.10	0.25	0	0	0.05	0.025

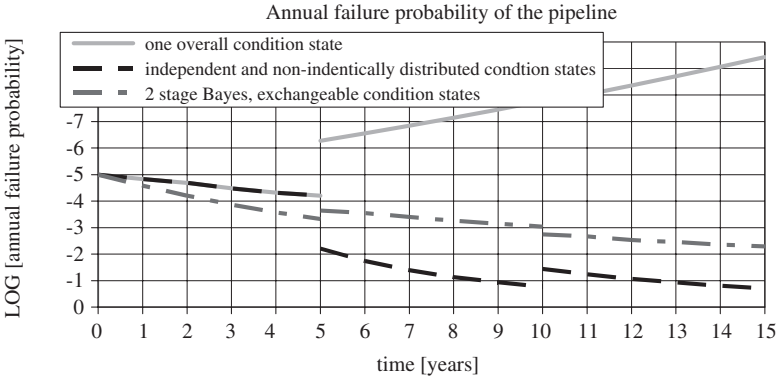

Figure 10. Annual failure probability as a function of time for two-stage Bayesian models.

The posterior probabilities for the hyper-parameter α after the first and second inspection are determined using (18) and shown in Table 1.

The annual failure probability $P_{F,pipeline}$ of the entire pipeline increases in time from its original a annual failure probability of 10^{-5} at time $\tau = 0$. The sectional limit states used in the reliability analysis are all of type:

$$g(\boldsymbol{z},\tau) = p_L(\boldsymbol{z},\tau) - p(\boldsymbol{z},\tau) \tag{42}$$

where τ is time, $\boldsymbol{z}$ is the vector of random variables (based on Table 3), $p_L(\boldsymbol{z})$ is the ultimate burst resistance given by the selected burst expression (one of the above burst capacities) and where $p(\boldsymbol{z})$ is the actual extreme pressure differential to which the pipeline is subjected during one year. The latter variable is Gumbel distributed with a mean based on the current operating pressure, as shown in Table 3. The conditional annual failure probability $P_{F,i|\theta}(\tau)$ at time τ given the CS θ_i in segment i, is then given by:

$$P_{F,i|\theta}(\tau) = \Pr(\, g_i(\boldsymbol{z},\tau|\,\theta_i) < 0) = \Pr(\, p_{L,i}(\boldsymbol{z},\tau) - p_i(\boldsymbol{z},\tau|\,\theta_i)) < 0) \tag{43}$$

which allows the system failure probability to be evaluated using (30) and the posterior joint density (25).

Fig. 10 shows the outcome of the reliability analysis. Also shown are the outputs of two limiting cases: one which assumes independent sections having the same condition state, and independent but non-identically distributed sections. It should be emphasized that all of these failure probabilities are conditional on the outcomes of the 5-year and 10-year inspections.

Based on the two-level exchangeable Bayes model, the probability that N of the 10 segments exceed a critical CS $\theta_{crit} = 8.0$ given the inspections at $\tau = \tau_{insp,1} = 5$ years and $\tau = \tau_{insp,2} = 10$ years is shown in Fig. 11. The expected mean value of the number of segments N which exceed the critical corrosivity is 1.8 after 5 years and 2.3 after 10 years.

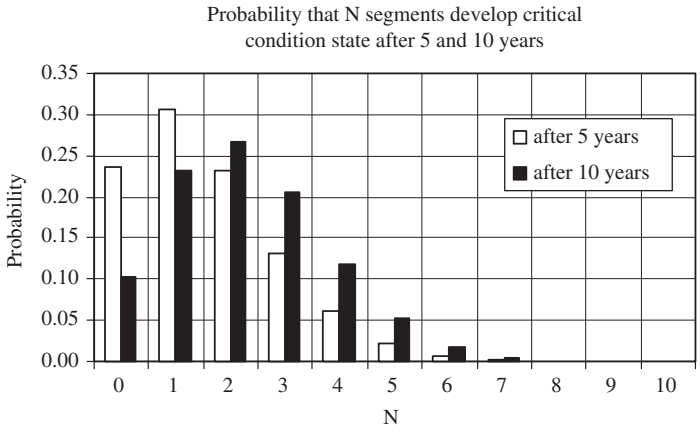

Figure 11. Probability that N segments exceed the critical corrosivity of $\theta_{crit} = 8.0$ after updating at 5 and 10 years.

7 CONCLUSIONS

Within large and complex structural systems as well as among different systems, statistical inference for decision making purposes often requires the assimilation of observed data from different sources, sub-systems or zones. After reviewing the basic concept of exchangeability, the present paper investigates the role of two-stage Bayesian models. It is shown that two-stage Bayesian models provide a rational basis for mixing system-specific or zone-specific data with data originating from similar systems or zones that behave or operate with different condition states.

Reliability updating for both local (sectional) and global limit states must be done very carefully in order to obtain a proper weighting of a fully local and a fully global inferential approach. A pipeline deterioration and inspection example shows that two-stage Bayesian modeling based on exchangeable condition states is an effective tool in modeling spatially distributed problems.

ACKNOWLEDGEMENTS

The first author is grateful for funding from the NSERC discovery grant program (Canada) and from ConocoPhillips. Assistance and input from Markus Dann, Mamdouh Salama, and Denijs Marcelis are greatly appreciated.

REFERENCES

Bunea, C., Charitos, T., Cooke, R.M. and Becker, G. 2005. Two-stage Bayesian models-application to ZEDB project, *Reliability Engineering and System Safety*, 90: pp. 123–130

Chatfield, C. 1996. *The analysis of time series: an introduction*, Chapman and Hall, London

Cronin, D.S., and Pick, R.J. 2002. Prediction of Failure Pressure for Complex Corrosion Defects, *Pressure Vessels and Piping*, pp. 279–287

de Finetti, B. 1937. La prevision, ses lois logiques, ses sources subjectives, *Annales de l'Institut Henri Poincare*, 7: pp. 1–68

de Finetti, B. 1974. *Theory of Probability*, Vols. 1 and 2, Wiley

deWaard, C. and Milliams, D.E. 1975. Carbonic Acid Corrosion of Steel, *Corrosion*, 31(5): pp.177

Faber, M.H. and Sorensen, J.D. 2002. Indicators for inspection and maintenance planning of concrete structures, *Structural Safety*, 24: pp. 337–396

Faber, M.H., Straub, D. and Maes, M.A. 2006. A computational Framework for Risk Assessment of RC Structures Using Indicators, *Computer-Aided and Infrastructure Engineering*, 21(3): pp. 216–230

Hofer, E. 1999. On two-stage Bayesian modeling of initiating event frequencies and failure rates, *Reliability Engineering and System Safety*, 67: pp. 97–99

Jensen, F.V. 2001. *Bayesian Networks and Decision Graphs*, Springer-Verlag

Jordaan, I.J. 2005. *Decision under Uncertainty*, Cambridge University Press

Kaplan, S. 1983. On a "Two-Stage" Bayesian Procedure for Determining Failure Rates from Experimental Data, *IEEE Transactions on Power Apparatus and Systems*, 102(1): pp. 195–202

Maes, M.A. 2002. Updating Performance and Reliability of Concrete Structures Using Discrete Empirical Bayes Methods, *International Journal of Offshore Mechanics and Arctic Engineering*, Transactions of the American Society of Mechanical Engineers, Vol. 124 pp. 239–246

Maes, M.A. 2003. Modelling infrastructure deterioration risks using Bayesian mixtures, *International Journal of Modelling and Simulation*, 23(1): pp. 43–51

Maes, M.A. and Dann, M. 2006. Two-stage Bayesian processes for spatially varying condition states, *Proceedings of the International Forum on Engineering Decision Making*, IFED2006, http://www.ifed.ethz.ch/events/secondforum_paper.html, ISBN 3-909386-62-8, Lake Louise, Canada, April

Maes, M.A. and Faber, M.H. 2006. Bayesian Framework for Managing Preferences in Decision Making, *Reliability Engineering and System Safety*, 91(5): pp. 556–569

Maes, M. A., Salama M.M. and Dann, M. 2006. Reliability of Burst Limit States for Damaged and Corroded High Strength Pipelines, *Proceedings of the 25th Offshore Mechanics and Arctic Engineering Conference*, OMAE2006, Hamburg, Germany, June

Malioka, V. and Faber, M.H. 2003. Condition Indicators Inspection and Maintenance Planning, *Proceedings of the 9th International Conference on Applications of Statistics and Probability in Civil Engineering*, ICASP9, San Francisco, USA

Maritz, J.S. and Lwin, T. 1989. *Empirical Bayes methods*, Chapman & Hall, London

Straub, D., Malioka, V. and Faber, M.H. 2006. A framework for the asset integrity management of large deteriorating concrete structures, *Structure and Infrastructure Engineering*, to be published

Vaurio, J.K. 1987. On analytical empirical Bayes estimation of failure rates, *Risk Analysis*, 17(3): pp. 329–338

Technical contributions

Reliability and Optimization of Structural Systems: Assessment, Design and Life-Cycle Performance – Frangopol, Kawatani & Kim (eds)
© 2007 Taylor & Francis Group, London, ISBN 978-0-415-40655-0

Practical assessments of risk and its uncertainty

A.H-S. Ang
University of California, Irvine, USA

ABSTRACT: The practical aspect of quantitative risk assessment (QRA) is highlighted for natural hazard mitigation. Besides the estimation of the expected risk measure, the distribution of the risk associated with the epistemic type of uncertainty is equally important; the latter permits the decision maker the selection of a risk-averse measure in order to minimize the error (or increase the confidence) in the decision. The process is illustrated with a hypothetical example of the risk assessment for New Orleans assuming that an assessment is performed in 1985; i.e., 20 years prior to the occurrence of Katrina in 2005. The process can also be applied to evaluate the reduction in the respective risks (for fatality, injury, and economic loss) accruable from an investment for mitigating future hazards. The practical implementation of QRA is emphasized.

1 INTRODUCTION

In formulating decisions for the design of infrastructures against the forces of natural hazards, the calculated risk in terms of potential damage and other adverse consequences is important. However, the uncertainty (of epistemic type) in the calculated risk is equally significant and relevant. In the case of natural hazards, it is the engineers' responsibility to provide the proper technical information to the decision-makers and stakeholders in the construction of protective infrastructure systems for mitigating a hazard. For this latter purpose, quantitative risk assessment (QRA) methodology provides the tools needed. The fundamental components of QRA are summarized below with an example illustrating the numerical process of assessing risk for natural hazard mitigation, and of estimating related risk reduction.

In the case of natural hazards, risk is most meaningful when expressed in terms of potential human sufferings and/or economic losses. Besides the probability of occurrence of a hazard, risk must include the potential adverse consequences that can result from the hazard event. The risk associated with natural hazards are very real, such as from strong earthquakes and associated tsunamis, high hurricanes (or typhoons), tornadoes, floods, and massive landslides. The forces created or induced by such natural hazards are usually extremely high and can cause severe damages and failures of engineered systems. Engineers, however, must still plan and design structures and infrastructures in spite of the extreme forces produced by one or more of these natural hazards. How safe should these infrastructures or facilities be for resisting the forces of natural hazards, of course, depends on the capital investments that the stakeholders, such as a government entity responsible for funding, is willing to invest (for safety and reliability) to prepare and protect against or reduce any impending risk to future hazards. In order to make the proper decisions on needed or optimal investments, information on risk and associated risk reduction accruable from additional investment, are clearly pertinent.

2 QUANTITATIVE RISK ASSESSMENT METHODOLOGY

Information on risk is often presented in qualitative terms; for example, as *high*, *medium*, or *low*. More often than not, information in this form is ambiguous and difficult to interpret; moreover, it

is not possible to perform risk-benefit trade off analysis. For this latter purpose, risk needs to be in quantitative terms, such as potential number of fatalities and injuries, and/or potential economic losses. Similarly, quantitative risk information is needed to assess the benefit of investment in risk reduction, from which the benefit associated with a reduction in risk can be made transparent and meaningful.

2.1 *Uncertainty in estimated risk*

In assessing risk, especially relative to natural hazards, significant uncertainties can be expected. The occurrence of a given hazard within a given time window, such as a strong-motion earthquake in a particular region of the world, is unpredictable; moreover, the damaging effects of the earthquake are highly variable and difficult to estimate with precision. Also, the human casualties and sufferings, as well as the financial and economic losses that are possible consequences following the earthquake are also highly variable and often difficult to estimate. It is, therefore, easy to recognize that there is considerable uncertainty in the quantitative assessment of risk associated with natural hazards. Such uncertainties, however, are important and must be taken into account in any quantitative assessment of risk.

Uncertainties may be classified into two broad types (see e.g., Ang and Tang, 2006) – namely, the *aleatory* and the *epistemic types.* The aleatory type is associated with the natural randomness or inherent variability of a phenomenon, whereas the epistemic type is based on our insufficient knowledge for predicting the phenomenon and in estimating the associated effects and consequences. In this regard, the aleatory uncertainty would give rise to a calculated risk, whereas the epistemic uncertainty would define the range or distribution of possible risk measures (representing the uncertainty in the calculated risk). Both the calculated risk and its uncertainty are equally important. It is, therefore, important to clearly differentiate the two types of uncertainty. Irrespective of the type of uncertainty, the basic tools for its modeling and the analysis of the respective effects require the same principles of probability and statistics.

2.2 *Probability models in QRA*

Probability models, therefore, are the basic tools for quantitative risk assessment (QRA). However, risk is more than just probability; it must include the potential consequences from the occurrence of an event. In the case of natural hazards, the occurrence of a particular hazard in time and location is invariably unpredictable, and its destructive effects on structures and infrastructures are highly variable; finally, the resulting consequences of the destructive effects generally contain significant uncertainty. Therefore, for quantitative considerations, each of these aspects may be evaluated using probability models as outlined below.

QRA will generally consist of three components which may be defined, respectively, as follows:

(1) *hazard analysis;* i.e., the determination of the probability of occurrence of a given hazard within a given time window;
(2) *vulnerability analysis*; i.e., the estimation of the extent and severity of damage to made-made and protective systems, and
(3) *consequence analysis*; i.e., the estimation of the potential consequences caused by the occurrence of the hazard.

The product of the above three components constitutes the estimated risk, *R*; that is

$$R = H_z \times V_u \times C_q \tag{1}$$

where: H_z = the result of a probabilistic hazard analysis;
V_u = the result of a vulnerability analysis; may be in terms of the probability or fraction of damage to a city or a region;
C_q = the estimated potential consequence resulting from the occurrence of the hazard.

As there are epistemic uncertainties in estimating or calculating each of the components in Eq. 1, the calculated risk will also contain uncertainty leading to a range (or distribution) of the possible risk measures. If the aleatory and epistemic uncertainties are combined, the resulting calculated risk will be the mean (or "best estimate") value of *R*.

2.3 *Analysis of hazard*

The determination of the occurrence probability of a natural hazard will obviously depend on the particular hazard. For example, probabilistic models for seismic hazard analysis are well established (e.g., Cornell, 1968; Der Kiureghian and Ang, 1977); such models and associated recent refinements (e.g., Harmsen, 2005) are now widely employed in practice. Similarly, models for the hazard analysis of tornado strikes have been developed by Wen and Chu (1973); whereas, for wind storms and hurricanes, and riverine floods, the respective occurrence probabilities at a given location over a specified period may be estimated from appropriate local or regional statistical data, modeled by extreme-value distributions (e.g., Gumbel, 1954) if appropriate.

2.4 *Vulnerability analysis*

Given the occurrence of a particular hazard, there is some chance that structures or infrastructures within the affected zone will be severely damaged or collapsed. This probability, of course, will depend on the distribution of the maximum force from the hazard relative to the capacity of the structures for resisting such forces. As the maximum forces and the structural capacities will both contain variability and uncertainty, each may be represented with a probability model. That is, the maximum forces and structural capacities can be represented with respective random variables and associated probability distributions.

2.5 *Analysis of consequences*

The adverse consequences caused by the destructive forces of a natural hazard can be very severe, particularly for extreme events such as large magnitude earthquakes, high category hurricanes (or typhoons), or massive landslides and mudflows. These would often involve large numbers of fatalities and injuries, high economic and financial losses, major disruptions of utilities and transportation facilities, and related indirect consequences caused by ripple effects. The estimation of the consequences associated with the occurrence of a given hazard is often difficult and may have to be largely judgmental; i.e., relying on judgments from experts with knowledge gained through experience from similar events. Even then, the estimated consequences would contain significant uncertainties (of epistemic type), which may be expressed only as respective ranges of possible losses.

3 A NUMERICAL ILLUSTRATION

An (hypothetical) example is described numerically below to illustrate the conceptual process of QRA as outlined above. In order to clarify the steps in the QRA process, the problem is necessarily idealized, although the assumptions are reasonably realistic. For this purpose, suppose that an analysis of the hurricane risk for New Orleans (for a period of 20 years) was performed 15 years (say in 1990) before the occurrence of Katrina, a Category 4 hurricane, in August 2005. In this illustrative example, the numerical values used are hypothetical and may not be accurate (as they are pre-Katrina). Nevertheless, they serve to illustrate the quantitative process of assessing the underlying risks and associated uncertainties[1] for the purpose of providing the essential quantitative information for making risk-informed decisions for mitigating a future hazard.

[1] All the calculations in the example were performed through Monte Carlo simulations using MATLAB software with the accompanying Statistics Toolbox.

Assume that upon careful examination of the recorded data on hurricanes in the gulf coast region, the return period of a Category 4 hurricane striking the vicinity of New Orleans is determined to be around 100 years; this means that there is a 1% probability each year, and approximately a 20% probability over a 20-year period, that a Category 4 hurricane can be expected to hit the city of New Orleans and its vicinity. A 20% probability of occurrence over a period of 20 years (which is not particularly long) is a significant probability.

A Category 4 hurricane, with a maximum sustained wind speed of 125–145 mph is bound to cause massive damages to ordinary dwellings and severe damages to some of the engineered infrastructures. Also, as the elevation of the city of New Orleans is 6 to 7 ft. below sea level, the city is protected by the levees and flood walls that kept the water of the surrounding lakes (such as Ponchartrain) and the Mississippi River from inundating the city. It has been widely reported that the levees were designed and constructed with an average height of around 8 ft for protection against hurricanes of Category 2 or 3. Suppose that the actual levee heights has a symmetric triangular distribution between 7 and 9 ft and that the surges from the lake caused by a Category 4 hurricane can be modeled with a lognormal random variable with an estimated median height of 10 ft and a c.o.v. of 30%. Therefore, under a Category 4 hurricane there is a high probability that the levees will be breached causing massive inundation of the city; with these assumptions, this probability can be calculated to be as follows: P(levee breached) = 0.78

Furthermore, the vulnerability of much of the houses in New Orleans and vicinity against the hurricane winds would also be very high. Assume that the distribution of sustained wind speed in a Category 4 hurricane is modeled with a Type I extreme-value distribution with a mean speed of 130 mph and a c.o.v. of 40%, and that the wind speed resistance of houses and other structures is a lognormal random variable with a median of 85 mph and a c.o.v. of 30%. On these bases, the vulnerability of the building stock and other structures in the city to the hurricane winds would be as follows: Vulnerability of structures = 0.785

The consequences of the destructive effects of a Category 4 hurricane to the city of New Orleans, therefore, must include those caused directly by the high winds as well as by the surges from the lakes. Assuming that up to 90% of the population (approximately 600,000) in New Orleans will be evacuated before the storm, the potential fatalities may be assumed to range from 1800 to 3000 (i.e., 3% to 5% of those who did not evacuate) and serious injuries between 5000 and 10,000, with respective mean values of 2400 fatalities and 7500 injuries; whereas, the economic loss could range between 75 and 150 billion dollars with a mean loss of $112.5 billion. It may be reasonable to assume (prior to the occurrence of Katrina) that the fatalities and injuries will be caused equally by the extreme wind and by the inundation of the city; whereas the economic loss will largely be caused by the failure of the levee system and subsequent inundation of the city.

On the basis of the above postulated information, the "best estimate" of the risks to the city of New Orleans can be summarized as follows (based on respective mean values):

$$\text{Fatality risk} = 0.5[0.20(0.785)(2400)] + 0.5[0.20(0.78)(2400)] = 376$$
$$\text{Risk of serious injuries} = 0.5[0.20(0.785)(7500)] + 0.5[0.20(0.78)(7500)] = 1{,}174$$
$$\text{Risk of economic loss (in dollar)} = 0.20(0.78)(112.5) = \$17.55 \text{ billion}$$

3.1 *On risk reduction*

The results of a quantitative risk assessment will permit also a quantitative analysis of the reductions in the respective risks that can accrue from an investment in strategies to mitigate the effects of a future natural hazard. A clear example are the risk reductions accruing from strengthening and raising the height of the levees around New Orleans for protection against a Category 4 hurricane. Suppose that (in 1990) the cost to improve the levee system is estimated to be $1.00 billion to insure against or mitigate any inundation of the city. This may require raising the height from the existing average height of 8 ft to a uniform height of 12 ft plus any needed strengthening of the levees and floodwalls. With 12-foot levees, the probability of breaching from a Category 4 hurricane will be

reduced to the following: P(levee breached) = 0.27; and the respective "best estimate" reduced risk would be as follows:

Reduced economic risk = 0.20(0.27)(112.5) = 6.08 billion dollarse
Reduced fatality risk = 0.5[0.20(0.27)(2400)] + 0.5[0.20(0.785)(2400)] = 253
Reduced injury risk = 0.5[0.20(0.27)(7500)] + 0.5[0.20(0.785)(7500)] = 791

Therefore, with the investment of $1.0 billion to improve the levee system, the "best estimate" net reductions in the respective risks would be as follows:

reduction in economic risk = (17.55 − 6.08 − 1.00) = $10.47 billions;
reduction in fatality risk = (376 − 253) = 123; and
reduction in injury risk = (1174 − 791) = 383,

which are significant reductions in the respective risks accruable from the $1.0 billion investment for improving the levee system.

3.2 *Uncertainties in estimated risks*

The risks calculated above are based on the estimated mean (or median) values of the respective components in Eq. 1, yielding the "best estimate" risk measures. Clearly, there are (epistemic) uncertainties in each of the estimated mean (or median) values; these uncertainties may be represented by realistic ranges (or distributions) of the respective estimated mean (or median) values. These will lead also to corresponding uncertainties in the estimated risk measures, which are equally as important as the calculated risks. In this example, these epistemic uncertainties would specifically include the following:

(1) The estimated return period of 100 years for a Category 4 hurricane occurring in New Orleans may actually be between 50 to 150 years. In this case, the annual occurrence probability would range between 0.7% and 2% (in 20 years would be 14% to 40%); the underlying uncertainty may then be represented by a c.o.v. of 29%, and may be modeled with a lognormal distribution with a median of 1.0 and a c.o.v. (coefficient of variation) of 0.29, i.e. LN(1.0, 0.29).
(2) Because the specified estimated median surge height of 10 ft in the surrounding lakes is uncertain, the actual median surge could vary between 8 ft and 12 ft. This is equivalent to a c.o.v. of 12% in the median surge height, which may be represented by a lognormal distribution of LN(1.0, 0.12). Therefore, the probability of breaching the levees would become a random variable and can be described by the histogram shown in Fig. 1 which has a mean value of 0.75.
(3) The mean wind speed of 130 mph in a Category 4 hurricane may actually be between 110 and 150 mph. Therefore, the associated c.o.v. would be 9% in the estimated mean wind speed. In this light, the vulnerability of structures would also have a distribution of possible values.
(4) Finally, the uncertainties in the estimated consequences may be postulated as follows:
   - the economic loss ranging from $75 billion to $150 billion, assumed to be uniformly distributed within the indicated range; whereas,
   - the fatalities ranging from 1800 to 3000, assumed to be uniformly distributed within this range; and
   - the injuries ranging from 5000 to 10,000, also assumed to be uniformly distributed within this range.

   To take account of the above uncertainties, the resulting economic risk can be evaluated as

$$\mathrm{Re} = 0.20 N_H(p_B)(C_E) \tag{2}$$

Eq. 2 is a convolution integral, in which

p_B = probability of breaching the levees; the histogram of Fig. 1 contains the uncertainty in the estimation of the median surge height;
N_H = uncertainty in the estimated mean hazard (i.e., return period), prescribed as LN(1.0, 0.29);

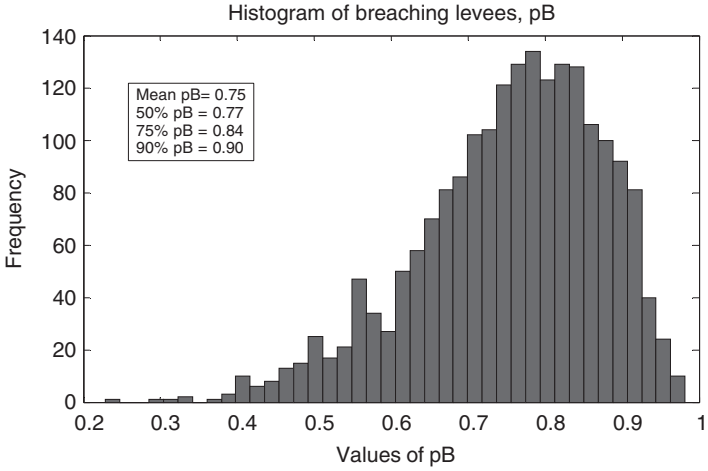

Figure 1. Histogram of probability of breaching levees, pB.

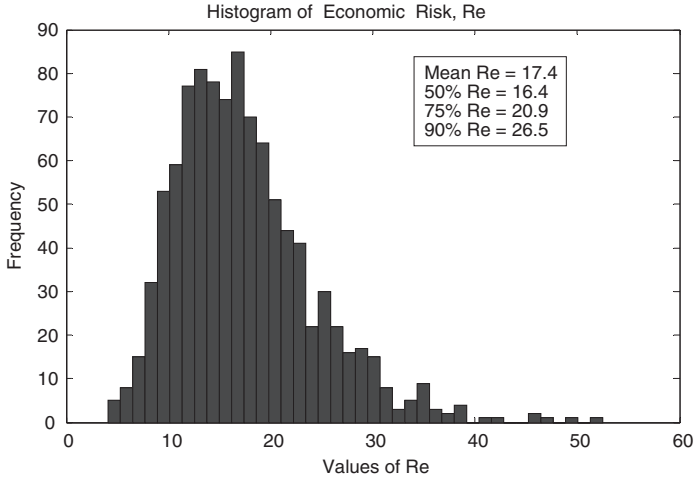

Figure 2. Histogram of economic risk, Re.

C_E = economic loss from inundation of city; assumed to be uniformly distributed between \$75 and \$150 billion.

In light of the above uncertainties, the economic risk, Re, would also be a random variable. By Monte Carlo simulation (with 1000 repetitions), we generate the corresponding histogram as shown in Fig. 2 with a mean value of \$17.4 billion.

Of particular interest for decision making are the following percentile values of Re:

50% value = \$16.4 billion; 75% value = \$20.9 billion; 90% value = \$26.5 billion

For example, for a risk aversive (i.e. conservative) decision, the 90% value may be selected or used; in which case, the economic risk from inundation would be specified as \$26.5 billion instead of the best estimate value (or mean value) of \$17.55 billion.

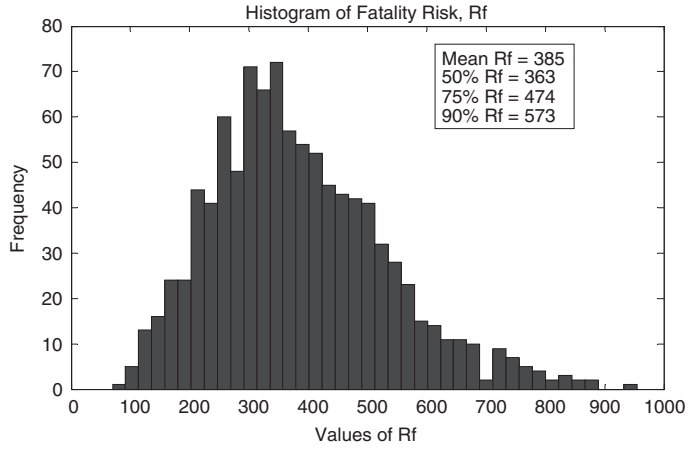

Figure 3. Histogram of fatality risk, Rf.

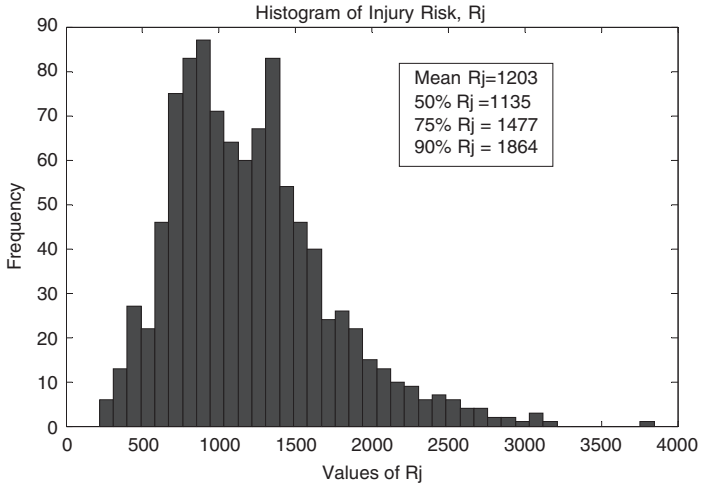

Figure 4. Histogram of injury risk, Rj.

Similarly, because of the uncertainty in the estimated mean wind speed, as well as in the occurrence probability of a Category 4 hurricane, and in the expected number of fatalities, the fatality risk is also a random variable with the histogram shown in Fig. 3 with a mean value of 385 fatalities.

Also, the following percentile fatality risk values may be of special interest for decision-making.

50% Rf = 363; 75% Rf = 474; 90% Rf = 593

For a risk averse (or conservative) decision, the 90% value of 593 fatalities may be specified.

Similarly, the distribution of the injury risk is shown in Fig. 4 with a mean of 1203 injuries.

Again, the following percentile values of the injury risk would be of special interest in decision making: 50% Rj = 1135; 75% Rj = 1477; 90% Rj = 1864 in which the 90% value of 1864 injuries would be a conservative risk value.

Finally, it is important to emphasize that by specifying a conservative risk value (e.g., the 90% value), the effects of uncertainty (of the epistemic type) in the calculated risk can be minimized.

4 INFORMATION AND ADVICE FOR DECISION MAKERS

Technical information obtained or generated from a QRA should be presented to the relevant stakeholders, in terms of the quantitative risk measures obtained as illustrated above, as well as of the benefit that can accrue from a given investment to reduce each of the respective risks. It is essential that this information be presented to decision makers who are responsible for allocating resources for minimizing risks. In the case of a natural hazard, the most important risk measures would include the fatality and injury risks, and the risk of economic losses, with the respective uncertainties.

Information and advice presented in quantitative terms, based on the expertise of engineers, should generally be more convincing to decision makers. These may be in terms of the "best estimate" value of the pertinent risk or the complete range (distribution) of all possible risk measures associated with its epistemic uncertainty; from this distribution risk-averse (i.e., conservative) values may be specified to reduce the uncertainties underlying the estimated risks. As with other technical information developed for engineering purposes which are invariably in quantitative terms, risk measures should and can also be developed in the same terms; society would generally expect such information (i.e., supported by quantitative analyses) from the expertise of the engineering community.

5 SUMMARY AND CONCLUDING REMARKS

The fundamentals for the systematic and quantitative assessment of risk, with particular emphasis for hazard mitigation, are summarized. Besides the assessment of the "best estimate" measure of a pertinent risk, the assessment of the uncertainty underlying the calculated risk is equally important. These are illustrated with a quantitative assessment of the risks (for a 20-year period) associated with the occurrence of a Category 4 hurricane in New Orleans on the assumption that the assessment was performed in 1990 (15 years prior to the occurrence of Katrina in 2005).

The fundamentals of QRA, as summarized and illustrated here, show that QRA is a valuable and practical tool available for engineers to generate quantitative technical information on risk and its associated uncertainty. A conservative (or risk averse) measure of risk may be specified to reduce the level of the underlying (epistemic) uncertainty. QRA can also be used to assess the benefit in risk reduction accruable from an incremental investment, and thus provide a quantitative basis for benefit-cost study that may be essential and useful for making risk-informed optimal decisions.

Civil engineers, in particular, among all engineers have the primary responsibility for the design and planning of civil infrastructures, including protective systems to minimize losses of lives and economies during extreme hazard events. In this light, there is every reason that practicing civil engineers should be equipped with the tools of QRA, especially when dealing with problems involving natural hazards.

REFERENCES

Ang, A. H-S., and Tang, W.H., 2006, *Probability Concepts in Engineering*, 2nd Edition, John Wiley & Sons, Inc,

Cornell, C.A., 1968, Engineering seismic risk analysis, *Bull. of Seismological Soc. of America*, Vol. 58

Der Kiureghian, A., and Ang, A. H-S.,1977, A fault rupture model for seismic risk analysis, *Bull. of Seismological Soc. of America*, Vol. 67

Gumbel, E.J.,1954, Statistical theory of extreme values and some practical applications, *Applied Mathematics Series 33*, National Bureau of Standards, Washington, DC

Harmsen, S., 2005, PSHA uncertainty analysis: applications to the CEUS and the Pacific NW, *Infrastructure Risk Management Processes*, Ed. C. Taylor and E. VanMarcke, ASCE, pp. 15–63

Wen, Y.K., and Chu, S.L.,1973, Tornado risk and design wind speed, *Proc. of ASCE, Jour. of Structural Div.*, Vol. 99, No. ST 12

Reliability and Optimization of Structural Systems: Assessment, Design and Life-Cycle Performance – Frangopol, Kawatani & Kim (eds)

Sampling strategies to detect threshold excursions in random fields

Jack W. Baker
Stanford University, USA

Michael H. Faber
Swiss Federal Institute of Technology (ETH Zurich), Switzerland

ABSTRACT: Sampling strategies are considered for efficiently detecting threshold excursions within realizations of random fields. By considering costs of sampling and costs of non-detection of excursions, a risk-based sampling framework is described. Computation of excursion probabilities, conditional upon observations from samples, is performed by using a conditional simulation technique to generate realizations of random fields that are consistent with the observed values. Simple numerical examples are used to demonstrate the use of the approach, and to illustrate how it might be used to identify adaptive sampling schemes that will aid in efficiently detecting threshold excursions. The problem is motivated by geotechnical sampling problems, where a limited testing budget is available to obtain information about the potential presence of interesting features underground (e.g., pockets of weak or liquefiable soil).

1 INTRODUCTION

The goal of many geotechnical testing activities is to understand the range of potential values that various soil properties might take. This includes intrinsic soil properties such as strength or soil type, as well as levels of contamination in the soil. Because these properties are unknown, they can be represented by random variables. As the properties also tend to be spatially dependent (due to, for example, similarities in materials and deposition patterns), the spatial distribution of soil property values might be represented by a random field.

Common goals in a geotechnical testing activity are to characterize the probability distribution of some soil property (or properties) at a given location, or to estimate the spatial dependence of the soil property [1]. A third goal might be to detect whether the soil property exceeds some given value within the region of interest. This may arise if an engineer is trying to identify areas within a site having low bearing capacity or high liquefaction susceptibility.

In this paper, sampling strategies to most effectively achieve this third goal of detecting excursions are considered. This goal is closely related to search theory, a topic studied in great detail (see, e.g., the survey of [2]). This study varies slightly from most search theory applications, which are concerned with detecting a discrete feature, in that here we are considering extreme values of a continuous random field, so that even non-excursions provide information about the likelihood of an excursion in nearby areas. The fact that all observations provide differing levels of information, however, can greatly increase the numerical complexity of the problem.

Here, a series of simple calculations are performed to illustrate the problem and to point to effective strategies for sampling. With these basic results obtained, potential extensions to more complex situations are discussed.

2 RANDOM FIELD DEFINITION

It is assumed that the property of interest is a Gaussian random field with known mean, variance and autocorrelation. In the example below, the following model is assumed:

$$\mu_F(x,y) = 0 \tag{1}$$

$$\sigma_F(x,y) = 1 \tag{2}$$

$$\rho(\Delta h) = e^{-\Delta h/d} \tag{3}$$

where $\mu_F(x,y)$ and $\sigma_F(x,y)$ are the mean and standard deviation, respectively, of the random field F at location $\{x,y\}$. The term $\rho(\Delta h)$ is the autocorrelation of the random field at two points separated by a distance Δh, and d is a constant controlling the scale over which correlations are significant. The field is assumed to be heterogeneous and isotropic to simplify the presentation, although those conditions can be relaxed without difficulty. The objective is to determine whether a given realization of the random field exceeds a given threshold within some finite domain, using as few samples as possible.

3 RISK-BASED SAMPLING

Although the computational expense can be severe, risk-based sampling approaches provide a useful and rational approach for optimizing sampling strategies [3, 4]. The concept of this approach is to take samples in a manner that minimizes the risk associated with the system. In this way, the cost of sampling and expected cost of potential failures can be minimized. In the most general sampling approach here, the number of samples and locations can be left unspecified, and further samples can be taken as long as the marginal cost of additional samples is less than the marginal value of information from the additional samples. A simpler problem is one where the number of samples is specified, and only the locations of the samples must be chosen. Sampling strategies will also change depending upon whether the sampling is adaptive (i.e., observed results from previous samples can be used when choosing future sample locations) or whether all sample locations must be chosen before sampling begins.

To illustrate this sampling approach, we first consider the case where samples are taken until the value of information provided by the sample is less than the cost of the sample. To illustrate, consider an example where each sample has a cost of 1 unit. Classifying a realization as containing an excursion leads to an additional cost of 10 units, due to mitigation measures that are needed; this cost is incurred regardless of whether an excursion actually exists. Failing to detect an excursion has a cost of 100, which represents the cost of a delay during construction to take remedial actions, or the cost of a failure in the future.

A decision tree for this example is shown in Figure 1. The classification decision (the shaded decision node in Figure 1) is straightforward to calculate. Because the number of samples and their locations is specified, it only remains to compute the probability of an excursion, denoted p, conditional upon the observed sample values (a method for computing this probability is discussed in the following section). For this example, if $p < 0.1$ then the minimum expected cost is obtained by classifying the site as having no excursions ($E[cost] = 100^* p + n$). If $p > 0.1$ then the minimum expected cost is obtained by classifying the site as having an excursion ($E[cost] = 10 + n$). For $p = 0.1$, the two choices are equivalent.

Pre-posterior decision analysis can in principle be used to determine the number of samples to be taken and their locations [5]. In practice, however, computing the costs required to evaluate this decision is very difficult. The value of information obtained from an additional sample must be maximized by optimally choosing the location at which the sample should be taken. But the location at which the sample should be taken, and its value, depends upon the number of further samples that might be taken (i.e., if this is the last sample, it should be placed in the middle of an

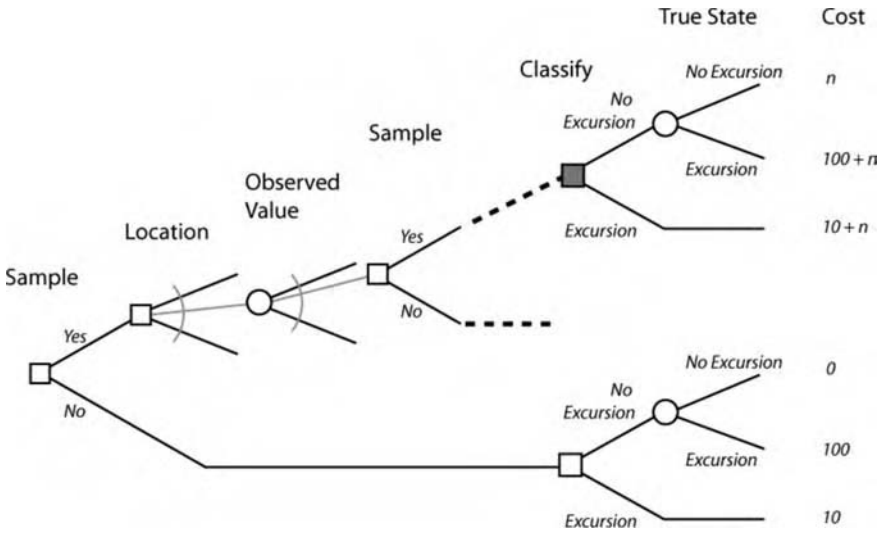

Figure 1. A decision tree for deciding the optimal number of samples and their locations.

area of interest, but if two more samples are to be taken, then they might be spaced to provide more uniform coverage).

Finding the optimal sampling strategy requires evaluating every possible path in Figure 1, because decision path will depend upon the (random) observed values of future samples. As a consequence of this, the problem differs from deterministic dynamic programming problems, where many branches do not need to be evaluated in order to locate the optimal decision path. Using symmetry arguments, some of the potential combinations are equivalent and the number of evaluations can be reduced. But because the excursion probabilities needed for formulating decision rules are calculated based on numerical simulations, it is prohibitively computationally expensive to evaluate decision trees having a large number of possible paths.

To simplify the decision problem, one could first fix the allowed number of samples so that the decision problem only involves choosing the locations of these samples. This is perhaps a realistic situation for many practical problems (e.g., the budget for testing is fixed before testing begins, or the sampling equipment is mobilized for a fixed amount of time). Because the number of possible decisions is greatly reduced in this case, it is possible to perform some calculations.

3.1 *Conditional excursion probability, given observations*

When deciding whether to classify a site as having an excursion or not, it is necessary to compute the probability of a threshold excursion, given the observed values from completed tests. Although many analytical results have been derived relating to properties of random fields [6–8], no methods exist for computing excursion probabilities conditional upon observations. Thus a conditional simulation procedure is used here. This procedure can be used to simulate realizations of the random field that are consistent with the specified mean, variance and autocorrelation of the field, but that also agree perfectly with observed values at specified locations (see, e.g., [9]). The procedure takes advantage of the fact that conditional distributions of joint standard Gaussian random variables are also Gaussian with the following distribution

$$\left(\mathbf{Y} \mid \mathbf{Y}_{obs} = \mathbf{y}\right) \sim N\left(\boldsymbol{\Sigma}_{12} \cdot \boldsymbol{\Sigma}_{22}^{-1} \cdot \mathbf{y},\ \boldsymbol{\Sigma}_{11} - \boldsymbol{\Sigma}_{12} \cdot \boldsymbol{\Sigma}_{22}^{-1} \cdot \boldsymbol{\Sigma}_{21}\right) \tag{4}$$

where $\mathbf{y}$ is the vector of observed values from previous measurements, $\mathbf{Y}$ is the vector of random variables at unobserved locations in the area of interest, $\boldsymbol{\Sigma}_{11}$ is the covariance matrix of

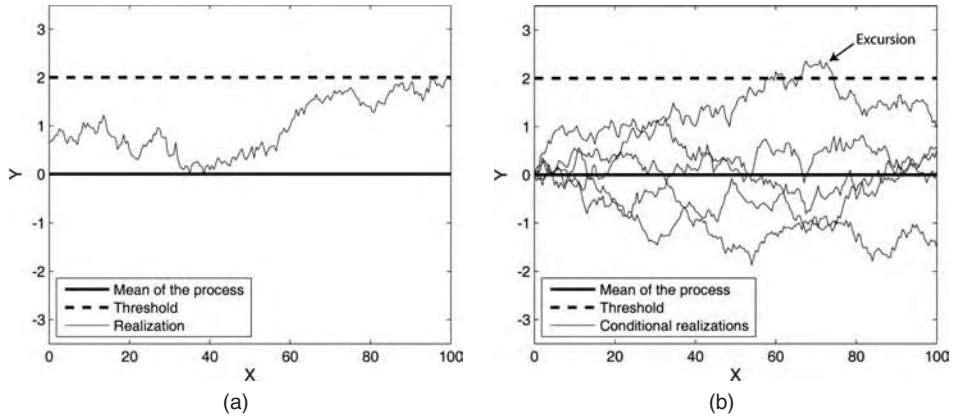

Figure 2. (a) A single realization of the random process in one dimension. (b) Five realizations of the random process, conditional upon observing a value of 0 at location $X = 0$.

the unobserved values $\mathbf{Y}$, $\mathbf{\Sigma}_{22}$ is the covariance matrix of the random variables associated with the observed locations, and $\mathbf{\Sigma}_{12}$ and $\mathbf{\Sigma}_{21}$ are the cross-covariance matrices between the random field values at the observed and unobserved locations. This approach is explained in more detail elsewhere [9].

It is in general not possible to compute excursion probabilities directly from the result of equation (4). One can, however, simulate samples from this distribution, and then count the number of samples that contain an excursion. Using this Monte Carlo approach, it is possible to estimate excursion probabilities conditional upon any set of observed values at any locations of interest. Example conditional simulations in one dimension are shown in Figure 2b.

4 EXAMPLE CALCULATIONS

Several simple examples are described in the following sections, to illustrate how the above framework can be applied.

4.1 *One-dimensional sample space*

The simplest possible example is to first consider only a one-dimensional domain of interest, and to consider a small number of samples in that area. The region of interest is assumed to be the interval from 0 to 100, and the random function is defined by Equations 1 through 3, with the distance parameter d equal to 25. The threshold level of interest is set equal to 2. The cost of classifying a site as having an excursion was set equal to 40, while the cost of not identifying an excursion is equal to 100 and the cost of samples was neglected because the number of samples is constant. An example realization is shown in Figure 2a, and conditional simulations of this one-dimensional random process are shown in Figure 2b. Because the marginal distribution of individual locations is standard Gaussian, their individual exceedance probabilities are equal to $1 - \Phi(2) = 0.023$, where $\Phi(\cdot)$ is the standard Gaussian cumulative distribution function. The probability that a given realization of the field will contain an excursion is estimated using Monte Carlo simulation to be 0.304.

This example can be used to confirm the potential benefit of an adaptive sampling scheme. Figure 3 shows expected costs, given that a second sample is taken after observing the value at location $X = 0$. The costs are conditional upon the observed value at the first location. If the first location is observed to have a value much below the threshold (i.e., on the left side of Figure 3),

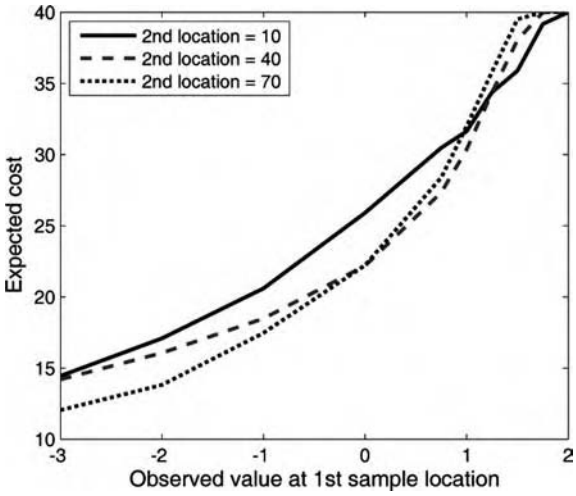

Figure 3. Expected cost of a second sample, conditional upon the observed value at the first location. The first sample is taken at $X = 0$, and results are shown for three potential second locations.

then the cost is minimized by taking the second sample at a location far from the location of the first sample. If, however, the first sample yields an observation near to the threshold value, then the cost is minimized by taking an additional sample near to the original sample. This makes intuitive sense: if the first sample suggests that the surrounding region is "safe" (far below the threshold) then additional samples should be taken elsewhere, but if the first sample indicates a potential nearby excursion, then additional samples at nearby locations will be useful.

By accounting for the probability distribution of the observed value at the first sample location, and assuming that the second sample is taken at whichever of the three locations minimizes the expected cost, one can compute that the expected cost of this adaptive sampling scheme is 27.1. In contrast taking two samples at {0, 10}, {0, 40}, and {0, 70} yields expected costs of 29.3, 27.5, and 28.0, respectively. Thus, as would be expected intuitively, the adaptive sampling scheme yields lower expected costs than the alternative non-adaptive schemes. The relative benefit of adaptive sampling schemes is expected to increase significantly as the number of samples increases.

4.2 *Two-dimensional sample space*

In this example, the sample region of interest is a surface of dimension 100×100, composed of discrete cells each having dimension 1×1. Examples of the simulations are shown in Figure 4. The Gaussian field was defined according to equations 1 through 3, and a threshold level of 3 was chosen. The marginal threshold exceedance probabilities of individual locations are equal to 0.0013, and the probability that a given realization of the field will contain an excursion is 0.28.

Direct simulation of these realizations is possible, but requires inversion of a $10{,}000 \times 10{,}000$ covariance matrix. To save computational expense, a conditional simulation approach was used (see [10] for details). Figure 5 shows the excursion regions of the simulations from Figure 4.

4.2.1 *One sample*

When only one sample is to be taken in the region, intuition suggests that it should be taken in the middle of the site. To confirm this using the proposed procedure, six sample locations are considered: in each case the y value of the sample location is 50, and x values of 0, 10, 20, 30, 40 and 50 are considered, as illustrated in Figure 6a. Because of symmetry, x values greater than 50 are not needed, and the x and y coordinates can be interchanged to reflect sampling along the vertical axis.

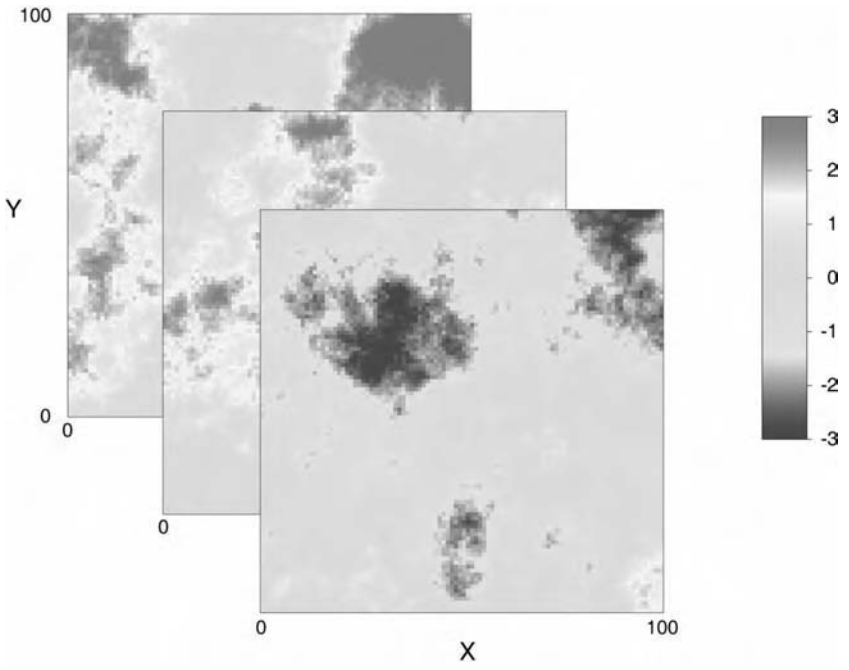

Figure 4. Example simulations of the random field used for calculations.

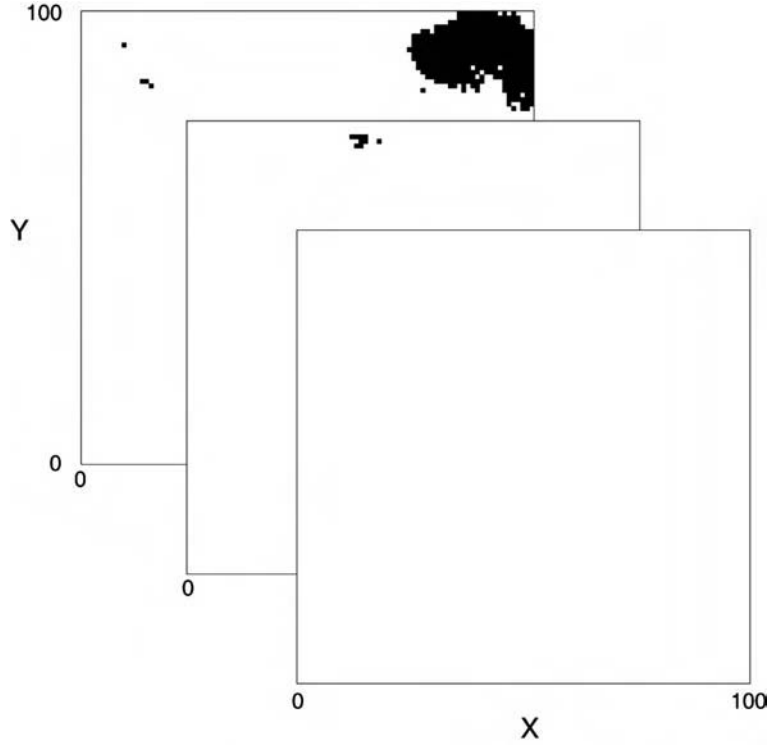

Figure 5. Threshold excursions of the random field simulations shown above.

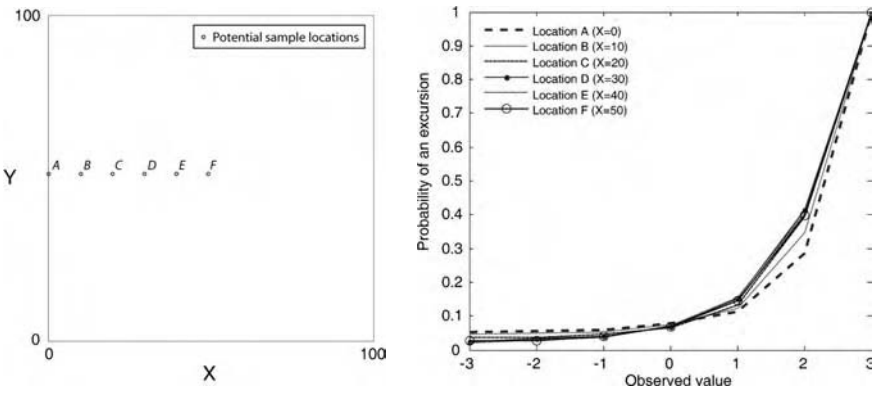

Figure 6. (a) Illustration of the six potential sample locations to be considered. (b) Probability of an excursion, conditional upon the observed value at the potential sample location.

For each sample location and potential observed value, simulations of conditional realizations can be used to compute the probability of an excursion. The results for a variety of observed values and sample locations are shown in Figure 6b. By using the excursion probabilities from Figure 6b, it is possible to compute the conditional expected cost conditional upon observing the specified value. Then, integrating all possible observed values and weighting each by its probability of occurrence, unconditional expected costs can be computed. The expected costs associated with taking samples at locations A through F are: 8.84 8.50 8.04 7.99 7.93 and 7.92. This indicates that the optimal strategy would be to take a sample near the center of the area of interest, as would be expected.

4.2.2 *Two samples*

If two samples are to be taken, an adaptive procedure can be used to choose the second sample location based on the result of the first location. To keep the number of considered situations manageable, the following system is proposed. First a sample is taken at location $\{x, y\} = \{25, 25\}$. In the adaptive sampling situation, the second location can be chosen once the outcome of the first sample is known. If the first sample is close to the excursion threshold, the second sample might be taken near to the first sample in order to learn more about this potentially critical region. If the first sample is far below the threshold, then the second sample should be taken at a location far from the first sample, under the assumption that the region near the first sample is of little concern, so other regions of the site should be studied. The considered locations for the second sample are $\{x, y\} = \{30, 30\}$, $\{60, 60\}$ and $\{90, 90\}$.

Conditional excursion probabilities are computed using the conditional simulation technique described above, and example results are shown in Figure 7 for a variety of sample locations and observed values. These can again be linked with expected costs associated with observing these values, and then by integrating over the probability of observing these values, expected costs of various sample strategies can be evaluated.

5 FUTURE WORK

The above work illustrates an approach by which decision theory can be used to identify optimal schemes for sampling to detect an excursion in a random field. More work is required, however, before the approach is ready for practical applications with large numbers of samples. Evaluation of the decision tree used to choose sampling strategies requires computation of excursion probabilities conditional upon every potential permutation of sample locations, and this is computationally

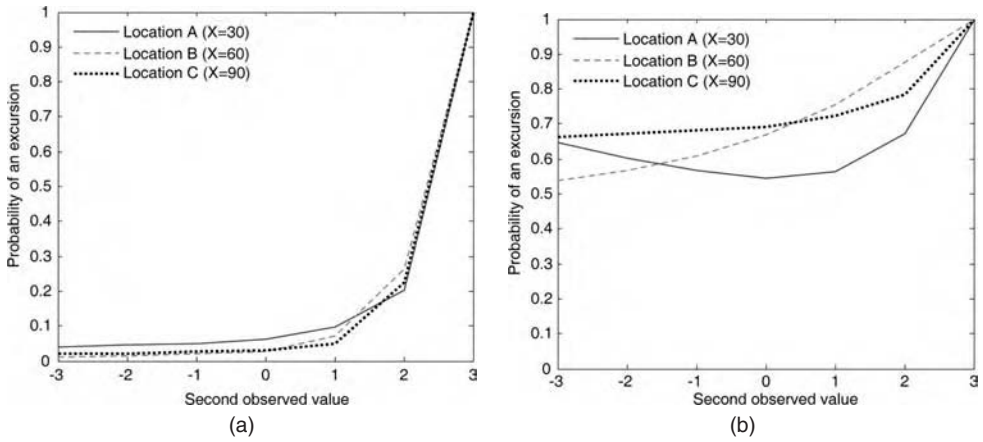

Figure 7. Probability of an excursion, conditional upon the observed values at the potential sample locations. (a) Results given that a value of -2.5 was observed at the first sample location. (b) Results given that a value of 2.5 was observed at the first sample location.

prohibitive because the probabilities are computed using simulation techniques. An approach will be developed to sample a representative subset of possible sample locations, in order to identify near-optimal strategies at a fraction of the computational cost. Analytic approximations to excursion probabilities will also be used to efficiently process large numbers of potential sample locations, and to identify the sample options where more careful (i.e., more computationally expensive) evaluations are needed.

The above approach focused only on detecting threshold excursions, while assuming that the properties of the random field were known. In reality, however, many sampling activities are concerned both with quantifying the relevant parameters of the random field as well as detecting excursions. Work relating to sampling strategies for characterizing random fields has been done (e.g., [11]), and those concepts could be combined with the ideas presented here. Evaluating tradeoffs between multiple objectives may be difficult, however.

6 CONCLUSIONS

A risk-based sampling framework for detecting excursions in realizations of random fields has been discussed. The goal of the framework is to identify optimal strategies for choosing sample locations to minimize expected costs, where there are costs associated with taking samples, with misclassifying a site as having no excursions and with classifying a site as having an excursion. The problem is motivated by, for example, geotechnical sampling problems, where a limited testing budget is available to obtain information about the potential presence of interesting features underground (e.g., pockets of weak or liquefiable soil).

Using decision theory, a decision tree was developed to frame this question. A critical need for evaluating the decision tree is an estimate for the probability of an excursion existing in a given sample realization, conditional upon the observed values from samples taken at a specified set of locations. This excursion probability was computed using a conditional simulation approach that allows for a great deal of flexibility in terms of the definition of the random field, the sample locations, and the shape and size of the region of interest. The approach should prove especially useful for developing adaptive sampling strategies, where the location of additional samples is dependent upon the observed values of previous samples. Simple numerical examples were presented to illustrate how this approach could be evaluated. By providing a quantitative method for evaluating these strategies, cost-saving improvements over typical sampling strategies can be formulated.

REFERENCES

Baecher GB, Christian JT. Reliability and statistics in geotechnical engineering. Chichester, West Sussex, England; Hoboken, NJ: J. Wiley; 2003.

Benkoski SJ, Monticino MG, Weisinger JR. A survey of the search theory literature.Naval Research Logistics 1991; 38469–94.

Straub D., Faber M.H. Risk based inspection planning for structural systems.Structrual Safety 2005; 27(4): 335–55.

Faber MH, Straub D., Maes M.A. A computational framework for risk assessment of RC structures using indicators. Computer-Aided Civil and Infrastructure Engineering 2006; 21(3): 216–30.

Benjamin JR, Cornell CA. Probability, statistics, and decision for civil engineers. New York: McGraw-Hill; 1970.

Vanmarcke E. Random fields, analysis and synthesis. Cambridge, Mass.: MIT Press; 1983.

Adler RJ. The geometry of random fields. Chichester [Eng.] ; New York: J. Wiley; 1981.

Adler RJ, Taylor JE. Random fields and geometry. (in press, preprint at http://iew3.technion.ac.il/~radler/publications.html); 2006.

Baker JW, Faber M. Accounting for soil spatial variability when assessing liquefaction risk Journal of geotechnical and geoenvironmental engineering 2006; (in review).

Deutsch CV, Journel AG. GSLIB geostatistical software library and user's guide. Version 2.0. ed. New York: Oxford University Press; 1997.

Degroot DJ, Baecher GB. Estimating autocovariance of in-situ soil properties. Journal of Geotechnical Engineering 1993; 119(GT1): 147–66.

Reliability and Optimization of Structural Systems: Assessment, Design and Life-Cycle Performance – Frangopol, Kawatani & Kim (eds)
© 2007 Taylor & Francis Group, London, ISBN 978-0-415-40655-0

Role of uncertainties in the lifetime performance of concrete structures

Fabio Biondini
Department of Structural Engineering, Politecnico di Milano, Milan, Italy

Dan M. Frangopol
Department of Civil and Environmental Engineering, ATLSS Research Center, Lehigh University, Bethlehem, Pennsylvania, USA

ABSTRACT: A general approach to the probabilistic nonlinear and limit analysis of framed structures in aggressive environments is used to investigate the role of the uncertainty effects associated with different parameters defining the time-variant performance of concrete structures. Based on suitable time-dependent sensitivity analysis the results of the probabilistic analysis shows that the relative importance of the uncertainty effects associated with each random variable may significantly vary during time due to the various sources of structural damage which may strongly affect the structural reliability.

1 INTRODUCTION

The design approach usually proposed by the codes mainly refers to undamaged structures and does not account for the effects of uncertainty associated with the unavoidable sources of structural damage which during time may strongly modify the reliability level. In fact, for concrete structures immersed in aggressive environments the structural performance must be considered as time-dependent, mainly because of the progressive deterioration of the mechanical properties of materials which makes the structural system less able to withstand the applied actions. In this context, a design procedure aimed to achieve the required level of structural performance not only at the initial time, but over the whole expected service life of the structure, must consider the relative importance of the uncertainty effects associated with each design parameter. To this aim, the role played by both the deterioration process and the corresponding evolution of the structural behavior on this variation needs to be investigated and clarified. In this way, it would be possible to calibrate the design procedures with respect to the random variables which actually affect the lifetime structural response.

Starting from the previous considerations, this paper investigates the time evolution of the uncertainty effects associated with different parameters which define the lifetime performance of concrete structures. The study is developed by using a novel methodology for time-variant reliability analysis of concrete structures subjected to diffusive attacks from external aggressive agents (Biondini et al. 2004, 2006*a*). The diffusion process is modeled by using cellular automata and the mechanical damage coupled to diffusion is evaluated by introducing proper material degradation laws. The lifetime performance is investigated by means of a probabilistic limit analysis procedure of framed structures which considers axial force and bending moment as active and interacting generalized plastic stressors (Biondini 2000).

Based on this procedure, the time evolution of the structural performance of an existing reinforced concrete arch bridge is investigated at the cross-sectional level by suitable indicators on the nonlinear behavior, as well as at the structural level with reference to the collapse load (Biondini and Frangopol 2006). The effects of the uncertainty associated with each random variable are finally quantified and compared by means of a time-dependent sensitivity factor based on a linear regression of the

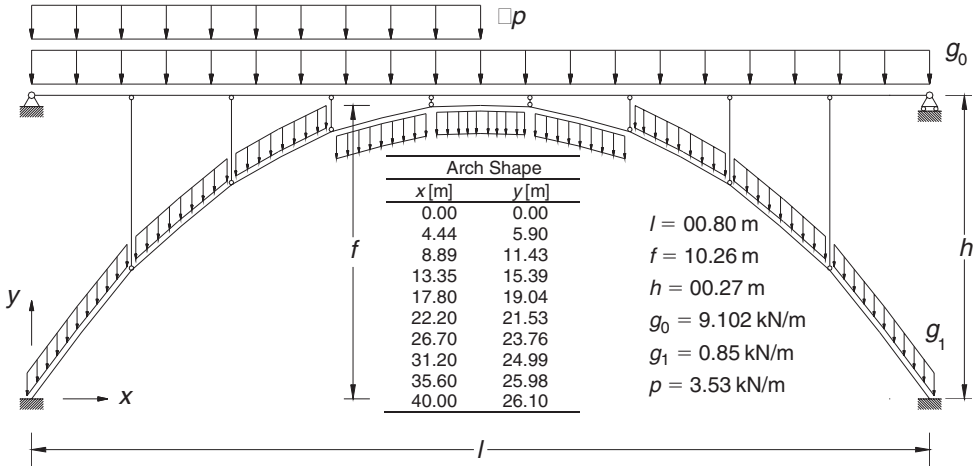

Figure 1. Arch bridge (nominal) structure. Overall dimensions, load condition, and beam cross-sections.

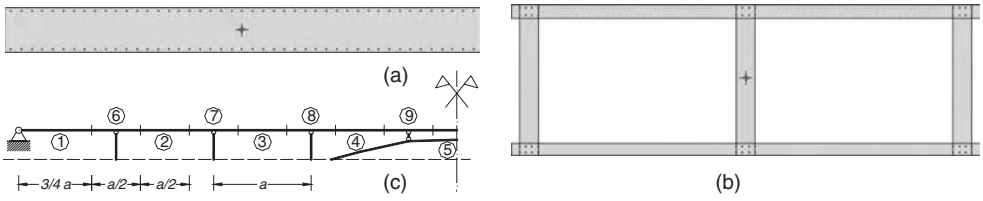

Figure 2. Details of the cross-sections. (a) Arch. (b) Beam. (c) Beam subdivision (see Table1).

Table 1. Distribution of the reinforcement along the beam (See Figure 2.c).

Span	1	2	3	4	5	6	7	8	9
A_s'	21Ø28	48Ø28	42Ø28	30Ø28	24Ø28	48Ø28	48Ø28	45Ø28	33Ø28
	130Ø8	130Ø8	130Ø8	130Ø8	130Ø8	130Ø8	130Ø8	130Ø8	130Ø8
A_s	21Ø28	30Ø28	42Ø28	24Ø28	24Ø28	21Ø28	36Ø28	27Ø28	24Ø28

data. The results shows that the relative importance of the uncertainty effects associated with each random variable may significantly vary with time due to the various sources of structural damage which may strongly modify the structural reliability.

2 LIFETIME PERFORMANCE OF CONCRETE STRUCTURES

2.1 *Case studied*

The present study refers to the arch bridge over the Corace river in Italy (Galli and Franciosi 1955). The structural model is shown in Figure 1. The arch has a rectangular cross-section with the following nominal dimensions $d_y = 0.57$ m and $d_z = 6.00$ m, and it is reinforced with $45 + 45 = 90$ bars having nominal diameter $\emptyset = 28$ mm (Figure 2(a)). The beam has a two-cellular cross-section with main nominal dimensions $d_y = 2.00$ m and $d_z = 6.00$ m (Figure 2(b)). The other nominal dimensions are: web thickness $= 0.20$ m; top slab thickness $= 0.18$ m; bottom slab thickness $= 0.16$ m. The distribution of the reinforcement along the beam refers to the subdivision shown in Figure 2(c), and is given in Table 1. The structure is subjected to a set of dead loads g and to a live load p.

The nonlinear bending behavior of the cross-sections is defined by assigning the constitutive laws of the materials. For concrete, the stress-strain diagram is described by the Saenz's law in compression and by an elastic perfectly plastic model in tension, with the following nominal parameters: compression strength $f_c = -30$ MPa; tension strength $f_{ct} = 0.25|f_c|^{2/3}$; initial modulus $E_{c0} = 9500|f_c|^{1/3}$; peak strain in compression $\varepsilon_{c0} = -0.20\%$; strain limit in compression $\varepsilon_{cu} = -0.35\%$; strain limit in tension $\varepsilon_{ctu} = 2f_{ct}/E_{c0}$. For steel, the stress-strain diagram is described by an elastic perfectly plastic model in both tension and compression, with the following nominal parameters: yielding strength $f_{sy} = 300$ MPa; elastic modulus $E_s = 206$ GPa; strain limit $\varepsilon_{su} = 1.00\%$.

2.2 *Diffusion process*

The structure is assumed to be subjected to a diffusive attack from an environmental aggressive agent located with concentration $C(t) = C_0$ along the free edges of both beam and arch. The kinetic diffusion process is described according to the Fick's laws and is effectively simulated by using a special class of evolutionary algorithms called cellular automata. In particular, it can be shown that the Fick's laws in two-dimensions can be simply reproduced by adopting the following evolutionary rule (Biondini et al. 2004):

$$C_i^{k+1} = \phi_0 C_i^k + \frac{1-\phi_0}{4}\sum_{j=1}^{2}(C_{i-1,j}^k + C_{i+1,j}^k) \tag{1}$$

where the discrete variable $C_i^k = C(\mathbf{x}_i, t_k)$ represents the concentration of the component in the cell i at time t_k, and ϕ_0 is a suitable evolutionary coefficient. The deterministic value $\phi_0 = 1/2$ usually leads to a good accuracy of the automaton. Clearly, to regulate the process according to a given diffusivity coefficient D, a proper discretization in space and time should be chosen in such a way that the grid dimension Δx and the time step Δt satisfy the following relationship:

$$D = \frac{1-\phi_0}{4}\frac{\Delta x^2}{\Delta t} \tag{2}$$

With reference to a nominal diffusivity coefficient $D = 10^{-11}$ m^2/sec, the automaton used in the case study is defined by a grid dimension $\Delta x = 50.2$ mm and a time step $\Delta t = 1$year. As an example, the diffusion process for the nominal scenario is described by the maps of concentration $C(\mathbf{x},t)/C_0$ shown in Figure 3(a) for the beam segment 6, and Figure 3(b) for the arch.

2.3 *Structural damage and cross-sectional nonlinear analysis*

Structural damage is modeled by introducing a degradation law of the effective resistant area for both the concrete matrix and the steel bars. This degradation is achieved by means of proper dimensionless *damage indices* δ_c and δ_s for steel and concrete, respectively, which provide a direct measure of the damage level of the materials within the range [0; 1]. The damage indices $\delta_c = \delta_c(\mathbf{x},t)$ and $\delta_s = \delta_s(\mathbf{x}, t)$ at point $\mathbf{x}$and time t are correlated to the diffusion process by assuming, for both materials, a linear relationship between the rate of damage and the mass concentration $C = C(\mathbf{x}, t)$ of the aggressive agent (Biondini et al. 2004):

$$\frac{\partial \delta_c(\mathbf{x},t)}{\partial t} = \frac{C(\mathbf{x},t)}{C_c \Delta t_c} \qquad \frac{\partial \delta_s(\mathbf{x},t)}{\partial t} = \frac{C(\mathbf{x},t)}{C_s \Delta t_s} \tag{3}$$

where C_c and C_s represent the values of constant concentration $C(\mathbf{x},t)$ which lead to a complete damage of the materials after the time periods Δt_c and Δt_s, respectively. In addition, the initial conditions $\delta_c(\mathbf{x},t_0) = \delta_s(\mathbf{x},t_0) = 0$ with $t_0 = \max\{t | C(\mathbf{x},t) \le C_{cr}\}$ are assumed, where C_{cr} is a critical threshold of concentration (Biondini et al. 2004).

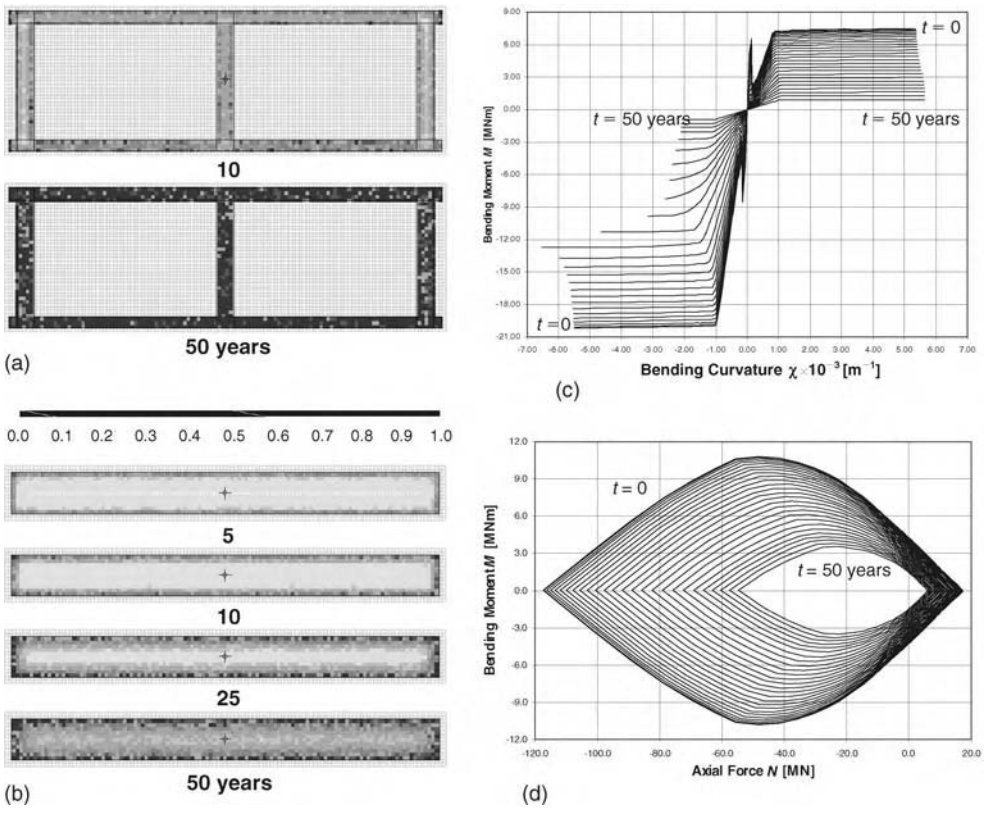

Figure 3. Maps of concentration $C(\mathbf{x},t)/C_0$ of the aggressive agent: (a) Beam (segment 6); (b) Arch. Time evolution of the structural performance ($\Delta t = 2$ years): (c) Bending moment M versus curvature χ diagrams (segment 6). (d) Axial force N versus bending moment M interaction diagrams for the arch.

In the present study, a very severe damage scenario with nominal values $C_{cr} = 0$, $C_c = C_s = C_0$, $\Delta t_c = 25$ years and $\Delta t_s = 50$ years, is considered. The mechanical damage induced by diffusion for the nominal scenario can be evaluated from the time evolution of the bending moment M versus curvature χ diagrams of the beam segment 6, shown in Figure 3(c), and of the axial force N versus bending moment M interaction diagrams of the arch, shown in Figure 3(d).

2.4 *Time-variant limit analysis*

Let $\lambda \geq 0$ be a scalar multiplier of the live loads. By assuming that the structure is safe for $\lambda = 0$, the collapse multiplier λ_c associated with its failure can be derived from the two fundamental theorems of limit analysis. In fact, based on a stepwise linearization of the resistance domains, it can be shown that the lower bound theorem and the upper bound theorem of the limit analysis allow to assess the collapse multiplier λ_c, as well as the stress distribution at the incipient collapse and the collapse mechanism, by solving a couple of dual linear programming problems.

Due to the progressive deterioration of the mechanical properties of materials, the quantities which define the resistance domains, as well as the corresponding collapse multiplier λ_c, vary during time. The time evolution of the resistance domains can be evaluated as previously shown by a lifetime cross-sectional analysis. In this way, a time-variant limit analysis leading to the time evolution of the collapse multiplier $\lambda_c = \lambda_c(t)$ can be performed by solving the linear programs at several time instants (Biondini and Frangopol 2006).

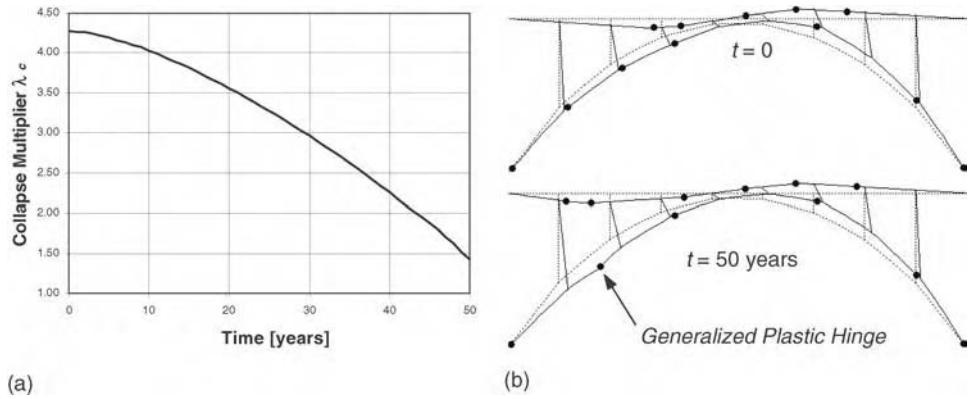

Figure 4. (a) Time evolution of the collapse multiplier λ_c. (b) Collapse mechanism at the initial time ($\lambda_c = 4.28$) and after 50 years of lifetime ($\lambda_c = 1.42$).

For the arch bridge, the time-variant limit analysis is performed with reference to the time evolution of the resistance bending moments of the axially unloaded beam and of the axial force-bending moments resistance curves of the arch, idealized at each time instant by a four-sides stepwise linearization. The deterioration of the five supporting walls, simply compressed, is not investigated since they are assumed as not critical with respect to collapse. Figure 4 shows the main results carried out for the nominal scenario. These results highlight that the time evolution of damage leads to a significant variation of the collapse multiplier, which decreases from $\lambda_c = 4.28$ to $\lambda_c = 1.42$ (Figure 4(a)), as well as to a noteworthy redistribution of the internal stress resultants and a consequent modification of the collapse mechanism (Figure 4(b)).

3 ROLE OF UNCERTAINTY IN LIFETIME PERFORMANCE

3.1 *Probabilistic model*

The probabilistic model assumes as random variables the location (x_h, y_h) of the nodal connections between the structural elements, the material strengths f_c and f_{sy}, the coordinates (y_p', z_p') of the nodal points $p = 1, 2, \ldots$ which define the two-dimensional model of the concrete cross-sections, the coordinates (y_m', z_m') and the diameter $\emptyset_m$ of the steel bars $m = 1, 2, \ldots$, the diffusivity coefficient D, the damage rates $q_c = (C_c \Delta t_c)^{-1}$ and $q_s = (C_s \Delta t_s)^{-1}$, the loads g and p in each beam element. These variables are considered to be statistically independent and are assumed to have the probabilistic distribution with the mean μ and standard deviation σ values listed in Table 2 (Biondini et al. 2006*a*).

3.2 *Probabilistic performance of the cross-sections*

The probabilistic performance of the cross-section of the beam segment 6 is now investigated in terms of bending moment versus curvature diagram (Figure 3.c). For the sake of synthesis, the cracking moment M_{cr} and the resistant moment M_r, as well as the curvature ductility $\varphi = \chi_u / \chi_y$ given by the ratio of curvatures at ultimate and yielding, respectively, are assumed as suitable indicators of structural performance. With reference to a sample of 5000 simulations, Figure 5 shows the time evolution of the statistical parameters (mean value μ, standard deviation σ, minimum and maximum values) of the performance indicators for both positive and negative bending responses during the first 50 years of service life (Biondini et al. 2006*b*). When directly compared with the random variability of the structural demand, the results of the probabilistic simulation allow to assess the time-variant reliability of the cross-section or, conversely, to assess the corresponding remaining service life which can be assured under prescribed reliability levels without maintenance.

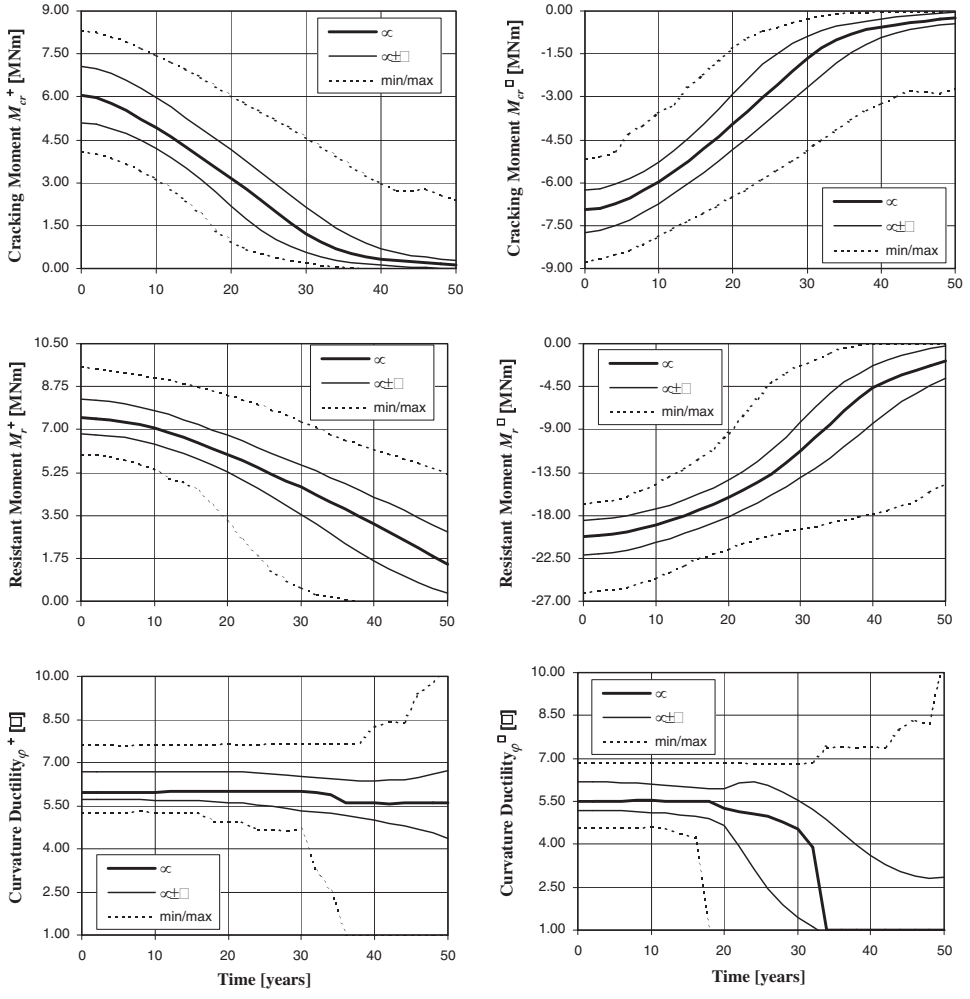

Figure 5. Time evolution of structural performance indicators during the first 50 years of lifetime: mean μ (thick line), standard deviation σ from the mean μ (thin lines), minimum and maximum values (dotted lines).

3.3 *Regression analysis and sensitivity factors*

The results of the simulation process highlight that the deterioration of structural performance tends to be associated with a significant increase of the spreading effects of uncertainty over time (Figure 5). This tendency is particularly emphasized for curvature ductility. However, as already pointed out, the relative importance of the uncertainty effects associated with each one of the random variables a_i listed in Table 2 may significantly vary during time.

In order to investigate the effects of the uncertainty associated with each parameter x_i on each performance indicator y_j, the following standard normal variates are introduced:

$$\xi_i(t) = \frac{x_i(t) - \mu_{x,i}(t)}{\sigma_{x,i}(t)} \qquad \eta_j(t) = \frac{y_j(t) - \mu_{y,j}(t)}{\sigma_{y,j}(t)} \tag{4}$$

where μ_x, σ_x, and μ_y, σ_y, are the time-variant mean value and standard deviation of the random variables x and y, respectively. Based on these variates, a set of time-variant least squares linear

Table 2. Probability distributions and their parameters.

Random variable ($t = t_0$)	Distribution type	μ	σ
Coordinates of the nodal points, (x_h, y_h)	Normal	$(x_h, y_h)_{nom}$	50 mm
Concrete strength, f_c	Lognormal	$f_{c,nom}$	5 MPa
Steel strength, f_{sy}	Lognormal	$f_{sy,nom}$	30 MPa
Coordinates of the nodal points, (y_p', z_p')	Normal	$(y_p', z_p')_{nom}$	5 mm
Coordinates of the steel bars, (y_m', z_m')	Normal	$(y_m', z_m')_{nom}$	5 mm
Diameter of the steel bars, $\emptyset_m$	Normal (*)	$\emptyset_{m,nom}$	$0.10\,\emptyset_{m,nom}$
Diffusivity coefficient, D	Normal (*)	D_{nom}	$0.10\,D_{nom}$
Concrete damage rate, $q_c = (C_c \Delta t_c)^{-1}$	Normal (*)	$q_{c,nom}$	$0.30\,q_{c,nom}$
Steel damage rate, $q_s = (C_s \Delta t_s)^{-1}$	Normal (*)	$q_{s,nom}$	$0.30\,q_{s,nom}$
Dead loads, g	Normal (*)	g_{nom}	$0.10\,g_{nom}$
Live load, p	Normal (*)	p_{nom}	$0.40\,p_{nom}$

(*)Truncated distributions with non negative outcomes are adopted in the simulation process.

regression is performed on the data samples obtained from the simulation in the following form:

$$\eta_j(t) = \alpha_{ij}(t)\xi_i(t) + \beta_{ij}(t) \tag{5}$$

In this way, the regression coefficients α_{ij} are assumed as time-dependent measures of the sensitivity of the dependent variable y_j with respect to the independent variable x_i.

The results of this analysis are shown in Figure 6 where, for the sake of synthesis, the sensitivity factors associated with the coordinates of the nodal points of the cross-sectional model, and with both the coordinates and areas of the steel bars, are computed with reference to the mean values of the corresponding standard variates over the whole cross-section and denoted as y_c, y_s, and A_s, respectively. The following remarks can be made (Biondini et al. 2006*b*):

- The cracking moments in the undamaged scenario mainly depend on the concrete strength. Such dependency quickly decreases during time, and after about 20 years the damage rate of concrete becomes the more important parameter. However, this contribution tends to progressively disappear. At the end of service life an important role is played by the damage rate of steel and, for the positive cracking moment, by the geometrical dimensions of the cross-section.
- The resistant moments in the undamaged scenario mainly depend on the steel strength. Such dependency quickly decreases during time and become negligible after about 25 years. At this point, for positive resistant moment the damage rate of steel becomes the more important parameter for the whole remaining service life. On the contrary, for negative resistant moment a clear dependency no longer holds until the last years of service life, when the damage rate of steel begins to give a significant contribution.
- The curvature ductility in the undamaged scenario mainly depend on the steel strength. For positive bending behavior such dependency is maintained along the whole service life. On the contrary, for negative bending behavior more complex correlations emerge after about 15–20 years, when the role played by the location of the steel bars and the damage rate of concrete becomes more important. However, these contributions tend to disappear at the end of service life, when a significant contribution is given by the area of the steel bars.

3.4 *Probabilistic performance of the structure*

A probabilistic time-variant limit analysis is carried out by using a set of about 28000 Monte Carlo simulations (1000 for each cross-section of the beam, 1000 for the cross-section of each span of the arch, 1000 for the global analysis of the structure). The time evolution of the collapse multiplier during the first 50 years of lifetime is shown in Figure 6.a for a selected sample of these

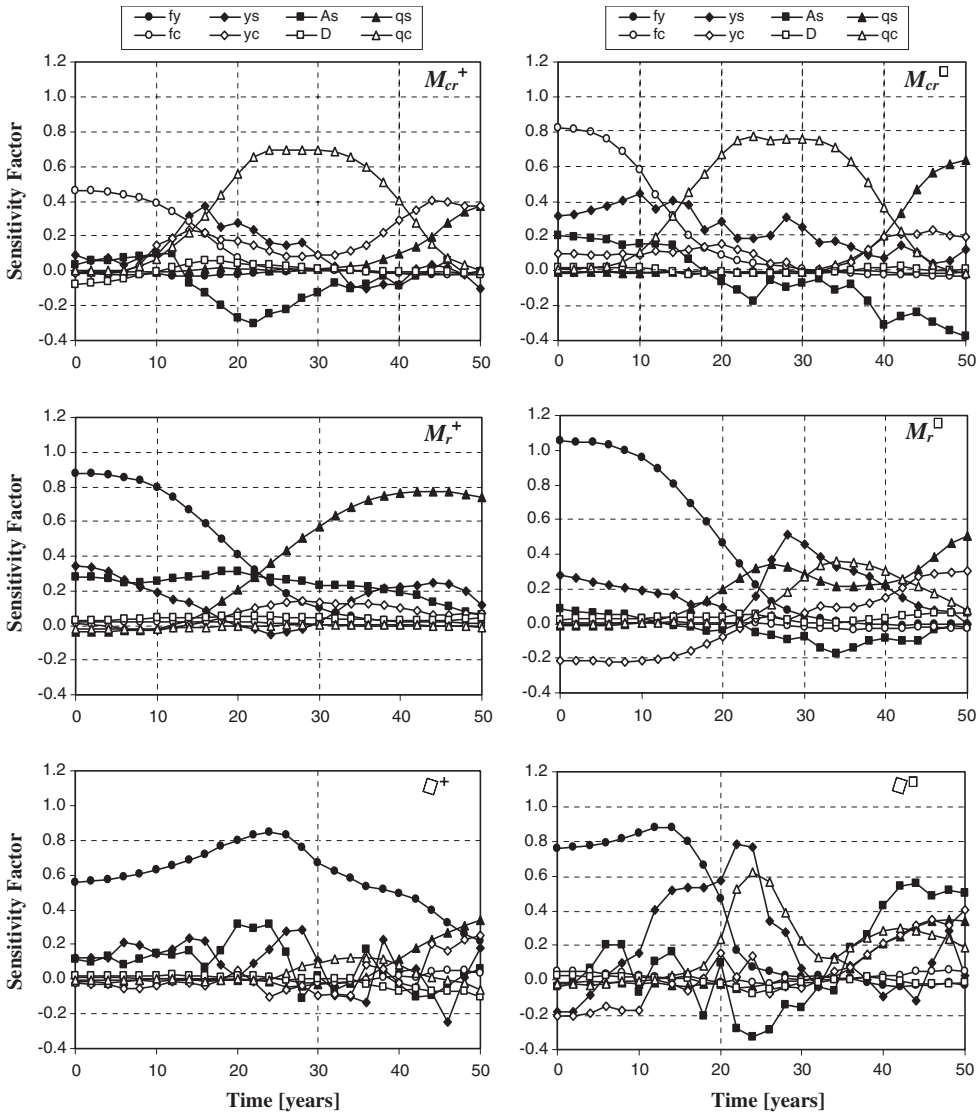

Figure 6. Sensitivity factors of the structural performance indicators.

simulations. In particular, Figure 6.a compares the nominal scenario with the scenarios associated with the minimum and maximum values of the collapse multiplier obtained at the initial time – min(0) and max(0) – and at the end of the structural lifetime – min(50) and max(50) –, as well as with the scenarios characterized by the maximum and minimum variation of the collapse multiplier over the investigated lifetime period – max(0–50) and min(0–50). With reference to the whole sample, Figure 6.b shows instead the time evolution of the statistical parameters (mean value μ, standard deviation σ, minimum and maximum values) of the collapse multiplier (Biondini and Frangopol 2006). The direct comparison of these results with those obtained a the cross-sectional level shows that the role of uncertainties at the structural level shows an opposite tendency. In fact, the deterioration of structural performance is no longer associated with a significant increase of the spreading effects of uncertainty, but they decrease over time due to the positive smoothing effect of the structural redundancy.

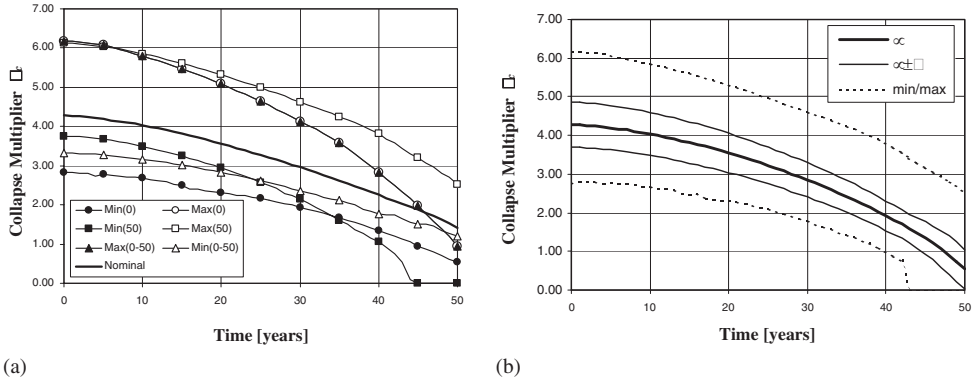

(a) (b)

Figure 7. Time evolution of the collapse multiplier λ_c. (a) Comparison among selected simulations. (b) Mean μ (thick line), standard deviation σ from the mean μ (thin lines), minimum and maximum values (dotted lines).

4 CONCLUSIONS

In design practice the complexity of the reliability problem is reduced by means of simplified probabilistic methods in which only a few uncertain parameters are considered as random variables, typically those which mainly affect the structural response. However, the results of this investigation proved that for concrete structures in aggressive environments the relative importance of the uncertainty effects associated with each design parameter may significantly vary during time. In particular, the classical view assuming that the main role in concrete design is played by the uncertainty associated with the material strengths needs to be reviewed to account for the effects of the unavoidable sources of structural damage which during time may strongly affect the structural performance and the corresponding reliability level. The role played by the topology of the structural system should be also taken into account, since it has been shown that redundancy could affect the spreading of uncertainty over time.

REFERENCES

Biondini, F., (2000). Probabilistic Limit Analysis of Framed Structures. *8-th ASCE Conference on Probabilistic Mechanics and Structural Reliability*, Paper 273, Notre Dame, July 24–26.

Biondini, F., Bontempi, F., Frangopol, D.M., and Malerba, P.G., (2004). Cellular Automata Approach to Durability Analysis of Concrete Structures in Aggressive Environments. *ASCE Journal of Structural Engineering*, **130**(11), 1724–1737.

Biondini, F., Bontempi, F., Frangopol, D.M., and Malerba, P.G., (2006*a*). Probabilistic Service Life Assessment and Maintenance Planning of Deteriorating Concrete Structures. *ASCE Journal of Structural Engineering*, **132**(5), 810–825.

Biondini F., Bontempi, F., Frangopol, D.M., and Malerba, P.G., (2006*b*). Lifetime Nonlinear Analysis of Concrete Structures under Uncertainty. *Bridge Maintenance, Safety, Management, Life-Cycle Performance and Cost*, P.J.S. Cruz, D.M. Frangopol, and L.C.Neves (Eds.), Taylor & Francis Group plc, London.

Biondini, F., Frangopol, D.M., (2006). Collapse Reliability and Lifetime Prediction of Deteriorating Reinforced Concrete Framed Structures. *Advances on Reliability and Optimization of Structural Systems*, J.D. Sorensen, and D.M. Frangopol (Eds.), Taylor & Francis, London, 269–279.

Galli, A., Franciosi, V., (1955). Il calcolo a rottura dei ponti a volta sottile ed impalcato irrigidente. *Giornale del Genio Civile*, **11**, 686–700 (in Italian).

Reliability and Optimization of Structural Systems: Assessment, Design and Life-Cycle Performance – Frangopol, Kawatani & Kim (eds)
© 2007 Taylor & Francis Group, London, ISBN 978-0-415-40655-0

Lifetime optimization of deteriorating structures

Fabio Biondini & Alessandra Marchiondelli
Department of Structural Engineering, Politecnico di Milano, Milan, Italy

ABSTRACT: A consistent approach to the optimal design of durable structures must consider the time evolution of the structural performance induced by the progressive deterioration of the system properties. To comply with this requirement, a new conceptual approach to the minimum lifetime cost design of deteriorating structures under multiple loading conditions is presented. The proposed procedure is applied to the lifetime structural optimization of a steel truss and of a reinforced concrete frame under different damage and maintenance scenarios. The obtained results highlight the fundamental role played by both the time-variant performance and the maintenance planning in the selection of the optimum structural design.

1 INTRODUCTION

For structures exposed to damaging environments the structural performance must be considered as time-dependent, mainly because of the progressive deterioration of the mechanical properties of materials which makes the structural system less able to withstand the applied actions. Therefore, a consistent approach to optimum design of durable structures should lead to find design solutions able to comply with the desired performance not only at the initial time of construction, but also during the whole expected service lifetime by taking into account the effects induced by unavoidable sources of mechanical damage and by eventual maintenance interventions.

This paper presents a new conceptual approach to the lifetime optimization of deteriorating structures under multiple loading conditions (Azzarello et al. 2006, Biondini and Marchiondelli 2006*a*). The structural damage is modeled by introducing a proper material degradation law and the structural analysis is carried out at different time instants in order to assess the time evolution of the system performance. The design constraints are related to both the time-variant stress and displacement state, as well as to the amount of structural damage. The objective function is formulated by accounting for both the initial cost of the structure and the costs of possible maintenance interventions, that are properly discounted over time and assumed to be proportional to the actual level of structural damage. The proposed procedure is initially presented for truss and framed structures made by homogeneous members. Finally, it is extended to the case of reinforced concrete structures by adopting different damage rates and material costs for both concrete and steel.

The lifetime structural optimization of a steel truss and of a reinforced concrete frame under different damage and maintenance scenarios proves the effectiveness of the proposed formulation. In particular, the obtained results highlight the fundamental role played by both the time-variant performance and the maintenance planning in the selection of the optimum structural design.

2 MODELING OF STRUCTURAL DAMAGE

With reference to truss and framed structures, damage is considered to affect the cross-sectional area $A = A(t)$, the elastic modulus $E = E(t)$, and the material strength $\overline{\sigma} = \overline{\sigma}(t)$ of each member:

$$A(t) = [1 - \delta_A(t)]A_0 \qquad E(t) = [1 - \delta_E(t)]E_0 \qquad \overline{\sigma}(t) = [1 - \delta_{\overline{\sigma}}(t)]\overline{\sigma}_0 \tag{1}$$

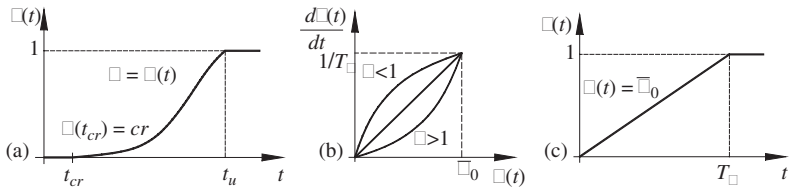

Figure 1. Modeling of structural damage. (a) Time evolution of the damage index $\delta = \delta(t)$. (b) Linear relationship between the rate of damage and the stress level $\sigma = \sigma(t)$. (c) Meaning of the damage parameter T_δ.

where $\delta_A, \delta_E, \delta_{\bar{\sigma}}$, are dimensionless damage indices which provide a direct measure of the damage level within the range [0; 1]. Proper correlation laws may be introduced to define the corresponding variation of other geometrical properties of the cross-section, like the inertia moment, etc.

The time evolution of the damage indices $\delta_A, \delta_E, \delta_{\bar{\sigma}}$, clearly depends on the physics of the deterioration process, usually related also to the stress state $\sigma = \sigma(t)$ (Figure 1.a). Therefore, a reliable assessment of the decreasing structural performance during time requires the formulation of deterioration models suitable to describe the actual damage evolution and its interaction with the structural behavior (Biondini *et al.* 2004). However, despite the inherent complexity of damage laws, very simple degradation models could be successfully adopted in order to define an effective hierarchical classification of the design alternatives (Biondini and Marchiondelli 2006*b*).

Without any loss of generality, in this study it is assumed that all material properties undergo the same damage process, or $\delta_A = \delta_E = \delta_{\bar{\sigma}} \equiv \delta$. In addition, the damage index $\delta = \delta(t)$ is correlated to the time-variant structural behavior by assuming the following relationship between the rate of damage and the acting stress $\sigma = \sigma(t)$ (Figure 1.b):

$$\frac{d\delta(t)}{dt} = \frac{1}{T_\delta}\left[\frac{\sigma(t)}{\bar{\sigma}_0}\right]^\alpha \qquad \bar{\sigma}_0 = \begin{cases} \bar{\sigma}_0^+ & \text{if } \sigma \geq 0 \\ \bar{\sigma}_0^- & \text{if } \sigma < 0 \end{cases} \tag{2}$$

where $\alpha \geq 0$ is a suitable constant, $\bar{\sigma}_0^-$ and $\bar{\sigma}_0^+$ are the minimum and maximum allowable stress at the initial time $t = t_0$, respectively, and T_δ represents the time period required for a complete damage under a constant stress level $\sigma(t) = \bar{\sigma}_0$ (Figure 1.c). In addition, the initial condition $\delta(t_{cr}) = 0$ with $t_{cr} = \max\{t \mid \sigma(t) \leq \sigma_{cr}\}$ is assumed, where $\sigma_{cr} \leq \bar{\sigma}_0$ is a critical stress threshold.

The index $\delta = \delta(t)$ fully describes the damage evolution in each point of the structure. However, due to its *local* nature, it does not seem handy for design purposes. A more synthetic *global* measure of damage $\hat{\delta} = \hat{\delta}(t)$ may be easily computed as the average of δ over the volume of the whole structural system (Biondini 2004, Azzarello et al. 2006).

3 LIFETIME OPTIMALITY CRITERIA

3.1 *Structural cost*

Several quantities able to represent the structural performance may be chosen as targets for the optimal design. In the following, the adopted design target is the total cost C of the structure over its service lifetime, given by the sum of the initial cost C_0 and maintenance cost C_m:

$$C = C_0 + C_m \tag{3}$$

The initial cost C_0 is computed as follows:

$$C_0 = cV_0 \tag{4}$$

where V_0 *is* the total volume of material and c is the corresponding unit cost. The maintenance cost C_m can be evaluated by summing the costs of the individual interventions:

$$C_m = \sum_{k=1}^{r} \frac{C_m^k}{(1+v)^{(t_k - t_0)}} \tag{5}$$

where the cost C_m^k of each intervention $k = 1, \ldots, r$ has been referred to the initial time t_0 by taking a proper discount rate v into account (Kong and Frangopol 2003).

3.2 *Maintenance scenario*

The previous general formulation is now specialized to a prescribed maintenance scenario. In this scenario an essential maintenance aimed to totally restore the initial structural performance is performed after each design period T_D, or at each time instant $t_k = (t_0 + kT_D)$. In this way, all the interventions have the same cost $C_m^k = C_m^1$, and the total number of interventions applied during a prescribed service lifetime T_S is $r = [\text{int}(T_S/T_D) - 1]$. Therefore, the cost of maintenance is:

$$C_m = C_m^1 \sum_{k=1}^{r} \frac{1}{(1+v)^{kT_D}} = C_m^1 q \tag{6}$$

where the factor $q = q(T_S, T_D, v) \leq r$ depends on the prescribed parameters T_S, T_D, and v only.

The cost C_m^1 of the single intervention is related to the level of structural damage developed during each design period T_D. Since damage is not recovered during time, a measure of this damage is given by the global damage index $\hat{\delta} = \hat{\delta}(t)$ evaluated at the end of each design period T_D, or:

$$\tilde{\delta} = \hat{\delta}(t_k) = \hat{\delta}(t_{k-1} + T_D), \qquad k=1,\ldots,r \tag{7}$$

Based on the lifetime global damage index $\tilde{\delta}$, the following linear relationship is assumed:

$$C_m^1 = C_0 \tilde{\delta} \tag{8}$$

and the total lifetime structural cost C is finally formulated as follows:

$$C = C_0(1 + \tilde{\delta} q) \tag{9}$$

3.3 *Role of maintenance cost*

To highlight the actual role played by a prescribed maintenance program, the design of the tensioned bar shown at the top of Figure 2 is investigated. By denoting with d_0 the diameter of the undamaged cross-section, the total cost of the bar over the prescribed service lifetime T_S is:

$$C = C_0(1 + \tilde{\delta} q) = cA_0 L(1 + \tilde{\delta} q) = c\frac{\pi d_0^2 L}{4}(1 + \tilde{\delta} q) \tag{10}$$

with $\tilde{\delta} = \tilde{\delta}(d_0)$. The diameter d_0 must be chosen in such a way that the acting stress $\sigma = \sigma(t)$ is no larger than the admissible stress $\overline{\sigma} = \overline{\sigma}(t)$ over the prescribed design period T_D:

$$\sigma(t) = \frac{F}{A(t)} = \frac{F}{A_0[1-\delta(t)]} = \frac{4F}{\pi d_0^2[1-\delta(t)]} \leq \overline{\sigma}(t) = \overline{\sigma}_0[1-\delta(t)] \tag{11}$$

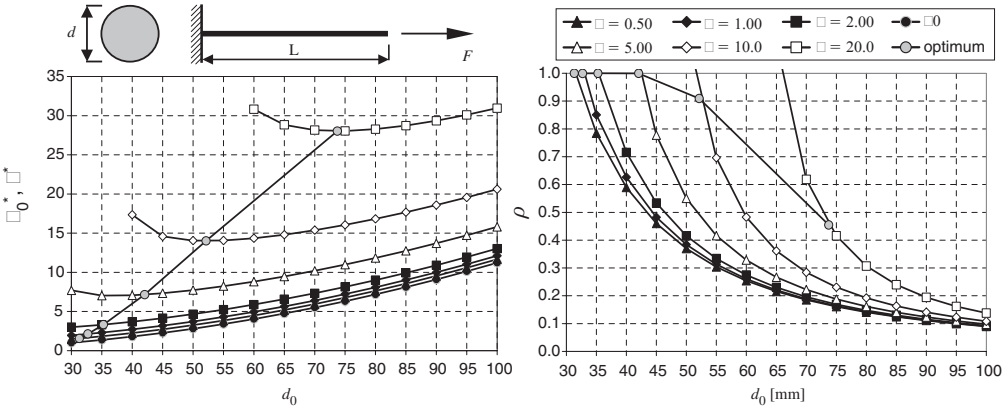

Figure 2. Lifetime cost and structural efficiency of a tensioned bar undergoing damage.

with $\delta(t) = \delta(d_0, t)$. In case damage is not considered ($\delta = \tilde{\delta} = 0$), the minimum cost solution d_0^* is simply given by the minimum diameter d_0 which satisfies the stress constraint:

$$d_0^* = d_{0,\min} = \sqrt{\frac{4F}{\pi \overline{\sigma}_0}} \qquad C^* = C(d_0^*) = C_0(d_0^*) = c\frac{FL}{\overline{\sigma}_0} \tag{12}$$

On the contrary, when damage is properly included in the design problem, the minimum cost solution d_0^* is, in general, no longer associated with the diameter $d_{0,\min}$. In fact, higher d_0^*-values may be required to achieve a balance between the maintenance cost and the amount of damage.

These aspects are highlighted in Figure 2, where both the cost and structural efficiency of the bar versus its diameter d_0 are shown for different values of the damage rate $\theta = T_S/T_\delta$, with $\sigma_{cr} = 0$, $\alpha = 1$, and with reference to the following case study: $F = 70$ kN, $\overline{\sigma}_0 = 100$ MPa, $T_S = 100$ years, $T_D = 10$ years, and $\nu = 0$ ($q = r$). In particular, the diagrams shown in Figure 2 refer to the following quantities:

$$\chi_0^* = C_0/C^* \qquad \chi_m^* = C_m/C^* \qquad \chi^* = \chi_0^* + \chi_m^* \qquad \rho = \sigma(T_D)/\overline{\sigma}(T_D) \tag{13}$$

where C^* denotes the optimal cost without damage ($\theta = 0$). The following remarks can be made:

- The minimum feasible diameter without damage is $d_{0,\min} = 29.9$ mm. Its value increases with θ.
- The initial cost χ_0^* increases and the maintenance cost χ_m^* decreases when d_0 increases. For a given value of d_0, the maintenance cost χ_m^* increases with θ.
- The total cost χ^* has a minimum for $d_0^* \geq d_{0,\min}$, and the optimal diameter d_0^* increases with θ.
- The stress ratio ρ decreases with d_0 and increases with θ. The optimal solution d_0^* at the end of the design period T_D may be not fully stressed ($\rho^* \leq 1$).

Similar results are obtained by varying the parameter T_D (Azzarello 2005).

4 LIFETIME STRUCTURAL OPTIMIZATION

4.1 *Formulation of the optimization problem*

The purpose of a one-target lifetime design process is to find a vector of design variables $\mathbf{x} \in \Re^n$ which optimizes the value of an objective function $f(\mathbf{x})$, according to both side constraints with

bounds $\mathbf{x}^-$ and $\mathbf{x}^+$, and inequality time-variant behavioral constraints $\mathbf{g}(\mathbf{x},t) \leq 0$:

$$\min_{\mathbf{x}\in D} f(\mathbf{x}) \qquad D = \left\{ \mathbf{x} \mid \mathbf{x}^- \leq \mathbf{x} \leq \mathbf{x}^+,\ \mathbf{g}(\mathbf{x},t) \leq \mathbf{0} \right\} \tag{14}$$

Based on the previously introduced cost concepts, the objective function $f(\mathbf{x})$ to be minimized is related to the total lifetime cost C of the structure as follows:

$$f(\mathbf{x}) \equiv C(\mathbf{x})/c = V_0(\mathbf{x})[1 + \tilde{\delta}(\mathbf{x})q] \tag{15}$$

The time-variant behavioral constraints are related to the corresponding structural response by means of the stress $\sigma_{i,\ell} = \sigma_{i,\ell}(t)$ and displacement $u_{j,\ell} = u_{j,\ell}(t)$ associated with each element i, nodal point j, and loading condition ℓ, as follows:

$$\begin{cases} \overline{\sigma}^-_{i,\ell}(\mathbf{x},t) \leq \sigma_{i,\ell}(\mathbf{x},t) \leq \overline{\sigma}^+_{i,\ell}(\mathbf{x},t) \\ -\sigma_{i,\ell}(\mathbf{x},t) \leq \overline{\sigma}^{cr}_{i}(\mathbf{x},t) \end{cases} \qquad \overline{u}^-_{j,\ell} \leq u_{j,\ell}(\mathbf{x},t) \leq \overline{u}^+_{j,\ell} \tag{16}$$

where $\overline{\sigma}^-_{i,\ell} = \overline{\sigma}^-_{i,\ell}(t)$ and $\overline{\sigma}^+_{i,\ell} = \overline{\sigma}^+_{i,\ell}(t)$ are the minimum and maximum allowable stress, respectively, $\overline{u}^-_{j,\ell}$ and $\overline{u}^+_{j,\ell}$ are prescribed displacement bounds, and $\overline{\sigma}^{cr}_i = \overline{\sigma}^{cr}_i(t)$ is the critical stability threshold. Constraints on both local and global damage may be also introduced (Azzarello *et al.* 2006). This optimization problem is solved by using a gradient-based method (Vanderplaats, 2001).

4.2 *The case of reinforced concrete structures*

The general approach previously presented can be easily extended to the special case of reinforced concrete structures. First, the damage evolution in concrete and steel is described by means of two damage indices $\delta_c = \delta_c(t)$ and $\delta_s = \delta_s(t)$, respectively. Second, the initial cost C_0 is computed as follows:

$$C_0 = c_c V_{c,0} + c_s V_{s,0} = c_c (V_{c,0} + \kappa V_{s,0}) = c_c V^*_{c,0} \tag{17}$$

where$V_{0,c}$, $V_{0,s}$, are the total volumes of concrete and steel, respectively, c_c, c_s, are the corresponding unit costs, $\kappa = c_s/c_c$ is the unit cost ratio, and $V^*_{c,0}$ is the equivalent volume of concrete. Finally, focusing the attention on the Serviceability Limit State (SLS), the time-variant behavioral constraints on the stress state associated with each loading condition ℓ are related to the stress in both concrete fibers $\sigma_{c,i,\ell} = \sigma_{c,i,\ell}(t)$ and steel bars $\sigma_{s,i,\ell} = \sigma_{s,i,\ell}(t)$ of each element i:

$$\begin{cases} \overline{\sigma}^-_{c,i,\ell}(\mathbf{x},t) \leq \sigma_{c,i,\ell}(\mathbf{x},t) \leq \overline{\sigma}^+_{c,i,\ell}(\mathbf{x},t) \\ \overline{\sigma}^-_{s,i,\ell}(\mathbf{x},t) \leq \sigma_{s,i,\ell}(\mathbf{x},t) \leq \overline{\sigma}^+_{s,i,\ell}(\mathbf{x},t) \end{cases} \tag{18}$$

Clearly, additional constraints related to the Ultimate Limit States (ULS) may be also introduced, even though they are not considered here.

5 APPLICATIONS

5.1 *Steel truss*

The proposed formulation is applied to the lifetime optimization of the truss structure shown in Figure 3.a. Three alternative loading conditions are considered: (a) $F_z = F = 1$ MN and $F_y = 0$; (b) $F_z = 0$ and $F_y = F$; (c) $F_z = F_y = F$. It is worth noting that, in general, the response to the loading condition (c) is not given by the superposition of (a) and (b), since the system properties vary during time.

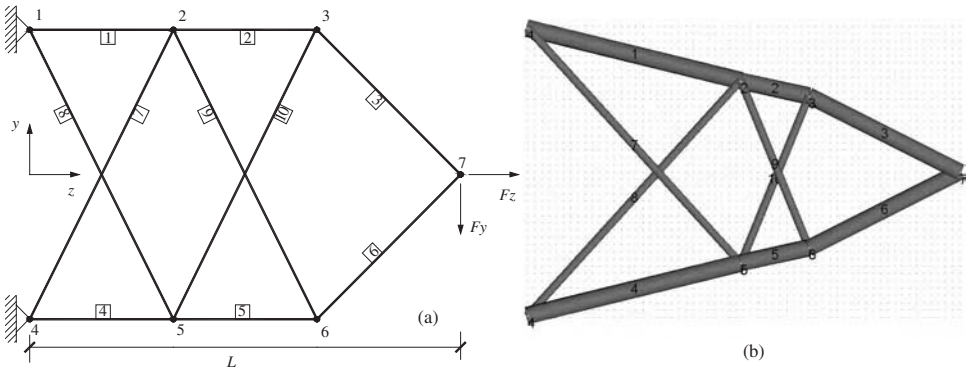

Figure 3. Truss structure. (a) Design model. (b) Optimal solution without damage ($\theta = 0$).

Table 1. Truss structure. Optimal value of the design variables without damage ($\theta = 0$).

d_1 [mm]	d_2 [mm]	d_3 [mm]	d_8 [mm]	d_9 [mm]	y_1 [mm]	z_2 [mm]	y_2 [mm]	z_3 [mm]	y_3 [mm]
120.5	116.5	115.7	57.7	57.8	988.9	1478.6	627.2	1952.2	522.2

A circular cross-section with diameter d_i is assumed for each member $i = 1, \ldots, 10$. The structural shape is defined by the coordinates (z_j, y_j) of each node $j = 1, \ldots, 7$. The design model is based on the following geometrical constraints: $d_1 = d_4$, $d_2 = d_5$, $d_3 = d_6$, $d_7 = d_8$, $d_9 = d_{10}$, $z_1 = z_4 = 0$; $y_1 = y_4$, $(z_2, y_2) = (z_5, y_5)$, $(z_3, y_3) = (z_6, y_6)$, $y_7 = 0$, $z_7 = L = 3\,\text{m}$. Therefore, the optimization problem is defined by $n = 10$ design variables $\mathbf{x} = [d_1 d_2 d_3 d_8 d_9 |\ y_1 z_2 y_2 z_3 y_3]^T$, for which the following side constraints are assumed: $0.05\,\text{m} \le d_i \le 0.50\,\text{m}$; $0.10\,\text{m} \le y_j \le 1.00\,\text{m}$; $0.10\,\text{m} \le z_2 \le 2.80\,\text{m}$; $0.20\,\text{m} \le z_3 \le 2.90\,\text{m}$. For the behavioral constraints the initial allowable stress $\overline{\sigma}^+_{0,i,\ell} = -\overline{\sigma}^-_{0,i,\ell} = \overline{\sigma}_0 = 160\,\text{MPa}$ is considered for each member i and loading condition ℓ.

In case damage is not considered, the optimal solution described in Figure 3.b and Table 1 is achieved. This solution is compared with the structures shown in Figure 4, obtained by solving the lifetime optimization problem with reference to a service lifetime $T_S = 100$ years and a damage rate $\theta = T_S/T_\delta = 10$, with $\sigma_{cr} = 0$ and $\alpha = 1$, for different design monitoring periods $T_D = \{1, 50$ years$\}$ and discount rates $v = \{0, 3\%\}$. This comparison, together with the results obtained for other values of the parameters v and T_D (Azzarello, 2005), leads to the following general conclusions:

- The optimal design solution $\mathbf{x}^*$ strongly depends on both the parameters T_D and v. In particular, both such parameters influence the optimal dimension of the cross-sections, while the v-values tend to significantly affect the optimal location of the nodal points only.
- The initial cost χ_0^* strongly increases with T_D, and does not significantly depend on v.
- The maintenance cost χ_m^* decreases with both T_D and v.
- The total cost χ^* increases with T_D, and decreases with v. This tendency highlights the expected higher cost-effectiveness of a maintenance planning with frequent interventions over more conventional maintenance-free design strategies.
- The lifetime damage index $\tilde{\delta}$ increases with T_D, and does not significantly depend on v.
- Despite no constraints are imposed on the nodal displacements, the maximum deflection does not significantly depend on T_D and v. In particular, the maximum vertical displacement of node 7 approximately equals the optimal value associated with the undamaged scenario ($u_{y7} = 5.1$ mm).

Similar results are obtained by varying the parameter θ in the range $0.50 \div 20$ (Azzarello, 2005). Clearly, higher θ-values lead to more ponderous optimal structures and, consequently, to higher values of the optimal cost components.

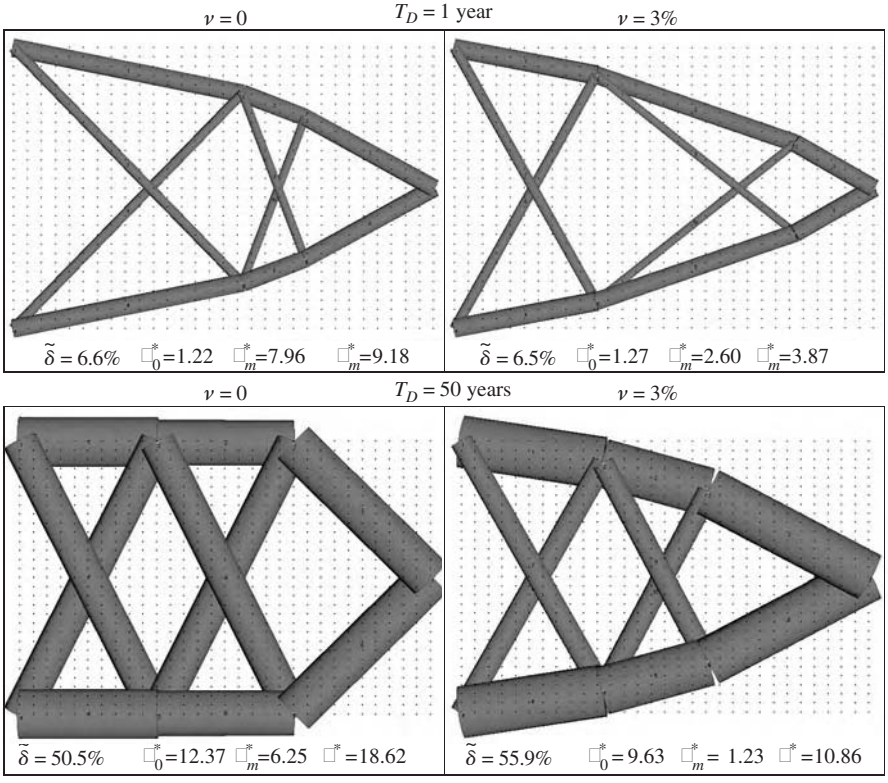

Figure 4. Truss structure. Optimal solutions in a design scenario with damage ($\theta = T_S/T_\delta = 10$, $T_S = 100$ years) for different values of the design monitoring period $T_D = \{1, 50$ years$\}$ and of the discount rate $\nu = \{0, 3\%\}$.

5.2 *Reinforced concrete frame*

The previous formulation is applied to the lifetime optimization of the reinforced concrete frame shown in Figure 5.a. A rectangular cross-section is assumed for both beam and columns. With reference to Figures 5.a and 5.b, the optimization problem is defined by $n = 9$ design variables $\mathbf{x} = [b\, h_1\, h_2 \,|\, A_1\, A_2\, A_2'\, A_3\, A_3' \,|\, d]^T$, for which the following side constraints are assumed: $b \geq 300$ mm; $1 \leq h_j/b \leq 2$, $i = 1,2$; $A_i \geq 2\,\text{Ø}\,12$ and $A_j' \geq 2\,\text{Ø}\,12$, $i = 1,2,3$; $0.10 \leq d/L \leq 0.50$.

The three alternative loading conditions shown in Figure 6 are considered. Since the SLS is investigated, the time-variant structural response in terms of nodal displacements and internal stress resultants are evaluated by assuming a linear elastic behavior. Based on the general criteria for concrete design, the corresponding stress in the materials are computed at the cross-sectional level by assuming for concrete a linear elastic behavior in compression with $E_c = 30$ GPa and no strength in tension ($\overline{\sigma}_c^+ = 0$), and for steel a linear elastic behavior in both tension and compression with $E_s = 15E_c$.

The same behavioral constraints are considered for each loading condition. The stress in the materials is verified in each member by assuming the initial allowable stress $-\overline{\sigma}_{c,0}^- = 15$ MPa for concrete, and $\overline{\sigma}_{s,0}^+ = -\overline{\sigma}_{s,0}^- = 180$ MPa for steel. The displacement constraints $u_x \leq 20$ mm and $u_y \leq 10$ mm over the whole service lifetime are also considered (Figure 5.a).

The lifetime performances are defined by the following parameters: service lifetime $T_S = 100$ years, design period $T_D = 10$ years, unit cost ratio $\kappa = 20$, discount rate $\nu = 3\%$, and damage rate $\theta = T_S/T_\delta = 10$, with $\sigma_{cr} = 0$ and $\alpha = 1$ for both concrete and steel. Moreover, to investigate the role of the spatial distribution of deterioration, the damage scenarios described in Table 2 are considered.

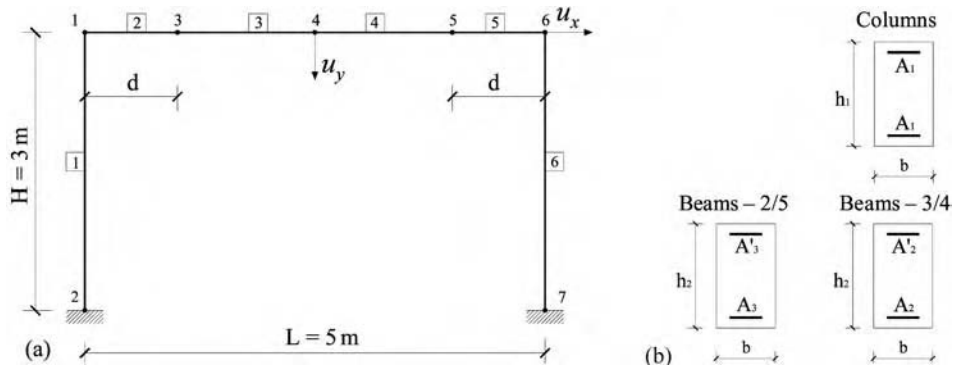

Figure 5. Reinforced concrete frame. (a) Geometrical dimensions and structural model. (b) Cross-sections of beam and columns.

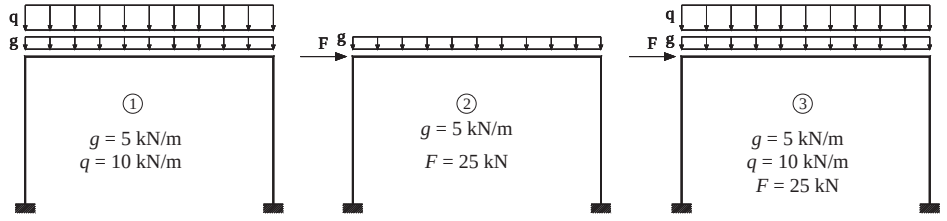

Figure 6. Reinforced concrete frame. Loading conditions.

Table 2. Reinforced concrete frame. Damage scenarios ($\theta = T_S/T_\delta = 10$, $T_S = 100$ years).

Damage scenario	Left column	Beam	Right column
A	–	–	–
B	Damage	Damage	Damage
C	–	Damage	–
D	Damage	–	Damage
E	Damage	Damage	–
F	–	Damage	Damage

The direct comparison of the optimal solutions shown in Figure 7 shows that the optimal dimensions of the cross-sections, as well as the optimal amount and distribution of reinforcement, strongly depend on the prescribed damage scenario. In particular, it is worth noting that damage leads to a more ponderous design not only for members affected by deterioration. In fact, due to redundancy, damage induces a time-variant redistribution process in which the internal stress resultants tend to progressively move towards the undamaged members.

6 CONCLUSIONS

A new conceptual approach to the minimum lifetime cost of deteriorating structures under multiple loading conditions has been presented. This approach allowed to overcome the inconsistencies involved in the classical formulation of the optimum design problem, where the time evolution of the structural performance induced by the progressive deterioration of the system properties is not adequately considered. In fact, in the proposed formulation, the structural damage is accounted

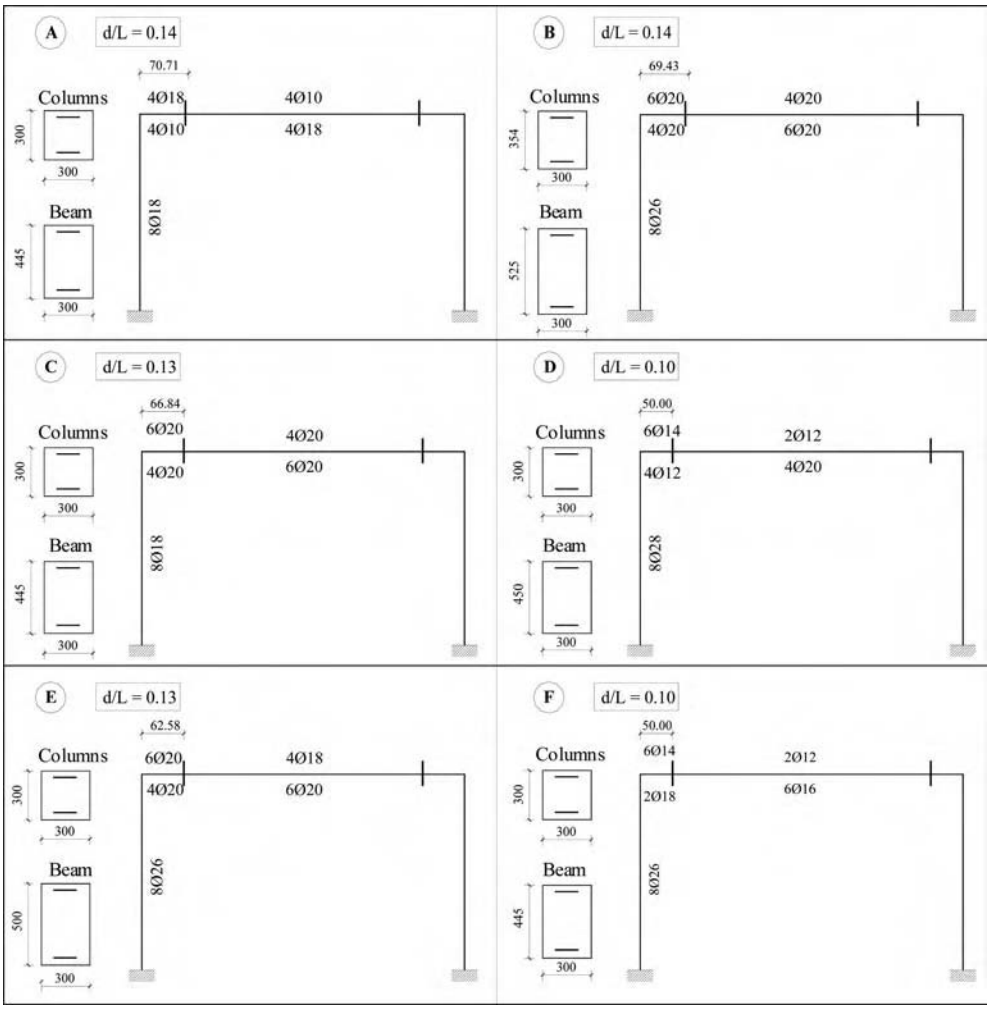

Figure 7. Reinforced concrete frame. Optimal design solutions associated with the damage scenarios described in Table 2 ($\theta = T_S/T_\delta = 10$, $T_S = 100$ years, $T_D = 10$ years, $\kappa = 20$, $\nu = 3\%$).

for by means of a proper material degradation law of the mechanical properties, and the design constraints of the optimization problem are related to the corresponding time-variant structural performance over the whole expected service lifetime of the construction. In addition, the objective function is formulated by accounting for both the initial cost of the structure and the costs of possible maintenance interventions, that are properly discounted over time and assumed to be proportional to the actual level of structural damage.

The lifetime optimization of a steel truss and of a reinforced concrete frame proved the effectiveness of the proposed approach by highlighting that the optimal solution strongly depends on both the time-variant structural performance and the maintenance planning.

REFERENCES

Azzarello, L., 2005. Ottimizzazione di Sistemi Strutturali con Prestazioni Variabili nel Tempo. Degree Thesis, Politecnico di Milano, Milan, Italy (In Italian).

Azzarello, L., Biondini, F., Marchiondelli, A., 2006. Optimal Design of Deteriorating Structural Systems. *3rd Int. Conference on Bridge Maintenance, Safety and Management (IABMAS'06)*, Porto, July, 16–19.

Biondini, F., Bontempi, F., Frangopol, D.M., and Malerba, P.G., 2004. Cellular Automata Approach to Durability Analysis of Concrete Structures in Aggressive Environments. *ASCE Journal of Structural Engineering*, **130**(10), 1724–1737.

Biondini, F., Marchiondelli, A., 2006*a*. Lifetime Structural Optimization. *European Symposium on Service Life and Serviceability of Concrete Structures (ESCS-2006)*, Helsinki, June 12–14 – Keynote Paper, 1–12.

Biondini, F., Marchiondelli, A., 2006*b*. Evolutionary Design of Structural Systems with Time-variant Performance. *Structure and Infrastructure Engineering* – Tentatively accepted for publication.

Biondini, F., 2004. A Three-dimensional Finite Beam Element for Multiscale Damage Measure and Seismic Analysis of Concrete Structures. *13th World Conference on Earthquake Engineering*, Vancouver, B.C., Canada, August 1–6, Paper No. 2963.

Kong, J.S., Frangopol, D.M., 2003. Evaluation of Expected Life-Cycle Maintenance Cost of Deteriorating Structures. *ASCE Journal of Structural Engineering*, **129**(5), 682–691.

Vanderplaats, G.N., 2001. *DOT – Design Optimization Tool*, Vanderplaats Research & Development, Colorado Springs, CO, USA.

Reliability and Optimization of Structural Systems: Assessment, Design and Life-Cycle Performance – Frangopol, Kawatani & Kim (eds)
© 2007 Taylor & Francis Group, London, ISBN 978-0-415-40655-0

Seismic reliability functions for complex systems based on a secant-stiffness reduction index

Luis Esteva & Orlando J. Díaz-López
Institute of Engineering, National University of Mexico

ABSTRACT: The stiffness-reduction index proposed in this study can be efficiently used for the determination of second moment probabilistic descriptions of Z_F, the natural logarithm of the minimum value of the intensity required to produce collapse of a complex nonlinear system and, therefore, for the determination of seismic reliability functions of those systems. This is achieved while avoiding the need to depend on the determination of a lateral deformation capacity, which is very sensitive to the strength and stiffness degradation of the system due to its cyclic response, as well as to its lateral configuration at the instant of impending collapse.

The determination of the reliability index β is based on the determination of the mean and standard deviation of Z_F, on the basis of a statistical sample of values of Z, the natural logarithm of the intensity, and I_{SSR}, the stiffness-reduction index, in the vicinity of $I_{SSR} = 1.0$. Information derived from sample points with I_{SSR} cannot be directly taken into account through a conventional least-squares regression analysis, because the corresponding intensities may be equal to or larger than the required minimum values. The maximum likelihood approach presented here is more efficient than one previously proposed by Esteva and Ismael (2004) when only the collapse failure mode is of interest in the evaluation of the seismic vulnerability of a system.

1 INTRODUCTION

In practical engineering applications related to performance-based earthquake-resistant design, the estimation of the seismic reliability of complex nonlinear systems for given values of the ground-motion intensity is ordinarily based on a measure of the probability that the ratio of the lateral deformation capacity of the system to the peak value of the corresponding nonlinear response demand for an ensemble of earthquake excitations with the specified intensity is greater than unity. For this purpose, the intensity must be measured by an adequate indicator, having a high statistical correlation with the seismic response of the system of interest. This is ordinarily achieved using the ordinate of the linear response spectrum for the fundamental period of the system. Approximate estimates of second-moment probabilistic indicators of both variables (response demand and deformation capacity) are often obtained with the aid of a simplified reference system, characterized by mechanical properties determined by means of a static pushover analysis of the detailed system. A normalized value of the intensity can then be used, such as the expected value of the ductility demand on the simplified reference system (Esteva et al, 2002a, b).

Probabilistic estimates of the deformation capacities of complex systems obtained by means of pushover analysis are tied to severe limitations, because according to this approach it is not possible to account for (a) the influence of cumulative damage associated with the cyclic response, and (b) the dependence of the lateral deformation capacity on the response configuration of the system when it approaches failure.

Trying to avoid the introduction of arbitrary assumptions about the determination of the deformation capacity, alternative criteria have been proposed, according to which system failure is assumed

to take place when the displacements predicted by the dynamic response analysis become indefinitely large and non-reversible. The effective values of the elements of the resulting stiffness matrix are then infinitely small. This condition is described as system collapse (Esteva, 1992; Shome and Cornell, 1999; Esteva and Alamilla, 2006). In order to determine the safety factor of a given system with respect to this type of failure for a given ground motion time history, it is necessary to obtain the scale factor that has to be applied to that time history in order to produce system collapse. The intensity leading to collapse is then denoted as "*failure intensity*". Because the determination of the needed scaling factor has to be attained by means of an iterative procedure, it may call for excessive demands of computer time.

The method of Incremental Dynamic Analysis (IDA, Vamvatsikos and Cornell, 2002) offers both possibilities for the estimation of probabilistic indicators of seismic reliability for given ground motion intensities: either on the basis of deformation capacities or using the concept of failure intensity. According to this method, the lateral deformation capacity of the system of interest is defined as the value of the peak roof displacement when the slope of the incremental dynamic response function (spectral acceleration vs peak roof displacement) becomes lower than a specified value; this point also serves to define the failure intensity. The possibility to visualize the evolution of the lateral roof displacement as the intensity grows, as well as to observe the values reached by the ground motion intensity before the occurrence of unbounded peak roof displacements constitutes a significant asset of the method. However, these advantages are often tied to excessive computer time demands (Dolsek and Fajfar, 2004).

In this paper an alternative approach is explored, aiming at estimating reliability functions relating the reliability index β (Cornell, 1969) with the ground motion intensity, including the influence of cumulative damage and avoiding the need to obtain probabilistic definitions of lateral deformation capacities. This approach is based on the concept of "*failure intensity*", mentioned above.

2 SECANT-STIFFNESS REDUCTION INDEX

Esteva and Ismael (2004) define the collapse condition in terms of a secant-stiffness reduction index $I_{SSR} = (K_0 - K)/K_0$, where K_0 is the initial tangent stiffness associated with the base-shear *vs* roof displacement curve resulting from pushover analysis and K is the secant stiffness (base shear divided by lateral roof displacement) when the lateral roof displacement reaches its maximum absolute value during the seismic response of the system. The failure condition is expressed as $I_{SSR} = 1.0$. For a given value of the intensity (y), the probability density function of $Q = \ln I_{SSR}$ is equal to $f_Q(q)$, which is continuous for $q < 0$ and includes a discrete concentration at q= 0, which is equal to $p_F(y) = P[Q = 0|y]$, the failure probability for an intensity equal to y. In order to permit the joint analysis of information including cases with values of Q smaller than or equal to 0, an auxiliary variable U is introduced, such that $Q = U$ for $Q < 0$ and $Q = 0$ for $U \geq 0$ (that is, for the failure condition). The probability density function of U is designated by $f_U(\cdot)$, and the associated cumulative distribution function by $F_U(\cdot)$. These functions are characterized by a set of parameters $\{\kappa\}$ that determine their basic properties, such as mean, standard deviation and skewness. (For instance, in the case of a Gaussian distribution, $\{\kappa\}$ may be made by the mean and the standard deviation.) These parameters can in turn be expressed as functions of y, $G(y|\alpha)$, with given form and unknown parameters. It is also assumed that we count with a set of $m + n$ pairs of values of the normalized intensity μ_{0i}, and the corresponding logarithmic damage index $Q = q_i$, the latter obtained by means of a step-by-step time history dynamic response analysis. Under the assumption that these pairs of values are ordered so that Q is smaller than 0 (survival condition) for the first m cases, and equal to 0 for the remaining n cases, the likelihood function is expressed as follows in terms of α:

$$L(\alpha) = \prod_{i=1}^{m} f_U\left(u_i|y_i,\alpha\right)\prod_{j=1}^{n}\left[1 - F_U\left(0|y_j,\alpha\right)\right] \tag{1}$$

The vector of parameters α is determined by means of a maximum likelihood approach applied to the sample of pairs of values of Y and Q.

This paper follows an approach proposed by Esteva and Díaz-López (2006). According to it, a reliability function $\beta(y)$ is obtained from a sample of pairs of values of I_{SSR} and y, where β is the safety index proposed by Cornell (1969) and y is the ground motion intensity. If the sample includes only cases with I_{SSR} smaller 1.0, the reliability function can be obtained by means of a regression analysis; if cases with $I_{SSR} = 1.0$ are also included, a maximum likelihood analysis must be performed. Instead of formulating the problem as that of obtaining an indicator of the probability that $I_{SSR} < 1.0$ (survival) for a given intensity, attention is focused on the determination of second moment indicators of the probability distribution of $Z_F = \ln Y_F$, where Y_F is the minimum value of the intensity leading to the condition $I_{SSR} = 1.0$ (collapse). For an earthquake with intensity equal to y, a safety margin Z_M can be defined equal to the natural logarithm of the ratio of the system capacity to the amplitude of its response to the given intensity; it can also be defined as the natural logarithm of the ratio Y_F/y. The reliability function can then be expressed as follows:

$$\beta(y) = \left(E(Z_F) - \ln y\right) / \sigma(Z_F) \tag{2}$$

Here, $E(\cdot)$ and $\sigma(\cdot)$ stand for *expected value* and *standard deviation*, respectively.

For the structural system of interest, a sample of pairs of random values of Z and the stiffness reduction index, I_{SSR}, can be used to estimate means and standard deviations of $Z(u)$, the latter defined as the natural logarithm of the random intensity Y that corresponds to $I_{SSR} = u$. The values of Z in the sample that correspond to values of I_{SSR} equal to 1.0 are upper bounds of $Z_F = \ln Y_F$, where Y_F is the minimum value of Y required to produce system failure. Therefore, the points corresponding to these values of Z_F cannot be incorporated into the sample used to estimate $E(\mathrm{Z}(u))$ and $\sigma(\mathrm{Z}(u))$ by means of conventional minimum-squares regression analysis. However, they can be included in the estimation process, through a maximum likelihood analysis slightly different from that proposed by Esteva and Ismael (2004).

The expected value and the standard deviation of $\mathrm{Z}(u)$ will now be represented by the functions $E(\mathrm{Z}(u)|\alpha_1)$ and $\sigma(\mathrm{Z}(u)|\alpha_2)$, with a given form and unknown vectors, α_1 and α_2, of the parameters to be estimated using a sample including m values of I_{SSR} smaller than 1.0 and n values equal to 1.0. For the observed sample, the likelihood function of (α_1, α_2) can be expressed as follows:

$$L(\alpha_1, \alpha_2) = \prod_{i=1}^{m} f_Z\left(z_i | u_i, \alpha_1, \alpha_2\right) \prod_{j=1}^{n} \left[1 - F_Z\left(z_j | u_j, \alpha_1, \alpha_2\right)\right] \tag{3}$$

In order to get sufficiently accurate estimates of the mean and the standard deviation of Z_F, without an excessively large computational effort, it is convenient to generate samples containing a large proportion of its points with values of I_{SSR} slightly smaller than 1.0. This can be achieved by means of an algorithm that includes two basic steps: (a) an approximate probabilistic relation between I_{SSR} and Z is first obtained from a small sample of those variables, and (b) a new sample of values of I_{SSR} is determined for a set of simulated ground motion records, with their intensities chosen in such a manner that they have high probabilities of producing damage levels in the required intervals. The probabilistic relation just mentioned may be as simple as the expected value of $Z = \ln Y$ as a function of I_{SSR}.

3 ILLUSTRATIVE EXAMPLES

3.1 *Systems studied*

Rangel (2006) has applied the algorithm proposed in the preceding section to the determination of the reliability functions of a number of multistory frame building systems, provided with hysteretic energy-dissipating devices (EDD). Among other cases, he has studied a set of multistory buildings

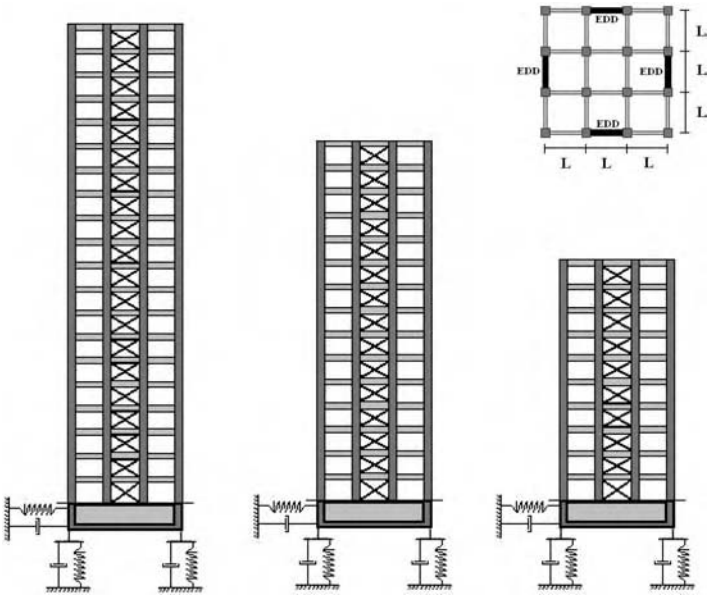

Figure 1. Cases studied: elevation and plan.

with the global geometrical properties shown in Figure 1. In all cases, the bay width L was taken equal to 600 cm, and the story height h was taken equal to 300 cm, except that of the ground story, which was taken equal to 400 cm. They were all assumed to be built at a soft soil site in the Valley of Mexico. Therefore, it was deemed adequate to account for the influence of soil-structure interaction on the dynamic responses of the systems and on their corresponding reliability functions. The sets of springs and dampers shown in the figure at the bases of the buildings are intended for this purpose. Three different levels of contribution of the EDD's to the lateral story strength and stiffness were considered for the combined systems (conventional frame plus EDD's) in each set: 0 (conventional frame system), 50 and 75 percent. The conventional system was designed in accordance with the 2004 edition of Mexico City seismic design code (NTCDS-RCDF, 2004). The systems including EDD's were designed in such a manner that the lateral strength and stiffness of each story was equal (within a 5 percent tolerance) to the values of the corresponding conventional system. These conditions were established on the basis of the expected values of the mechanical properties of the structural members.

3.2 *Seismic excitations*

The systems ere assumed to be built at the SCT soft-soil site, in the Valley of Mexico, with a dominant ground period of 2.0 seconds. A sample of ground motion time histories with evolutionary statistical properties similar to those of the earthquakes likely to occur at that site was generated. For each system considered, the intensities were expressed in terms of the ordinates of the linear pseudo-acceleration response spectra for the fundamental period of the system (calculated using the expected values of gravitational loads and mechanical properties). The sample contained both low- and moderate-intensity actual records, and high-intensity artificial ground motion time histories; the latter were simulated in accordance with the hybrid method proposed by Ismael & Esteva (2006). Figure 2 shows the ground acceleration time histories and the pseudo-acceleration response spectra for several elements of the sample.

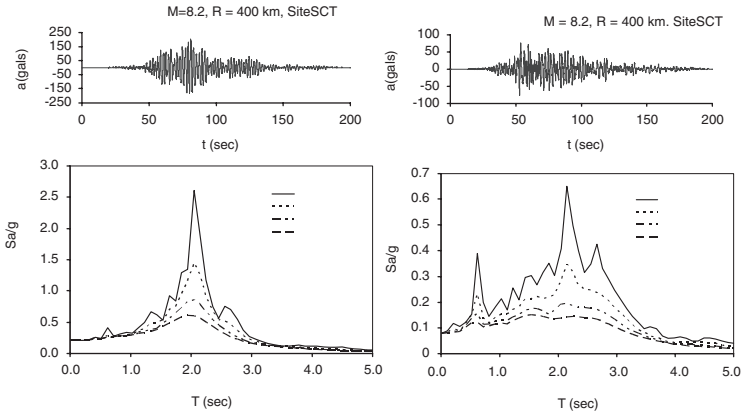

Figure 2. Acceleration time history and linear response spectra for two large-magnitude earthquakes generated at seismic sources affecting Mexico City, SCT site: soft soil, dominant ground period = 2 s.

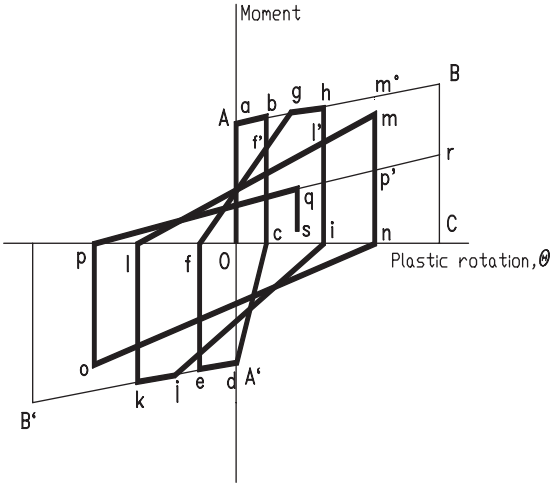

Figure 3. Constitutive function for moment *vs* plastic-rotation at bending member ends.

3.3 *Nonlinear seismic response models*

For the purpose of evaluating the nonlinear seismic response of each system to a ground acceleration time history, the mechanical behavior of each structural member subjected to alternating-sign deformation cycles was represented by assuming that nonlinear behavior in bending was concentrated at each beam or column, in the form of a hinge with a moment *vs* rotation constitutive function similar to that shown in Figure 2. The model (Esteva et al, 1999, adapted from Wang and Shah, 1987) considers that both local strengths and stiffness values in each loading direction deteriorate gradually, as functions of the damage accumulated in that direction. The model is defined by six parameters: F_y, K_1, K_2, X_F, a and α. The first three are respectively the yield strength and the tangent stiffness before and after yielding; they determine the force-deformation envelope curve. X_F is the deformation associated with the peak value of the load, while a and α serve to transform the low-cycle-fatigue index given by the summation term in the second member of Equation 4 into the damage index D (Equation 5). This index measures the degradation of the internal force corresponding to the maximum deformation amplitude reached during previous loading cycles (See Figure 3).

According to the model proposed here,

$$q = a\sum_{i=1}^{N}\frac{X_i}{X_F} \tag{4}$$

and

$$D = 1.0 - \exp(-\alpha q) \tag{5}$$

where X_i is the deformation-amplitude in the direction of interest during the i-th cycle and N is the number of cycles. These functions are used here to represent the degrading hysteretic behaviour of plastic hinges at critical sections of flexural members. On the basis of experimental evidence given by Wang and Shah (1987), a was taken equal to unity, and α equal to 0.602. According to Equation 5, the load carrying capacity of the element considered is not completely lost when $q = 1$. This is in better agreement than the original model with both the laboratory results and the behavior of full-scale systems responding to real earthquakes.

A bilinear model with stable hysteresis loops for a large number of cycles will be used to represent the cyclic behavior of energy-dissipating devices. The form and the parameters of the model adopted here are consistent with the laboratory tests performed on assemblages of U-shaped devices developed by Aguirre and Sánchez (1992). An expression of the form given by Equation 6 was fitted to their results:

$$N_F(x) = \exp(ax^{-b} - c) \tag{6}$$

Here, $N_F(x)$is the number of cycles to failure under a sequence of cycles with a constant amplitude equal to x(cm); $a = 128$, $b = 0.02$ and $c = 121$.

3.4 *Determination of seismic reliability functions*

In order to obtain the reliability functions of the form given in Equation 2, uncertainties about gravitational loads and mechanical properties of structural members were taken into account in accordance with the probabilistic models described by Esteva and Ruiz (1989), based on information provided by Meli (1976) and Mirza & McGregor (1979). These properties were used to generate a sample of possible random realizations of each structural system, with the aid of Monte Carlo simulation. For each system studied, each simulated realization was randomly assigned to one of the ground motion time histories in the sample obtained as described in Section 3.2, in order to generate a sample of pairs of values of $Y$and I_{SSR}. For this purpose, a step-by-step nonlinear dynamic response analysis was performed for each combination of structural system and seismic excitation. Some results are plotted in Figures 4–6, which show values of Z, defined here as the natural logarithm of the normalized intensity $S_aM/\overline{V}_y$ for different values of the stiffness reduction index $D = I_{SSR} = (K_0 - K)/K_0$, where M is the mass of the system and $\overline{V}_y$ is the expected value of the yield value of the base shear, determined by means of a pushover analysis. In these figures, N denotes the number of stories and p_d is the percentage of the strength and stiffness taken by the EDD at each story.

The information contained in Figures 4–6 was used to obtain expected value functions of $Z = \ln(S_aM/\overline{V}_y)$ in terms of the stiffness reduction index $D = I_{SSR}$. For the three buildings studied here, these functions are shown in Figure 7. Together with the values of Z shown in Figures 4–6, they were used to obtain the values of $(Z - \mathrm{E}(Z))^2$ that were used to obtain the functions representing the standard deviation of Z in terms of $D = I_{SSR}$. The expected value and the standard deviation of Z_F was directly obtained from the expected value and standard deviation functions, taking $I_{SSR} = 1.0$. These values were used to determine the reliability function $\beta(Z)$, in accordance with Equation 2.

As shown in Figure 7, the expected values of Z_F grow systematically with p_d, the contribution of the EDE's to the lateral strength and stiffness of the system. According to the results of Rangel

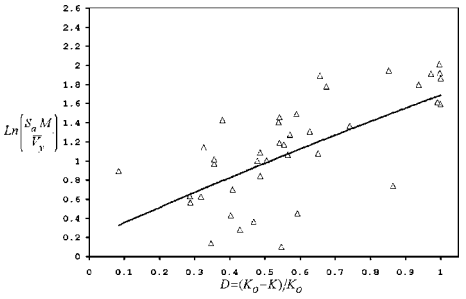

Figure 4. Normalized intensity vs I_{SSR}, $N = 20$, $p_d = 0$.

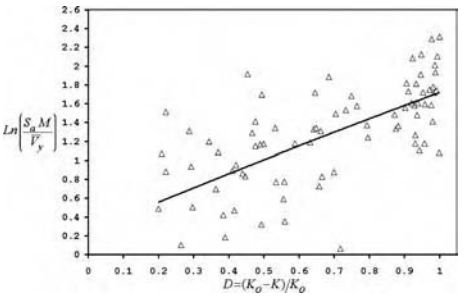

Figure 5. Normalized intensity vs I_{SSR}, $N = 20$, $p_d = 25$.

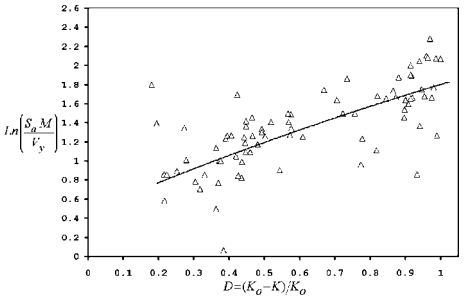

Figure 6. Normalized intensity vs I_{SSR}, $N = 20$, $p_d = 50$.

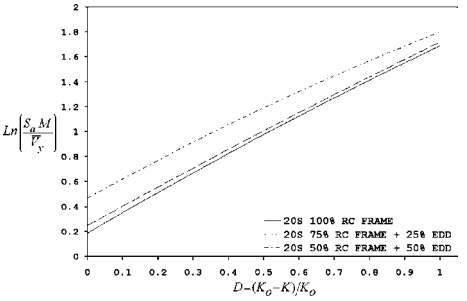

Figure 7. Expected values of normalized intensity vs I_{SSR}, $N = 20$, $p_d = 0$, 0.25, 0.5.

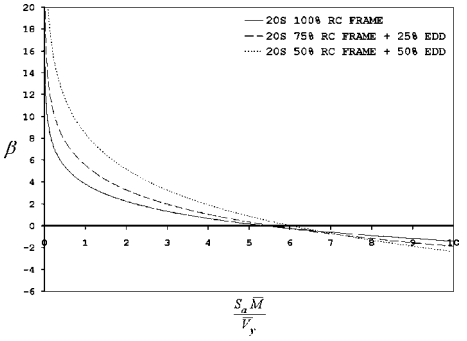

Figure 8. Reliability functions for the buildings studied, with different values of p_d.

(2006), the standard deviation of Z_F decreases when p_d increases. Both effects contribute to the higher values adopted by $\beta(Z)$ for higher values of p_d, as observed in Figure 8.

4 CONCLUDING REMARKS

The stiffness-reduction index proposed in this study can be efficiently used for the determination of second moment probabilistic descriptions of Z_F, the natural logarithm of the minimum value of the intensity required to produce collapse of a complex nonlinear system and, therefore, for the determination of seismic reliability functions of those systems. This is achieved while avoiding the need to depend on the determination of a lateral deformation capacity, which is very sensitive

to the strength and stiffness degradation of the system due to its cyclic response, as well as to its lateral configuration at the instant of impending collapse.

The determination of the reliability index β is based on the determination of the mean and standard deviation of Z_F, on the basis of a statistical sample of values of Z, the natural logarithm of the intensity, and I_{SSR}, the stiffness-reduction index, in the vicinity of I_{SSR} = 1.0. Information derived from sample points with I_{SSR} cannot be directly taken into account through a conventional least-squares regression analysis, because the corresponding intensities may be equal to or larger than the required minimum values. The maximum likelihood approach presented here is more efficient than one previously proposed by Esteva and Ismael (2004) when only the collapse failure mode is of interest in the evaluation of the seismic vulnerability of a system.

REFERENCES

Alamilla, J. & Esteva, L. 2006. Seismic reliability functions for multistory frame and wall-frame systems. *Earthquake Engineering and Structural Dynamics, accepted for publication.*

Cornell, C. A. 1969. A probability based structural code. *Journal of the American Concrete Institute* **66** (12).

Díaz-López, O. & Esteva, L. 2006. Seismic reliability analysis of complex nonlinear systems, using secant-stiffness-reduction indicators. *Proc. 1st European Conference on Earthquake Engineering and Seismology*, Geneva, Switzerland.

Dolsek, M. and Fajfar, P. 2004. IN2 – A simple alternative for IDA. *Proc. 13th World Conference on Earthquake Engineering*, Vancouver, Canada: Paper 3353.

Esteva, L. 1992. Nonlinear seismic response of soft-first-story buildings subjected to narrow-band accelerograms. *Earthquake Spectra* **8** (3): 373–389.

Esteva, L., Díaz-López, O. & García-Pérez, J. 1999. Life cycle optimization of structures with seismic energy-dissipating devices. *Case Studies in Optimal Design and Maintenance Planning of Civil Infrastructure Systems, American Society of Civil Engineers*. Edited by D. Frangopol.

Esteva, L., Díaz-López, O., García-Pérez, J. Sierra, G. & Ismael, E. 2002a. Simplified reference systems in the establishment of displacement-based seismic design criteria. *Proc. 12th European Conference on Earthquake Engineering*, London, England: Paper 419.

Esteva, L., Alamilla, J. & Díaz-López, O. 2002b. Failure models, significant variables and reference systems in the reliability-based seismic design of multistory buildings. *Proceedings of the 7th US National Conference on Earthquake Engineering*, Boston, Mass., USA.

Esteva, L. & Ismael, E. 2004. A maximum likelihood approach to system reliability with respect to seismic collapse. *Proc. International Federation for Information Processing, WG7.5 Working Conference*, Banff, Canada.

Ismael, E. & Esteva, L. 2006. A hybrid method for simulating strong ground motion records. *Proc. 1st European Conference on Earthquake Engineering and Seismology.* Geneva, Switzerland.

Meli, R. 1976. Bases para los criterios de diseño estructural del proyecto del Reglamento de Construcciones para el Distrito Federal. (Bases for structural design criteria in the draft for the Federal District Building Code) *Report 375, Institute of Engineering, National University of Mexico.*

Mirza, S. A. & McGregor, J. 1979. Variation in dimensions of reinforced concrete members. *J. Struct Div, ASCE* **105** (ST4): 751–766.

NTCDS-RCDF. 2004. Normas Técnicas Complementarias para Diseño por Sismo del Reglamento de Construcciones del Distrito Federal (Complementary Technical Norms for Seismic Design, Federal District Building Code), Mexico City.

Rangel, J. G. 2006. Funciones de confiabilidad sísmica de sistemas con elementos disipadores de energía (Seismic reliability functions for systems with hysteretic energy dissipators). *M. Sc. Thesis, Graduate Program in Engineering, National University of Mexico* (in process).

Shome, N. & Cornell, C.A. 1999. Probabilistic Seismic Demand Analysis of Nonlinear Structures. *Report No. RMS*.35, *Department of Civil Engineering, Stanford University*, Stanford, California, USA.

Vamvatsikos, D. & Cornell, C. A. 2002. Incremental dynamic analysis. *Earthquake Engineering and Structural Dynamics* **31** (3): 491–514.

Wang, M. L. & Shah, S. P. 1987. Reinforced concrete hysteresis model based on the damage concept. *Earthquake Engineering and Structural Dynamics* **15**: 993-1003.

Reliability and Optimization of Structural Systems: Assessment, Design and Life-Cycle Performance – Frangopol, Kawatani & Kim (eds)
© 2007 Taylor & Francis Group, London, ISBN 978-0-415-40655-0

Redundancy and robustness of structures: A retrospective

Michel Ghosn & Dan M. Frangopol
Department of Civil Engineering, The City College of New York/CUNY, New York, NY, USA
Department of Civil and Environmental Engineering, ATLSS Research Center, Lehigh University, Bethlehem, PA, USA

ABSTRACT: Issues related to structural redundancy and robustness have gained increased importance after a number of recent major collapses due to man-made or natural hazards. As a result, several recent and on-going studies have focused on determining the failure mechanisms in typical structural systems and are making recommendations to improve the overall system safety of civil structures including buildings and bridges. Yet, despite major advances in developing methodologies for the structural analysis of cascading failures and in understanding the behavior of different types of systems under suddenly applied extreme loads, a main issue related to defining objective measures of redundancy and quantifying the levels of redundancy that exist in structural systems remains vastly unresolved. This paper revisits some of the work done by the authors and their colleagues on the quantification of system redundancy and reviews previously made proposals for including system redundancy and robustness during the structural design and safety assessment of structural systems. These proposals, which are based on system reliability principles, consider structural system safety, system redundancy and system robustness in comparison to member safety, and account for the uncertainties associated with determining member and system strengths as well as future loads in a consistent and rational manner.

1 INTRODUCTION

A 1985 "State of the Art Report on Redundant Bridge Systems" concluded that although analytical techniques to study the response of damaged and undamaged flexural systems to high loads are available, "little work has been done on quantifying the degree of redundancy that is needed" (ASCE-AASHTO Task Committee; 1985). Some two decades later and following several tragic failures caused by terrorist attacks and natural hazards, the issues related to structural safety, redundancy, and robustness have gained increased importance. In fact, several recent and on-going studies have focused on determining the failure mechanisms of typical structural systems and are making recommendations to improve the overall system safety of civil structures including buildings and bridges (NCSRT; 2005). Yet, despite all the advances made in developing structural analysis methodologies and in understanding the behavior of different types of systems under suddenly applied extreme load events, the issue raised in the 1985 state of the art report pertaining to the quantification of the required levels of redundancy remains vastly unresolved. In this paper, the authors review previously made recommendations on the quantification of system redundancy and revisit proposals for including system redundancy and robustness during the structural design and safety assessment of buildings and bridges. These proposals, which are based on system reliability principles consider structural system safety, system redundancy and system robustness in comparison to member safety, and account for the uncertainties associated with determining member and system strengths as well as future loads in a consistent and rational manner.

2 SYSTEM RELIABILITY BACKGROUND

Current structural design specifications evaluate a structural system's safety based on the capacity of the weakest member. This approach may lead to the design of over-conservative systems by ignoring the ability of ductile and redundant systems to redistribute their loads when a single member reaches its maximum load carrying capacity. Also, and more importantly, the approach may lead to the design of non-redundant systems, which may be susceptible to cascading collapse after the accidental failure of one of their members. To understand the relationship between member properties and the reliability of parallel multi-member systems, Hendawi & Frangopol (1994) analyzed the two-member system described in Figure 1 considering the effect of post-failure behavior (or ductility capacity), the correlation between member capacities, resistance sharing parameters, and load variability. To perform the comparison, the members of the system are assumed to have been designed to satisfy a system safety factor, SSF, defined as:

$$SSF = \frac{\sum_i \overline{R}_i}{\overline{P}} \tag{1}$$

where $\overline{R}_i$ is the mean resistance of member i, and $\overline{P}$ is the mean of the applied load. The deterministic resistance-sharing factor is defined in terms of the member stiffness K_i, as:

$$RSF_i = \frac{K_i}{\sum K_i} \tag{2}$$

Damage of member i is evaluated using the damage factor $DF(i)$ defined as:

$$DF(i) = \frac{A_i(\text{int act}) - A_i(\text{damaged})}{A_i(\text{int act})} \tag{3}$$

where A_i is the area of member i

A reliability analysis is performed for several hypothetical cases, the results of which were represented by the reliability index $\beta_{sys} = \Phi^{-1}(P_f)$ where P_f is the probability of failure and Φ^{-1} is the inverse of the cumulative Guassian function. The results presented in Figs. 2, 3 and 4 for the two-member parallel system illustrate the following system characteristics (see also Hendawi and Frangopol; 1994):

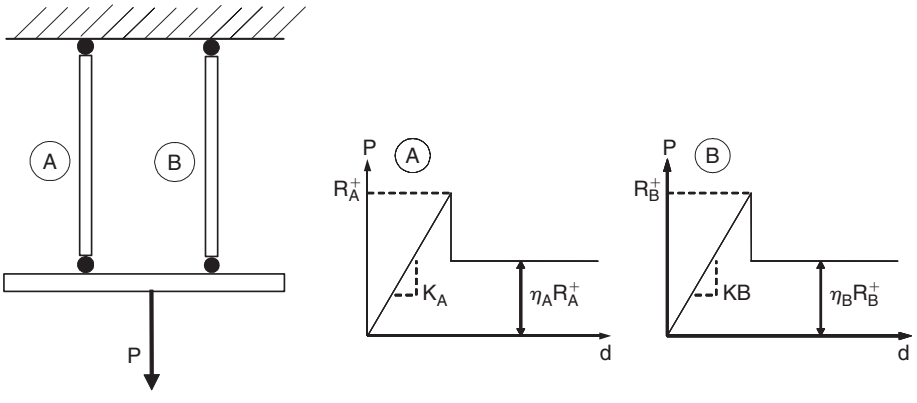

(a) Two-member system

(b) Force-deformation characteristics of members

Figure 1. Idealized two-member parallel system.

- Correlation in member strengths, leads to lower system reliability. (Fig. 2).
- Brittle systems are less sensitive to member correlation than ductile systems (Fig. 2).
- Equal resistance sharing as represented by $RSF_1 = RSF_2 = 0.5$ for a two-member system produces maximum system reliability for ductile systems but minimum system reliability for brittle systems. (Fig. 3)
- As indicated in Fig. 4, under increasing damage of member 1, the system reliability is decreased for both ductile and brittle systems. If no damage exists and if resistance correlation is not perfect, a two-member ductile system is more reliable than a single ductile member having the cross-sectional area of the two members. Whereas, for the same conditions, two-member brittle system produces less reliability.

Based on these and other similar analyses, Hendawi & Frangopol (1994) and Ghosn & Moses (1992, 1998) recommended the application of a system redundancy factor during the design and safety evaluation of structural systems to account for system safety and robustness by modifying the

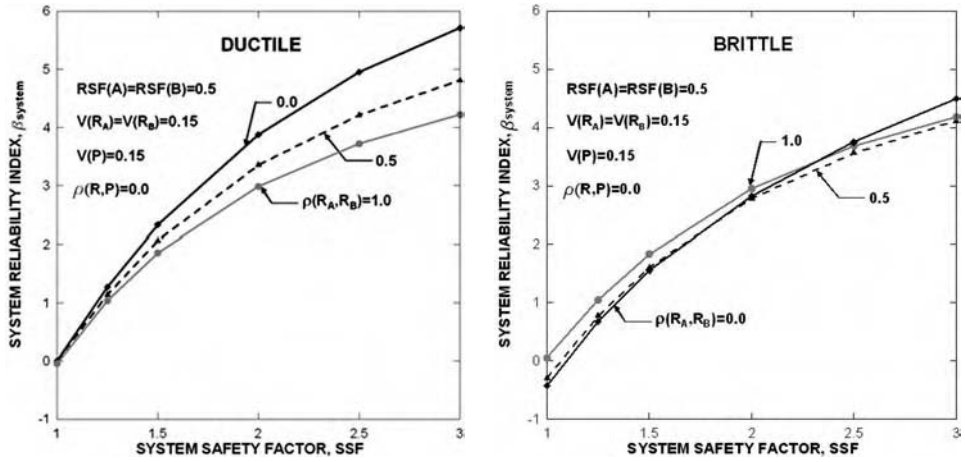

Figure 2. Effect of member resistance correlation and SSF on system reliability.

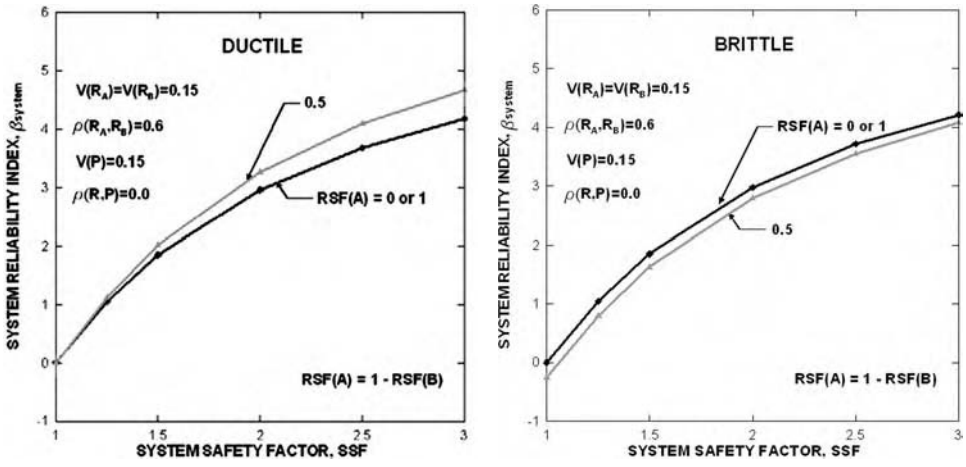

Figure 3. Effect of resistance sharing on system reliability.

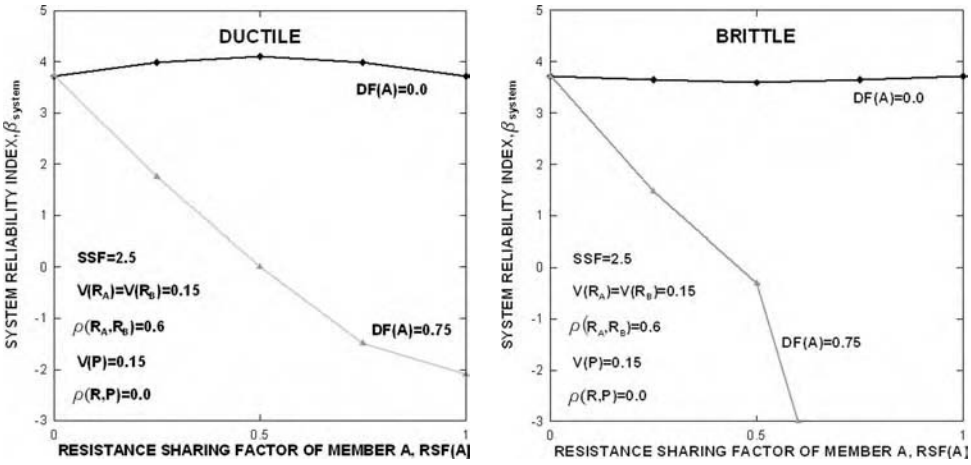

Figure 4. Effect of member damage on system reliability.

traditional safety-check equations that are normally used in design specification. The modification lead to safety-checking equation that takes the form:

$$\phi_s \phi R_n \geq \sum_i \gamma_i Q_i \tag{4}$$

where ϕ_s is the system factor, ϕ is the member resistance factor, R_n is the nominal member resistance, γ_i are the load factors and Q_i are the nominal design loads. The application of a system factor $\phi_s < 1.0$ would lead to increasing the system reliability of designs that traditionally have been shown to have low levels of system reserve and redundancy. Alternatively, $\phi_s > 1.0$ would lead to rewarding the design of adequately redundant systems by allowing their members to have lower capacities than those of non-redundant systems. Because the presence of redundancy does not necessarily guarantee sufficient levels of safety, upper and lower limits should be set on ϕ_s to ensure that minimum levels of member and system reliability are met.

3 IMPLEMENTATION IN BRIDGE SYSTEMS

To evaluate the safety of a bridge structural system, Ghosn & Moses (1998) reviewed commonly accepted criteria and concluded that a bridge can be considered safe if: (a) it provides an acceptable level of reliability against first member failure, (b) it is unlikely to reach its ultimate capacity under extreme loading conditions, (c) it does not loose its functionality by producing large deformations under expected loading condition and (d) has sufficient robustness to carry some traffic load after the brittle failure of a main component. These limit states can be schematically represented as shown in Fig. 5.

Specifically, Fig. 5 provides a conceptual representation of the behavior of a structure and the different levels of safety that should be considered. For example, the solid line labeled "actual behavior" may represent the live load versus maximum vertical displacement of a multi-girder bridge superstructure. Assuming that the live load applied has the configuration of the nominal design vehicle, then the first main member will fail when the design vehicle load is multiplied by a factor LF_1. But, the ultimate capacity of the whole bridge is not reached until the load is multiplied by a factor LF_u. Large vertical deformations rendering the bridge unfit for use are reached when the load is multiplied by a factor LF_f. At this point, the bridge is said to have lost its functionality. If the bridge has sustained major damage due to the brittle failure of one or more of its members,

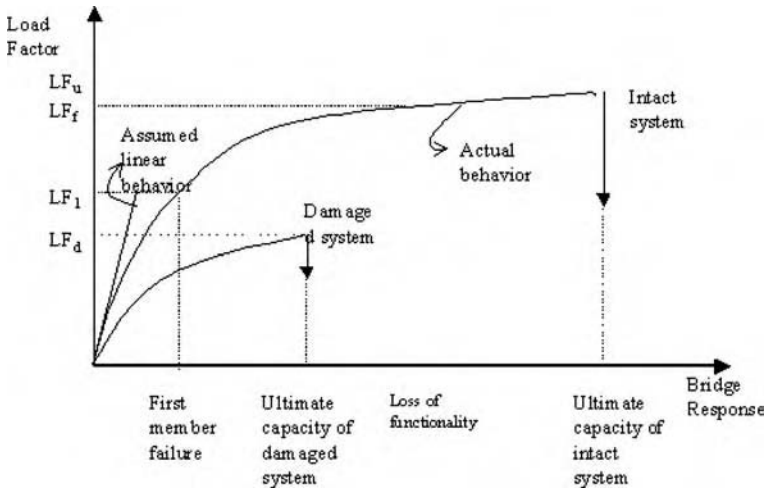

Figure 5. Representation of typical behavior of bridge systems.

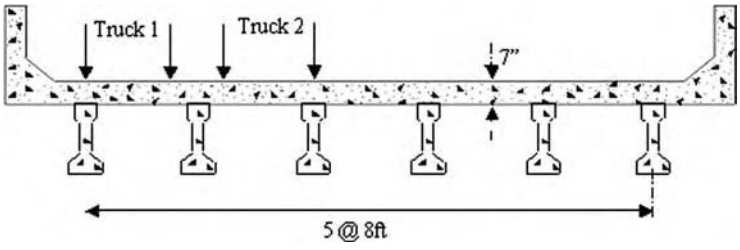

Figure 6. Cross section of typical multi-girder bridge.

its behavior after damage is represented by the curve labeled "damaged system". In this case, the ultimate capacity of the damaged bridge is reached when the design live load is multiplied by a factor LF_d. This situation may arise when say a fracture critical member has failed or after the brittle failure of a main load carrying member due to collisions or other impacts.

In most typical applications, bridge specifications have focused on ensuring that bridge members meet minimum safety requirements and failure is defined as the point at which the first member reaches its load capacity. Thus, the design process controls the most critical member's capacity designated as LF_1. However, for many bridges, the failure of a main carrying member may not necessarily lead to bridge collapse neither would the deflections be necessarily sufficiently high to render the bridge unfit for use. Even after the brittle failure of a main load-carrying member, the bridge may still be able to carry significant levels of live load. As observed from the analyses of the parallel systems performed in the previous section, different types of bridges may have different degrees of redundancy and robustness depending on their topology, resistant sharing factors, member strength correlation and material behavior. Current specifications encourage the design of redundant bridges. However, as mentioned earlier, there currently are no widely accepted objective measures of redundancy.

3.1 *Modeling of bridge structures*

To understand the behavior of typical multi-girder highway bridge superstructures, a large number of prestressed concrete and steel I-beam bridges designed to satisfy the AASHTO Standard

specifications are analyzed (AASHTO; 2002). Thus, the safety factor SSF is implicitly controlled by the code requirements.

During the analysis, the weights of the AASHTO HS-20 design trucks were incremented and the moment-rotation relationship updated as the moments in each individual member reached critical values. In addition to the determination of the internal moments and forces at each load step, the analysis led to a load versus vertical displacement curve similar to that shown in Fig. 5 for each of the bridge configurations analyzed. To determine the appropriate value for the functionality limit, the literature was reviewed and different options were considered. It was determined that a deflection limit equal to span length/100 is appropriate to ensure traffic safety while simultaneously avoiding visible permanent deformations. Finally, to analyze the capacity of a damaged bridge to sustain live load after the brittle failure of one main girder, the external girder under the live load was completely removed from the model simulating situations where the beam is shattered due to a collision or a blast.

The nonlinear reliability analysis is performed assuming that the slab, the remaining portion of the girder and other secondary elements can still provide sufficient strength to redistribute the load to the remaining girders. This is deemed to be a realistic scenario based on observations made in the field about bridges whose exterior girders were badly damaged due to collisions or other accidental loads. The stiffness of the slab and secondary members provide for the realistic modeling of the resistance-sharing factor RSF_i of Eq. 2.

3.2 *Reliability analysis*

A common probabilistic measure of safety that is used in structural design and evaluations is the reliability index, β. For example, a $\beta_{\text{member}} = 3.5$ for member safety was used as the target for the development of the AASHTO-LRFD Specifications (AASHTO; 2004). For illustration and assuming that bridge capacity, R, and the applied load, S, follow lognormal distributions, the reliability index can be calculated using the equation:

$$\beta = \frac{ln\left(\frac{\overline{R}}{\overline{S}}\right)}{\sqrt{V_R^2 + V_S^2}} = \frac{ln\left(\frac{\overline{LF}\ HS20}{\overline{LL}\ HS20}\right)}{\sqrt{V_{LF}^2 + V_{LL}^2}} = \frac{ln\left(\frac{\overline{LF}}{\overline{LL}}\right)}{\sqrt{V_{LF}^2 + V_{LL}^2}} \tag{5}$$

where $\overline{R}$ = mean value of resistance, $\overline{S}$ = mean value of applied load effect, $HS20$ = load effect of HS-20 truck, V_{LF} = coefficient of variation of the bridge resistance defined as the standard deviation divided by the mean value, V_{LL} = coefficient of variation of the applied live load. Both the resistance and the applied live load are expressed as a function of the HS-20 truck load effect which can then be factored out so that the resistance is expressed in terms of the load factor LF obtained from the incremental analysis and the applied live load factor LL.

In general, the reliability index can be calculated using either simple LogNormal models or advanced reliability methods such as the response surface method whereby the bridge's ability to withstand the applied load, LL, without reaching a limit state is represented by the load factor LF_i corresponding to the limit state under consideration. The probability of failure can then be represented by:

$$P_f = Pr\,(LF_i < LL) = \Phi^{-1}(\beta) \tag{6}$$

where Φ^{-1} is the inverse of the cumulative Gaussian function.

To calculate the reliability index, β, for the four limit states represented by LF_1, LF_f, LF_u and LF_d the results of the deterministic analysis are used in addition to the statistical data assembled during the calibration of the AASHTO-LRFD specifications (AASHTO; 2004). Based on the analyses performed in the previous section and normal bridge design and construction procedures, the main members of the bridge are assumed to be fully correlated as this assumption is both reasonable

based on construction practices and it provides a conservative estimate of the reliability of both ductile and brittle systems.

Probabilistic measures of redundancy are obtained by examining the differences between the reliability indices of the systems for the three limit states LF_u, LF_f and LF_d expressed in terms of $\beta_{ultimate}$, $\beta_{functionality}$ and $\beta_{damaged}$ which are compared to the reliability of the most critical member β_{member}. This could be done through the relative reliability indices $\Delta\beta_u$, $\Delta\beta_f$, $\Delta\beta_d$ defined as:

$$\begin{aligned} \Delta\beta_u &= \beta_{ultimate} - \beta_{member} \\ \Delta\beta_f &= \beta_{functionality} - \beta_{member} \\ \Delta\beta_d &= \beta_{damaged} - \beta_{member} \end{aligned} \tag{7}$$

3.3 *Analysis of reliability results*

The reliability analysis of hundreds of bridge configurations in addition to the sensitivity analyses demonstrated that the proposed measures of redundancy are robust in the sense that the relative reliability indices of equation (7) are not very sensitive to variations in the stiffnesses of the individual members, member strengths, the magnitude of the applied dead load or skew angles less than 45°. To be sure, the member and system reliability indexes would change but the difference between the system and member indexes remains relatively insensitive.

The level of redundancy was found to be not only a function of the number of beams as commonly assumed, but also a function of the combination of number of beams and beam spacings. For example, multi-girder bridges with wide spacings have low system reserve ratios independent of the number of beams. On the other hand, because the load distribution factors of narrow bridges with very closely spaced beams is high, these bridges show little system reserve as the failure of one beam would cause a cascading failure of the adjacent beams.

The presence of diaphragms was found to help in redistributing the load to the intact members when a bridge is damaged after the brittle failure of one of its members. However, the diaphragms do not significantly contribute to the redundancy of undamaged bridges.

Bridges whose members are not sufficiently ductile do not exhibit adequate levels of system reserve regardless of the number of supporting girders.

Finally, bridges known to have adequate levels of redundancy are shown to produce relative reliability indices which exceed $\Delta\beta_u = 0.85$, $\Delta\beta_f = 0.25$ $\Delta\beta_d = -2.70$. Based, on this observation, an objective measure of redundancy can be obtained based on target $\Delta\beta$ values. Thus, bridges that do not meet the above $\Delta\beta$ criteria are classified as non-redundant and should be either redesigned with modified topological configurations to improve their levels of redundancy or alternatively should be penalized by requiring that their members and system strengths be higher than those of similar bridges that show adequate levels of redundancy. Thus, a bridge that has a low level of redundancy can still be so "over-designed" that collapse would have a low probability of occurring. This can be achieved by calibrating system resistance factor, ϕ_s, to be applied on the member strengths to ensure that the system reliability will meet a target value $\beta_{system} = 3.5 + \Delta\beta$ and provide adequate system safety even if member safety may not meet the traditionally accepted minimum target $\beta_{member} = 3.5$.

Although the steps involved in the calculation of the system reliability and subsequently the determination of the applicable system factor are easy to follow for engineers familiar with the application of reliability theory, the process may be too involved for routine applications on typical bridge configurations. Thus, code writers may calibrate a set of system factors as shown in Eq. 4 that can be directly applied during the design or the load capacity evaluation of existing bridges to ensure that the system capacity of these bridges are adequate.

3.4 *System factors for bridge superstructures*

To illustrate how Eq. 4 can be calibrated for application in bridge design and evaluation, values for the system factor, ϕ_s, have been proposed to provide a measure of the system reserve strength as

Table 1. System factors for girder superstructures.

Loading type	System/member type	ϕ_{su}	ϕ_{sd1}	ϕ_{sd2}
Bending of	Two-girder bridges	0.85	0.80	0.80
members of	Three-girder bridges with spacing: $\leq$1.8m	0.85	1.20	1.10
multi-girder	Four-girder bridges with spacing: $\leq$1.2rn	0.85	1.20	1.10
systems	Other girder bridges with spacing: $\leq$1.2m	1.00	1.20	1.15
	All girder bridges with spacing: $\leq$1.8m	1.00	1.20	1.15
	All girder bridges with spacing: $\leq$2.4m	1.00	1.15	1.05
	All girder bridges with spacing: $\leq$3.0m	0.95	1.00	0.90
	All girder bridges with spacing: $\leq$3.6m	0.90	0.80	080
	All girder bridges with spacing: $>$3.6m	0.85	0.80	0.80
Slab bridges	For bending		1.00	
All bridge types	Members in shear		0.80	
All joints & connections			0.80	

it relates to ductility, redundancy and operational importance, and their interaction. The proposed system factors are calibrated such that overall system safety of a bridge structure as represented by the system's reliability index meets a target value. Assuming that members of adequately redundant bridges are designed to satisfy the current AASHTO LRFD criteria, then their reliability index should be on the order of $\beta_{member} = 3.5$. The proposed redundancy criteria have been calibrated so that the reliability index of an intact bridge system will exceed $\beta_{ultimate} = 4.35$. Furthermore, the reliability index for a maximum deflection of span length/100 will exceed, $\beta_{functionality} = 3.75$. Finally, the system reliability of a bridge that has lost a major member will exceed $\beta_{damaged} = 0.80$. As an example, the latter value implies that a superstructure that has sustained major damage or the complete loss in the load carrying capacity of a main member will still have an 80% probability of survival under regular truck loading. The target system reliability index values are obtained based on the observation made earlier that adequately redundant bridges have been found to have relative reliability indices $\Delta\beta_u = 0.85$, $\Delta\beta_f = 0.25$ and $\Delta\beta_d = -2.70$.The introduction of the system factors ϕ_s into Eq. (4) will serve to add member and system capacity to less redundant systems such that the overall system reliability is increased. When adequate redundancy is present, a system factor, ϕ_s, greater than 1.0 may be used.

For members of superstructures of bridges classified to be critical or that are susceptible to brittle damage, the system factor should be determined as follows:

$\phi_s = \min(\phi_{su}, \phi_{sd1})$ for multi-girder systems with diaphragms spaced at not more than 7600 mm.
$\phi_s = \min(\phi_{su}, \phi_{sd2})$ for all other multi-girder systems.

For the superstructures of all other bridges:
$\phi_s = \phi_{su}$

where ϕ_{su} = system factor for superstructure ultimate capacity, ϕ_{sd1} = system factor for damage of superstructures with regularly spaced diaphragms, and ϕ_{sd2} = system factor for damage of superstructures with no diaphragms as given in Table 1 for different number of beams and beam spacing. A minimum value of $\phi_s = 0.80$ is recommended but in no instance should ϕ_s, be taken as greater than 1.20. These limits have been proposed as a temporary measure until the practicing engineering community builds its confidence level in the proposed methodology.

Bridges susceptible to brittle damage include bridges with fatigue-prone details, those with members that are exposed to collisions from ships, vehicles, and debris carried by swelling streams and rivers, or bridges that may be susceptible to blast.

As was proposed in (AASHTO, 2004) for the seismic design of bridges, it is recommended that bridge owners or those having jurisdiction classify each bridge into one of three importance categories as follows: (a) Critical bridges, (b) Essential bridges, or (c) other bridges. Such classification should be based on social/survival and/or security/defense requirements following the guidelines for the design for earthquakes (AASHTO, 2004). In addition, bridge owners should

identify bridges that are susceptible to brittle damage as mentioned earlier. The use of more stringent criteria for critical bridges is consistent with current trends to use performance-based design in bridge engineering practice.

Members in shear as well as all joints and connections are assigned a system factor $\phi_s = 0.\ 80$. This assumes that the resistance factor ϕ was calibrated to satisfy a target member reliability index $\beta_{member} = 3.5$. Since shear failures and connection failures are brittle, the application of a system factor $\phi_s = 0.80$ will increase the reliability index of the member and also that of the system so that $\beta_{member} = \beta_{system} \approx 4.35$ which is the target value for system safety.

4 CONCLUSIONS

This paper presented a retrospective on structural system redundancy and robustness. This retrospective was mainly based on the work of the authors and their co-workers and is limited to the period 1984–2000. A framework for considering structural redundancy during the design and assessment of structural systems was presented. This was achieved by proposing a method to penalize designs with insufficient levels of redundancy and requiring that their members be more conservatively designed than allowed by current standard specifications. This could be done by applying system factors that are calibrated using reliability techniques so that nonredundant bridges would provide a minimum level of system reliability. The development of the design methodology was based on a proposed set of objective measures of redundancy that compared system safety to member safety. These measures accounted for system reserve after the brittle or ductile failure of a main load-carrying member. The calibration process was illustrated by studying the performance of typical multi-girder bridges. Additional work of the authors and their co-investigators on structural redundancy can be found in Ghosn (1988), Ghosn and Moses (1992, 1998), Ghosn and Casas (1995), Liu, Ghosn et al. (2001), Ghosn et al. (1992), Frangopol ed. (1987), Frangopol (1992), Frangopol and Curley (1987), Frangopol et al. (1987, 1998, 1991, 1992), Frangopol and Klisinski (1989), Frangopol and Nakib (1990a,1990b,1991), Frangopol and Iizuka (1992a,b), Frangopol and Yoshida (1996), Fu and Frangopol (1989, 1990), Gharaibeh and Frangopol (2000), Gharaibeh et al. (2000a,b), Hendawi and Frangopol (1994), Nakib and Frangopol (1991).

REFERENCES

AASHTO (2002), Standard Specifications for Highway Bridges, 17th edition, Washington, D.C.

AASHTO (2004), Load & Resistance Factor Design (LRFD) Bridge Design Specifications, 3rd edition, Washington, D.C.

ASCE-AASHTO Task Committee (1985), "State if the Art Report on Redundant Bridge Systems," ASCE Journal of Structural Engineering, Vol. 111, No. 12.

Frangopol, D.M. (1992). "Bridge loading, reliability and redundancy: Concepts and applications," *Lecture Notes in Engineering*, C.A. Brebia, and S.A. Orzag, eds., *Reliability and Optimization of Structural Systems '91*, R. Rackwitz, and P. Thoft-Christensen, eds., Springer-Verlag, Berlin, 1–18.

Frangopol, D.M., and Curley, J.P. (1987). "Effects of damage and redundancy on structural reliability," *Journal of Structural Engineering*, ASCE, **113** (7), 1533–1549.

Frangopol, D.M., and Iizuka, M. (1992a). "Reliability-based redundancy measures for bridge evaluation and design," *Proceedings of the Third NSF Workshop on Bridge Engineering Research in Progress*, La Jolla, California, 139–142.

Frangopol, D.M., and Iizuka, M. (1992b). "A survey of system redundancy measures," *Structures Congress '92*, Jim Morgan, ed., ASCE, New York, 153–156.

Frangopol, D.M., and Klisinski, M. (1989). "Weight-strength-redundancy interaction in optimum design of three-dimensional brittle-ductile trusses," *Computers and Structures*, Pergamon Press, **31**(5), 775–787.

Frangopol, D.M., and Nakib, R. (1990). "Bridge redundancy assessment," *Second Workshop on Bridge Engineering Research in Progress*, University of Nevada, Reno, 167–170.

Frangopol, D.M., and Nakib, R. (1990). "Damage-redundancy-reliability interaction in bridge analysis," *Developments in Short and Medium Span Bridge Engineering '90*, B. Bakht, R.A. Dorton, and L.G. Jaeger, eds., Canadian Society of Civil Engineers, **1**, 343.

Frangopol, D.M., and Nakib, R. (1991). "Redundancy in highway bridges," *Engineering Journal*, American Institute of Steel Construction, **28** (1), 45–50.

Frangopol, D.M., and Yoshida, K. (1996). "Loading and material behavior effects on system redundancy," *Building an International Community of Structural Engineers*, S.K. Ghosh and J. Mohammadi, eds., ASCE, New York, **2**, 674–681.

Frangopol, D.M., ed. (1987). *Effects of Damage and Redundancy on Structural Performance*, ASCE (ISBN 0-87262-587-7), New York, 85 pages.

Frangopol, D.M., Gharaibeh, E.S., Hearn, G., and Shing, P.B. (1998). "System reliability and redundancy in codified bridge evaluation and design," *Structural Engineering World Wide 1998*, N.K. Srivastava, ed., Paper Reference T121-2, Elsevier, Amsterdam, 1998, 9 pages on CD-ROM.

Frangopol, D.M., Goble, G.G., Trautner, J.J., and Scholfied, M.M. (1987). "Redundancy evaluation of existing bridges," *Bridge and Transmission Line Structures*, L. Tall, ed., ASCE, New York, 1–14.

Frangopol, D.M., Iizuka, M., and Yoshida, K. (1991). "Redundancy measures for design and evaluation of structural systems," *Proceedings of the 10th International Conference on Offshore Mechanics and Arctic Engineering* (OMAE 1991); ASME Paper No. OMAE -91-1242, Vol. II: Safety and Reliability, ASME, Stavanger, Norway, 157–163.

Frangopol, D.M., Iizuka, M., and Yoshida, K. (1992). "Redundancy measures for design and evaluation of structural systems," *Journal of Offshore Mechanics and Arctic Engineering*, ASME, **114** (4), New York, 285–290.

Fu, G., and Frangopol, D.M. (1989). "System reliability and redundancy in a multiobjective optimization framework," *New Directions in Structural System Reliability*, D.M. Frangopol, ed., University of Colorado Press, Boulder, 147–157.

Fu, G., and Frangopol, D.M. (1990). "Balancing weight, system reliability and redundancy in a multiobjective optimization framework," *Structural Safety*, **7** (2–4), 165–175.

Gharaibeh, E.S., and Frangopol, D.M. (2000). "Safety assessment of highway bridges based on system reliability and redundancy," *Congress Report, 16th Congress of IABSE*, Lucerne, Switzerland, 274–275; *Structural Engineering for Meeting Urban Transportation Challenges*, IABSE Congress Lucerne, Switzerland, 8 pages on CD-ROM.

Gharaibeh, E.S., Frangopol, D.M., and Enright, M.P. (2000b). "Redundancy and member importance evaluation of highway bridges," *Applications of Statistics and Probability*, R.E. Melchers, and M.G. Stewart, eds., Balkema, Rotterdam, **2**, 651–658.

Gharaibeh, E.S., Frangopol, D.M., Shing, P.B., and Hearn, G. (2000a). "System function, redundancy, and component importance: Feedback for optimal design," *Advanced Technology in Structural Engineering*, M. Elgaaly, ed., ASCE, Reston, Virginia, 8 pages on CD-ROM.

Ghosn, M., and Casa, J.R. (1995). "System Performance of I-Beam and Spread Box Beam Prestressed Concrete Bridges," by M. Ghosn and J.R. Casas, IABSE Congress, San Francisco.

Ghosn, M., 1988, "Reliability of Multistate Structural Systems," ASCE -Joint Specialty Conference on Probabilistic Methods, Blacksburg, VA.

Ghosn, M., and Moses, F. (1992) "Calibration of Redundancy Factors for Highway Bridges," ASCE Specialty Conference on Probabilistic Mechanics and Structural & Geotechnical Reliability, Denver, CO.

Ghosn, M., and Moses, F. (1992) "Redundancy & Reliability of Highway Bridges," ASCE Tenth Structures Congress, San Antonio, TX.

Ghosn, M., and Moses, F. (1998) *Redundancy in Highway Bridge Superstructures*, National Cooperative Highway Research Program, NCHRP Report 406, Transportation Research Board, National Academy Press, Washington DC.

Ghosn, M., Moses, F., and Khedekar, N. (1993) "System Reliability of Redundant Structures using Response Functions," ICOSSAR'93, Innsbruck, Austria.

Hendawi, S., and Frangopol, D.M. (1994). "System reliability and redundancy in structural design and evaluation," *Structural Safety*, Elsevier, **16** $(1+2)$, 47–71.

Liu, D., Ghosn, M., Moses, F., and Neuenhoffer, A. (2001) *Redundancy in Highway Bridge Substructures*, National Cooperative Highway Research Program, NCHRP Report 458, Transportation Research Board, National Academy Press, Washington DC.

Nakib, R., and Frangopol, D.M. (1991). "Redundancy and reliability analysis of existing bridges," *Proceedings of ICASP6, Sixth International Conference on Applications of Statistics and Probability in Civil Engineering*, L. Esteva and S.E. Ruiz, eds., Mexico City, Mexico, **2**, 849–856.

National Construction Safety Team on the Collapse of the World Trade Center Towers (2005), "Federal Building and Fire Safety Investigation of the World trade Center Disaster, Draft Report, NIST NCSTAR 1, U.S. Department of Commerce, Washington, DC.

Reliability and Optimization of Structural Systems: Assessment, Design and Life-Cycle Performance – Frangopol, Kawatani & Kim (eds)
© 2007 Taylor & Francis Group, London, ISBN 978-0-415-40655-0

Case study of a hands-on inspection for optimal maintenance planning for railway bridges

T. Kamizono, Y. Okamoto & F. Yamada
Kyobashi Mentec Co., Ltd., Osaka, Japan

H. Namiki
Kyobashi Corporation, Osaka, Japan

ABSTRACT: Railway Bridge inspections are roughly divided into Initial Inspection, Routine Inspection and In-Depth Inspection. An Initial Inspection is the first inspection of a bridge. A Routine Inspection is an inspection consisting of observations and measurements needed to identify deterioration of damage and any changes of circumstances of a bridge, since the Initial Inspection. If the results of the Routine Inspection show that the identified damage is unsound, an In-Depth Inspection, which is a close-up and hands-on inspection, is conducted to investigate the causes of damage in detail and to take appropriate measures to repair the damage. In order to acquire an optimal maintenance method for a structure in railway bridges, some examples of an In-Depth Inspection are given in this paper and the results are investigated. Moreover, an effective combination of In-Depth Inspections and efficient interval periods between In-Depth Inspections were investigated.

1 INTRODUCTION

The steel structures of railway bridges in Japan were initially designed using the technology of Britain, the United States, and Germany. Since then as Japan's economy has grown, many steel structures have been constructed, using the original technology of Japanese engineers according to the environmental background of Japan. These steel structures play an extremely important role in Japan's infrastructure today. Many of these structures, which have functioned effectively for about 100 years, are still in use. Since they have been used for a long time and their performance has been required increasingly, the maintenance management for the steel structures in a railway is a great challenge.

In order to keep railway bridges in sound condition, it is important to prioritize repair according to the severity of damage and weak points detected during inspections. As each structure is unique, it is necessary to understand the environmental conditions and other circumstances of a structure well and to maintain it accordingly. If appropriate maintenance is performed before defects and damage become fatal to a structure, the structural life can be prolonged considerably.

Bridge inspections are conducted to determine the physical and functional condition of the bridge. They also help to establish priorities for repair and rehabilitation programs.

Railway Bridge inspections are roughly divided into Initial Inspection, Routine Inspection and In-Depth Inspection. An Initial Inspection is the first inspection of a bridge as it becomes a part of the bridge file. The purpose of this inspection is the determination of baseline structural conditions and the identification and listing of any existing problems, or locations in the structure that may have potential problems. A Routine Inspection, which has to be done in two-year intervals, is an inspection consisting of observations and measurements needed to determine the physical and functional

condition of the bridge. It also identifies deterioration of damage and any changes of circumstances of a bridge since the Initial Inspection, and ensures that the structure continues to satisfy present service requirements. If the results of the Routine inspection show that the identified damage is unsound, an In-Depth Inspection, which is a close-up and hands-on inspection, is conducted to investigate the cause of damage in detail and to take appropriate measures to repair the damage.

In order to acquire an optimal maintenance method for a structure in railway bridges, some examples of an In-Depth Inspection are given in this paper and the results are investigated. Moreover, an effective combination of In-Depth Inspections, and efficient interval periods between In-Depth Inspections, are investigated.

2 A HANDS-ON INSPECTION

2.1 *Deflection measurement*

A deflection measurement is conducted to investigate the running safety of trains, the riding comfort of trains and the soundness of the bridge. The evaluations are examined as compared with the allowable values for each category.

Railway bridge "A" over the Kakogawa River in Kakogawa, Hyogo, Japan, which was constructed in 1922, has 30 simple steel deck girders, as shown in Fig. 1. The riveted structure consists of two steel girders, upper lateral bracing, sway bracing, supports and two piers and an abutment. The span length from the 1st to the 6th span is 13.411 meters and from the 7th to the 30th span is 13.793 meters. The total length of the bridge is about 410 meters. As an example, the vertical deflection response to moving trains was measured at the span center of the 2nd and the 30th simple girders of the inbound and outbound lines.

To measure the deflection of these girders, a deflection recorder, deflection sensors, probes and sectional temporary measurement tools, consisting of steel pipes, were used. One end of the tool was fixed to the girder at the span center, and the distance of the other end and the probe placed on the ground was measured by the sensor as shown in Fig. 2. The sampling frequency of the deflection measurement was 50 Hz. The operating speed of trains was about 65 km/h.

The deflection responses at the span center are shown in Fig. 3. The deflection response at the span center of the 2nd inbound line girders differed from the left and right girders. This difference resulted from the fact that the track center was not aligned with the beam center, the girders were in the transition curve section of the 550 meter curvature radius, and the differential settlement was generated at supports of the girders under running trains. The differential settlement generated at the supports had the greatest effect on the difference especially since each support had settled at four different levels: 2 mm, 0.5 mm, 0.5 mm and 0 mm. If the differential settlement was completely resolved, it is estimated it would decrease the deflection difference by approximately 40%.

Figure 1. Bridge "A".

However, this deflection difference has the potential to induce a fatigue crack from the hole of the rivet fastening secondary members, or to loosen a rivet fastening secondary members, and to induce a rolling vibration of trains.

Figure 4 shows the maximum deflection values as compared with the maximum deflections calculated by the simplified formula which does not contain a dynamic deflection. This deflection difference was generated on the 2nd inbound line girders and the 30th outbound line girders.

All the observed maximum deflections were less than the deflection limits L/800, which is 16.76 mm for the 1st to the 6th girders and 17.24 mm for the 7th to the 30th girders, for a bridge with the span length of less than 20 meters. The trains passed through the bridge with about 0.8 Hz slow vibration produced by static deflection. The vertical vibration of less than 1 Hz is not so noticeable for passengers as shown in Fig. 5. For the noticeable frequency range from 5 Hz to 20 Hz, the combined vibration of the girder and vehicle was not noticeable. The vibration of more than 10 Hz was not investigated. The riding comfort was not severely affected by the vertical vibration.

2.2 *Impact vibration test*

The impact vibration test is now regarded as a method to evaluate the conditions of bridge substructures based on the effect of earthquakes and the scour around the bridge pier base. The natural frequency of a bridge pier is measured by giving an impact vibration to the bridge pier. This value is compared with the standard value of the natural frequency. In this case, the standard value of the natural frequency is calculated by the formula derived statistically for each foundation type using several parameters, such as the height of the pier, weight of the superstructure and width of the

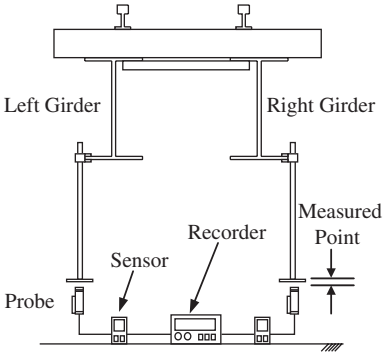

Figure 2. Measuring method.

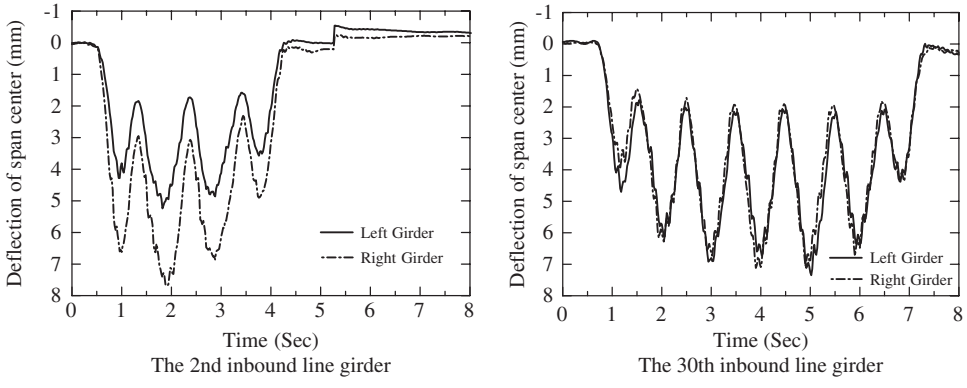

Figure 3. The deflection response at the span center.

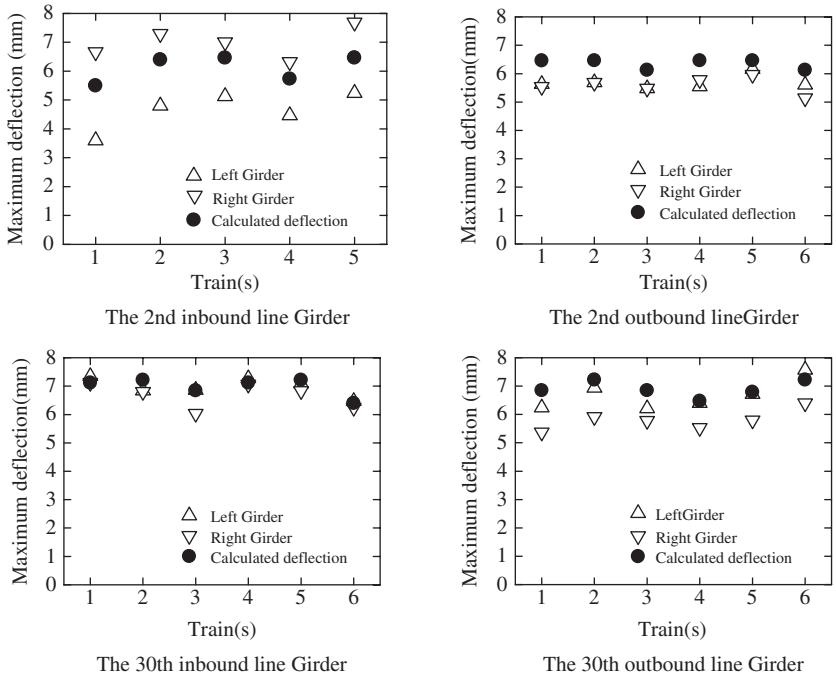

Figure 4. The maximum deflection.

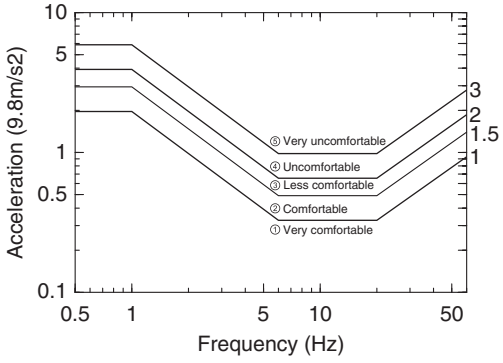

Figure 5. Riding comfort of Janeway (Vertical).

pier, not by using eigen value analysis. It is judged that a bridge substructure is sound if a measured natural frequency is higher than the calculated standard value.

The bridge "A" has 29 piers and 2 abutments supporting the double track. These piers use the caisson type foundation. The measured points were at the pier top, the middle pier and the span center of the girder.

The top of the pier was given the impact vibration at a right angle to the bridge axle using a heavy bob, which weights 50 kg, dangled at the end of the timber overhanged from the upper flange of the girder as shown in Fig. 6 and Fig. 7. The dynamic responses at the top and middle pier were measured by the velocimeters placed at these points. The sampling frequency of the velocity measurement was 100 Hz. The test was conducted 10 times at each bridge pier and the measured responses were superposed for the purpose of eliminating unrelated noise. The natural frequency was calculated from the superposed response using Fourier analysis.

Figure 6. Impact vibration test.

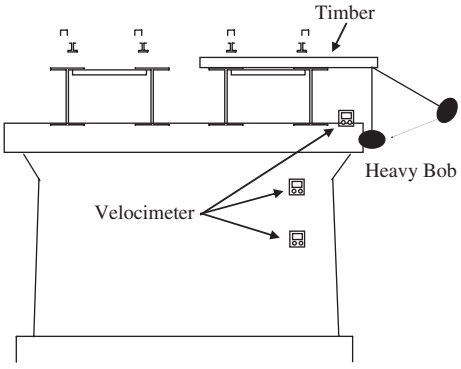

Figure 7. Measuring method.

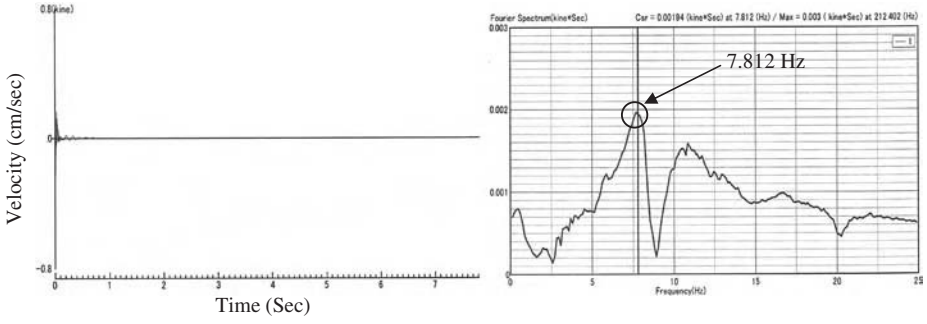

Figure 8. The superposed response to the impact vibration at the top of the 2nd pier.

For example, Fig. 8 shows the superposed response to the impact vibration at the top of the 2nd pier. Since there was a cold joint in the middle of the pier, the points above and below the cold joint were also measured, and the pier behavior was investigated. The measured natural frequencies at the pier top and middle were of the equal value: 7.812 Hz, and the value was higher than the standard value: 6.523 Hz. Therefore, it was judged that the pier was without harmful effects from the cold joint and scour.

The impact vibration test was also conducted at other bridge. For the type of the bridge piers, since there was no appropriate formula to calculate the standard of the natural frequency, the data we measured can be used for future maintenance management by using this measurement data as initial data.

2.3 *Fatigue assessment of reinforced stringers*

2.3.1 *New method to reinforce stringers*

The bridge “B”, which was constructed in 1899, has a double track under-road plat truss with a span of 31.6 meters. In a routine inspection many cracks were found at the upper flanges and the gusset plates of the stringer of the truss. The stiffened angle members were placed below the existing upper flange, and the existing lateral bracing was removed after the new lateral bracing was placed to the stiffen members through the gusset plate. The lateral load was suspected to cause fatigue failure of the web between the upper flange and stiffened angles because the new lateral bracing was placed to the stiffened angle below the existing upper flange. The lateral deformation of the railway rail was measured to estimate the lateral load.

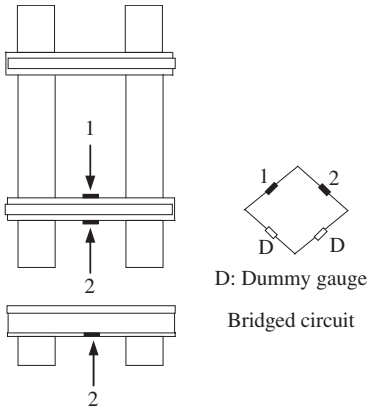

Figure 9. Bending strain measuring method.

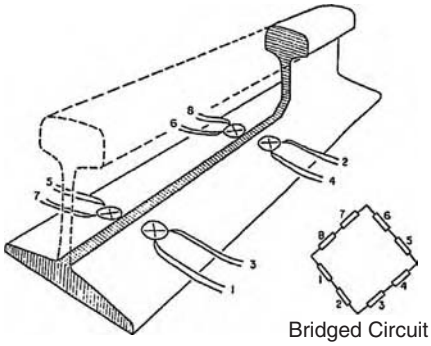

Figure 10. Shear strain measuring method.

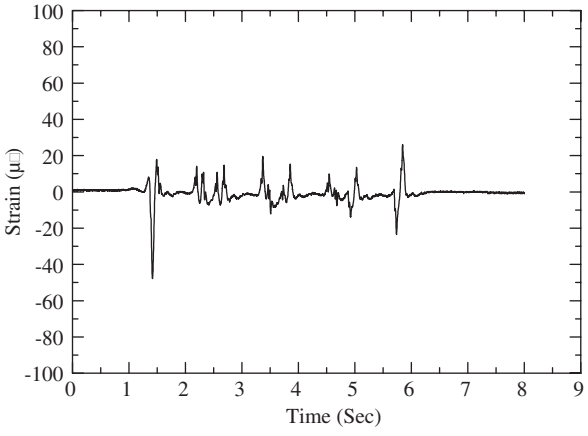

Figure 11. Measured bending strain.

2.3.2 *Dynamic approach*

The lateral load is a load generated when a bogie runs at an angle on a railway track. Strain gauges were placed on the lower part of one of the rails and the value of the load was obtained by measuring the dynamic strain of the rail under running trains. There are 2 ways of measuring this load. One method measures the bending strain at the base of a rail under running trains as shown in Fig. 9. The other method measures shear strain at the lower part of a rail web under running trains as shown in Fig. 10. Using the bending strain measuring method makes it difficult to observe the lateral load exactly, because the measured value is affected by the neighboring axle of the train. Since the measured value using the shear strain measuring method, which uses 4 gauges, is not affected by the neighboring axle of the train, the load is measured clearly. However, since connecting the 4 gauges is complicated, it is easy to make a mistake.

Since the bending strain measuring method has the advantage that connecting gauges are simple, the lateral load was measured at the rail base above the floor beam, near the rail joint and above the lattice point of the lateral bracing, using the bending strain measuring method. The load was calculated from the measured strain, assuming that the rail was a continuous beam since it is attached to the sleepers using a rail anchor. Figure 11 shows the measured strain, using the bending strain measuring method. The load calculated from the dynamic strain was about 7 kN at the most.

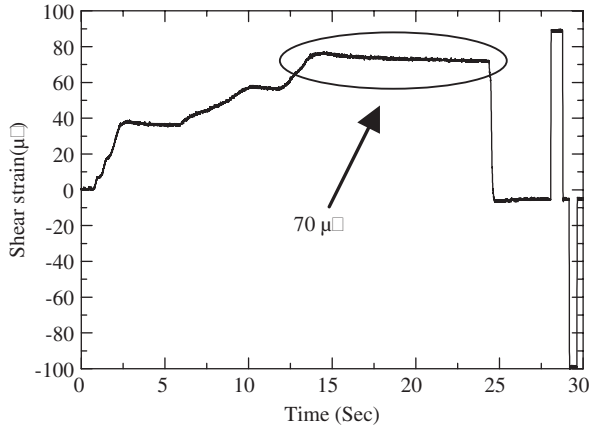

Figure 12. Calibration data.

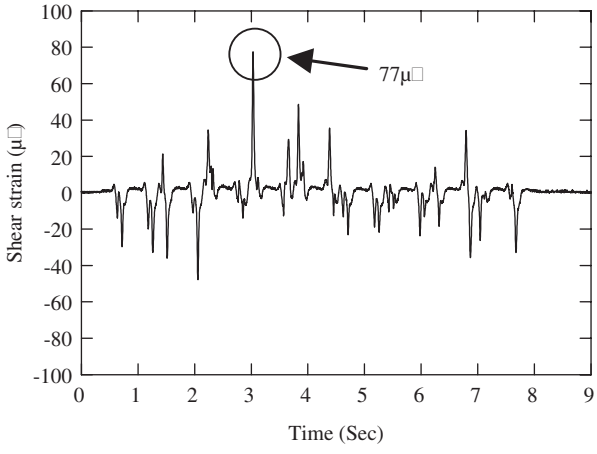

Figure 13. Measured shear strain at site.

Then, since the lateral load was suspected to cause fatigue failure of the web between the upper flange and stiffened angles above the lattice point of the lateral bracing, the load was measured at the lower part of the rail web above the lattice point of the lateral bracing using the shear strain measuring method. A gauge test was performed to check the gauges' connection and the bonding by applying a lateral force to the head of the rail before measuring the load. Moreover, the calibration of the shear strain measuring was performed. The measured strain at the lower part of the rail web above the lattice point of the lateral bracing was about 70 με when applying the lateral force of 9.8 kN to the head of the rail, as shown in Fig. 12. Figure 13 shows the dynamic strain at the lower part of the rail web above the lattice point of the lateral bracing when measured as a train passed. Since the measured strain was 77 με at the most, it is assumed that the lateral load was about 10 kN in this section of the rail. For this line, the design lateral load is 60 kN and the measured load was less than the design load.

2.3.3 *Static calibration*

For the purpose of investigating the local bending of the web between the upper flange and stiffened angles above the lattice point of the lateral bracing while applying the lateral load, the static loading test was performed. The special gauge, which is used to measure stress concentration, was placed

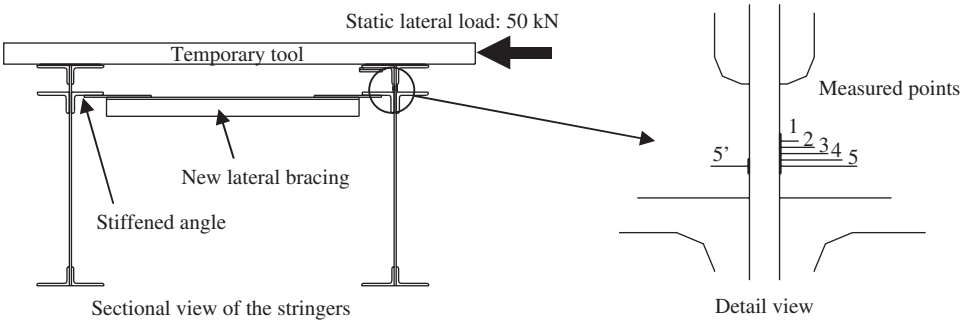

Figure 14. The measuring method of static loading test.

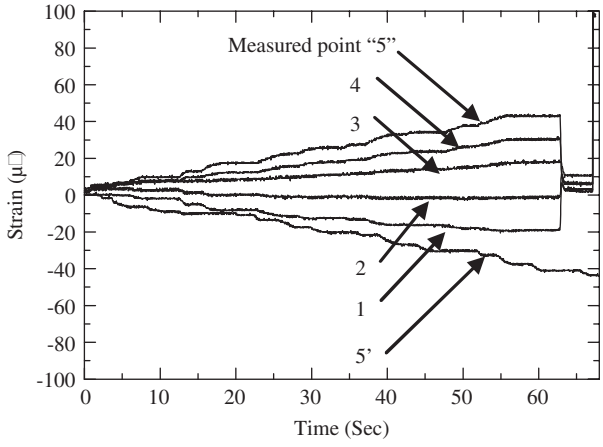

Figure 15. The response of the static loading test.

on the web. The behavior of the web was observed by applying the lateral force of 50 kN to the temporary measurement tool fixed on the upper flange above the web as shown in Fig. 14. The measured static strain of the web is shown in Fig. 15. The strain at the point of 2 mm lower than the middle of the web, which was at the measured point "2", was about 0. The compression strain was observed at the web above the point and the tensile strain was observed at the web below the point. When applying the lateral load (50 kN) to the rail, the web between the upper flange and stiffened angles was bent locally. The stress distribution of the web was calculated from measured strains and the extrapolation curve of the stress obtained from the calculated stress distribution is shown in Fig. 16. The maximum stress of the web is estimated to be about 34 MPa. When applying the lateral load of 60 kN, which is the design load, to the rail, the maximum stress of the web is estimated to be about 41 MPa.

2.3.4 *Estimation of fatigue life*

The fatigue limit of the web plate under consideration should be classified into the category "B", because currently available steel beams are made of basic material with surface roughness of lower than 50s. But considering the fact that it is an old beam, it is classified into category "C", which is one grade lower, and the stress allowed is 115 MPa.

The dynamic strain at the web was observed under running trains. Since the strain generated due to the lateral load at the measured point "2" was 0 from the result of the static loading test, the strain generated due to the lateral load at the measured point "5" was obtained by subtracting

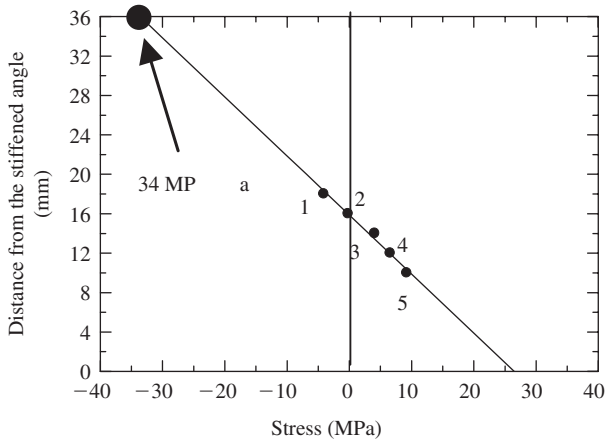

Figure 16. The extrapolation curve of the stress at the web.

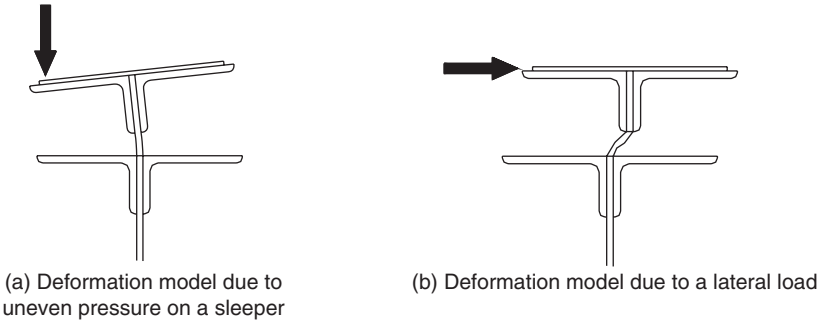

Figure 17. The deformation model.

the strain value observed at the measured point “5” from the strain value observed at the measured point “2”. The strain at the measured point “2” was mainly generated in the upper flange angle due to uneven pressure on the sleeper. The uneven pressure on the sleeper was estimated to be equal at each measured point, as shown in Fig. 17. Since the subtracted strain at the measured point “5”, which was generated due to the lateral load, was 8 $\mu\varepsilon$ at the most, as shown in Fig. 18, the stress calculated from the strain was 1.6 MPa. The maximum stress of the web was estimated to be about 5.5 Mpa. If the generated stress at the most was 5.5 Mpa when applying the lateral load 10 kN to the rail, the generated stress at the most was estimated to be about 33 kN when applying the lateral load 60 kN, which is the design load, to the rail. The fatigue limit of the web plate is classified into category “C” and the stress allowed is about 115 MPa. Therefore, it was determined that the web is safe in regard to fatigue from results of the static loading test and the dynamic response under running trains.

3 OPTIMAL INTERVALS AND TYPE COMBINATIONS OF INSPECTIONS

Successful bridge inspections are dependent on proper planning and techniques, adequate equipment, and experience and reliability of the personnel performing the inspections. Inspections should not be confined to searching for defects which may exist, but should include anticipating problems. Thus, inspections are performed in order to develop both preventive as well as corrective maintenance programs.

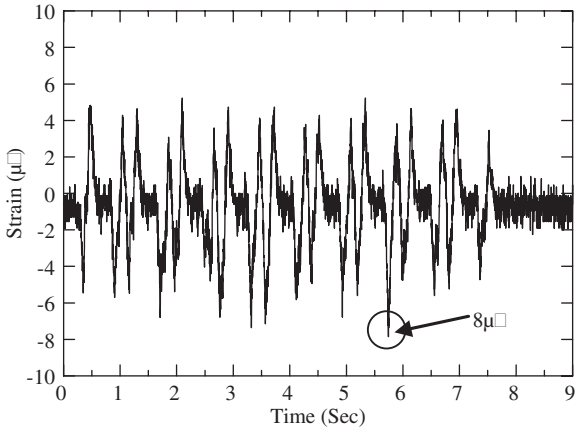

Figure 18. The strain generated due to the lateral load at the measured point “6”.

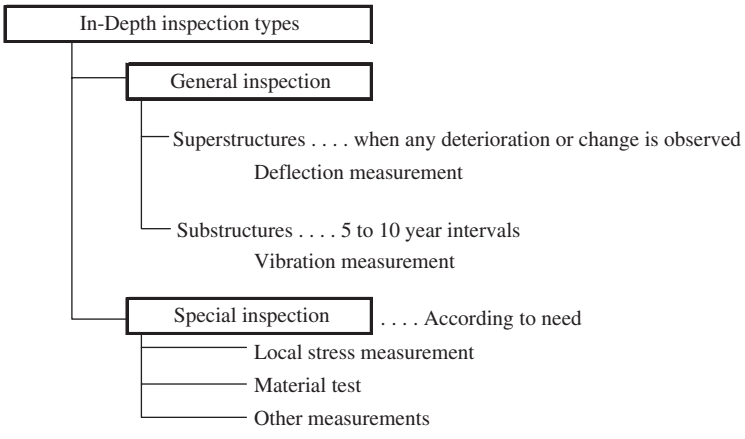

Figure 19. The intervals and type combinations of In-Depth inspections.

General kinds of an In-Depth inspection have a deflection measurement, a vibration measurement and a quantity of rust measurement.

For a superstructure of a bridge, a deflection measurement should be performed to assess structural damage resulting from environmental factors or any change, since a load carrying capacity which a bridge has can be identified by performing a deflection measurement. A deflection measurement needs to be performed before a service period. When any deterioration or change is observed, a deflection measurement should be performed to determine the need for a repair, an improvement or a monitoring compared with the initial deflection.

For a substructure of a bridge, it is advisable to measure vibration at intervals, because a substructure is constantly affected by scour. Since bridges often deteriorate over a 10 year period, it is preferable that a vibration measurement be conducted in 5 to 10 year intervals.

Special kinds of an In-Depth inspection use a local stress measurement, a material test and a live load measurement. An appropriate inspection using these measurements should be conducted according to need. The inspection is also conducted to obtain the detail data for the purpose of selecting an appropriate repair. Figure 19 shows the intervals and type combinations of In-Depth inspections.

4 CONCLUSION

The deflection measurements were conducted to investigate the running safety of trains, the riding comfort of trains and the soundness of the bridge. This deflection difference was generated on the 2nd inbound line girders. Even if the differential settlement were resolved, the deflection difference would have remained. However, it has an extremely low feasibility rating to eliminate the deflection difference completely by adjusting the track and beam center and straightening the track alignment.

The impact vibration tests were performed to evaluate the conditions of bridge substructures based on the effect of earthquakes and the scour around the bridge pier base. The soundness of the substructures was identified, and the natural frequencies of the substructures were gathered as initial data. For the bridges which have not been observed, the impact vibration tests should be performed as soon as possible, to identify the soundness of the structures, to obtain the natural frequency as initial data, and to manage the structures in the future.

The lateral load was observed using the bending and shear strain measuring method, and the static and dynamic strain was measured at the web between the upper flange and stiffened angles above the lattice point of the lateral bracing. The interrelation between the lateral load and the generated stress at the web was investigated from these results. The web is safe in regard to fatigue. The maximum stress of 33 Mpa at the web calculated from the dynamic strain measured at the web under running trains was less than the maximum stress of 41 Mpa at the web calculated from the result of the static loading test. One of the main reasons is the fact that the lateral load was distributed by the sleepers and rail.

An effective combination of In-Depth Inspections, and efficient interval periods between In-Depth Inspections, were investigated. The intervals and combination type of inspections are not decided in detail at present, and In-Depth inspections are not often performed. Moreover, the appropriate measure, which is a repair, an improvement or a monitoring, should be decided reflecting the result of In-Depth inspections. However, it is actually difficult to implement the optimal maintenance management, because of financial resource restrictions and the effects of other strategic projects.

REFERENCES

Railway Technical Research Institute. 2000. The design standard and description for steel railway structures in Japan

American Association of State Highway and Transportation Officials. 1994. Manual for Condition Evaluation of Bridges

Railway Technical Research Institute. 1990. The standard and description of maintenance management for steel railway structures in Japan

Japan Association of Railway Institutions. 1980. The View of Civil Structure Replacement

Reliability and Optimization of Structural Systems: Assessment, Design and Life-Cycle Performance – Frangopol, Kawatani & Kim (eds)
© 2007 Taylor & Francis Group, London, ISBN 978-0-415-40655-0

Condition rating methodology on RC bridges with chloride induced deterioration

H. Kano
Kinki Region Branch, Japan Bridge Engineering Center, Chuo, Osaka, Japan

H. Morikawa
Department of Civil Engineering, Kobe University, Nada, Kobe, Japan

ABSTRACT: To evaluate performance simply by using grading technique (i.e. using visual inspection result) and judging need of the detailed inspection play a key role in executing effective maintenance by the limited budget. Therefore, authors adopted the condition rating as one of the simple performance evaluation techniques, and improved a little to become more reliable. And authors tried to apply the condition rating to some cases of RC superstructure damaged by chloride induced deterioration. Furthermore, the trial calculation results of the condition rating were compared with the inspection results of actual structure which was associated with the loading test result concerning mass loss of RC test beam. Consequently, it turned out that the parameters of simple performance evaluation in the condition rating could be evaluated as value including the parameter about the uncertainty of inspection result.

1 INTRODUCTION

As the concrete structure that has been used for a long term increases, the maintenance expense will be expected to increase in the future, too. Therefore, a research and technological development to do reasonable maintenance management more at a low price are conducted as a problem of the pressing need in relevant field of maintenance. The authors took up the CEB condition rating (the condition rating) as one of the simple performance evaluation technique. The authors examined whether the technique is applicable and also tried to improve the technique to give a useful judgment index about necessity of a detailed inspection. These are discussed in this paper as follows.

2 ROLE AND IMPORTANCE OF SIMPLE PERFORMANCE EVALUATION BASED ON ROUTINE AND PERIODIC INSPECTION RESULT

In executing maintenance, a maintenance plan, which is based on the deterioration prediction considering the importance, the threat posed to third parties, and the environmental condition of the target structure, is settled on (Japan Society of Civil Engineers. 2001). An example of the maintenance flow chart shows in Figure 1.

Routine or periodic inspection which is composed mainly of visual inspection is carried out in order to check on the condition of a structure. These inspections are the most basic measure paying attention to the presence of deterioration factors or something defective at the performance degradation that is the feature of concrete structure. Though the evaluation and the judgment of a detailed inspection necessity are based on these inspection results, semi-quantitative evaluation

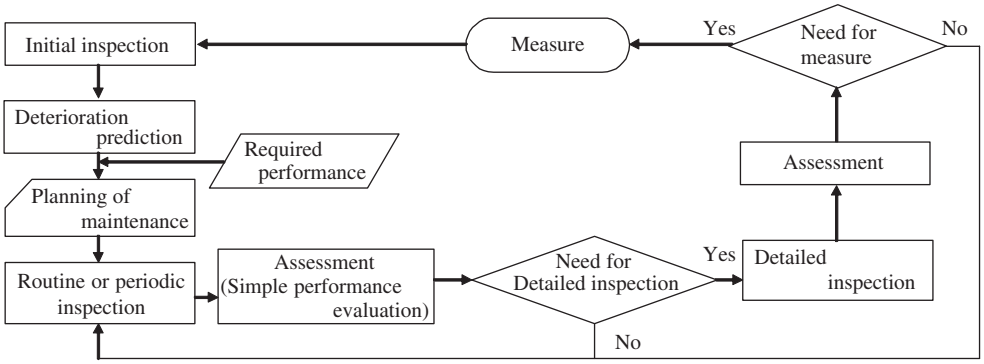

Figure 1. An example of maintenance management flow.

measure such as grading has been researched and developed as a useful evaluation measure of the qualitative data obtained at routine and periodic inspection (Japan Society of Civil Engineers. 1995).

However, because neither the accuracy nor reliability is able to clarified, it is difficult to evaluate performance enough such as safety performance of the structure according to these inspection data as yet. It will be necessary to judge the necessity of a detailed inspection according to more appropriate timing as the structure to be maintained increases in the future.

Therefore, it is hoped for not only the improvement of accuracy and reliability obtained from routine and periodic inspection data but also the development of more reliable measure that the performance evaluates simply from those data.

3 THE SIMPLE PERFORMANCE EVALUATION MEASURE APPLYING THE CONDITION RATING METHODOLOGY

The CBE condition rating is taken up as an example of the simple performance evaluation methodology by routine and periodic inspection result, and basic idea and calculation method are shown.

3.1 *Outline of the condition rating*

The condition rating is a measure that has developed aiming at the quantification to evaluate the level of deterioration and to place in the preliminary order for detailed inspection, and remedial measures. The feature of the condition rating is the following two points.

First of all, rating value is shown not in the total adding point based on the table set for every damage type, level, range, etc. but in the ratio between the value at the time of the inspection and the maximum state value of deterioration that could realistically occur in the environmental condition.

Secondly, the simple performance evaluation index is given by calculating safety factor *RF* of the member by using capacity reduction factor, which is defined according to the deterioration class classified by the rating value.

3.2 *Calculation procedure*

The general expression for condition rating of a damaged structure is defined by the sum of damage values V_D:

$$V_D = B_i \times K_{1i} \times K_{2i} \times K_{3i} \times K_{4i} \tag{1}$$

Table 1. Damage types, associated basic values B_i and criteria for evaluation of the degree (intensity).

		Degree of damage			
Damage type	B_i	I ($K_{2i} = 0.5$)	II ($K_{2i} = 1.0$)	III ($K_{2i} = 1.5$)	IV ($K_{2i} = 2.0$)
Plastic shrinkage and plastic settlement cracks, crazing, cracks caused by inefficient joints	1	Single smaller	Several smaller	Few stronger	Many stronger
Cracking caused by direct loading, imposed deformations and restraint	3	Single <0.5 mm	Several <0.5 mm	Single >0.5 mm	Several >0.5 mm
Mech. Damages, erosion, collision	1	I. Damage is small size, generally appearing on single locations of a member. II. Damage is of medium size, confined to single localities, or, damage is of small size appearing on few localities or on a small area of a member.			
Efflorescence, exudation, popouts	1	III. Damage is of large size, appearing on many localities or on greater area of a member. IV. Damage is of very large size, appearing on the major part of a member.			
Leakage through concrete	2	I. Light and medium II. Heavy and severe Chlorides < 0.4% cement		III. Light and medium IV. Heavy and severe Chloride > 0.4% cement	
Leakage at cracks, joints, embedded items	2	ditto		ditto	
Wet surface	1	ditto		ditto	
Cover defects caused by reinforcement corrosion	2	Rust stains, light	Rust stains, heavy	Cracks over stirrups	Delaminations over stirrups
Spalling caused by corrosion of reinforcement	3	I. Finer cracks along reinforcing bars in corners, II. Finer cracks along other reinforcing bars, and/or, wider longitudinal cracks or exposed reinforcement along corners, III. Wider cracks along other bars or exposed reinforcement, IV. Hollow areas and surface spalling.			

Table 2. Factor K_{3i} – general criteria for the extent of a damage type.

Criterion	K_{3i}
Damage is confined to a single unit of the same bridge member	0.5
Damage is appearing on several units (e.g. less than 1/4) of the same bridge member	1.0
Damage is appearing on the major part of unit (e.g. 1/4 to 3/4) of the same bridge member	1.5
Damage is appearing on the great majority of unit (e.g. more than 3/4) of the same bridge member	2.0

where:

V_D: damage type value, only the parameters taken up by this paper were shown in Table 1.

B_i: basic value associated with the damage type "i", expressing the potential effect of the damage type "i" on the safety and/or durability of the observed structural component, ranging from 1 to 4 (see Table 1);

K_{1i}: factor of the structural member, which is part of the structural component, on which the damage type "i" is appearing, accounting for the member's effect on the overall safety and/or durability of the component. The value of K_{1i} was defined as 1 ($K_{1i} = 1$) because of discussion only for a structural member in this paper;

K_{2i}: factor indicating the intensity/degree of the type "i". Values and general descriptive criteria are given in Table 1, while the numerical criteria, associated with certain damage types are shown together with basic values in Table 1;

K_{3i}: factor covering the extent of propagation of the damage type "i" on the entire observed member or on all items of same member type. Values and selection criteria are given in Table 2;

K_{4i}: factor emphasizing the urgency of necessary intervention in case that the damage type "*i*" is directly jeopardizing the safety of the component or the users (within the range from 1 to 5).

The rating value R_c of the observed structure is defined as:

$$R_C = \frac{\sum V_D}{\sum V_{D.ref}} \times 100 = \frac{\sum_1^k K_{1m} \times M_m}{\sum_1^k K_{1m} \times M_{m.ref}} \times 100 \quad (2)$$

$$M_m = \sum_1^n B_i \times K_{2i} \times K_{3i} \times K_{4i} \quad (3)$$

$$M_{m.ref} = \sum_1^t B_i \times K_{2i} \times K_{3i} \times K_{4i} \quad (4)$$

where:

ΣV_D: effective sum of damage values calculated for the observed structure or its part (e.g. bridge component), related to the detected damage types from the list in Table 1(K_2, K_3, and K_4 as allotted by the inspector at the inspection)

$\Sigma V_{D.ref}$: reference sum of damage values obtained by taking into account every damage type listed in Table 1, that could potentially occur on the same observed structure or its part, multiplied by unit values of factors of intensity and extent. ($K_{2i} = K_{3i} = 2$, $K_{4i} = \text{const.} = 1$)

K: number if members "*m*" within the observed structure; *n*: number of detected and evaluated damage types "*i*" on a member "m"; *t*: total number of potential damage types on the member "*m*" (from Table 1)

The deterioration class of a structural element and/or a member is judged based on the rating value R_c calculated from the inspection result. Moreover, the capacity reduction factor Φ is calculated by equation (5) when no visible deterioration of the structure is observed, and rating factor (safety factor) RF of the member is evaluated by equation (6):

$$\Phi = B_R \times e^{-\alpha_R \times \beta_c \times V_R} \quad (5)$$

$$RF = \frac{\Phi * R_d - \gamma_G * G_n}{\gamma_Q * Q_n (1 + I)} \quad (6)$$

where:

Φ: capacity reduction factor for the observed member (0.5 (bad) – over 1.0 (well)), B_R: bias, i.e. ratio between the true and the designed mean resistance of the relevant member section ($B_R = R_a/R_d$), R_a: mean remaining capacity in the relevant section, and for the relevant action effect (bending, shear), R_d: design capacity of the critical section ($G + Q$), α_R: deterioration factor, in relation to the obtained rating value (see Table 3), V_R: coefficient of variation, to be chosen with regard to the level of reliability of the test and inspection data, β_c: target reliability index (e.g. for bridge super structure: $\beta > 2.5$), RF: safety factor, I: impact value (in case bridge structures), G_n, Q_n, γ_G, γ_Q: dead load and live load effect, and partial safety factors of dead and live load effect in the critical section.

4 TRIAL CALCULATION OF THE RATING VALUES

4.1 *Partial improvement of the parameter table*

When the condition rating is applied as a simple performance evaluation technique, it is necessary to consider that the appearing location of deterioration affects its performance. For instance, on evaluating that pays attention to bending, it is considered that the location where lage bending

Table 3. Deterioration classes and deterioration factor.

Deterioration class	Description of the condition, necessary intervention	Rating values R_c	α_R
I	No defects, only construction deficiencies. No repair only regular maintenance needed.	0 to 5	0.3
II	Low degree deterioration, which only after longer period of time might be the cause for reduced serviceability or durability of the affected structural component, if not repaired in proper time. Deterioration locations can be repaired with low costs as part of regular maintenance works.	3 to 10	0.4
III	Medium degree deterioration, which can be the cause for reduced serviceability and durability of the affected structural component, but still not requiring any limitation of use of the structure. Repair in reasonably short time is required.	7 to 15	0.5
IV	High degree deterioration, reducing the serviceability and durability of the structure, but still not requiring serious limitation of use. Immediate repair to preserve the designed serviceability and durability is required.	12 to 25	0.6
V	Very heavy deterioration, requiring limitation of use (e.g. restricted vehicle weight on bridges), propping of most critical components, or other protective measures. Immediate repair and strengthening of the structure is required or the carrying capacity shall be adequately reduced.	22 to 35	0.7
VI	Critical deterioration, requiring immediate propping of the structure and strong limitation of the use, e.g. closing of the bridge. Immediate and extensive rehabilitation works are needed, however the design serviceability and use of the structure, as well as acceptable remaining service can be no more be achieved with economic costs.	over 30	–

moment is affecting influences its performance more than any other location in a girder. In this paper, weight concerning the location of appearing deterioration was given to factor K_{3i} covering the extent of propagation, so the calculation method was improved to raise the evaluation value of K_{3i} by one rank (+0.5) within the range where 2.0 is not exceeded, if the critical section is included within the location, and to consider the influence.

4.2 *Trial calculation procedure*

Japan Society of Civil Engineers: Appendix of "Standard Specifications for Concrete Structures (Maintenance)" illustrated structures deteriorated by chloride induced deterioration. Referring the case of accelerating period and deteriorating period, the rating values R_c assumed routine and periodic inspection were tried to calculate based on the following assumption ((a) to (d)).

(a) The photograph assumed state of deterioration in RC superstructure girder, and assumed the simple performance evaluation concerning the bending moment.
(b) Though only half one side (1/4 in the entire girder) of the girder of the total length was able to be confirmed in the photograph, it was assumed that the state of deterioration extended to overall.
(c) Only damage types shown in Table 1 were considered because of unclear environmental condition etc., though the definition of the value $M_{m.ref}$ of equation (2) was the reference sum of every damage type that could realistically occur.
(d) Factor of the structural member K_{1i} and factor emphasizing the urgency of necessary intervention K_{4i} assumed to be $K_{1i} = K_{4i} = 1$, as it was discussing about a girder.

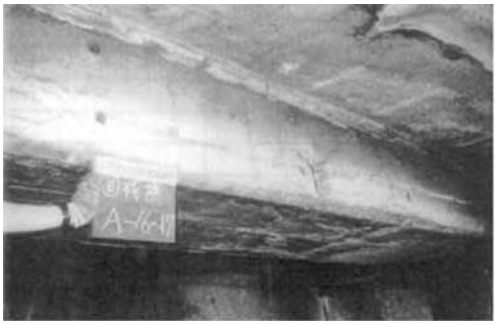

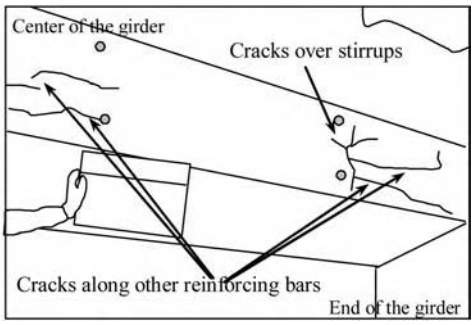

Photograph 1. Figure 2. The case of latter accelerating period with chloride induced deterioration.

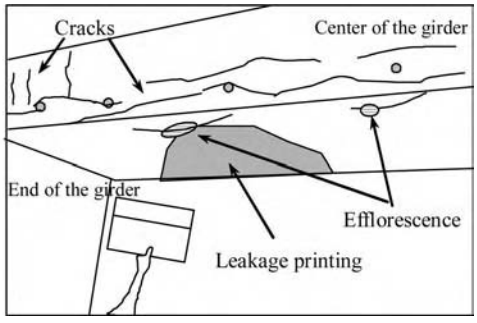

Photograph 2. Figure 3. The case of deteriorating period with chloride induced deterioration.

The case of latter accelerating period with chloride induced deterioration is shown in Photograph 1 and Figure 2, and the case of deteriorating period is shown in Photograph 2 and Figure 3.

Table 4 shows the results of trial calculation for the condition rating. Table 5 also shows deterioration classes according to the rating values. The evaluated deterioration classes (Table 3) were almost same as the definition of deterioration grade on appearance shows in Japan Society of Civil Engineers: “Standard Specifications for Concrete Structures (Maintenance)”.

5 CONSIDERATION OF SIMPLE PERFORMANCE EVALUATION PARAMETER BY COMPARISON WITH DETAILED DETERIORATION PREDICTION RESULT

It was considered tendency of the deterioration factor α_R and the coefficient of variation V_R given by the rating value R_c and how to give the parameter in the formula of capacity reduction factor Φ in such a way that the simple performance evaluation result obtaining from the rating value R_c compared to the inspection result for similar structure and bending destruction test result of RC beam specimen in consideration of mass loss ratio of reinforcing bars reported by Morita et al.

5.1 *Proposal for calculation function of α_R*

When a simple performance is evaluated, the deterioration factor α_R value is given by deterioration class depending on the rating value R_c in Table 3. But, range in each deterioration class might overlap, so two α_R or Φ is given to one R_c. The relation of R_c and α_R should be 1 for 1 from the viewpoint of the performance evaluation. Therefore, median within the range of R_c of each deterioration class and α_R were Involution approximation by the least-squares method as shown in

Table 4. The results of trial calculation for the condition rating.

Damage type	B_i	(1) Latter accelerating period				(2) Deteriorating period			
		K_{1i}	K_{2i}	K_{3i}	K_{4i}	K_{1i}	K_{2i}	K_{3i}	K_{4i}
Plastic shrinkage and plastic settlement cracks, crazing, cracks caused by inefficient joints	1	1.0	–	–	1.0	1.0	–	–	1.0
Cracking caused by direct loading, imposed deformations and restraint	3		–	–			–	–	
Mech. Damages, erosion, collision	1		–	–			–	–	
Leakage through concrete	1		–	–			0.5	0.5 + 0.5	
Leakage at cracks, joints, embedded items	2		–	–			–	–	
Wet surface	2		–	–			–	–	
Cover defects caused by reinforcement corrosion	1		–	–			–	–	
Spalling caused by corrosion of reinforcement	2		1.5	1.0			1.5	1.5 + 0.5	
Leakage through concrete	3		0.5	1.5 + 0.5			0.5	2.0 + 0.0	
Calculation result		$M_{m(1)} = 3.0 + 3.0 = 6.0$, $M_{m,ref(1)} = 64$ $R_{c(1)} = 6.0/64 \times 100 = 9.4\%$				$M_{m(2)} = 0.5 + 6.0 + 3.0 = 9.5$, $M_{m,ref(2)} = 64$ $R_{c(2)} = 9.5/64 \times 100 = 14.8\%$			

Table 5. Deterioration classes according to the rating values.

Deterioration process	Rating value R_c (%)	Deterioration class (See Table 3)
(1) Latter accelerating period	9.4	II or III
(2) Deteriorating period	14.8	III or IV

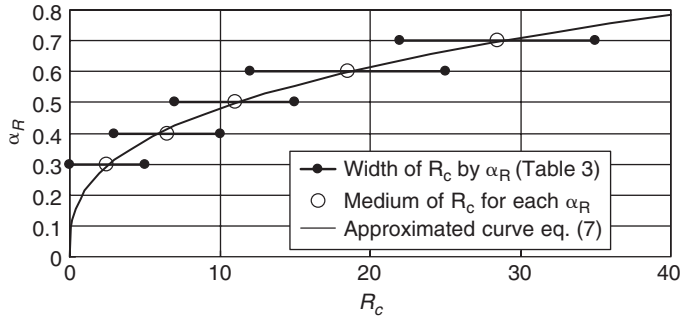

Figure 4. Involution approximation by the least-squares method.

Figure 4, then it assumed to be α_R calculation function shown in equation (7).

$$\alpha_R = 0.214 R_c^{0.353} \tag{7}$$

5.2 *Consideration of reasonableness for calculating parameter of capacity reduction factor*

Φ U_d as a simple performance evaluation result given by the rating value was compared with bending capacity reduction of the RC beam specimen considering mass loss ratio of reinforcing

Table 6. Calculation result of α_R, β_c ,V_R.

	Rating value R_C(%)	α_R eq. (7)	U	$\beta c \cdot V_R$	βc	V_R
(1) Latter accelerating period	9.4	0.47	0.88	0.272	2.3	0.118
					4.3	0.063
(2) Deteriorating period	14.8	0.55	0.76	0.497	2.3	0.216
					4.3	0.115

bars, and validity of the capacity reduction factor Φ calculation parameters were examined. In general, because the crack width and the crack pattern (flaking off crack and crack along reinforcing bar) by corrosion mass loss of reinforcing bar is different for each cover or diameter of reinforcing bar according to Takewaka et al. and Tsutsumi et al., it is difficult to discuss as an enough object of comparison. At the same time, following conditions were assumed within the range in which it did not deviate from definition of deterioration process on appearance of structure, state of deterioration and standard performance reduction (JSCE. 2001). It was assumed that the simple performance evaluation result (capacity $\Phi\ U_d$) and the experiment result of the RC beam (capacity U) were concerned in bending moment capacity of the same structure.

Then, the capacity set $\Phi\ U_d = U = 1.0$ when it was healthy. The corrosion mass loss ratio of reinforcing bars, which is in the case of latter accelerating period shown in Photograph 1 and Figure 2, was assumed to be 10% based on measurement average value 11.8% on an actual structure at the location on just about spalling that is defined as a boundary between accelerating period and deteriorating period (by Morita et al.). Moreover, the bending moment capacity at this time was assumed to be 0.88 from the experiment value when the mass loss of reinforcing bars in weight rate was 10% (by Morita et al.). In the same manner as former, the corrosion mass loss ratio of reinforcing bars, which is in the case of deteriorating period shown in Photograph 2 and Figure 3, was assumed to be 20%, as it was considered initial stage comparatively of deteriorating period because no large area flaking or spalling at cover was appearing though the number of cracks increased and local area flaking appeared. Moreover, the bending moment capacity at this time was assumed to be 0.76 from the experiment value when the mass loss of reinforcing bars in weight rate was 20% (by Morita et al.). α_R, β_c, and V_R obtained from equation (5) and equation (7) were brought together in Table 6. However, β_c was assumed to be a constant within range (2.3 to 4.3) of target reliability index to the state of ultimate limit in ISO/CD13822; Structure design standard – Assessment for existing structure.

Table 6 shows that the value V_R of deteriorating period is larger than accelerating period. Although this means the value V_R has to be given not constant but large as terrible defective level on external of inspected structure, it is so difficult to set relation between external defectives level and V_R so far, which is one of the key factors that influence uncertainty of inspection result; it is large depending on the research in the future. From Figure 4 and Table 6, however, it is considered that the reduced capacity according to β_c would be able to evaluate by the evaluation value given by R_c with $\alpha_R \cdot V_R$ at $\beta_c = 2.3$ including uncertainty of inspection result because of α_R and V_R are in proportional relation according to the rating value R_c. The least-squares approximation of R_c and $\alpha_R \cdot V_R$ on assuming $\beta_c = 2.3$ is shown in equation (8).

$$\alpha_R \cdot V_R = 0.0079 R_c \quad (\beta_c = 2.3) \tag{8}$$

As an annotation, the approximation function is considered as a straight line, and none variation to the inspection result of $R_c = 0.0$ (none defective) because there are only two cases of trial calculation results this time, and the segment of the approximation straight line is assumed to be 0. Moreover, if $\Phi \cdot U_d$ of an important structure is assessed, the evaluated value will be able to be considered its importance, applying larger β_c to equation (5). For example, it is meant for $\beta_c = 4.3$

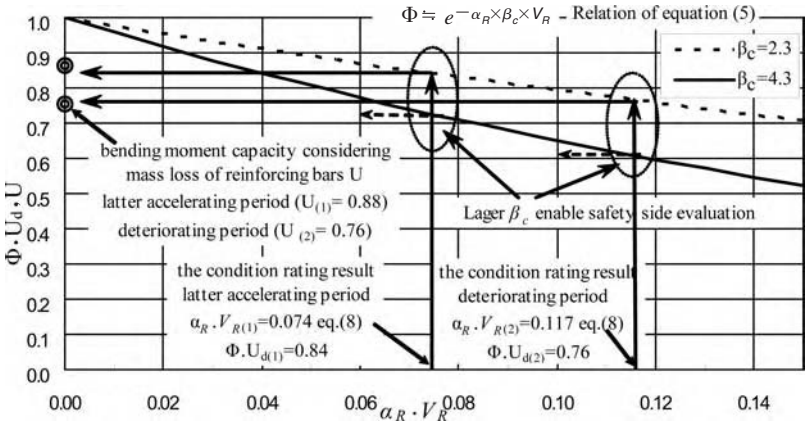

Figure 5. Re-calculation result of $\Phi \cdot U_d$, safety factor for β_c and an image of safety side evaluation.

to consider the safety factor of 1.87 times against $\beta_c = 2.3$. The result of re-calculation of $\Phi \cdot U_d$ by equation (5) and (8), and an image of safety side evaluation adopting large β_c is shown in Figure 5.

6 SUMMARY

For development of the simple performance evaluation technique based on routine and periodic inspection result, the improvement considered the appearing location of deterioration and trial calculation were executed. Moreover, according to a comparative study of tendency to α_R calculation parameter in the simple performance evaluation referring to inspection result of an actual structure and to the bend destruction experiment result, the authors propose that $\alpha_R \cdot V_R$ was able to express performance evaluation parameter based on rating value R_c. But, it is only a stage where several cases under a lot of assumption were provisionally calculated so far. A lot of data including cases of actual structures will be studied in order to consider reasonableness and to improve accuracy in the future.

REFERENCES

CEB Bulletin 243. 1998. *Strategies for Testing and Assessment of Concrete Structures Guidance Report*: CEB.

Japan Society of Civil Engineers. 1996. *Maintenance for Concrete Structures Guidance Report (draft).*

Japan Society of Civil Engineers. 2001. *Standard Specifications for Concrete Structures (Maintenance).*

Japan Society of Civil Engineers. 2001. *Standard Specifications for Concrete Structures (Maintenance) (Appendix).*

Morita, Y. Morikawa, H. & Kobayashi, H. 2002. Corrosion Process Model of RC Members Considering Seasonal Condition and Performance Evaluation. *Proceedings of the Japan Concrete iunstitute*.Vol. 24. No. 2: 1519–1524. Japan.

Takewaka, K. & Matsumoto, S. 1984. Influence that corrosion of reinforcing bars exerts dynamic properties of RC Member. *Proceedings of the Japan Concrete iunstitute*.Vol.24: 177–180. Japan.

Tsutsumi, T., Matsushima. Murakami. & Seki. 1996. Study on Crack Models Causes by Pressure Due to Corrosion Products. Research on Generation Mechanism of Corrosion Crack. *Journal of Materials. Concrete Structures and Pavements*. No.532. V-30: 159–166. Japan.

Reliability and Optimization of Structural Systems: Assessment, Design and Life-Cycle Performance – Frangopol, Kawatani & Kim (eds)
© 2007 Taylor & Francis Group, London, ISBN 978-0-415-40655-0

A new performance-based maintenance approach for infrastructures

A. Kawamoto
Aratani Construct Consultant Inc, Tottori, Japan

W. Shiraki
Kagawa University, Kagawa, Japan

K. Yasuda
Newjec Inc, Tokyo, Japan

N. Ito
CAE Inc, Tottori, Japan

M. Dogaki
Kansai University, Osaka, Japan

ABSTRACT: In Japan, the Specifications for highway bridges have been revised from specification-based design to performance-based approach in order to accommodate smart structures. As one of the important revision tasks, there is a consideration of limit states and performance at limit states during and after hazards. However, there has not been sufficient attention to limit-states of smart structures. As main revision tasks for performance-based design, we consider the manifestation of limit sates and required performance levels, the proposition of methods for guaranteeing safety of each structure, and the planning for evacuation for disaster. In this study, a new concept is proposed for design and maintenance following hazards in performance-based design system. This concept is named as live design and live management. Two concepts such as conventional maintenance concept and live design concept in emergency are fused into a new maintenance management concept of highway bridges in performance-based design system.

1 INTRODUCTION

We interest in transforming current specification-based design provisions to a performance-based approach especially for incorporating a smart structure. However, the limit states and performance criteria have to be expanded in order to take advantage of the special opportunities provided by a smart structure. For example, we expect smart structures not only to mitigate damage during a hazard, and inform occupants and evacuation personnel regarding where the occupants are, which evacuation paths may be blocked, whether the structure is gravely damaged and whether there is a risk of collapse. We also expect a smart structure to inform and guide engineers regarding where it may be damaged and how to best implement maintenance for its use during post-emergency use. The energy dissipation, fire-resistance and any other smart devices as well as sensing, communication and computing systems that are incorporated in smart structures require a major re-thinking of the maintenance regimes, as well as a re-definition of performance limit states for which the smart elements are expected to offer an enhancement of performance. That is, it is expected that smart structures make have live feature. Among these, this paper discusses about the way of making a design method about the performance-based design have live concept.

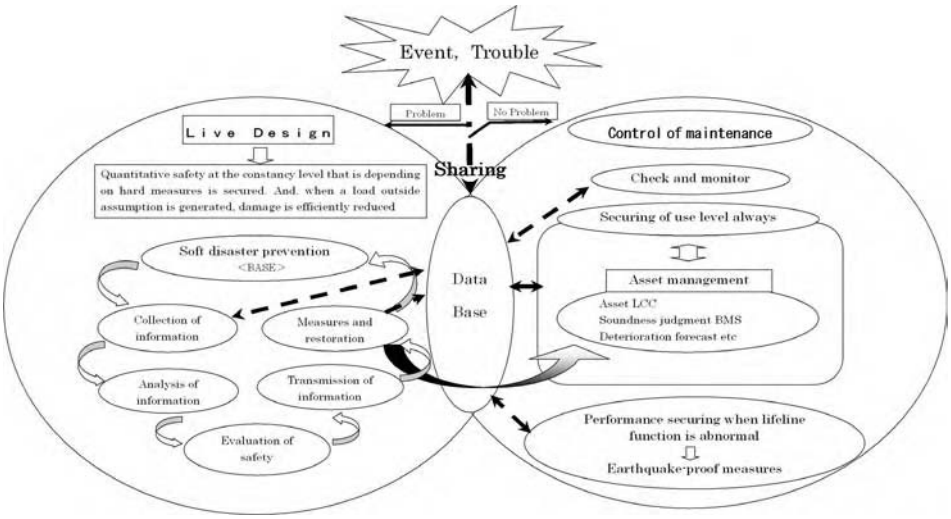

Figure 1. Intelligent constructed system to have considered live design[2].

The performance-based design of infrastructures is defined as “Design with high degree of freedom so as to satisfy their demand performance specified clearly” [1]. However, there are a lot of problems that should be clarified until its achievement. One is to establish maintenance methodology of structures according to the performance-based design rule. Unfortunately, such idea is not clearly introduced into current maintenance method of highway bridges based on specification-based design rule. Then, highway administrators correspond to each structure individually, and secure the performance level so as to be able to endure its serviceable state. In the performance-based structural design, however, it is necessary to consider structural performances for the object structure in the plan, design, construction, maintenance such as replacement of members and the update structure during the whole life of structure by the same architecture. In addition, the required performances in the specified limit states should be cleared, and the counter measures should be described clearly when the structure fall into the limit state with respect to exceeding deformation and failure in performance-based design.

Therefore, the highway administrators should be examining the strategy of a live design concept[2,3] for reducing damage by a quick measures of the struck situation. Also, they should secure the escape route and induce people to the escape route, if unexpected circumstances occur with the situation of structural performance determined after enough discussion at that time.

The authors have proposed a new management methodology[3]. It consists of two concepts such as a conventional maintenance in usual service and a live design management in emergency. Its approach is based on the performance-based design. The method is introduced for the maintenance of infrastructures during their whole life as shown in Fig. 1. It is a data exchange and the one in each other to enable smooth correspondence in normal and abnormal circumstances while updating it through a common database. In Fig. 1, the event is defined as the state of exceeding deformation and collapse by an accidental earthquake during the service time of structure. The trouble is defined as the state of deteriorating and damaging under usual service in run and the state of losing their functions. Then, a new maintenance approach named as a live management approach is proposed that consists of the conventional maintenance and live design at the event, and then its effectiveness is discussed through an illustrative example. Firstly the current state and existing problem of maintenance are presented, and its performance-based design is described. Next, a new maintenance approach based on the performance-based design is considered as live management, and the content and administrative procedure of live management are given. Finally, the problem

to be solved and the claims postulated are pointed out, for the case of which live management is applied to practical maintenance problems in the future.

2 CURRENT STATE AND PROBLEM OF HIGHWAY BRIDGE MANAGEMENT

The idea and execution method on the maintenance up to the present are described. The problem with which it should be going to grapple in the future is extracted.

2.1 *Current management of highway bridges*

This chapter discusses the maintenance method of highway bridges. Here is described how their maintenance has been defined in the law up to the present.

There is Article 42 clause 2 of the highway law as a law concerning to the maintenance. This content is defined as 'A technical standard concerning maintenance or mending the road and other matters are provided by the government ordinance'. However, only not to be enacted yet and old was putting out of the following notices.

- Direct control maintenance mending execution points (Final revision on Oct. 1962, First edition on June 1958).
- Management points such as maintenance mending of road (Road notice No.368, From the head of Road Bureau to each administrative divisions governor and a five great mayor on 28th Aug. 1962).
- Therefore, the highway administrator is executing the maintenance referring to the following technical standards.
- Highway maintenance mending points, Japan Highway Association, 1978.8.
- Highway bridge repair handbook, Japan Highway Association, 1979.
- Tiredness of steel bridge, Japan Highway Association, 1997.
- Bridge check points (idea), Ministry of Construction Pubic Works Research Institute, 1988.
- Bridge regular check points (idea), The Ministry of Land, Infrastructure and Transport national road and disaster prevention section, 2004.3 etc.

Especially, the bridges as social infrastructure facilities are maintained by a breakdown maintenance that diagnoses realities grasp of the bridge by the check due to daily and periodic checks, and abnormal circumstances, and appropriate repair is carried out.

2.2 *New management approach for highway bridges*

There is a severe financial picture by long-term economical recession in Japan. The amount of investment for managing the social infrastructure facilities has been reduced year by year. On the other hand, the number of bridges stocked as social infrastructure facilities exceeds 50,000 only even for national and state highways without toll, and those with service in run over 50 years after construction become more than 20,000 in 2020. As a result, the mending expense for maintaining retrofitting bridges is feared to increase rapidly, and to press the expense for managing new social infrastructure facilities. Then, it seems that the maintenance approach shifts from a breakdown measures to preventative ones, and is executed various examinations that achieve an efficient maintenance within limited fiscal resources. A typical management technique can be enumerated as follows:

(1) Scenario based management
In general, structural performances decrease as their material deteriorates. It thinks making the structure a life prolongation is attempted by management due to the scenario based on the deterioration forecast of the material so as to maintain the health of the structure in the Concrete Committee of the Japanese Society of Civil Engineers[4]. That is, the basic of management is to

carefully carry out inspection according to the scenario from before appearing of deterioration, and to take appropriate measures usually so that the structures do not deteriorate.

(2) Life cycle cost management
The concept of life cycle cost (LCC)[5] is to set update time that is more appropriate to make it last long putting expenditure on an initial investment and the maintenance so as to minimize an initial, maintenance and repair costs. LCC may be evaluated taking into account the deflator, interest rate and so on. In this idea, it considers or the idea whether to consider the interest rate exists with infinity or limited with service in run of the targeted structure. The basic of LCC concept is to plan the maintenance scheduling from the design phase to the mind, and one means to set the specification at the designing.

(3) Asset management
The concept of Asset Management (AM)[6] is to treat the social infrastructure facilities as a common property for the whole people, and to evaluate the current state objectively. AM is also to estimate the state of property during mid/long terms, and to analyze what is the best solution for the problems deciding when, which and how repair and reinforcement measures in the forecast under the restriction of budget. Therefore, AM can say that the social infrastructure facilities are the conceptions of the strategic maintenance management to aim at a premeditated, efficient management. That is, it can be said 'Strategic maintenance' that consists of prior and the breakdown maintenance that starts appropriately executing the improvement plan based on the forecast of changing of the object structure time while considering the distribution of the budget.

3 PROBLEMS ON MANAGEMENT OF HIGHWAY BRIDGES

Recently, the structural design method tends to be modified from conventional specification-based design to performance-based design. It does not stay only in the design field, and the field of the maintenance clearly specified is similarly necessary the examination for this flow now. In this chapter, is examined the management requested the infrastructures in the performance-based design.

3.1 *What is management in the performance-based design?*

In the current specification-based design, the maintenance treatment of infrastructures was not specified clearly. Therefore, the highway administrators have been carried out by breakdown maintenance, i.e., the maintenance is done only for the damage found at usual inspection. Recently, action is starting for shifting from breakdown maintenance to preventive maintenance, i.e, maintenance carrying out day by day before finding of severe deterioration and damage. The concept of Asset management systematized is useful to manage the infrastructure facilities effectively and efficiently in the background of the fund shortage. However, the management is targeted in the serviceability state, and the maintenance of structures damaged by the event is separately treated by different concept.

On the other hand, it is necessary to consider a structural performance for object structure and to think about giving and the maintenance of a necessary performance furthermore in the maintenance in the performance-based design through whole life cycle of substitution and the update structure as for the plan, design, construction, and maintenance by the same architecture, and to describe the limit state of structures when the unexpected limit state at its design occurs clearly in the maintenance in the performance-based design. Moreover, the engineers who manage the highway bridges should induce to a prompt grasp of the struck situation, securing the escape route when unexpected circumstances are generated after the performance that the structure has now is understood enough, and be examining the strategy that attempts the reduction of damage. Thus, a clear policy and measures are requested for various situations of the object structure to be managed expecting it in the maintenance of the performance-based design.

3.2 *Problems on management in performance-based design*

Because the structure designed by the performance-based design method is designed so as to fill the demand performance, to the problem in management in the state of the load and the usage condition assumed by the design few. However, the existing structure by the specification-based design approach and constructed hardly fills the demand performance in the earthquake force among various kinds of design loads determined by the performance-based design. Therefore, whole structural performance from serviceable state to closely limit state is revalued, and correspondence that secures the demand performance requested by the performance-based design according to each importance degree is necessary in the management of an existing structure.

Moreover, the possibility that the state that has not been considered for the management period in the design is generated rises when a management period as long as the engineering works structure is demanded. In this case, it is necessary to consider how to reduce the damage by executing a prompt grasp of the evaluation of a structural performance in the current state of the object facilities and the struck situation at the event, securing the escape route, and the inducements to the escape route.

4 LIVE MANAGEMENT OF HIGHWAY BRIDGES

In the maintenance of structure due to the performance-based design, it is necessary to reduce the damage outside assumption in addition to the maintenance of the long-term demand performance that has been done by a usual maintenance. It is necessary that it practice a live design. The frame of a new maintenance, that takes the idea of a live design to the maintenance of the structure under the performance-based design, is defined as live management. In this study, the content and procedure of such management are proposed.

Live management consists of three parts, i.e., conventional maintenance, live design in usual service and live design at the event occurrence as shown in Fig. 2. It is considered that effective management in emergency is quickly achieved by efficiently synchronizing this management part. The outline of three management parts is as follows:

(1) Usual maintenance in usual service
This part aims at the maintenance of the structural performance that can be endured in a long-term state of use, and the content of AM that works in a present maintenance is executed.
(2) Live design management in usual service
The following contents are executed in the live design management.

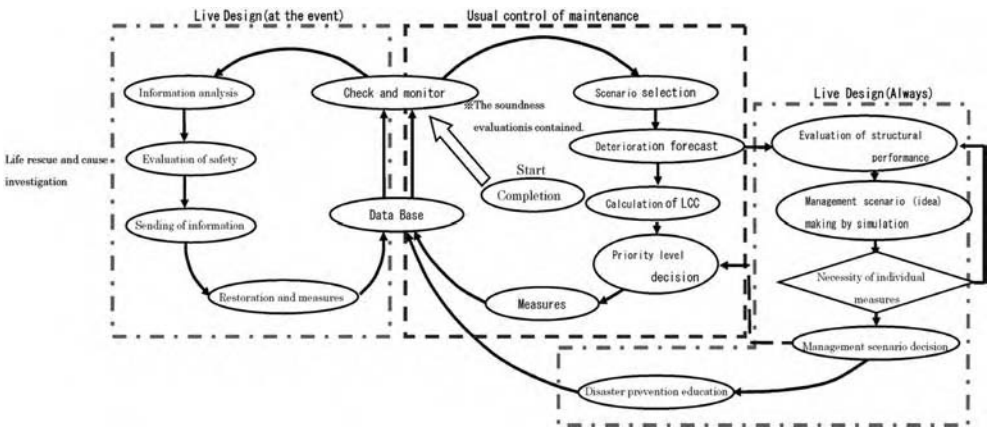

Figure 2. Proceed of live management.

① Evaluation of structural performance

The evaluation of structural performance in current state of the structure that does the deterioration progress based on the scenario set with the usual maintenance is executed. Among these, the structural performance shown here is the one to show the performance from the serviceable state to the limit state.

② Making of management scenario (idea) by simulation

The damage situation is estimated by the simulation technique under the different loadings in event occurrence, and then is made a management scenario based on usual maintenance management results within the target.

③ Necessity of individual measures

It is judged whether the maintenance and improvement of a structural performance in the management scenario at the event should be attempted or not. And, revaluation and the management scenario (idea) of structural performance are reexamined return back to ① when it is judged that measures are necessary, and then measures are executed.

④ Decision of management scenario

The management scenario is planned according to the process from ① to ③ referring to the result obtaining by the repetition. And, information on the individual structure set by this management scenario is transmitted to a usual maintenance, and it is reflected in the priority level decision of management.

⑤ Need of education for preventing disaster

It is quite difficult to defense the infrastructures from severe disaster only by hardware measures such as their strengthening, stiffening, and so on. It is important to measure by software techniques. One of them is an education for mitigating the damage of infrastructures. In the education for preventing disaster, the manager and citizen recognize as a common problem based on the decided management scenario, and both of them should be studied before the disaster occurs.

(3) Live design at the event

The following contents are executed in these departments of management.

① Collection of information

The object collecting information is to immediately understand an outline of struck situation after the occurrence of event in this part.

② Analysis of information

It examines whether information necessary for the analysis of information and the examination in the future is insufficient closely. If collecting information is insufficient, more detailed information is collected again.

③ Evaluation of safety

It is compared with the management scenario that had been set before it is struck based on the result of the analysis of information, and it is judged whether the struck situation is within its assumption or not. And, the restoration plan is made with securing the urgent transportation highway if the struck situation is a departure from normal assumption.

④ Sending of information

Necessary information is sent in each stage of the route that can be used, the situation of the emergency facilities, and the situation of the rescue operation among the results of evaluating safety as the grasp of the struck situation.

⑤ Restoration and measures

Restoration and measures according to the restoration plan examined by evaluating safety are progressed, and information is stored in the database.

5 EXAMPLE OF LIVE MANAGEMENT

The live management for Tottori city downtown is carried out as an illustrative example. The claims postulated and the problem that should be solved when live management is developed is discussed.

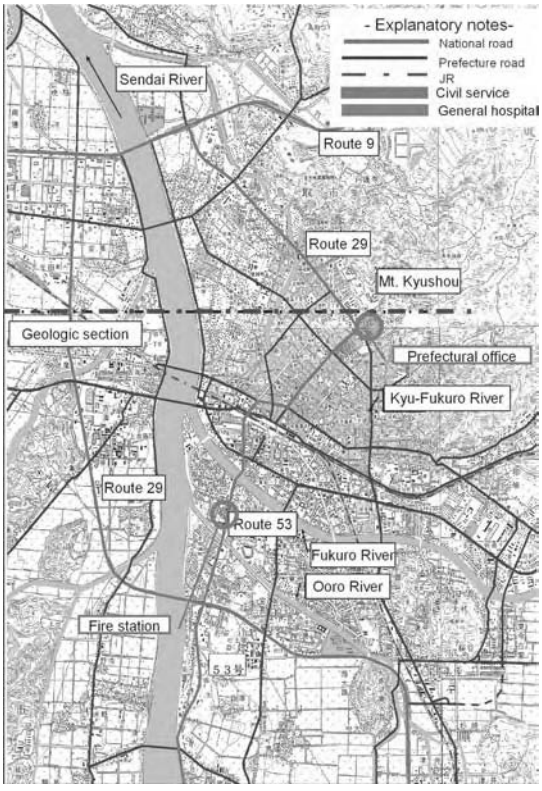

Figure 3. Administrative information chart.

5.1 *Current state and struck history of Tottori city downtown*

(1) Current state of central Tottori city

The downtown of Tottori city is located in plains that are developed to the delta in the Sendai river mouth of a river as shown in Fig. 3, and has concentrated on the part enclosed by branch (Ooro river) in the Sendai river and the Tottori Castle constructed at the top of Mt. Kyusho. It is possible to visit the town Tottori city prosperous as a castle town, and the old Fukuro river that flows like surrounding Mt. Kyusho was playing the role as the defense line in the age. As the main highways, the route 9 expands from east to west, and the route 29 and 53 have expanded from south to north. And, it expands radially from the Prefectural government where the prefecture highway exists in the Mt. Kyusho the foot of a mountain like accessing these roads and the highway network is formed.

The state of geological features in a region concerned originates in the delta in the Sendai river mouth of a river the generation process of plains and the huge back low ground blockaded to the dune. As a result, it is a structure that a weak alluvium (Ums – Uc layer) piles up on the comparatively steady as show in Fig. 4 the diluvium ground (Ls – Lmg layer) by about 30 m.

(2) Struck history

31 earthquake damages[8] were experienced by the earthquake in the west of Tottori Prefecture on Oct. 6, 2000 according to the earthquake record that remained in Tottori Prefecture. Tottori city was hited by the Tottori earthquake on 10th Sept. 1943. Its scale was over the epicenter of Magnitude 7.4 in which 10 km of the vicinity of Tottori city in the underground is made a Hypocenter. The damage extends it to 7,500 households or more in the collapse house and 1,000 dead or more and as much as 16 places in the fire occurrence part. The index, that is

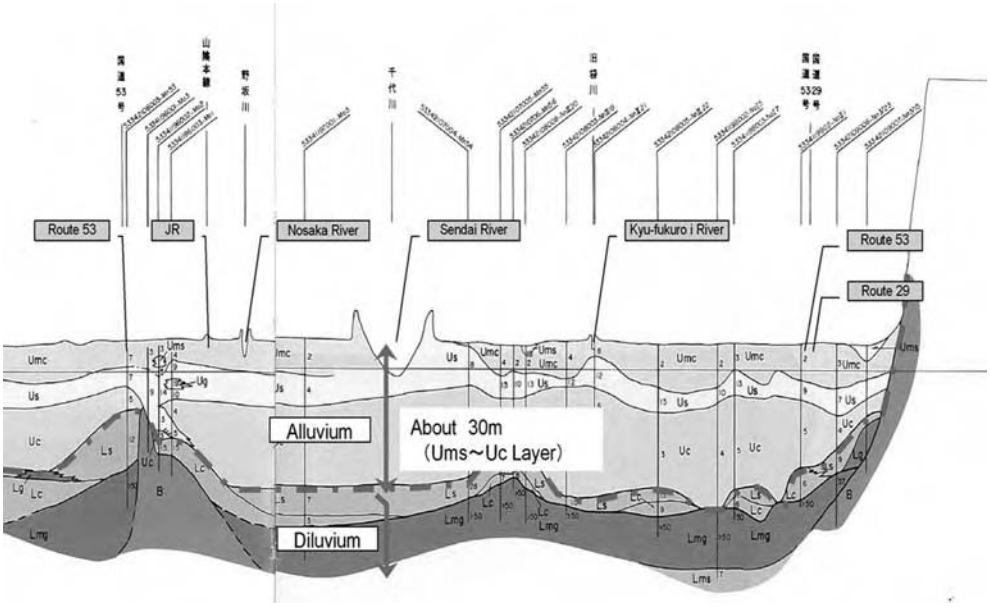

Figure 4. Geologic section [7].

the ratio of the numbers of perfectly collapsed house to the total numbers of house shown by the percentage, is defined as the damage rate, and the range is shown on the map in struck material[8] of that time. The area in which the damage rate is more than 50 percent is shown in Fig. 5. It is overlapped on the administrative information chart of present Tottori city. It is obvious that the area in which the damage rate is more than 50 percent is expanded over the downtown, and extends it even to suburbs. It can be found that this reaches the whole area almost of a present downtown.

5.2 *Demand and problem on live management*

We examine the correspondence requested in live management immediately after the event.

(1) Securing of trunk line route
The highway network of a part concerned is shown in Fig.3. Center basic facilities of distribution are routes 9, 29 and 53. These routes have the important function as access road to JR, the city hall, the general hospital and so on. Therefore, it is necessary to think about maintenance, the emergency measures, and the restoration of the function by assuming these routes to be the most important route at the event.

We are experiencing the concentration of the victim and the rescue vehicle on the route that can pass, falling into a violent traffic jam, and interfering to shelter and the rescue operation after all in Hanshin-Awaji (Kobe) Earthquake. Therefore, it is necessary to examine raising the importance degree such as the state highways besides these important routes, securing two or more routes that can pass, and doing a prompt traffic arrangement and the information transmission.

(2) Securing of the escape route and the injured person's treatment, and the search and rescues of missing person.
We are maintaining the action manual that shows the shelter place and the escape route of each district to which it lives. However, the action method when the highway is blocked by the situation of the escape route after the earthquake occurs, for instance, the collapse of the house and

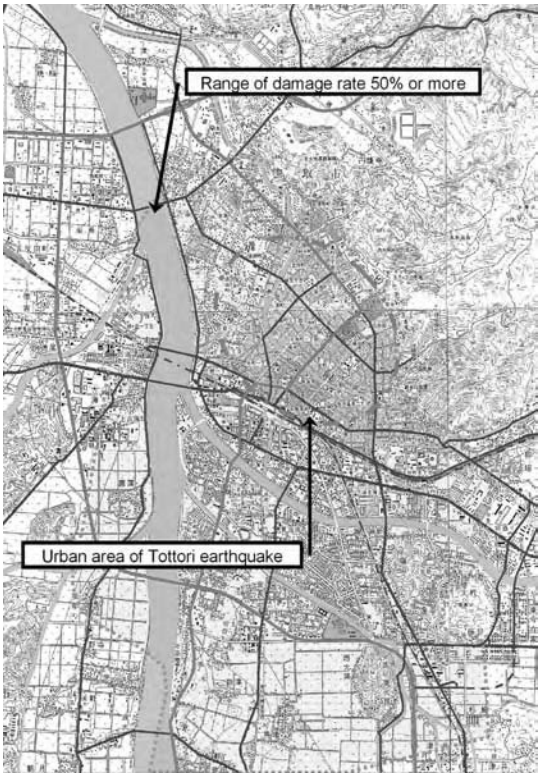

Figure 5. Struck situation chart.

it is not possible to pass by the fire occurrence is not included in this manual. Therefore, a prior preparation of the selection of the shelter place and the escape route of some substitutions etc. becomes necessary indispensable.

Moreover, the fire station with large scale becomes the base of the life rescue immediately after the disaster and the transportation of the injured person. It is necessary to raise the importance degree from other routes and to examine route 53 so that the fire station with wide place in a region concerned may transport it to the general hospitals that are along route 53, and exist in the rescue activity and suburbs of the downtown by using this route.

In the downtown besides above, the old Fukuro river flows like dividing into two parts of the south and north, and it is possible that the defense line before becomes an obstacle that isolates the resident when becoming a situation in which the bridge that spans this river collapses. Therefore, the maintenance of these bridges in daily life becomes much important.

6 CONCLUSIONS

In this study, it is considered that the contents requested for the maintenance of the highway bridge in the performance-based design are as follows.

① Secure a structural performance of the object structure through its life cycle, and maintain it.
② Specify the limit state of the structure when the unexpected limit state at the design occurs under service in run.

③ The highway administrator should be examining the strategy for the reduction of damage to the generation of unexpected circumstances after understanding the performance that the highway structure has now enough.

And, this content has both the content that attempts the long-term securing that a usual maintenance corresponds used and the reduction of the damage at the event. Here, such management method was defined as live management, and the problem was examined with the possibility of live management.

This research is just attached to the fence. In the future, we review about the grasping of event occurrence time status of being suffered, the management of the highway structure one, the setting of a best management scenario and the establishment of the smart structure and so on by the prototype model (the Tottori city model) of live management.

Then, it plans to proceed with the research to build intelligent constructed system which introduced the concept of live design.

REFERENCES

1) Design and construction of bridge substructure in performance design age “Chapter of outline”. Sankaido, 2002.12.1 (Japanese).
2) Dasgupta, G., Connor, J., and Sutner, K.: Information-Based Security for Civil Infrastructure: Deep Domain Bayesian Models-case studies of office buildings, NSF Proposal No.0331054, 2002.3.
3) Kawamoto, A., Shiraki, W., Yasuda, K., Ito, N., and Dogaki, M. : Concept of live design for maintenance of infrastructures, Proc. of Safety Problems, Japan Society of Civil Engineers, 2006.11 (Japanese).
4) Concrete standard specifications “Chapter of maintenance management” in 2001, Civil Engineering association, 2001.1 (Japanese).
5) Nishikawa, K. : Longevity and control of maintenance of road bridge, Journal of ?, Japan Society of Civil Engineers, No.501/I-29, pp.1–10, 1994.10 (Japanese).
6) The Ministry of Land, Infrastructure and Transport, Chapter of advisory committee concerning ideal ways of management and renewal, etc. of road structure in the future, : Proposals of how for being of management and renewal, etc. of road structure in the future, 2003.4 (Japanese).
7) 96 Tottori ground chart, The Corporation ground engineering association Chugoku branch, 1996.11 (Japanese).
8) Tottori earthquake disaster material (research by the Ministry of Education specific research expenditure in 1982), Technical Colleges regional Yonago industry disaster prevention research group, 1983.4 (Japanese).
9) Road earthquake measures handbook (chapter of earthquake restoration), Japan Road Association, 2002.4 (Japanese).

Reliability and Optimization of Structural Systems: Assessment, Design and Life-Cycle Performance – Frangopol, Kawatani & Kim (eds)
© 2007 Taylor & Francis Group, London, ISBN 978-0-415-40655-0

Earthquake-proof reliability-based design for steel rigid-frame piers of highway bridges

Mitsuo Kawatani
Department of Civil Engineering, Kobe University, Kobe, Japan

Yasutoshi Nomura & Shingo Kato
Graduate School of Science and Technology, Kobe University, Kobe, Japan

ABSTRACT: In order to upgrade design codes for highway bridges, reliability-based design methods covering a limit state design and a load and resistance factor design (LRFD) have been investigated. In this study, limit state probabilities of analytical models designed by the LFD considering both different load factors for various geometric shapes of structures and load combinations of D + E and D + L + E are evaluated. As the results, it is clarified that the condition of the load combinations of D + L + E is more critical as an ultimate limit state than that of D + E. This study also confirms that extremely uniform limit state probabilities of the group of rigid frame piers designed by considering various load factors can be calculated.

1 INTRODUCTION

In order to upgrade design codes for highway bridges, reliability-based design methods covering a limit state design and a load and resistance factor design (LRFD) have been investigated by many researchers. In regard to the LRFD method theoretical studies have been carried out for load combination methodology (Shinozuka 1986) and optimum determination of load factors (Kawatani et al. 1990) in the LRFD format, based on limit state probabilities taking account of both the probabilistic characteristics of each load and the probabilities of simultaneous occurrences of various loads.

In the practice of structural design, both extreme and abnormal loading conditions must be considered. This requirement possibly results in a large number of load combinations in the design criteria. Under each load combination, limit state probability can be obtained by means of convolution integral and is calculated through the load coincidence method. An appropriate objective function which measures the difference between the computed limit state probability and target one will be minimized to determine load factors.

This study discusses an effectiveness of load factor design (LFD) considering two points. First, the issue with the treatment of live load in a limit state design is referred. Structural models to be considered are gate-shaped steel rigid-frame piers of relatively short-span continuous girder bridges of Hanshin Expressway. As representative loads for the design of bridge piers, dead load and earthquake load have been considered. However, Japan has a frequency earthquake and also chronic traffic conjunction problems in urban area. The probability of simultaneous occurrences of an earthquake and a traffic conjunction is not low. In the current design load combinations, it is impossible to evaluate the limit state probability of structures in these situations. The live load that is the vehicle load caused by daily traffic conjunctions of urban highway bridges has to be considered. Secondly, another attempt is made to discuss the earthquake-proof characteristics due to different skeleton shapes of analytical models. In the past study (Kawatani et al. 1994), response acceleration for earthquake load is calculated considering a natural period and a damping constant

of each structure. Furthermore an effect of the elastic-plastic response of a structure has been dealt with in approximation by taking into consideration reduction of the response acceleration according to ductility factor μ. Differences of response accelerations of each structure affect calculations of limit state probabilities. The LFD design format provides structures that have more uniformly limit state probabilities to in comparison with these of ASD, however there is no consideration of the problem mentioned above.

In this study, limit state probabilities of analytical models designed by the particular LFD are investigated. The LFD proposed in this study considers both different load factors for various geometric shapes of structures and load combinations of D + E and D + L + E, where D, L and E indicate a dead load, a live load and an earthquake load, respectively. For calculations of limit state probabilities, the elastic-plastic analysis using a plastic hinge method is carried out from a yield point to an ultimate limit state. The large amount of observed data accumulated by Hanshin Expressway Company on weight characteristics, traffic conditions and earthquake-loading conditions are also used for modeling the actual loads to calculate it (Konishi et al. 1990).

2 PLASTIC HINGE METHOD

Because the structures dealt with in this study are one-layer gate-shaped rigid-flame piers, a degree of statical indeterminacy is three. Therefore when the 4th plastic hinge is formed, this structure can be judged to be an ultimate limit state for collapse, however a probability of occurrence of the 4th plastic hinge formed is very small. So, in this study an occurrence of the 1st plastic hinge being formed is considered as an ultimate limit state. The horizontal force capacity acting to a beam member of a gate-shaped pier in case that the 1st plastic hinge is formed is taken as P_u, and an equivalent weight W is determinate, so the limit state function Z is expressed as follows:

$$Z = P_u - K_{he} W \tag{1}$$

where K_{he}: equivalent horizontal seismic coefficient. Here, the equivalent weight includes the weight of the beam part and the half of the weight of a column part of a bridge pier, and the reaction force from a superstructure.

The calculation procedure of the horizontal force capacity in which the 1st plastic hinge is formed is explained in the following three sections.

2.1 *Modeling of bridge pier and superstructure*

The analytical model of the steel bridge pier of one-layer gate-shaped rigid-flame is divided into 20 finite elements, and an elasto-plastic analysis is carried out. At the predicted point of a plastic hinge formed a stress is calculated. Six points are predicted in both ends of columns and a beam of a rigid-flame bridge pier as shown in Fig. 1. The exact locations of these points are explained as follows:

(a) Each point of A and F is located at a half of the plastic hinge length L_{pc} from the base of a column to the upper part.
(b) Each point of B and E is located at a half of the plastic hinge length L_{pc} from the lower end of the corner area of a column to the lower part.
(c) Each point of C and D is located at a half of the plastic hinge length L_{pb} from the corner area of both ends of a beam to the center.

The plastic hinge length of a beam and a column L_{pc}, L_{pb}, respectively is estimated as follows:

$$L_{pc} = L_{pb} = 0.1(H' - b') \tag{2}$$

$$\text{Note: } 0.1b' \leq L_{pc}(L_{pb}) \leq 0.5b' \tag{3}$$

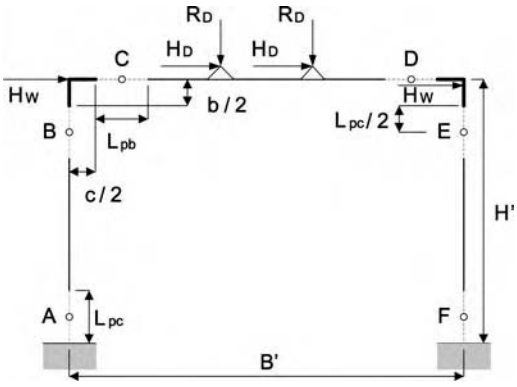

Figure 1. Check point of stress.

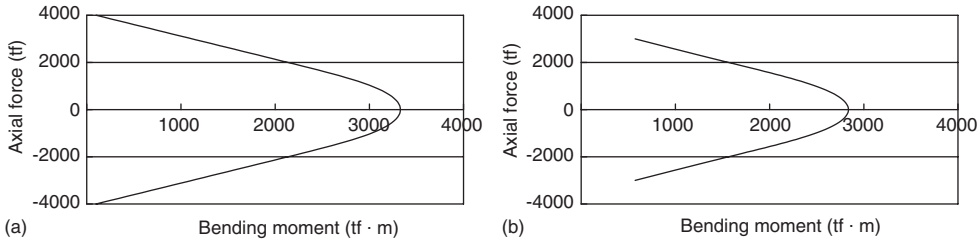

Figure 2. Correlation of axial force-bending moment; (a) column and (b) beam.

where H': height of a column, and b′: width of a box section in column($b' = c$), or in beam($b' = b$), b is web height of a box section. In addition, the corner area of the beam-column intersection covered in the column width c and the beam height b is assumed as rigid. An acting position of an inertia force of superstructure is the undersurface of the RC slab.

The rotation spring of the plastic hinge of a column and a beam is a perfect elasto-plastic element with the same stress-strain relationship in both tension and compression sides. An ultimate strain ε_u may be $\varepsilon_u = 5\%$. When a bending moment of the predicted point reaches the ultimate bending moment M_u, the section becomes the plastic hinge and its bending stiffness EI becomes 0. The other elements are elastic.

2.2 *Calculation of the relation between axial force and ultimate bending moment in a plastic hinge element*

Since that the axial force and the bending moment may act on a structural element simultaneously, the correlation of an axial force-ultimate bending moment is needed for the judgment of yielding in a plastic hinge element. The correlation in the case of model number No.1 and the thickness 10 mm of a beam is shown in Fig. 2 for example. In this study, the same nonlinear stress-strain relationship of a steel in both tension and compression sides is assumed and therefore the correlation of the axial force-ultimate bending moment is symmetry for the bending moment, and here the bending moment can be treated in an absolute value.

2.3 *Calculation of the relation between horizontal force and horizontal displacement*

A horizontal force acting on a beam at the center of the framework model is increased gradually, and among all plastic hinge elements an element is reached firstly to plastic. Therefore, the relation of a horizontal force-horizontal displacement of a pier is calculated.

3 COMPUTATIONAL METHOD OF LOAD FACTORS

3.1 *Limit state probability of structures*

Load factors should be determined on the basis of a reliability concept, such as minimizing the scattering of limit state probabilities of structures from a target probability in a certain limit state. Due to the reliability-based concept, structures having an uniform safety can be designed.

3.2 *Computational procedure of load factors*

A suitable value of the earthquake load factor γ_E is given, and the sections of selected structures are designed together with the death load. Next, the limit state probability P_i is calculated. Here, the objective function Ω shown as follows is introduced.

$$\Omega = \sum_i w_i \{(\log P_i - \log P^*)/\log P^*\}^2 \quad (4)$$

where w_i: weight coefficient, and P^*: the target limit state probability.

The load factor is chosen so as to minimize the objective function among several load factors.

3.3 *Computational method of limit state probability*

Under a load combination, the limit state probability can be obtained by means of convolution integral. The limit state probability of structures are calculated through the load coincidence method (Wen 1977) as follows:

$$P(x) = 1 - \exp[-\sum n_j P_j(x)] \quad (5)$$

where P(x): limit state probability of limit state x during the structure's lifetime,
n_j: expected number of occurrence of load combination j during the structure's lifetime,
$P_j(x)$: limit state probability under the condition of one occurrence of load combination j.

4 ANALYTICAL MODELS OF BRIDGE STRUCTURES AND LOADS

4.1 *Structural models*

Representative structural models to be considered are gate-shaped steel rigid-frame piers of relatively short-span continuous girder bridges as shown in Fig. 3. Twelve substructures consisting of steel box beam-columns with various geometric dimensions are selected as listed in Table 1 for analytical models. The member dimensions a, b and c of piers are determined with reference to standard design examples as follows: (Kawatani et al. 1994)

$$a=L/20,\ b=0.0425(B+H)+0.717,\ c=0.0392(B+H)+0.876 \quad (6)$$

Symbols in Table 1 can be referred to Figs. 1 and 3. These structural models reasonably well cover the entire spectrum of steel piers of Hanshin Expressway.

A skeleton of structural model for transverse analysis is shown in Fig. 4 with points of interest also indicated by circled numbers. These points of interest are important in the sense that critical stresses are usually observed at these locations, and hence thickness of the plates, which is considered as the only design variable in this study, is determined depending on these critical stresses. Other geometric dimensions (except plate thickness) and stiffness of structures are assumed to be constant.

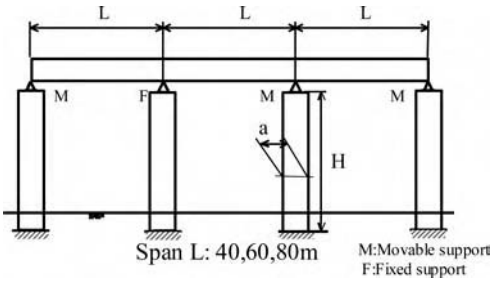

Figure 3. Structural models.

Table 1. Geometric dimensions of support structures for transverse analysis.

No.	L	H	B	H'	B'	a	b	c
1	40.0	10.0	20.0	9.01	17.95	2.0	1.99	2.05
2	40.0	10.0	30.0	8.79	27.56	2.0	2.42	2.44
3	40.0	20.0	20.0	18.79	17.56	2.0	2.42	2.44
4	40.0	20.0	20.0	18.79	27.16	2.0	2.84	2.84
5	60.0	10.0	20.0	9.01	17.95	3.0	1.99	2.05
6	60.0	10.0	30.0	8.79	27.56	3.0	2.42	2.44
7	60.0	20.0	20.0	18.79	17.56	3.0	2.42	2.44
8	60.0	20.0	30.0	18.58	27.16	3.0	2.84	2.84
9	80.0	10.0	20.0	9.01	17.95	4.0	1.99	2.05
10	80.0	10.0	30.0	8.79	27.56	4.0	2.42	2.44
11	80.0	20.0	20.0	18.79	17.56	4.0	2.42	2.44
12	80.0	20.0	30.0	18.58	27.16	4.0	2.84	2.84

Note: $H' = H - b/2$, $B' = B - c$ (unit: m).

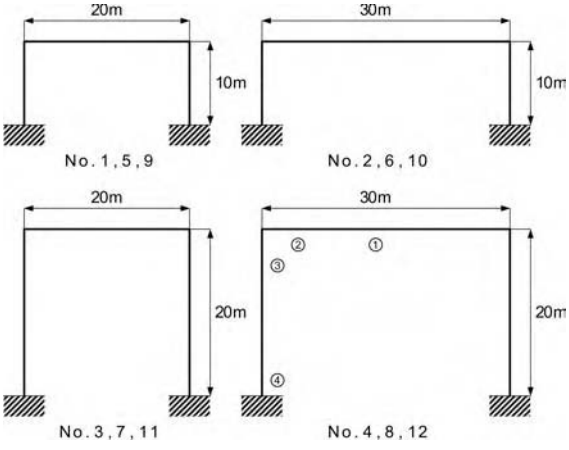

Figure 4. Skeleton of structures and points of interest.

4.2 *Load models*

As representative loads for the design of bridge piers, dead, live and earthquake loads are considered. The large amount of observed data accumulated by Hanshin Company on weight characteristics, traffic conditions and earthquake-loading conditions are used for modeling the actual loads. Temporal occurrences of these loads are modeled after Borges-Castanheta (Borges & Castanheta 1972) model based on the observational data.

Table 2. Reaction of intermediate support.

Span (m)	Mean (tf)	Standard deviation δ (tf)	α	u
40	106.01	5.707	0.2142	103.39
60	132.48	8.902	0.1368	128.39
80	158.70	10.887	0.1121	153.71

Note: Ordinary congestion without impact (proportion of large size trucks of 20%).

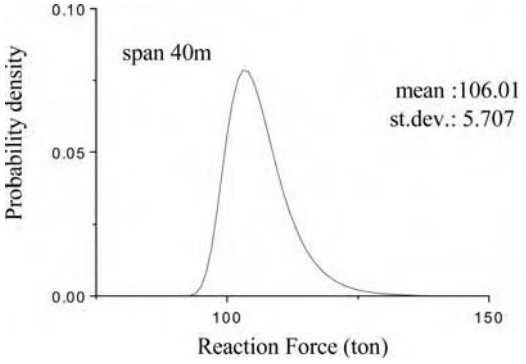

Figure 5. Probability density function for live load.

Table 3. Natural Period T, Damping Constant h and Parameter of Weibull distribution function.

No.	T (sec)	h	α	β	X_0 (gal)
1	0.3676	0.1632	0.922	31.97	33.91
2	0.2447	0.1899	0.925	37.50	36.43
3	0.9594	0.0291	0.854	18.98	18.25
4	0.6679	0.0947	0.884	24.66	22.67
5	0.3690	0.1620	0.922	31.63	33.85
6	0.2460	0.1897	0.925	37.46	36.43
7	0.9595	0.0291	0.854	18.98	18.25
8	0.6697	0.0943	0.884	24.67	22.60
9	0.3701	0.1617	0.921	31.57	33.81
10	0.2471	0.1894	0.925	37.43	36.43
11	0.9608	0.0288	0.853	18.95	18.23
12	0.6712	0.0940	0.884	24.67	22.55

4.2.1 *Dead load*

The actual dead load is slightly larger than a design dead load and is assumed to be 1.05 times the nominal load.

4.2.2 *Live load*

Live loads are modeled, especially simulating traffic loads by using Monte Calro method based on stochastic data of traffic flows measured on Hanshin Expressway. In this study, Traffic condition is considered as an ordinary congestion with proportion of large size trucks of 20%. The probability characteristic is set up based on Type I extreme value (Gumbel) distribution. (see Table 2 and Fig. 5)

4.2.3 *Earthquake load*

An earthquake load is modeled considering seismic records more than magnitude of five in Hanshin area. A response acceleration for earthquake load is calculated considering a natural period of each structure. The natural periods of the steel bridge piers are in the range from 0.24 sec to 0.96 sec as shown in Table 3.

Damping constants of bridge structures are closely related with the natural period. In case where the natural period is below 1.0 sec, damping constants have great effects on the response of structures. Therefore, for modeling more rational earthquake load, response acceleration should be estimated by changing a damping constant due to the natural period. In the specifications (JSHB) a damping constant is 0.02 beyond the natural period of 1.0 sec and is 0.2 to 0.4 in the natural period of 0.5 sec. Damping constants can be estimated in $h = -0.225T + 0.245$ where $h = 0.02$ in the natural period of 1.0 sec, and $h = 0.20$ in the natural period of 0.2 sec in this study.

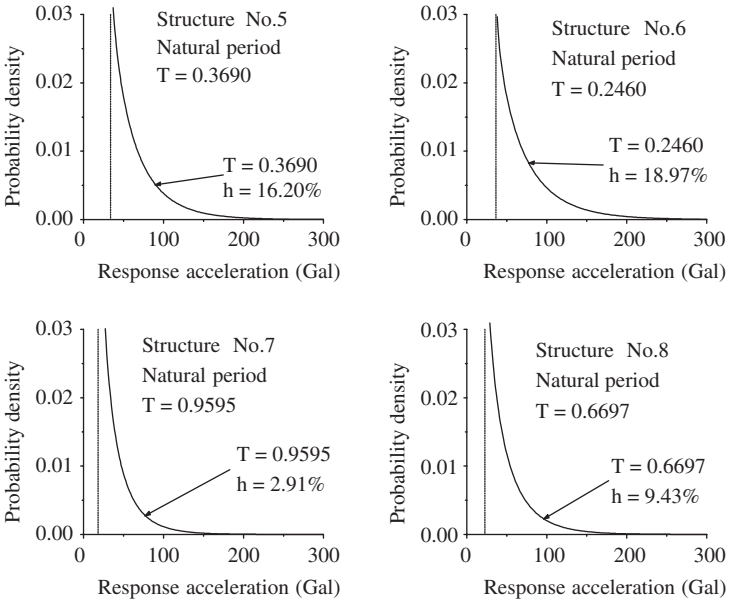

Figure 6. Probability density function of earthquake load.

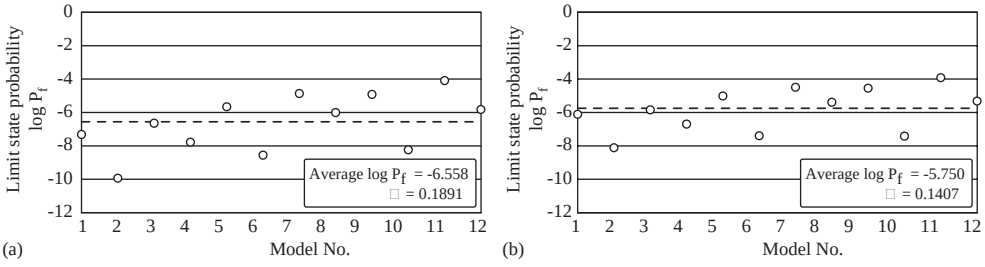

Figure 7. Limit state probabilities of analytical models designed by ASD under each condition: (a) D + E and (b) D + L + E.

Weibull distribution function is chosen to represent seismic load effects on pier structures as shown in Fig. 6.The damping constant and the distribution parameter of Weibull distribution function of each structure are shown in Table 3.

5 ANALYTICAL RESULTS

5.1 *Live load at the earthquake-proof design*

Under actual load combinations of D + E and D + L + E, Fig. 7 shows limit state probabilities of 12 analytical models designed by ASD considering a design load combination of D + E. These mean values are also calculated. Average log P_f of D + L + E is larger in comparison with that of D + E. This result means that the load combination of D + L + E is more critical as an ultimate limit state of steel rigid-frame piers. Therefore, it is observed that live load has to be included in the design load combination as D + L + E in this study.

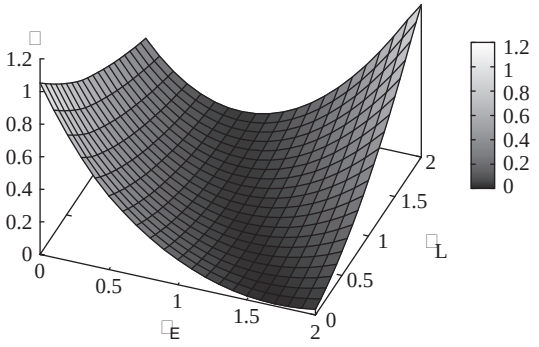

Figure 8. Relation of load factor-objective function (No. 1,5 and 9, D + L + E).

Table 4. Load factors for LFD.

Load combination	No.	γ_L	γ_E
D + E	1,5,9	–	1.4
	2,6,10	–	0.6
	3,7,11	–	1.6
	4,8,12	–	1.2
D + L + E	1,5,9	0.0	1.7
	2,6,10	0.0	1.0
	3,7,11	0.0	1.8
	4,8,12	0.0	1.5

Table 5. Thickness according to load factor (No. 1, 5 and 9, D + L + E).

					Thickness (mm)			
					Beam		Column	
Case	γ_L	γ_E	Ω	No.	Center	End	Top	Base
1	0.0	1.7	0.0140	1	4.4	15.2	17.3	15.8
				5	5.2	21.5	22.8	18.0
				9	5.9	28.8	28.9	19.8
2	0.3	1.5	0.0181	1	4.9	16.1	18.3	16.1
				5	5.6	22.3	23.7	18.0
				9	6.3	29.5	29.6	19.7

5.2 *Load factors under each design load combinations of D + E and D + L + E*

In this study, different load factors for various geometric shapes of structures and load combinations are estimated to minimize their objective functions. Fig. 8 shows the relation between load factors and the values of objective function at analytical model Nos.1, 5 and 9, where the D + L + E is considered as the load combination. When the value of objective function is less than 0.2, the object function has a tendency to decrease a live load factor. The same tendency is observed in other analytical cases. Load factors calculated under considerations of the analytical result mentioned above are shown in Table 4. It would be found that these live load factors do not have any suitableness for evaluations of the live load in a load combination of D + L + E. However, from Table 5 it is observed that the effectiveness of the load factor design method using different load factors can be evaluated adequately because a little difference of load factors gives little influence in designing.

5.3 *Limit state probability and objective function for actual load combination of D + L + E*

Figure 9 shows limit state probabilities and objective function Ω of structures designed by ASD and LFD under each load combinations. Not only values of the objective function but also all of average log P_f of LFD are lower than those of ASD. These results prove that LFD considering various load factors following geometric shapes of steel ridged-frame piers and the load combination of D + L + E can be more reliable structural design method in comparison with ASD.

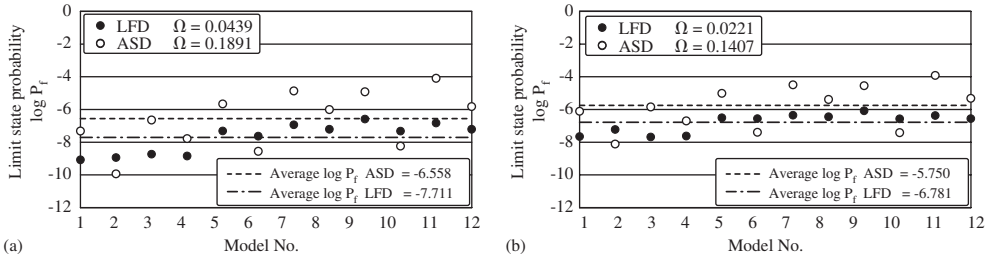

Figure 9. Limit state probability under each condition: (a) D + E and (b) D + L + E.

6 CONCLUSIONS

Concluding remarks obtained in this study can be described as follows.

1. The ultimate limit state under the load combination of D + L + E is more critical in comparison with that of D + E.
2. It is shown that the load factor design method using various load factors following geometric shapes of steel ridged-frame piers may provide more uniform reliability of structures than the allowable stress design method.

REFERENCES

Borges, F. & Castanheta, J. 1972. *Structural Safety, 2nd ed*, Laboratorio Nacional de Engengaria Civil, Lisbon, Portgal.

Kawatani, M., Hamada, H. & Kudo, H. 1994. Load Factors Based on Limit State Probability of Steel Piers of Highway Bridges, *Computational Stochastic Mechanic, Proc. of Second International Conference Computational Stochastic Mechanics*, Athens: 618–629.

Kawatani, M., Kitazawa, M., Kubo, M. & Shinozuka, M. 1990. Reliability-Based LRFD for Bridges: Determination of Load Factors, *Structural Safety & Reliability. Proc. 5th ICOSSAR*, San Francisco 1989:Addendum.

Konishi, I., Kameda, H., Matsuhashi, K., Emi S. & Kitagawa, M. 1990. Safety Assessment of Urban Expressway Bridges Based on Probabilistic Modeling of Multiple Load Enviroments. *Structural safety*, Vol.7, No.1: 33–55.

Shinozuka, M. 1986. Load Combination and Load Resistance Factor Design. *IABSE Symposium*: 65–69.

Wen, Y. K. 1977. Statistical Combination of Extreme Loads, *Proc. of ASCE*, Vol.103, No.ST5: 1079–1093.

Reliability and Optimization of Structural Systems: Assessment, Design and Life-Cycle Performance – Frangopol, Kawatani & Kim (eds)

Effect of dynamic wheel loads on fatigue performance of RC slabs

Chul-Woo Kim & Mitsuo Kawatani
Department of Civil Engineering, Kobe University, Kobe, Japan

ABSTRACT: This paper presents an examination of the effect of dynamic wheel loads of vehicles on fatigue performance of RC slabs. The dynamic wheel load effect is considered by means of the impact coefficient. A three-dimensional (3D) traffic-induced dynamic response analysis of bridges is carried out to simulate the impact coefficient for RC slabs along with the Monte Carlo simulation (MCS) technique. The simulation incorporates randomness of the surface roughness of bridges, the bump height, the vehicles' traveling positions, the vehicles' axle weights, and vehicle speed. It is observed that the slab located near the expansion joint, which is rendered stronger by its deeper cross section, has a lower probability of fatigue failure than other panels even though the slab near the expansion joint experiences the most severe dynamic loading effect.

1 INTRODUCTION

A reinforced concrete (RC) slab that is directly subjected to wheel loads is the most important structural element in distributing wheel loads of vehicles, and is suffered from many factors such as salt application, traffic, etc. Japan's Ministry of Land, Infrastructure and Transportation has determined that about 67% of the need for steel bridge reconstruction in Japan is attributable to damage to RC slabs (PWRI 1997). A rational criterion for performance of the slab thus provides a useful assessment tool for decision-making in relation to bridge management because the maintenance, rehabilitation and replacement of the slab comprise a large fraction of the bridge's life-cycle cost (Furuta, Tsukiyama, Dogaki & Frangopol 2003).

One of the important factors for performance of RC slabs in Japan is fatigue failure. Fatigue of the RC slab is caused by the total moving wheel load of static truck loads and dynamic load effects. Generally in bridge design, dynamic load effects exerted by moving vehicles on bridges and RC slabs are considered using the impact coefficient.

A fatigue test for RC slabs by Matsui (1984) shows that the equivalent loading cycles is proportional to the load ratio raised to the twelfth power. The test indicates that the axle load, including the impact coefficient raised to the twelfth power, affects the RC slab fatigue performance. However, only the probability distribution of axle loads is considered in fatigue assessment and design of the RC slab. In contrast, the worst case scenario is considered in the code-specified impact coefficient because of deficient data. This conservative approach is acceptable for the design of new structures. For existing structures, however, it may lead to unnecessary and costly strengthening. Another important point to be examined is whether the code-specified impact coefficient for slabs provides a conservative design for RC slabs or not. It indicates that better understanding of the RC slab's impact coefficient is crucially important to elucidate the deterioration process of RC slabs, including fatigue. This study is intended to clarify the effect of the impact coefficient on the fatigue performance of RC slabs.

2 ANALYTICAL PROCEDURE

2.1 *Impact coefficient of RC slabs*

The dynamic wheel load effect to RC deck slab is considered by using the impact coefficient simulated from a dynamic response analysis of bridges (Kim, Kawatani & Kim 2005, Kim & Kawatani 2006). It includes the process of considering the randomness of influencing factors to dynamic responses of a bridge. For estimating the impact coefficient, in this paper the dynamic increment has been determined in accordance with EMPA's procedure (Cantieni 1992) as shown in Equation 1.

$$i = (M_{dy,\max} - M_{st,\max}) / M_{st,\max}, \tag{1}$$

where, $M_{dy,\max}$ is the maximum bending moment at the observation position under dynamic vehicular loadings and $M_{st,\max}$ is the bending maximum moment at the observation position under static vehicular loadings.

2.2 *Performance function for fatigue of RC slabs*

In this study spalling of concrete with holes punched through the deck before yielding of reinforcement is assumed as the fatigue failure mode of the RC deck, because, at this stage of deterioration, the serviceability of the deck is so impaired that a decision on rehabilitation, or repair should be taken (Okada, Okamura & Sonoda 1978, Perdikaris, Petrou & Wang 1993).

The performance function for fatigue of RC slabs is

$$g(R,S) = R - S, \tag{2}$$

where R and S respectively represent the load-carrying capacity of an RC slab and the load effect. The failure probability is obtainable by counting the total events of $g < 0$ during a given lifetime.

The punching shear strength (P_{sx}) of an RC slab, which can be estimated using Equation 3 (Matsui & Muto 1992), is adopted as the load-carrying capacity of the RC slab:

$$R = P_{sx} = 2B\left(f_{s\max} x_m + f_{t\max} C_m\right), \tag{3}$$

where B is the effective width of fatigue failure of RC decks ($B = b + 2D_d$), b is the contact width of the loading plate or tire in the direction of distribution bars, D_d is the effective depth of distribution bars, f_{smax} is the maximum shear stress of concrete ($f_{smax} = 0.252 f_{ck} - 0.000246 f_{ck}^2$), f_{ck} is the compressive strength of concrete, f_{tmax} is the maximum tensile stress of concrete ($f_{tmax} = 0.583 f_{ck}^{2/3}$), x_m is the distance between the neutral axis and the edge of compression part of the main section, and C_m is the depth of concrete covering the main section.

A relationship between the load effect and the number of loading cycles can be expressed as the following equation (Matsui & Muto 1992) of the Miner's rule based on the S-N curve for RC slabs taken from a moving wheel load test, and Perdikaris, Petrou & Wang (1993) suggest a similar formulation.

$$\mathrm{Log}(P/P_{sx}) = -k\,\mathrm{Log}\,N + \mathrm{Log}\,C = -0.07835\,\mathrm{Log}\,N + \mathrm{Log}1.52, \tag{4}$$

where P is the wheel load and N is the total number of loading cycles ($N = N_{eq} \times$ fatigue life in year) caused by P, and the N_{eq} is the equivalent loading cycle defined in Equation 5.

The equivalent loading cycle for a standard load P_0 considering randomness of the axle load and impact coefficient can be defined as Equation 5 (HEPC 1991).

$$N_{eq} = \int_0^{i_{\max}} \int_0^{P_{\max}} \left\{\kappa \cdot (1+i) \cdot (P/P_0)\right\}^m f(i) \cdot f(P) \cdot dP \cdot di \times N_i \tag{5}$$

In that equation, N_{eq} is the equivalent loading cycle corresponding to a standard wheel load P_0; κ is a deviation factor to consider the difference between the wheel load effect under a real traffic condition and the load effect during the fatigue test of RC slabs; i represents the impact coefficient; N_i indicates total loading cycles of an axle load per year; P is the random axle load; $f(i)$ denotes the probability density function of impact coefficients; and $f(P)$ is the probability density function of axle loads.

To simplify the numerical example, κ in Equation 5 is estimated by assuming that the probability of fatigue failure of the RC slab at the middle section of the bridge is 100% within 50 years (the given life time) under consideration of the deterministic impact coefficient of 0.38 specified in the JRA code, even though the deviation factor should be determined precisely using FE method. In other words, using the estimated κ indicates that the slab is designed to have a fatigue life of 50 years by considering the code-specified impact coefficient. Next, the equivalent loading cycle N_{eq} for a standard load P_0 is calculated considering randomness of the impact coefficient according to Equation 5. The P_{sx} taken from Equation 4 by substituting the N_{eq} estimated from Equation 5 illustrates the load effect on the RC slab. The load-carrying capacity of the RC slab is calculated by considering the normal distribution of the compressive strength of concrete f_{ck} in Equation 3. Equation 2 gives the final probability of fatigue failure of each slab in a given fatigue life span. The standard wheel load P_0 is set as 9.81 kN.

3 MODEL DESCRIPTION

3.1 *Bridge model*

The bridge considered in this study is a simple-span composite steel-plate girder bridge. Figure 1 shows that it comprises three girders with a span length of 40.4 m. As for RC slabs, the slab thickness at the approaching side is 23 cm thick. That at the middle section is 17 cm thick and the span length is 2.65 m. The slab is assumed to act compositely with main girders. Table 1 presents a summary of the bridge characteristics. Figure 1 also gives observation points denoted as P1, P2, P3, P4 and P5. The panel where point P1 is located has 23 cm thickness. The other panels have 17 cm thickness. The validity of the analytical responses of RC slabs was verified through comparison with field-test data (Kawatani & Kim 1998), and omitted in this paper.

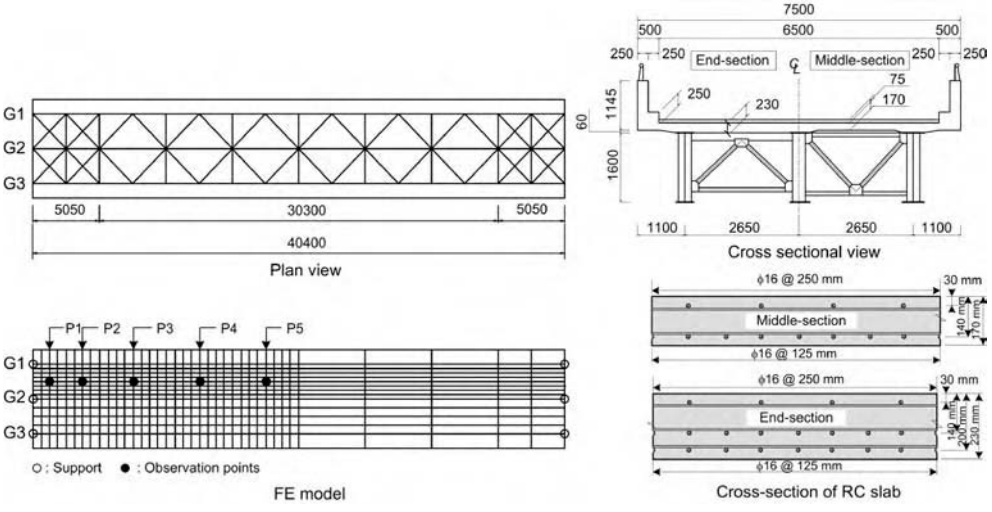

Figure 1. Simply supported steel plate girder bridge with RC deck (unit: mm).

Table 1. Steel bridge properties.

Mass per unit length (ton/m)	7.550
Section area of girders (m2)	0.142
Moment of inertia (m4)	0.212
Torsional constant (m4)	0.0548
Damping constant (1st and 2nd modes)	0.0254
Fundamental natural frequency (Hz)	
1st (Bending)	2.34
2nd (Torsion)	3.81

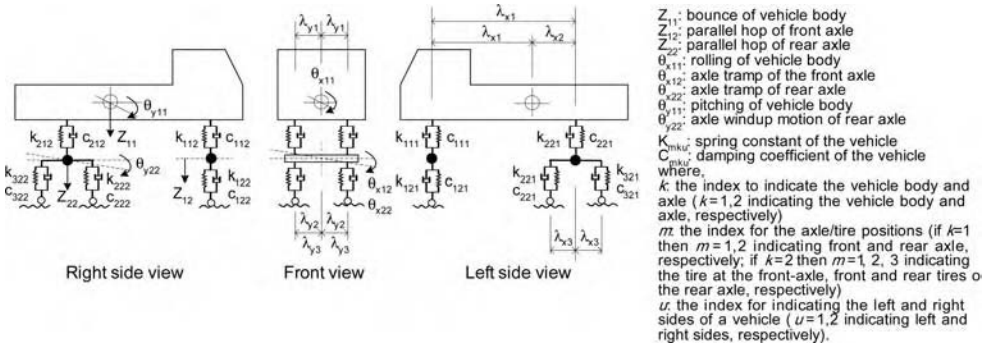

Figure 2. Three-axle dump truck model with 8 DOFs.

Table 2. Vehicle properties.

Parameters		Three-axle dump truck
Geometry (m)	Tread	1.80
	Distance between front and rear axle	3.99
	Distance of tandem axle	1.32
	Distance between front axle and CG	2.99
Weight (kN)	Gross	191.00
	Sprung mass including payload	171.40
Damping constant	Steer axle unsprung mass	4.90
	Drive axle unsprung mass	14.70
	Sprung mass (suspension)	0.03
	Unsprung mass (tire)	0.17
Fundamental frequency (Hz)	Bounce	3.30
	Axle hop	17.90

CG: Center of Gravity

3.2 *Vehicle model*

Traffic including a high proportion of heavy trucks on highway bridges usually occurs at night. The maximum traffic constitution among heavy trucks has been reported as three-axle vehicles in Japan (Sakano, Mikami & Miyagawa 1993). Therefore, a dump truck with a tandem axle idealized as an eight-degree-of-freedom model (see Figure 2) is adopted as a vehicle model for the simulation of the impact coefficient of RC slabs through the traffic-induced dynamic response analysis of bridges. Table 2 presents a summary of vehicle model properties. A detailed summary of the validation and experiment is available in another work (Kim, Kawatani & Kim 2005). Vehicles are assumed to move from the left to the right end of the bridge.

3.3 *Roadway profile*

Fluctuation of the roadway surface can be treated as a homogeneous Gaussian random process with zero mean (Dodds & Robson 1973). The probability can be defined as a power spectral density (PSD) function. The following analytical description has been proposed to fit the measured PSD (Honda, Kajikawa & Kobori 1982a).

$$S(\Omega) = \alpha/(\Omega^n + \beta^n), \tag{6}$$

where Ω ($= \omega/2\pi$) is the space frequency (cycle/m) and α, β and n are the roughness coefficient, shape parameter and parameter to express the distribution of power of the PSD curve, respectively; ω represents the circular frequency of the road surface.

Regarding parameters in Equation 6, $\alpha = 0.001$, $\beta = 0.05$ and $n = 2.0$ are used in this study based on measured data of Meishin Expressway, which links Nagoya with Kobe in Japan, before service. The PSD curve, with $\alpha = 0.003$, $\beta = 0.05$ and $n = 2.0$, is also considered in order to investigate the effect of roadway surface conditions on the impact coefficient of RC slabs.

3.4 *Bump height*

The lognormal distribution is selected to describe the probability distribution of bump heights at expansion joints of bridges based on survey results of national roadway bridges in Japan (Honda, Kajikawa & Kobori 1982b). Among the measured bump profiles, the sine-shaped bump profile that gives the most severe effect on the impact coefficient of decks from a preliminary study is adopted in the simulation. The respective mean value and standard deviation of the measured bump heights were 20.4 mm and 7.0 mm (Honda, Kajikawa & Kobori 1982b); the sine wave length of the bump profile in the driving direction is assumed as 100 cm. The highway bridges' pavement is generally better maintained than that of national roadway bridges. Consequently, half of the measured height is also considered in the simulation. The measured bump height on national roadway bridges is also used in the simulation to investigate the effect of bump height on the impact coefficient of the RC slab. The bump location considered in this study is on the bridge expansion joint.

3.5 *Traffic data*

A normal distribution is assumed for the travelling speed and position of vehicles on highway bridges based on the Hanshin Expressway database. Even though today's traffic environment shows a tendency toward increase in the travelling speed, the mean value and standard deviation of vehicle speeds are assumed respectively as 70 km/h and 10 km/h according to the previous research (Sakano, Mikami & Miyagawa 1993). To simulate the impact coefficient of RC slabs on national roadway bridges, a vehicle speed model with respective mean and standard deviation values of 50 km/h and 10 km/h is used in the analysis. The mean value and standard deviation for the travelling positions of vehicles are 0.0 m and 0.2 m from a target passage (HEPC 1991).

A lognormal distribution is assumed for the axle load of the three-axle vehicles according to the Hanshin Expressway measured data. The mean value and standard deviation of the axle load are 49.805 kN and 12.056 kN respectively for the front axle, 90.507 kN and 34.276 kN for the front wheel of the tandem axle, and 67.571 kN and 31.637 kN for the rear wheel of the tandem axle (HEPC 1991).

4 SIMULATION OF IMPACT FACTOR

A number of sample roadway profiles, bump heights, vehicle speeds, travelling positions of vehicles, and axle loads are generated using the MCS technique. A 3D dynamic response analysis of the steel plate girder bridge with moving vehicles is conducted to estimate the impact coefficient of the panels according to each sample of random variables.

Table 3. Impact coefficients taken from simulation.

Panel Scenario	P1 Mean (SD)*	P2 Mean (SD)	P3 Mean (SD)	P4 Mean (SD)	P5 Mean (SD)	G1 Mean (SD)
SCN-1	0.168	0.114	0.126	0.108	0.110	0.049
	(0.1083)	(0.0895)	(0.0894)	(0.0895)	(0.0897)	(0.0352)
SCN-2	0.227	0.150	0.147	0.156	0.152	0.084
	(0.2033)	(0.1193)	(0.1157)	(0.1236)	(0.1218)	(0.0550)

SCN-1: $S(\Omega) = 0.001/(\Omega^{2.0} + 0.05^{2.0})$; v(mean, SD) = (70, 10) km/h; bump (mean, SD) = (10.2, 3.5) mm
SCN-2: $S(\Omega) = 0.003/(\Omega^{2.0} + 0.05^{2.0})$; v(mean, SD) = (50, 10) km/h; bump (mean, SD) = (20.4, 7.0) mm
* SD means the standard deviation value.

This study creates two scenarios that illustrate how the impact coefficient changes based on different roadway surface condition and traffic speed. The scenarios are as follows:

- Scenario 1 (SCN-1): the roadway profile with $\alpha = 0.001$, $\beta = 0.05$ and $n = 2.0$ as parameters of the PSD function defined in Equation 6; bump heights' mean and standard deviation values are 10.2 mm and 3.5 mm, respectively; mean and standard deviation values of the vehicle speed are 70 km/h and 10 km/h, respectively.
- Scenario 2 (SCN-2): the roadway profile with $\alpha = 0.003$, $\beta = 0.05$ and $n = 2.0$ as parameters of the PSD function defined in Equation 6; bump heights' mean and standard deviation values are 20.4 mm and 7.0 mm, respectively; mean and standard deviation values of the vehicle speed are 50 km/h and 10 km/h, respectively.

The scenario SCN-1 assumes a situation of highway bridges, whereas the SCN-2 is for national roadway bridges. The two scenarios consider the same data of the traveling position and axle load described in section 3.5.

Three hundred samples of each random variable are taken into account to simulate the impact coefficient considering all the random variables to save computation time because a preliminary investigation demonstrates that the mean and standard deviation values of the simulated impact coefficient tend to converge within the 300 samples. No correlation is assumed among the random variables described in section 3. A previous work by authors (Kim & Kawatani 2006) suggests that the simulated impact coefficient of the RC slab can be characterized as the lognormal distribution. The impact coefficients obtained by simulation are shown in Table 3, which also provides the simulated impact coefficient of an external girder (specified as G1 in Table 3) at the span center. A noteworthy point in Table 3 is that the P1 panel experiences more severe dynamic loading effects than the other panels do. Moreover, comparing SCN-2 for national roadway bridges with SCN-1 for highway bridges shows that the slab on national roadway bridges experiences more severe dynamic load effect than highway bridges as expected.

5 EFFECT OF IMPACT COEFFICIENT ON RC SLAB'S FATIGUE PERFORMACNE

Simulation of the impact coefficient of RC slabs demonstrates that the traffic-induced dynamic response of the P1 panel located at the approaching side of the bridge is greater than that of other panels because of the bumps at expansion joints. Generally, design codes specify that the panel near expansion joints should be stronger than other panels. A question here is whether or not the severe wheel load affects fatigue performance of the RC slab located near an expansion joint. A simple reliability analysis for fatigue performance of the RC slab shown in Figure 1 is conducted

Table 4. Properties of the RC deck.

	Panel	Value
Concrete		
Compressive strength (f_{ck}; MPa)		20.58
Normal (μ: 20.58, V: 0.165)		
μ: mean, V: coefficient of variation		
Young's modulus (MPa)		230300.0
Slab thickness (cm)	P1	23.0
	P2-P5	17.0
Reinforcing steel		
Yield strength (f_y; MPa)		295.0
Young's modulus (MPa)		2058000.0

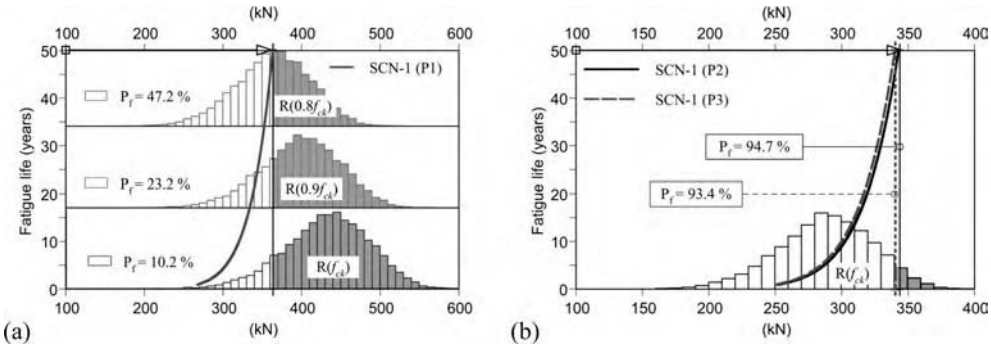

Figure 3. Fatigue life of RC decks (SCN-1). (a) P1 panel, (b) P2 and P3 panels.

to answer that question. Investigations specifically address the effect of the impact coefficient on fatigue performance of the RC slab as a numerical example. The fatigue performance of the RC slab is estimated using the probability of fatigue failure for a given lifetime. In this study, the RC slab lifetime is assumed as 50 years. The fatigue failure probability is estimated by comparing the punching shear strength of the RC slab and traffic load effects over the 50-year lifetime.

Traffic data are the same as those described in section 3.5. For the impact coefficient with lognormal distribution, the mean and standard deviation values summarized in Table 3 are used. The average daily truck traffic (ADTT) is assumed as 10,000 vehicles. Table 4 lists properties of concrete and reinforcing bars of RC slabs used in reliability analysis to assess the fatigue performance of the RC slab. The MCS is conducted to estimate the RC slab's probability of fatigue failure.

The fatigue performance of each panel according to the simulated impact coefficient is investigated next. The RC slab is assumed to have a design fatigue life of 50 years under the impact coefficient of 0.38 according to the JRA code. The probability of fatigue failure of each panel within the design fatigue life considering the simulated impact coefficients according to respective scenarios is summarized in Figures 3 and 4.

The P1 panel located near the expansion joint usually adopts a deeper cross-section and more reinforcing bars to resist the expected severe wheel load effects. However, congested areas containing much reinforcing steel may engender poor concrete quality because of rock pockets and sand streaks that result from the difficulty of placing concrete. Therefore, to consider the situation of poor concrete quality for the P1 panel, the ninetieth and eightieth percentiles of the compressive strength of concrete are also considered in this investigation. The R(f_{ck}), R(0.9f_{ck}) and R(0.8f_{ck})

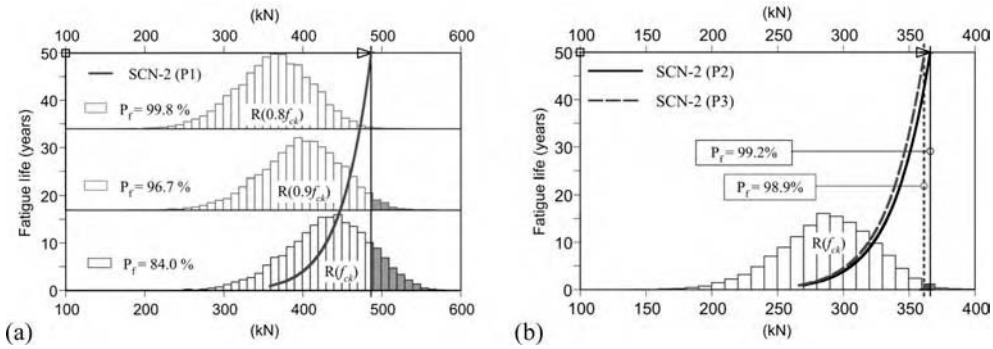

Figure 4. Fatigue life of RC decks (SCN-2). (a) P1 panel, (b) P2 and P3 panels.

in Figures 3 and 4 respectively demonstrate the load carrying capacity of the RC slab taken from considering full, ninetieth and eightieth percentiles of the concrete strength.

Regarding SCN-1 (see Figure 3), which denotes the scenario for general highway bridges, the probability of fatigue failure of the P1 panel distributed between 10.2% and 47.2% with respect to the concrete strength of the P1 panel, whereas those probabilities of other panels, especially P2 and P3 panels, are 94.7% and 93.4%, respectively. It indicates that the code-specified impact coefficient can provide a conservative design for fatigue of RC slabs because the failure probability is set as 100% under the code-specified impact coefficient. The situation for national roadway bridges of Japan, as illustrated in SCN-2, is also examined and summarized in Figure 4. It has worse roadway surface conditions and lower traffic speeds than highway bridges resembling SCN-1.

Observations from Figure 3 to Figure 4 show that the failure probability of the P1 panel is lower in comparison with other panels because of the deeper cross-section, even though the P1 panel experiences greater dynamic effects than other panels. On the other hand, the probability of fatigue failure tends to increase with decreasing concrete quality. Based on these observations, it can be concluded that the code-specified impact coefficient may lead to a conservative fatigue design for RC decks for well-maintained highway bridges. However, the increase of the impact coefficient as a result of the worse roadway surface conditions and traffic speed may cause fatigue failure of RC slabs earlier than the design life.

6 CONCLUSIONS

Impact coefficients of the RC slab on a steel girder bridge were simulated in this study using 3D traffic-induced dynamic response analysis of bridges combined with the Monte Carlo simulation technique. The respective effects of each random variable on the impact coefficient of the RC slab were investigated. Reliability analysis using the fatigue limit state based on the existing experimental result was also conducted to assess the influence of the impact coefficient on the probability of failure resulting from fatigue.

This study shows that the P1 panel located near bumps experiences more severe dynamic loading effect than that of other panels. On the other hand, observations through this study demonstrates that the probability of the P1 panel's fatigue failure is lower than that of the other panels located at the bridge's middle section because of the higher strength of the P1 panel resulting from the deeper cross section, even though the P1 panel experiences more severe dynamic loading effect than that of other panels. However, this study also suggests that the probability of the fatigue failure of the P1 panel tends to increase with decreasing concrete quality.

Based on those observations, it can be concluded that the code-specified impact coefficient may lead to a conservative fatigue design for RC slabs for well maintained highway bridges. However

the increased impact coefficient resulting from the worse roadway surface conditions may cause fatigue failure of RC slabs earlier than the design life.

Results of this study demonstrate the importance of the impact coefficient of RC slabs through analytical approaches. A collection of impact coefficients of RC slabs is necessary to create a rational criterion for the slab performance level and decision-making in relation to bridge management.

REFERENCES

Catieni, R. 1992. Dynamic behavior of highway bridges under passage of heavy vehicles. EMPA report No.220, Dübendorf.

Dodds, C.J. & Robson, M.M. 1973. The description of road surface roughness. *Sound and Vibrations* 31(2): 175–83.

Furuta, H., Tsukiyama, I., Dogaki, M. & Frangopol, D.M. 2003. Maintenance support system of steel bridges based on life cycle cost and performance evaluation. Reliability and optimization of structural systems. In: H. Furuta, M. Dogaki & M. Sakano (ed.), *Reliability and Optimization of Structural Systems*; *Proc. 10th IFIP WG7.5 Working Conf., Osaka, Japan, 25–27 March, 2002*. Lisse: Balkema.

Hanshin Expressway Management Technology Center (HEPC). 1991. Crack damage of RC deck slabs of highway bridges and its resistance. (in Japanese)

Honda, H., Kajikawa, Y. & Kobori, T. 1982a. Spectra of road surface roughness on bridges. *Structural Division, ASCE* 108(ST9): 1956–66.

Honda, H., Kajikawa, Y. & Kobori, T. 1982b. Roughness characteristics at expansion joint on highway bridges. *Proceedings of JSCE* 328: 173–76. (in Japanese)

Kawatani, M. & Kim, C.W. 1998. Effects of gap at expansion joint on traffic-induced vibration of highway bridge. *Proc. of Developments in Short and Medium Span Bridge Engineering'98, Calgary, Canada, July, 1998. CSCE* [CD-ROM].

Kim, C.W., Kawatani, M. & Kim, K.B. 2005. Three-dimensional dynamic analysis for bridge-vehicle interaction with roadway roughness. *Computers and Structures* 83(19–20): 1627–1645.

Kim, C.W. & Kawatani, M. 2006. Probabilistic investigation on dynamic response of deck slabs of highway bridges. In John Cagnol & Jean-Paul Zolesio (ed.), *System Modeling and Optimization, IFIP International Federation of Information Processing* 166: 217–228, *Proc. 21st IFIP TC7 Conf., Sophia Antipolis, France*, 21–25 July, 2003.

Matsui, S. 1984. Study about fatigue of RC slab of highway bridges and design method. *Doctoral thesis*, Osaka University. (in Japanese)

Matsui, S. & Muto, K. 1992. Rating of lifetime of a damaged RC slab and replacement by steel plate-concrete composite deck. *Technology Reports of the Osaka University* 42(2115): 329–40.

Okada, K., Okamura, H. & Sonoda, K. 1978. Fatigue failure mechanism of reinforced concrete deck slabs. *TRB, Transportation research record* 664: 136–44.

Perdikaris, P.C., Petrou, M.F. & Wang, A. 1993. Fatigue strength and stiffness of reinforced concrete bridge decks. *Final report to ODOT, FHWA/OH*-93/016, March 1993, Department of Civil Engineering, Case Western University, Cleveland, OH.

Public Work Research Institute. 1997. Results of survey on replacement of existing bridges. *Technical Memorandum of PWRI* 3512, Public Works Research Institute, Japan. (in Japanese)

Sakano, M., Mikami, I. & Miyagawa, K. 1993. Simultaneous loading effect of plural vehicles on fatigue damages of highway bridges. In Thoft-Christensen P & Ishikawa H (ed.), *Reliability and optimization of structural systems V. IFIP Transactions* B-12: 221–28, Elsevier Science Publishes.

Reliability and Optimization of Structural Systems: Assessment, Design and Life-Cycle Performance – Frangopol, Kawatani & Kim (eds)
© 2007 Taylor & Francis Group, London, ISBN 978-0-415-40655-0

Effect of uncertainty in cross-sectional property on reliability-based topology optimization of frame structures

Nozomu Kogiso & Keigo Nishida
Osaka Prefecture University, Sakai, Osaka, Japan

Katsuya Mogami, Shinji Nishiwaki, Kazuhiro Izui & Masataka Yoshimura
Kyoto University, Kyoto, Japan

ABSTRACT: Topology optimization methods using discrete elements such as frame elements can provide useful insights into the underlying mechanics principles of products, however the majority of such optimizations are performed under deterministic conditions. In order to consider variations of design parameters during the optimization, part of the authors presented a reliability-based topology optimization method for frame structures that considers uncertainties in applied loads and nonstructural mass at the early conceptual design stage. System reliability for multiple criteria, namely stiffness and eigen-frequency, is evaluated by regarding them as a series system, where mode reliabilities can be evaluated using first order reliability methods. In this study, the reliability-based optimization is expanded to consider variations on cross-sectional property of frame element on the optimum topology. Through numerical calculations, reliability-based topology designs of typical three-dimensional frames are obtained. The effect of uncertainties of cross-sectional property of frame element is investigated on the optimum topology.

1 INTRODUCTION

The conceptual design is a critical stage in the development process of mechanical products, since design factors pertaining to the most important characteristics of the product are decided in this stage (Fabrycky & Blanchard 1991). If the conceptual design process is well organized, the final products will likely offer the desired set of performance features and have been developed in a competitively short product development time.

Topology optimization methods offer the greatest potential for exploring ideal and optimized structures. Topology optimization methods include two major approaches: (i) the continuum approach, and (ii) the discrete element approach.

In the continuum approach, the optimal configuration is searched for using an infinite number of infinitesimal design variables. The continuum approach can be traced back to research first proposed by (Bendsøe & Kikuchi 1998), the so-called homogenization design method. The approach has been extensively applied to a variety of structural optimization problems (e.g., (Allen *et al.* 2004), (Maute & Allen 2004)). However, the optimization results are provided as a distribution of material, which gives little insight into the underlying reasons for the achieved optimality. Thus, this approach is unsuitable for supporting the decision-making of design engineers as they work to optimally configure such mechanical structures at the conceptual design phase.

On the other hand, the discrete element approach, also termed the ground structure approach, is based on formulations of structural elements derived from fundamental mechanics, such as the mechanics of materials, so design engineers can easily get insight of the reasons for optimality and the mechanical aspects of the structure. Therefore, this type of structural optimization can offer valuable decision-making support for design engineers working at the conceptual design

phase. In this approach, the design domain is configured with members such as trusses or frames, which implies dealing with a finite number of design variables During the structural optimization, unnecessary elements are eliminated. Comprehensive literature on the ground structure approach to structural optimization is found in review articles, e.g. (Rozvany *et al.* 1995).

Topology optimization methods using the discrete element approach are effective at the conceptual design stage, but actual mechanical structures are subject to, and cannot avoid uncertain conditions such as applied loads, material properties, and dimensional variation due to manufacturing factors. Since these uncertainties may negatively affect desired performances, there is a great need for optimization methods that can work effectively despite their presence.

Part of the authors have proposed the reliability-based topology optimization approach for frame structure design in the conceptual design phase (Mogami *et al*. 2006). For the frame structure with a nonstructural mass, system reliability for multiple criteria, namely stiffness and eigen-frequency, is evaluated by regarding them as a series system, where mode reliabilities can be evaluated using first order reliability methods (FORM) (Thoft-Christensen & Murotsu 1986). In the study, applied loads and nonstructural mass are treated as random variables. Through numerical calculations for two-dimensional and three-dimensional frame structures, it is demonstrated the importance of considering uncertainty of applied loads and nonstructural mass.

However, cross-sectional area of each frame element was treated as a deterministic design variable in that study. Even in the conceptual design phase, it is important to consider the effect of variations of cross-sectional property of frame elements, because the variations directly relate to variations of the stiffness and eigen-frequency. Therefore, the authors expand the previous research to include the cross-sectional property in random variables. In the topology optimization problem, the mean values of the cross-sectional property of frame elements are treated as design variables.

2 TOPOLOGY OPTIMIZATION

The optimization presented here is based on topology optimization techniques. The key ideas of the proposed method are the introduction of a fixed and extended design domain D that includes the original design domain Ω_d, and the utilization of characteristic function below that indicates the existence of a frame element. Suppose that a fixed and extended design domain D is composed of n frame elements. The existence of the i-th frame element is expressed by the following characteristic function:

$$\chi_i = \begin{cases} 1 & \text{if exists in } \Omega_d \\ 0 & \text{if does not exist in } \Omega_d \end{cases} \qquad \text{for } i = 1, \ldots, n \tag{1}$$

An optimal structure is obtained via this characteristic function when only necessary elements exists in the design domain Ω_d. This approach is also termed the ground structure approach. The optimization problem can be interpreted as a combinatorial problem that includes finite discontinuities that express the existence or non-existence of elements. To overcome this difficulty, Equation (1) is approximated using the following equations, whose formulation is based on the concept of the density approach, which is also called the Solid Isotropic Material with Penalization (SIMP) method (Bendsøe & Sigmund 1999).

$$\chi_i \approx {\rho_{A_i}}^p \tag{2}$$

where ρ_{A_i} is a normalized design variable ($0 \leq \rho_{A_i} \leq 1$) for the i-th element, and p is a penalization parameter emphasizing the influence that design variable ρ_{A_i} has on calculations.

In this study, frame structures are considered where the frame elements support an axial load as well as bending and twisting moments. The cross-sectional area of the i-th element, A_i, is defined as follows.

$$A_i = {\rho_{A_i}}^p A_{\max} \qquad (i = 1, \ldots, I) \tag{3}$$

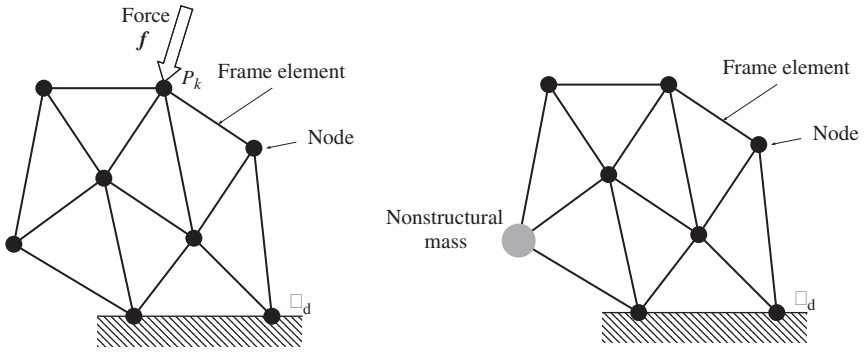

(a) Stiffness problem (b) Vibration problem

Figure 1. Configuration of design domain of frame structure.

where $A_{\max}$ is the maximum cross-sectional area and ρ_{A_i} is adopted as a normalized design variable. The other cross-sectional properties are easily obtained, assuming that the cross-sectional shape is a solid circle. The moment of inertia and polar moment of inertia are described in terms of the cross-sectional area as follows.

$$I_{y_i} = I_{z_i} = \frac{\pi d_i^4}{64} = \frac{A_i^2}{4\pi}, \qquad J_{x_i} = \frac{\pi d_i^4}{32} = \frac{A_i^2}{2\pi} \tag{4}$$

Using these parameters, we can construct a stiffness matrix $\boldsymbol{K}_e$ for each element.

For the topology optimization, two criteria are introduced. One is the mean compliance, used for static criterion, the other is the mean eigen-frequency, used for dynamic criterion.

2.1 *Mean compliance*

Consider that an elastic mechanical structure consisting of I elastic frame elements is subjected to a static load $\boldsymbol{f}$ at point P_k and fixed at boundary Γ_d, as shown in Fig. 1 (a). Body forces are assumed to be ignored for simplicity in the formulation. Let $\boldsymbol{f}$ and $\boldsymbol{d}$ be the load and displacement vectors, respectively. The mean compliance l is introduced as a measure of the stiffness at point P_k, expressed as follows (Bendsøe & Sigmund 1999; Suzuki & Kikuchi 1991).

$$l = \boldsymbol{f}^T \boldsymbol{d} = \boldsymbol{d}^T \boldsymbol{K} \boldsymbol{d} \tag{5}$$

where $\boldsymbol{K}$ is the global stiffness matrix of the entire structure.

2.2 *Mean eigen-frequency*

Eigen-frequency is adopted as a dynamic criterion. Consider a frame structure consisting of I frame elements and a nonstructural mass, as shown in Fig. 1 (b). A vibration equation can be formulated as follows.

$$(\boldsymbol{K} - \lambda_m \boldsymbol{M})\boldsymbol{\psi}_m = \boldsymbol{0}, \quad (m = 1, \ldots, M) \tag{6}$$

where $\boldsymbol{M}$ is the global mass matrix of the entire mechanical structure, λ_m $(m = 1, \ldots, M)$ is the m-th eigenvalue, and ψ_m $(m = 1, \ldots, M)$ is the m-th eigenvector.

In usual mechanical design situations, the first eigen-frequency is maximized to avoid resonance phenomenon but optimum designs that focus on an eigen-frequency often encounter significant

problems with mode shifting. To avoid the mode shifting problem, the following mean eigenvalue (Ma *et al.* 1995) is adopted.

$$\Lambda = 3\left(\frac{1}{\lambda_1}+\frac{1}{\lambda_2}+\frac{1}{\lambda_3}\right)^{-1} \tag{7}$$

During topology optimization under vibration criteria, local vibration modes that have no physical meaning will appear for excessively thin frame elements during the optimization search. In this study, Tcherniak's proposed method (Tcherniak 2002) is adopted to avoid such a phenomenon. When the design variable ρ_{A_i} is lower than the threshold value ρ_{thr}, the corresponding element mass matrix is regarded to zero, as follows.

$$\boldsymbol{M}_e = \begin{cases} \boldsymbol{M}_e & \text{if} \quad \rho_{A_i} > \rho_{\text{thr}} \\ \boldsymbol{0} & \text{if} \quad \rho_{A_i} \leq \rho_{\text{thr}} \end{cases} \tag{8}$$

where, ρ_{thr} is set to be 0.01 in this study.

3 RELIABILITY ANALYSIS

In addition to the applied load and the nonstructural mass, ρ_{A_i}, $(i = 1, \ldots, n)$ are treated as random variables in order to describe variations of cross-sectional area and the moment of inertia of the frame elements as shown in Equations (3) and (4). With variations of these random variables, the mean compliance in Equation (5) and the mean eigen value in Equation (7) also exhibit variations, which has a deleterious effect upon the structural performance. The degree of degradation in performance is evaluated based on structural reliability theory.

The frame structure is regarded as a failure when the mean compliance l exceeds the upper limit l_U or the mean eigenvalue Λ is lower than the lower limit Λ_L. Therefore, the following two limit state functions are introduced.

$$G_1(\boldsymbol{Z}) = h_1(\boldsymbol{U}) = l_U - l(\boldsymbol{U}) \tag{9}$$

$$G_2(\boldsymbol{Z}) = h_2(\boldsymbol{U}) = \Lambda(\boldsymbol{U}) - \Lambda_L \tag{10}$$

where $\boldsymbol{Z}$ indicates a random vector consisting of applied load, the nonstructural mass and cross-sectional property of the frame element. $\boldsymbol{U}$ is the random vector transformed to a normalized standard deviation $\boldsymbol{U} = T(\boldsymbol{Z})$ that is required to apply the FORM.

The reliability of each mode is evaluated through the FORM. In the FORM, the shortest distance from the origin to the limit state surface in $\boldsymbol{U}$-space is evaluated as reliability index β_i as shown in Figure 2 (Thoft-Christensen & Murotsu 1986). The Hasofer-Lind Rackwitz-Fiessler (HL-RF) method is adopted to evaluate the mode reliability index β_i and the design point $\boldsymbol{u}_i^*$ using the following iterative calculation.

$$\boldsymbol{u}_i^{(j+1)} = \left[\boldsymbol{\alpha}_i^{(j)T}\boldsymbol{u}_i^{(j)} - \frac{h_i(\boldsymbol{u}^{(j)})}{|\nabla_{\boldsymbol{u}} h_i(\boldsymbol{u}_i^{(j)})|}\right]\boldsymbol{\alpha}^{(j)}, \qquad \boldsymbol{\alpha}_i^{(j)} = \frac{\nabla_{\boldsymbol{u}} h_i(\boldsymbol{u}_i^{(j)})}{|\nabla_{\boldsymbol{u}} h_i(\boldsymbol{u}_i^{(j)})|} \tag{11}$$

where superscript (j) is the number of iterations and $\boldsymbol{\alpha}_i^{(j)}$ is the unit vector of the j-th trial point, $\boldsymbol{u}_i^{(j)}$. In convergence, the mode failure probability P_i is evaluated by linearizing the limit state function at the design point $\boldsymbol{u}_i^*$ as shown in Figure 2.

The frame system is regarded as a failure, if either of the limit state functions in Equations (9) and (10) has a negative value. That is, the system is modeled as a series system consisting of the

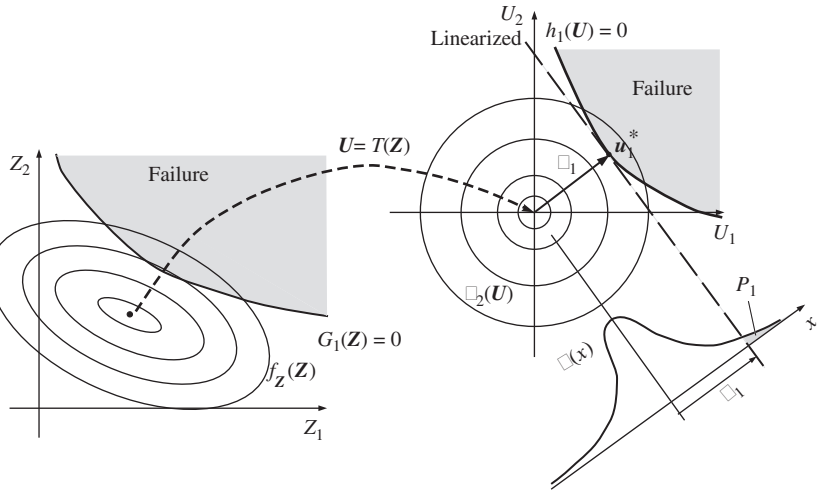

Figure 2. First order reliability method (FORM).

two failure modes. In this study, the system failure probability P_f is obtained as follows.

$$P_f = P_1 + P_2 - P_{12} = \Phi(-\beta_1) + \Phi(-\beta_2) - \Phi_2(-\beta_1, -\beta_2; \rho_{12}) \tag{12}$$

where P_{12} indicates a joint probability that is evaluated through a two-dimensional standard normal distribution function $\Phi_2()$ and ρ_{12} indicates the correlation between the modes, as shown in Figure 3.

A system reliability index, β_s in correspondence with the system failure probability P_f is defined as follows.

$$\beta_s = -\Phi^{-1}(P_f) \tag{13}$$

The system reliability index is used as the constraint or the objective function in reliability-based topology optimization.

4 FORMULATION OF RELIABILITY-BASED TOPOLOGY OPTIMIZATION

In this study, the expected values of normalized cross-sectional areas ρ_{A_i}, $(i = 1, \ldots, n)$ for frame elements are adopted as design variables. The reliability maximization under a volume constraint problem is obtained.

$$\begin{aligned} &\text{Maximize:} && \beta_s(E[\rho_{A_i}]) \\ &\text{subject to:} && V(E[\rho_{A_i}]) \le V_U \\ & && \boldsymbol{K}\boldsymbol{u} = \boldsymbol{f} \\ & && (\boldsymbol{K} - \lambda_m \boldsymbol{M})\boldsymbol{\psi}_m = \boldsymbol{0}, \quad (m = 1, \ldots, M) \\ & && 0 \le \rho_{A_i} \le 1, \qquad (i = 1, \ldots, I) \end{aligned} \tag{14}$$

where $V(E[\rho_{A_i}])$ is the expected value of the total volume of frame structure and V_U indicates the volume upper limit.

For numerical optimization, the convex linearization method (CONLIN) (Fleury & Braibant 1986), a type of sequential convex programming, is adopted. This approach offers advantage in convergence for stiffness problems (Takezawa *et al.* 2003).

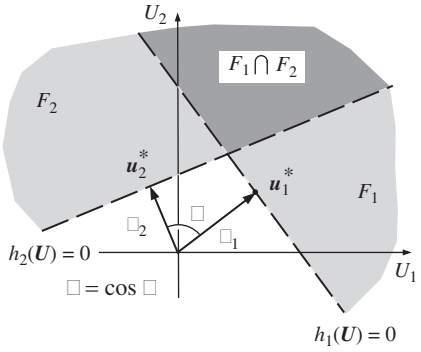

Figure 3. Joint failure probability.

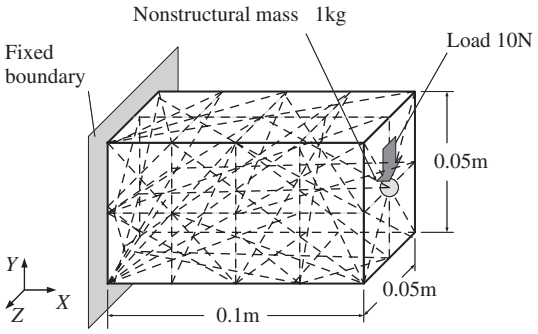

Figure 4. Ground structure of 3-D frame.

For the sensitivity analysis, the derivatives of the system reliability index in terms of design variables ρ_{A_i} is evaluated as follows (Enevoldsen & Sørensen 1994).

$$\frac{\partial \beta_s}{\partial \rho_{A_i}} = \frac{\partial \beta_s}{\partial P_s}\left(\frac{\partial P_1}{\partial \beta_1}\frac{\partial \beta_1}{\partial \rho_{A_i}} + \frac{\partial P_2}{\partial \beta_2}\frac{\partial \beta_2}{\partial \rho_{A_i}} - \frac{\partial P_{12}}{\partial \rho_{A_i}}\right) \tag{15}$$

where each derivative term is evaluated according to the reference (Enevoldsen & Sørensen 1994).

$$\frac{\partial P_j}{\partial \beta_j} = -\phi(-\beta_j), \qquad (j = 1,2), \tag{16}$$

$$\frac{\partial P_{12}}{\partial \rho_{A_i}} = \sum_{j=1}^{2} \frac{\partial \Phi_2}{\partial \beta_j}\frac{\partial \beta_j}{\partial \rho_{A_i}} + 2\frac{\partial \Phi_2}{\partial \rho_{12}}\frac{\partial \rho_{12}}{\partial \rho_{A_i}}, \tag{17}$$

$$\frac{\partial \beta_j}{\partial \rho_{A_i}} = \frac{1}{|\nabla_{\boldsymbol{u}} h_j(\boldsymbol{u})|}\frac{\partial h_j(\boldsymbol{u})}{\partial \rho_{A_i}}, \qquad (j = 1,2), \tag{18}$$

$$\frac{\partial \Phi_2}{\partial \beta_j} = -\phi(-\beta_j)\Phi\left(-\frac{\beta_k - \rho_{12}\beta_j}{\sqrt{1-\rho_{12}^2}}\right), \qquad (j,k = 1,2, j \neq k). \tag{19}$$

5 NUMERICAL EXAMPLES

Numerical examples are presented to examine verify the effect of variation of the cross-sectional property. The obtained optimum topology is compared with the optimum design that the cross-sectional property has no variations (Mogami *et al.* 2006). In the example, Young's modulus, Poisson's ratio, and mass density are set to 209 GPa, 0.3, and 7784 kg/m^3, respectively. These material constants are assumed to have no variations. The penalization parameter p is set to 1.0 and the allowable maximum cross-sectional diameter of each frame element is set to 0.01 m. For simplicity, all of random variables are assumed to be normally distributed.

A numerical example is given for a 3-D frame structure considering both the compliance and the eigen-frequency criteria. The design region is configured as a rectangular solid, as shown in Figure 4, where the left side plane is fixed. Applied load in the $-Y$ direction at the central node of the right side plane and the nonstructural mass at the same node are both treated as random variables, where the mean values are 10 N and 1 kg, respectively. The ground structure consists of

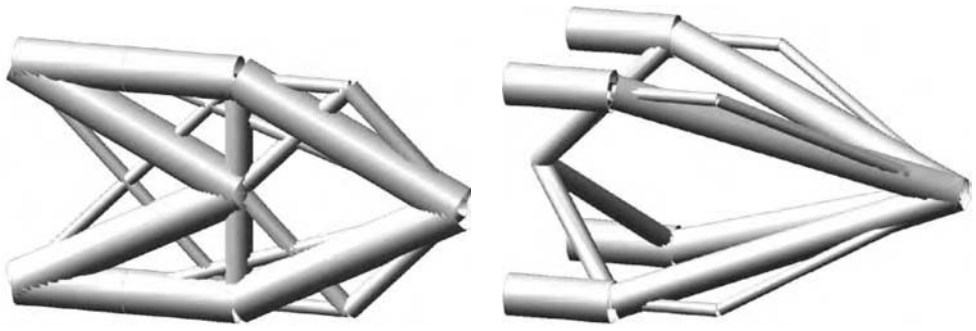

(a) Mean compliance minimization design (b) Mean eigenvalue minimization design

Figure 5. Deterministic optimal topology designs.

832 frame elements connecting any two nodes that are arranged at four equally divided locations in the X direction and two equally divided locations in the Y and Z directions, though all of the frame elements are not shown in Fig. 4.

5.1 *Deterministic design*

Deterministic designs for the mean compliance minimization and the mean eigenvalue maximization designs are obtained, where the mean applied load and the mean nonstructural mass are treated as deterministic values. The optimum designs are illustrated in Figure 5. The optimum mean compliance and eigen-frequency are 1.897×10^{-6}J and 36.37 Hz, respectively. The mean compliance maximization design reduces to the two-dimensional configuration, since only a vertical load is applied. On the other hand, the eigen-frequency optimum configuration is three-dimensional, with frame elements allocated at the outer-most nodes at the left side boundary plane that are become concentrated at the point where the nonstructural mass is located, at the center of right side plane.

5.2 *Reliability-based design without variations of cross-sectional property*

The reliability-based topology optimum designs are obtained for three cases having different standard deviation settings of only applied load and nonstructural mass, Case 1) $\sigma_l = 4\,\mathrm{N}, \sigma_m = 0.2\,\mathrm{kg}$, Case 2) $\sigma_l = 3\,\mathrm{N}, \sigma_m = 0.3\,\mathrm{kg}$ and Case 3) $\sigma_l = 2\,\mathrm{N}, \sigma_m = 0.4\,\mathrm{kg}$. For the limit state functions, the upper limit of the mean compliance is four times that of the deterministic optimum design; namely $4 \times 1.897 \times 10^{-6}$J, while the lower limit of the mean eigen-frequency is 0.4 of the deterministic optimum design; i.e., 0.4×36.37 Hz. The optimum configurations are illustrated in Figure 6 (a) and the obtained reliability indexes are listed in Table 1.

When the variance of the load is comparatively larger than the nonstructural mass, the frame elements in the central vertical plane area have large cross-sectional areas, since the load is vertically applied in this structure. On the other hand, when the variation of the mass is larger than the load, the configuration approaches what is seen in configurations where the deterministic eigen-frequency is maximized.

5.3 *Reliability-based design with considering variations of cross-sectional property*

Finally, the reliability-based optimum designs including variation of cross-sectional property are obtained. The variation of normalized cross-sectional area for each frame element, ρ_{A_i}, is modeled by setting the coefficient of variations (COV) for all of frame elements. Note that not only the cross-sectional area, but also moment of inertia and polar moment of inertia defined in Equation 4 have varied according to variation of ρ_{A_i}. Consider the two types of COV values, (a) COV $= 0.05$ and (b) COV $= 0.10$ with normal distribution. The total number of random variables is 834 consisting of the cross-sectional property of frame elements, as well as applied load and nonstructural

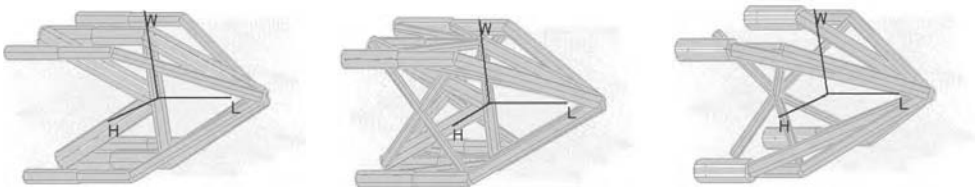

(i) Case 1 (ii) Case 2 (iii) Case 3

(a) No variations of cross-sectional property.

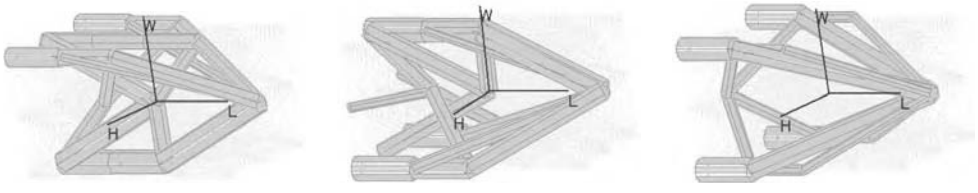

(i) Case 1 (ii) Case 2 (iii) Case 3

(b) COV = 0.05.

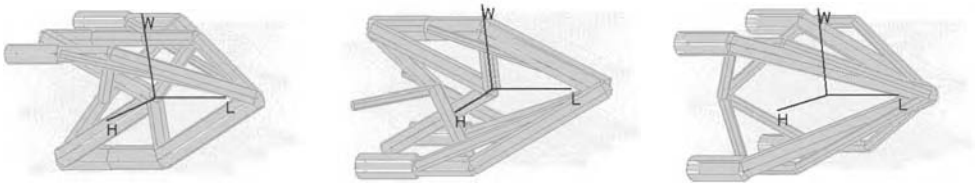

(i) Case 1 (ii) Case 2 (iii) Case 3

(c) COV = 0.10.

Figure 6. Reliability-based optimum topology without and with variations of cross-sectional property.

Table 1. Reliability index of optimum design with variations of cross-sectional property.

Coefficient of variation	Case 1			Case 2			Case 3		
	β_l	β_m	β_s	β_l	β_m	β_s	β_l	β_m	β_s
0.00	2.245	3.250	2.227	2.814	3.411	2.774	3.735	3.825	3.599
0.05	2.286	3.354	2.272	2.909	3.488	2.870	3.779	3.946	3.676
0.10	2.287	3.337	2.273	2.913	3.488	2.873	3.793	3.947	3.686

mass. The mean value of ρ_{A_i} is adopted as design variables. The other conditions are same as the previous example.

The optimum topologies for the two set of COVs under the two cases are illustrated in Fig. 6. In all cases, the optimum topology is changed from the previous example. In Case 1 and 2, the number of frame elements connected to the left boundary plane is reduced to the three elements with unsymmetrical layout. In Case 3, the thin central four frame elements are connected at the central node of the left plane. That is different from the previous example that the thin four frame elements from the corner nodes at the left side plane is connected at middle node. For both cases, the left-side frame elements becomes thicker than previous examples. This is considered to be reasonable to reduce the effects of variations of cross-sectional property.

The obtained reliability indexes are listed in Table 1. This result indicates that the optimum reliability seems to have little effect of variations of cross-sectional property. In addition, the

difference between the optimum designs in cases of COV = 0.05 and COV = 0.10 is small, though the topology designs are much different from that without considering variations of cross-sectional property. Though the iteration process does not seem to have numerically instability problem, further investigation is required to make clarify the effect of variations of cross-sectional property on the reliability.

6 CONCLUSION

In this paper, the reliability-based topology optimization methods for frame structure proposed by the authors is expanded to investigate the effect of variations of cross-sectional property of each frame element on the reliability from the previous study that considers variations of applied load and nonstructural mass. System reliability for multiple criteria, namely stiffness and eigen-frequency, is evaluated by regarding them as a series system, where mode reliabilities can be evaluated using first order reliability methods. In order that mechanical design engineers should find obtained solutions reasonable in conceptual design phase, the ground structure approach that uses discrete elements to represent the design space is adopted for the topology optimization.

The proposed methods were applied to the design problem of three-dimensional frame structure. It is demonstrated that the reliability-based optimum topology with variations of cross-sectional property of the frame element is different from that without variations. Further investigations, e.g., different cross-sectional shape, is required to clarify the effect of the variations.

REFERENCES

Allen, M., Raulli, M., Maute K. and Frangopol, D.M. 2004. Reliability-Based Analysis and Design Optimization of Electrostatically Actuated MEMS. *Computers and Structures 82*, 1007–1020.

Bendsøe, M.P. and Kikuchi, N. 1998. Generating Optimal Topologies in Structural Design using a Homogenization Method. *Comput. Methods Appl. Mech. Engrg. 71*, 197–224.

Bendsøe, M.P. and Sigmund, O. 1999. Material Interpolations in Topology Optimization. *Arch. Appl. Mech. 69*, 635–654.

Enevoldsen, I. and Sørensen, J.D. 1994. Reliability-Based Optimization in Structural Engineering. *Structural Safety 15*, 169–196.

Fabrycky, W.J. and Blanchard, B.S. 1991. *Life-Cycle Cost and Economic Analysis – International Series in Industrial and Systems Engineering*. Englewood Cliffs, NJ: Prentice-Hall.

Fleury, C. and Braibant, V. 1986. Structural optimization: A new dual method using mixed variables. *Int. J. Num. Methods in Engrg. 23*, 409–428.

Ma, Z.D., Kikuchi, N. and Cheng, H.C. 1995. Topology Design for Vibrating Structures. *Comput. Methods Appl. Mech. Engrg. 121*, 259–280.

Maute, K. and Allen, M. 2004. Conceptual Design of Aeroelastic Structures by Topology Optimization. *Struct. Multidisc. Optim. 27*, 27–42.

Mogami, K., Nishiwaki, S., Izui, K., Yoshimura, M. and Kogiso, N. 2006. Reliability-based Structural Optimization of Frame Structures for Multiple Failure Criteria Using Topology Optimization Techniques. *Struct. Multidisc. Optim. 32*, 299–311.

Rozvany, G. I. N., Bendsøe, M. P. and Kirsch, U. 1995. Layout Optimization of Structures. *Applied Mechanics Review 48*, 41–119.

Suzuki, K. and Kikuchi, N. 1991. A Homogenization Method for Shape and Topology Optimization. *Comput. Methods Appl. Mech. Engrg. 93*, 291–318.

Takezawa, A., Nishiwaki, S. Izui, K. and Yoshimura, M. 2003. Topology Optimization Using Function-oriented Elements Based on the Concept of First Order Analysis. In *ASME Design Automation Conference 2003*, pp. ASME DAC 2003/DAC–48773.

Tcherniak, D. 2002. Topology Optimization of Resonating Structures Using SIMP Method. *Int. J. Numer. Meth. Engrg. 54*, 1605–1622.

Thoft-Christensen, P. and Murotsu, Y. 1986. *Application of Structural Systems Reliability Theory*. Berlin: Springer-Verlag.

Reliability and Optimization of Structural Systems: Assessment, Design and Life-Cycle Performance – Frangopol, Kawatani & Kim (eds)
© 2007 Taylor & Francis Group, London, ISBN 978-0-415-40655-0

The applications of the third-order normal polynomial to structural reliability assessment

Zhao-Hui Lu & Yan-Gang Zhao
Nagoya Institute of Technology, Nagoya, Japan

ABSTRACT: In this paper, the third-order normal polynomial is investigated. First, a four parameters distribution based on the polynomial is defined, and the flexibility for fitting statistical data by using the distribution is illustrated by two practical examples. Second, a fourth-moment reliability index is derived, and several examples are presented to demonstrate the efficiency of the reliability index for structural reliability assessment.

1 INTRODUCTION

In structural reliability evaluation, the basic random variables representing uncertain quanties, such as loads, environmental factors, material properties, structural dimensions, and variables introduced to account for modeling and prediction errors, are assumed to have known cumulative distribution functions (CDFs) or probability density functions (PDFs). Determination of the probability distributions of these basic random variables is essential for the accurate evaluation of the reliability of a structure or structure system.

Many methods for determining the probability distributions have been developed, such as Bayesian approach (Der Kiureghian & Liu, 1986; Der Kiureghian, 2001), B-spline function (Zong & Lam, 1998; Zong & Lam, 2000; Zong & Lam, 2001), theoretical approach(Dan & Kanda 1999), and others. Usually, the basic method for determining the required distribution is to fit the histogram of the statistical data of a variable with a candidate distribution (Ang & Tang, 1975), and apply statistical goodness-of-fit tests. Generally, such candidate distributions would have parameters that may be evaluated from the mean value and standard deviation of the statistical data. It has been reported that the two-parameter (2P) distributions may not be appropriate when the skewness of the statistical data is important and must be reflected in the distribution. Thus, the three-parameter (3P) distributions (Zhao & Ang, 2002), which can effectively reflect the information of skewness as well as the mean value and standard deviation of statistical data, have been suggested as the candidate distribution. However, the 3P distributions may be not flexible enough to reflect the kurtosis of statistical data of a random variable, and distributions that can be determined by effectively using the information of kurtosis as well as the mean value, standard deviation, and skewness of the statistical data are required.

On the other hand, in structural reliability analysis, for a performance function $z = G(\mathbf{X})$, if the first four moments of $G(\mathbf{X})$ are obtained, the probability of failure P_f can be estimated from the relationship between the CDF of $G(\mathbf{X})$ and its first four central moments. Therefore, it is convenient to have a distribution whose parameters are determined by its first four moments.

In the present paper, a four-parameter (4P) distribution based on the third-order normal polynomial is defined, in which the parameters can be determined in terms of the mean value, standard deviation, skewness, and kurtosis of the sample data, and the flexibility for fitting statistical data by using the distribution is illustrated by two practical examples. A fourth-moment reliability index

is derived, and several examples are presented to demonstrate the efficiency of the reliability index for reliability analysis.

2 THE DISTRIBUTION BASED ON THE THIRD-ORDER NORMAL POLYNOMIAL

2.1 *Definition of the distribution*

The distribution is defined on the base of the following third-order polynomial normal transformation (Fleishman, 1978)

$$\frac{x-\mu}{\sigma} = S_u(u) = a_1 + a_2 u + a_3 u^2 + a_4 u^3 \tag{1a}$$

The CDF and PDF corresponding to Eq. 1a are expressed as

$$F(x) = \Phi(u) \tag{1b}$$

$$f(x) = \frac{\phi(u)}{\sigma(a_2 + 2a_3 u + 3a_4 u^2)} \tag{1c}$$

where F, f, μ, and σ are the CDF, PDF, mean value, and standard deviation of x, respectively; Φ and ϕ are the CDF and PDF of a standard normal variable u; and a_1, a_2,a_3, and a_4 are deterministic coefficients.

2.2 *Parameter estimation*

Several methods for determining the coefficients are reported by Chen & Tung (2003). These include Moment-matching method (Fleishman 1978), Least-square method (Hong & Lind 1996), and L-moments method (Tung 1999). Because the first four moments (mean, standard deviation, skewness, and kurtosis) having clear physical definitions are common in engineering and can be easily obtained using the sample data, the determination of the four coefficients using the first four moments will be focused on in this paper.

For a random variable, if the first four moments (mean value μ, standard deviation σ, skewness α_3, and kurtosis α_4) are known, the parameters of μ and σ can be obtained directly. And the parameters a_1, a_2, a_3, and a_4 are obtained by making the first four central moment of $S_u(u)$ equal to those of $x_s = (x-\mu)/\sigma$ with the aid of Eq. 1a, i.e.

$$a_1 + a_3 = 0 \tag{2a}$$

$$a_2^2 + 2a_3^2 + 6a_2a_4 + 15a_4^2 = 1 \tag{2b}$$

$$6a_2^2a_3 + 8a_3^3 + 72a_2a_3a_4 + 270a_3a_4^2 = \alpha_3 \tag{2c}$$

$$3(a_2^4 + 20a_2^3a_4 + 210a_2^2a_4^2 + 1260a_2a_4^3 + 3465a_4^4) + 12a_3^2(5a_2^2 + 5a_3^2 + 78a_2a_4 + 375a_4^2) = \alpha_4 \tag{2d}$$

Simplifying Eq. 2, the following equations of parameters a_2 and a_4 can be obtained as,

$$2A_1A_2 = \alpha_3^2 \tag{3a}$$

$$3A_1A_3 + 3A_4 = \alpha_4 \tag{3b}$$

where

$$A_1 = 1 - a_2^2 - 6a_2a_4 - 15a_4^2 \tag{3c}$$

$$A_2 = 2 + a_2^2 + 24a_2a_4 + 105a_4^2 \tag{3d}$$

$$A_3 = 5 + 5a_2^2 + 126a_2a_4 + 675a_4^2 \tag{3e}$$

$$A_4 = a_2^4 + 20a_2^3a_4 + 210a_2^2a_4^2 + 1260a_2a_4^3 + 3465a_4^4 \tag{3f}$$

Since the values α_3 and α_4 are known, the parameters a_2 and a_4 can be obtained from Eq. 3, which can be solved using common subroutines of nonlinear equations such as the "FindRoot" function in "Mathematica" software (Wolfram, 1999). After the parameters a_2 and a_4 have been obtained, the parameters a_1 and a_3 can be readily given as

$$a_3 = -a_1 = \frac{\alpha_3}{2A_2} \tag{4}$$

3 APPLICATIONS IN DATA ANALYSIS

In order to investigate the efficiency of the introduced distribution in fitting statistical data of a random variable, the following two examples use the practical data of H-shape structural steel collected by Ono et al. (1986). The fitting results of the histogram of the ratio between measured values and nominal values of the thickness are shown in Figure 1a, in which the number of data is 885 and the first-four moments of the data are obtained as $\mu = 0.986$, $\sigma = 0.0457$, $\alpha_3 = 0.883$, and $\alpha_4 = 5.991$. In Figure 1a, the PDFs of the normal and lognormal distributions, with the same mean value and standard deviation as the data, the PDF of the 3P-Gamma distribution whose mean value, standard deviation, and skewness are equal to those of the data, and the PDF of the present 4P distribution whose mean value, standard deviation, skewness, and kurtosis are equal to those of the data, are depicted. Figure 1a reveals the following:

(1) The PDFs of the normal distribution and lognormal distribution have the greatest differences from the histogram of the statistical data among the four distributions. Since the normal distribution is a symmetrical distribution with the skewness=0.0 and the kurtosis=3.0, respectively, it obviously cannot be used to fit the histogram that has such a large skewness (0.883) and kurtosis (5.991), respectively. Although the lognormal distribution can reflect skewness and kurtosis in some degree, the skewness and kurtosis of the lognormal distribution are functions of the coefficient of variation (COV). In the present case, the COV of the lognormal distribution is very small (0.0463), thus its skewness and kurtosis are 0.139 and 3.03 respectively, which are too small to match those of the data.

(2) Since the first three moments of the 3P Gamma distribution are equal to those of the data, it fits the histogram much better than the normal and lognormal distributions. However, the kurtosis of this distribution is depending on the skewness. The kurtosis corresponding to the skewness of the data is obtained as 4.17, which is too small to match that of the data.

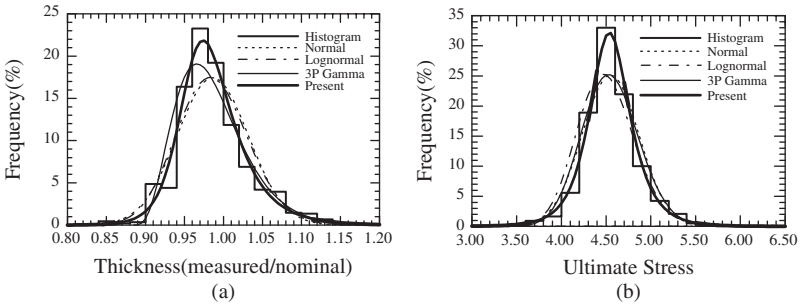

Figure 1. Data fitting for thickness and ultimate stress.

Table 1. Results of test for thickness.

		Predicted frequency				Goodness of fit			
Intervals	Freq.	Nor.	Log.	3P.	Pre.	Nor.	Log.	3P.	Pre.
<0.92	54	65.8	62.3	31.1	39.7	2.12	1.11	16.86	5.15
0.92–0.94	39	73.2	76.3	97.1	66.8	15.98	18.23	34.76	11.57
0.94–0.96	145	113	117.9	153	138.3	9.06	6.23	0.42	0.32
0.96–0.98	206	144.3	147.7	166.4	188.6	26.38	23.01	9.42	1.61
0.98–1.00	170	152.7	151.9	145.3	169.5	1.96	2.16	4.20	0.00
1.00–1.02	105	133.8	129.7	109.6	116.7	6.20	4.70	0.19	1.17
1.02–1.04	61	97.2	92.9	74.5	70.8	13.48	10.95	2.45	1.36
1.04–1.06	37	58.4	56.4	46.9	40.7	7.84	6.67	2.09	0.34
1.06–1.08	35	29	29.3	27.8	23.1	1.24	1.11	1.86	6.13
>1.08	33	17.6	20.6	33.3	30.3	13.48	7.46	0.0	0.23
Sum	885	885	885	885	885	97.74	81.64	72.26	27.81

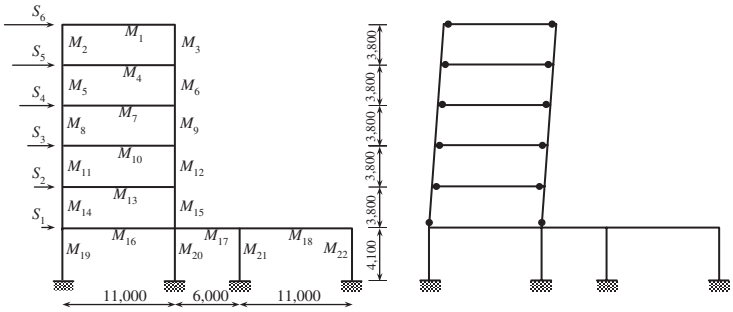

Figure 2. A six-story three bay frame and its most likely failure mode.

(3) The first four moments of the present 4P distribution can be equal to those of the data, and thus it can fit the histogram much better than the normal, lognormal, and 3P-Gamma distributions.

Results of the Chi-square tests of the four distributions are listed in Table 1, in which the goodness-of-fit tests were obtained using the following equation (Ang & Tang, 1975)

$$T = \sum_{i=1}^{k} \frac{(O_i - E_i)^2}{E_i} \tag{5}$$

where O_i and E_i are the observed and theoretical frequencies, respectively, k is the number of intervals used, and T is a measure of the respective goodness-of-fit. From Table 1, one can see that the goodness-of-fit of the introduced distribution is $T = 27.81$ which is much smaller than those of other distributions.

Similarly, the fitting results of the histogram of the ultimate stress are shown in Figure 2b, in which the number of data is 1932 and the first-four moments of the data are obtained as $\mu = 4.549$, $\sigma = 0.317$, $\alpha_3 = 0.153$, and $\alpha_4 = 6.037$. From the figure, one can see that since the skewness of the data is quite small, the 3P Gamma distribution cannot show significant improvement upon the normal and lognormal distributions, whereas the introduced distribution can effectively fit the histograms of the available data. Also, from Table 2, the goodness-of-fit tests verify that the introduced distribution has the best fit with $T = 14.67$ among all the distributions.

Table 2. Results of test for ultimate stress.

		Predicted frequency				Goodness of fit			
Intervals	Freq.	Nor.	Log.	3P.	Pre.	Nor.	Log.	3P.	Pre.
<4.0	64	80.5	67.5	71.1	73.1	3.38	0.18	0.71	1.13
4.0–4.2	108	181.3	189.7	187.7	130.8	29.64	35.19	33.84	3.97
4.2–4.4	365	354.9	377.8	371.6	345.4	0.29	0.43	0.12	1.11
4.4–4.6	638	472.8	480.4	477.9	589.5	57.72	51.70	53.63	3.99
4.6–4.8	424	428.6	410.9	415.3	459.1	0.05	0.42	0.18	2.68
4.8–5.0	193	264.4	247.6	252.2	204.8	19.28	12.04	13.90	0.68
5.0–5.2	82	110.9	109.4	110.1	78.1	7.53	6.86	7.17	0.19
>5.2	58	38.6	48.7	46.1	51.2	9.75	1.78	3.07	0.9
Sum	1932	1932	1932	1932	1932	127.64	108.60	112.62	14.67

Note: Freq. = Frequency, Nor. = Normal, Log. = Lognormal, 3P. = 3P Gamma, Pres. = Present.

From the examples above, one can clearly see that since the first four moments of the present 4P distribution are equal to those of the statistical data, it fits the histogram much better than the normal, the lognormal, and the 3P Gamma distributions.

4 APPLICATIONS IN STRUCTURAL RELIABILITY ASSESSMENT

4.1 *The fourth-moment reliability index*

The third-order polynomial normal transformation was first suggested by Fleishman (1978) to generate random numbers for Monte Carlo Simulation (MCS). Hong & Lind (1998) presented an approximate method to calculate the probability of failure of a structural system with the aid of this polynomial. And it has been used as a third-order polynomial normal transformation technique by Chen & Tung (2003). In this paper, a fourth-moment reliability index based on this distribution is derived and its applications in structural reliability assessment are discussed.

Consider a performance function $z = G(\mathbf{X})$ of a structure or a structural system. If the first four moments of $G(\mathbf{X})$ can be obtained, the probability of failure, $P(G \leq 0)$, can be readily obtained by assuming$G(\mathbf{X})$ obey the introduced distribution.

For the standardized random variable z_u

$$z_u = \frac{z - \mu_G}{\sigma_G} \tag{6}$$

Since

$$P_f = P[z = G(\mathrm{X}) \leq 0] = P\left[z_u \leq -\frac{\mu_G}{\sigma_G}\right] = P[z_u \leq -\beta_{2M}] \tag{7}$$

where μ_G and σ_G are the mean value and standard deviation of $z = G(\mathbf{X})$, respectively; β_{2M} is the second-moment (2M) reliability index; and P_f is the probability of failure.

According to Eq. 1a, the standardized random variable z_u can be expressed as

$$z_u = S_u(u) = a_1 + a_2 u + a_3 u^2 + a_4 u^3 \tag{8}$$

The fourth-moment (4M) reliability index based on the 4P distribution can be given as

$$\beta_{4M} = -S_u^{-1}(-\beta_{2M}) \tag{9a}$$

The probability of failure is expressed as

$$P_f = \Phi(-\beta_{4M}) \tag{9b}$$

4.2 *Moment computation for the performance function*

In order to conduct structural reliability analysis using the 4M reliability index, one should firstly compute the first four moments of the performance function.

A common encountered performance function in structural reliability is a linear sum of independent random variables in the original space:

$$G(\mathrm{X}) = \sum_{i=1}^{n} a_i x_i \tag{10}$$

where $x_i,\ i = 1, \ldots, n$ are mutually independent random variables and $a_i, i = 1, \ldots, n$ are coefficients.

The first four moments of Eq. 10 are obtained as follows

$$\mu_G = \sum_{i=1}^{n} a_i \mu_i \tag{11a}$$

$$\sigma_G^2 = \sum_{i=1}^{n} a_i^2 \sigma_i^2 \tag{11b}$$

$$\alpha_{3G}\sigma_G^3 = \sum_{i=1}^{n} \alpha_{3i} a_i^3 \sigma_i^3 \tag{11c}$$

$$\alpha_{4G}\sigma_G^4 = \sum_{i=1}^{n} \alpha_{4i} a_i^4 \sigma_i^4 + 6\sum_{i=1}^{n-1}\sum_{j>i}^{n} a_i^2 a_j^2 \sigma_i^2 \sigma_j^2 \tag{11d}$$

where $\mu_i(\mu_G), \sigma_i(\sigma_G), \alpha_{3i}(\alpha_{3G})$, and α_{4i} (α_{4G}) are the mean value, standard deviation, skewness, and kurtosis of x_i $(G(\mathbf{X}))$, respectively.

For complicated and implicit performance functions including those corresponding to correlative random variables, point estimates method (Zhao & Ono, 2000) will be used for moment computation.

4.3 *Numerical examples*

Example 1: Reliability analysis involving variables with unknown distribution.

In the first- or second- order reliability method, the probability distributions of the basic random variables are necessary to perform the normal transformations (the $x - u$ transformation and its inverse the $u - x$ transformation). Usually, in practical applications, the probability distributions of some of the basic random variables may be unknown, and the probabilistic information may be defined only in terms of the respective first few statistical moments. With Eq.1a and its inverse transformation, first- or second-order reliability analysis can be conveniently performed using the first four moments μ, σ, α_3, and α_4 in the $x - u$ and $u - x$ transformation.

Furthermore, random samples of the variables can easily generated using Eq. 1a for MCS.

For illustrations, consider an elasto-plastic frame structure with six stories and three bays as shown in Figure 2, the most likely failure model of this structure is also shown in Figure 2. The corresponding performance function may be expressed as

$$G(\mathrm{X}) = 2M_1 + 2M_4 + 2M_7 + 2M_{10} + 2M_{13} + M_{14} + M_{15} - 3.8S_2 - 7.6S_3 - 11.4S_4 - 15.2S_5 - 19S \tag{12}$$

The probabilistic of the member strength and loads are listed in Table 3. The CDFs of S_2 and S_3 are unknown, and the known information is their first four moments. With the aid of Eq. 11,

Table 3. Random variables in example 1.

Variables	PDFs	Mean	V	α_3	α_4
$M_1, M_4, M_7, M_{17}, M_{18}$	Lognormal	90.8 t-m	0.1	0.301	3.162
M_2, M_3, M_5, M_6	Lognormal	145.2 t-m	0.1	0.301	3.162
M_8, M_9, M_{21}, M_{22}	Lognormal	145.2 t-m	0.1	0.301	3.162
M_{10}, M_{13}, M_{16}	Lognormal	103.4 t-m	0.1	0.301	3.162
M_{11}, M_{12}, M_{14}	Lognormal	162.8 t-m	0.1	0.301	3.162
M_{15}, M_{19}, M_{20}	Lognormal	162.8 t-m	0.1	0.301	3.162
S_1	Gumbel	2.5 t	0.4	1.140	5.400
S_2	Unknown	5.0 t	0.4	1.264	5.969
S_3	Unknown	7.5 t	0.4	1.264	5.969
S_4	Lognormal	10.0 t	0.4	1.264	5.969
S_5	Lognormal	12.5 t	0.4	1.264	5.969
S_6	Lognormal	15.0 t	0.4	1.264	5.969

Table 4. Formula insensitivity of the present 4M reliability index.

	$G(\mathrm{X})$	μ_G	σ_G	α_{3G}	α_{4G}	β_{2M}	Present
Case 1	$R-S$	50.000	21.213	-0.0539	3.1323	2.357	2.294
Case 2	$\ln R - \ln S$	0.4116	0.1795	-5.19×10^{-7}	3.0000	2.294	2.294
Case 3	$1-S/R$	0.3267	0.1218	-0.5486	3.5399	2.682	2.293
Case 4	$R/S-1$	0.5338	0.2775	0.5486	3.5399	1.924	2.291
Case 5	$1/S-1/R$	3.492×10^{-3}	1.675×10^{-3}	0.3285	3.2627	2.085	2.294

the mean value, standard deviation, skewness, and kurtosis of $G(\mathbf{X})$ are obtained as $\mu_G = 619$, $\sigma_G = 154.285$, $\alpha_{3G} = -0.694$, and $\alpha_{4G} = 4.084$. The 2M reliability index is readily obtained as $\beta_{2M} = 4.012$. Using the suggested formula in the present paper, the 4M reliability index is readily obtained as $\beta_{4M} = 2.953$. The corresponding probability of failure is equal to 0.001572.

Although the CDFs of S_2 and S_3 are unknown, since the first four moments are known, the $x-u$ and $u-x$ transformations can be easily realized using Eq. 1a and its inverse transformation instead of Rosenblatt transformation and FORM can be readily conducted with results of $\beta_F = 3.100$ and $P_f = 0.000968$. Furthermore, using Eq. 1, the random sampling of S_2 and S_3 can be easily generated without using their CDFs and MCS can be thus easily conducted. The probability of failure of this performance function is obtained as $P_f = 0.001598$ and the corresponding reliability index is equal to 2.948 when the number of samplings is taken to be 500,000. One can see that the results of the present 4M method are in close agreement with the results of MCS and FORM.

Example 2: The formula insensitive of the present fourth-moment reliability index.

Consider a simple reliability problem as shown in Table 4, in which both R and S are lognormal variables with mean value, standard deviation, skewness, and kurtosis of $\mu_R = 150$, $\sigma_R = 15$, $\alpha_{3R} = 0.301$, $\alpha_{4R} = 3.1615$, $\mu_S = 100$, $\sigma_S = 15$, $\alpha_{3S} = 0.453$, and $\alpha_{4S} = 3.3677$. Because both R and S are positive, the five performance functions listed in Table 4 are equivalent. The first four moments of the performance functions obtained using the point estimates method (Zhao & Ono, 2000) are also listed in Table 4, together with the results of the 2M reliability index, and the present 4M reliability index.

From Table 4, one can see that although the 2M reliability index is much different for the different formulations, the present 4M reliability index gives almost the same results. The example is shown that the present 4M reliability index is insensitive to the formulations of the performance function.

Example 3: Parabolic limit surface with two design point.

Consider the following performance function:

$$G(\mathbf{X}) = b - x_2 - k(x_1 - e)^2 \tag{13}$$

where $b = 5$, $k = 0.5$ and $e = 0.1$.

If FORM is used to solve this problem, there are two design points which are successfully obtained by Der Kiuregian & Dakessian (1998) as: $X_1^* = [-2.741, 0.965]^T$ with $\beta_1 = 2.906$, and $X_2^* = [2.916, 1.036]^T$ with $\beta_2 = 3.094$.

If the proposed method is used, using the point estimates method (Zhao & Ono 2000), the first four moments of $G(\mathbf{X})$ can be easily obtained as $\mu_G = 4.495$, $\sigma_G = 1.229$, $\alpha_{3G} = -0.555$, and $\alpha_{4G} = 4.3684$. The 2M reliability index and its corresponding probability of failure are readily obtained as $\beta_{2M} = 3.657$ and $P_f = 0.000128$. The suggested 4M reliability index is readily obtained as $\beta_{4M} = 2.767$ with the aid of Eq. 9 and the corresponding probability of failure is equal to 0.00283. Apparently, for the proposed method there is no worry about the problem of multi-design points.

The reliability index using MCS obtained by Der Kiuregian and Dakessian (1998) is $\beta = 2.751$ and the corresponding failure probability is 0.00297. One can see that the results of the present method are in close agreement with the MCS results, whereas the 2M method provides significantly wrong results.

5 CONCLUSIONS

(1) The distribution has more flexibility for fitting statistical data of the basic random variables and can more effectively fit the histograms of available data than 2P or 3P distributions.
(2) The structural reliability evaluation can be conducted with the aid of the suggested 4M reliability index even when the CDFs or PDFs of random variables are unknown.
(3) The present 4M reliability index is insensitive to the formulations of the performance function.
(4) The present method has no shortcoming with the design points, and thus it is convenient to conduct structural reliability analysis in engineering.

ACKNOWLEDGEMENT

This study is partially supported by Grant-in-Aid from Ministry of ESCST. Japan (No. 17560501). The supports are gratefully acknowledged.

REFERENCES

Ang, AH-S. and Tang, W.H. 1975. *Probability concepts in engineering planning and design. Vol I: Basic Principles*. New York: J. Wiley & Sons.

Ang, AH-S. and Tang, W.H. 1984. *Probability concepts in engineering planning and design. Vol II: Decision, Risk, and Reliability*. New York : J. Wiley & Sons.

Chen, X. and Tung, Y.K. 2003. Investigation of Polynomial normal transformation. *Structural Safety* 25(4): 423–445.

Der Kiureghian, A. and Liu, P.L. 1986. Structural Reliability under incomplete probability information. *ASCE,J. Engrg. Mech.* 112(1): 85–104.

Der Kiureghian, A. 2001. Analysis of structural reliability under model and statistical uncertainties: a Bayesian approach. *Computational structural engineering* 1(2): 81–87.

Fleishman, A.L. 1978. A method for simulating non-normal distributions. *Psychometrika* 43(4): 521–532.

Hong, H.P. and Lind, N.C. 1996. Approximation reliability analysis using normal polynomial and simulation results. *Structural Safety* 18(4): 329–339.

Ono, T., Idota, H. and Kawahara, H. 1986. A statistical study on resistances of steel columns and beams using higher order moments. *AIJ, J. Structural and construction engineering*, 370: 19–37. (in Japanese)

Wolfram, S. 1999. *The Mathematica book. 4th edition*. Wolfram Media / Cambridge University Press.

Zhao, Y.G. and Ang, AH-S. 2002. Three-Parameter Gamma Distribution and its significance in structure. *International Journal of Computational Structural Engineering* 2(1): 1–10.
Zhao, Y.G. and Ono, T. 2000. New point estimates for probability moments. *ASCE, J. Engrg. Mech.* 126(4): 4–732.
Zhao, Y.G., Ono, T. and Kiyoshi, I. 2002. Monte Carlo simulation using moments of random variables. *Journal of Asian Architecture and Building Engineering* 1(1): 13–20.
Zong, Z. and Lam, K.Y. 1998. Estimation of complicated distributions using B-spline functions. *Structural Safety* 20(4): 341–355.
Zong, Z. and Lam, K.Y. (2000). Bayesian estimation of complicated distributions. *Structural Safety* 22(1): 81–95.
Zong, Z. and Lam, K.Y. (2001). Bayesian estimation of 2-dimensional complicated distributions. *Structural Safety* 23(2): 105–121.

Reliability and Optimization of Structural Systems: Assessment, Design and Life-Cycle Performance – Frangopol, Kawatani & Kim (eds)
© 2007 Taylor & Francis Group, London, ISBN 978-0-415-40655-0

Bridge live load effects based on statistics of extremes using on-site load monitoring

Thomas B. Messervey
Department of Mathematical Sciences, United States Military Academy, West Point, NY, USA

Dan M. Frangopol
Fazlur R. Khan Endowed Chair of Structural Engineering and Architecture, Department of Civil and Environmental Engineering, ATLSS Center, Lehigh University, Bethlehem, PA, USA

ABSTRACT: The initial (i.e., at time $t = 0$) reliability index, the time-variant live load, and the resistance deterioration processes are some of the most important factors in conducting a reliability-based life-cycle analysis of a highway bridge structure. In such an analysis, at least for a newer structure, there is likely more confidence in the geometry and material properties of the structure that determine its capacity than there is in the various loading conditions and scenarios that will place demand upon the structure. Structural health monitoring (SHM) offers a potentially powerful means to obtain site-specific data. However, questions that must be addressed are: what information to collect? how often? and how it should be processed? This paper examines the potential of utilizing the statistics of extremes to answer these questions. By using on-site SHM and observing only the maximum daily peak strain values over time, it is determined that one can successfully modify an initial estimate of truck weight and volume to determine the actual distribution and volume observed at the site. Although a newly developed idea in this work and specific to an initial assumed Gumbel distribution, the method shows interesting potential in the monitoring and assessment of structural systems.

1 INTRODUCTION

1.1 *Background*

In its most basic sense, the reliability of a structure is determined by its safety margin (i.e. performance function):

$$Safety\ Margin = Resistance - Demand \tag{1}$$

Typically, performance functions describe this relationship with respect to different failure modes for individual components or systems. A calculation of the initial reliability of a structure is obtained, and then the performance functions are predicted 75 years into the future in a probabilistic manner. Corrosion effects and deterioration decrease the resistance, while increased uncertainty about the loads increases the uncertainty in the demand. The goal of such an analysis is a holistic, life-cycle treatment of cost, performance, and safety from which to make the best possible decisions for maintenance and resource allocation.

This work will focus entirely upon *Demand* (see (1)), and is part of a framework to introduce structural health monitoring into the reliability-based life-cycle bridge management models as presented in (Messervey & Frangopol, 2006). In this study, the objective is to obtain the best possible estimate of the live load demand after a reasonable amount of time using structure specific on-site load monitoring via strain recordings. The *Resistance* (see (1)) is not treated in this analysis

to allow focus upon a method which investigates live-load effects. In a practical sense, this would be applicable to a newer structure where deterioration has not yet begun, or to a structure where a known load could be placed on it periodically to calibrate the resistance. In itself, demand is an intricate topic. Design codes such as the AASHTO LRFD Bridge Design Code (1994) certainly specify design parameters, but it must be considered that the calibration of the design HS-20 truck was based on a two week study of 9,250 trucks (Nowak, 1993). The trucks were weighed in Ontario, Canada, heavier trucks may have avoided the survey station, and the data is now over 30 years old. Additionally, it has been shown that traffic live-load effects vary from site to site and also are sensitive to the length of the time window utilized to capture the data (Gindy & Nassif, 2006). The initial distribution and volume of traffic is especially important in a bridge reliability analysis. The further the analysis projects in time, the greater the load that must be considered as the probability of encountering a truck on the extreme upper tail of the distribution increases with each truck crossing (Nowak, 1993).

1.2 *Scenario of interest*

This study is motivated by any typical short to medium-span, simply supported, steel beam/girder highway bridge. The bridge would likely not be state of the art, would be part of a larger network, and the bridge manager might be adverse to a monitoring/management solution that was expensive or required much oversight. Perhaps the HS-20 design load for this bridge and the initial traffic volume estimate was overly conservative and if this conservativeness can be identified, the information could be used to make the best possible resource allocations amongst the bridge network and for maintenance and inspection scheduling of the bridge of interest. Within this scenario, the idea is what could be done with the least amount of information and with an appropriate level of confidence?

1.3 *Proposed model and configuration*

Several strain gauges located at or near midspan of a simply supported beam capture maximum daily strain demands via a simple, but continuous on-board monitoring system employing peak picking at a specified time interval. Assuming elastic linear operational behavior, Hooke's law is utilized to transform strain to moment. With maximum values recorded, the statistics of extremes is utilized to characterize the underlying moment demand distribution in the transformed (extreme) space. This information can then be mapped back to the original space for inclusion in the 75-year reliability analysis. The calculation of the initial reliability index β_0 is of specific consequence as it has been shown as the most important parameter when using the eight random variable Frangopol model for predicting the reliability index over time (Frangopol 1998, Frangopol et al. 2001, van Noortwijk & Frangopol 2004, Kong & Frangopol, 2005). The mean value of the traffic distribution (average truck) or mean moment demand is also of significance as this value is utilized to calculate live load effects along with the initial volume of traffic. The result of this study will be utilized to build upon an ongoing analysis of a simply supported highway bridge (Messervey & Frangopol, 2006).

2 STATISTICS OF EXTREMES: THEORETICAL BACKGROUND

Although the total distribution of cars, trucks, and motorcycles crossing a bridge may take any form, close attention is given specifically to the characterization of the truck traffic which populates the upper tail, or the extreme values of the distribution. Since traffic is an ongoing, perpetual process, the behavior of the upper tail can be modeled as a random variable itself and its characteristics can be determined over time as the process repeats itself. Weigh-in-motion (WIM) studies have shown that Gamma or truncated normal distribution often provide a reasonable fit to model gross vehicle truck weights (Cohen, et al. 2003). Extreme statistics deal with what happens to the extremes

Table 1. 10 simulations of differing sample sizes, maximums, averages, and standard deviations.

Sample size n	10th random realization (kN)	Sample maximum, Yn (kN)	Avg of sample maximum values, μ_{Yn} (kN)	Std dev of sample maximum values, σ_{Yn} (kN)
1	147.5	147.5	169.5	64.3
2	300.7 167.7	300.7	198.5	59.2
3	121.1 154.9 161.7	161.7	195.1	17.0
4	101.1 161.3 242.9 99.6	242.9	207.2	51.0

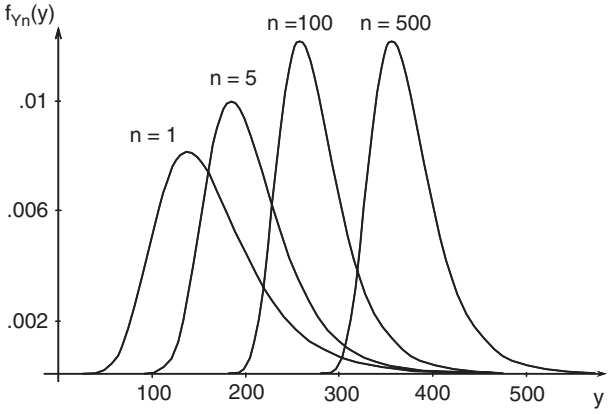

Figure 1. Effect of sample size n on the probability density function of the extreme value Y_n.

(i.e., the largest or smallest) values of random variables. As indicated in Ang & Tang (1984), "statistically, these pertain to the maximum and minimum values from a set of observations . . . (samples of size n)." For distributions with an exponentially decreasing upper tail, such as traffic, the behavior of the extremes will always converge to a Type I asymptotic (Gumbel) distribution as the size of the sample space surpasses 25 (Ang & Tang, 1984). A simple example illustrates this concept and highlights the difference between the sample of size n, and the number of observations or realizations required to characterize what is happening in that sample space.

Let

$$Y_n = \max (X_1, X_2, X_3, \ldots, X_n) \tag{2}$$

where X is the initial random variable with known initial distribution function, and X_i is the realization of the moment demand created by a truck on a simply supported beam or girder at the point of maximum moment. Let X have an initial Gamma distribution $\sim$ Gamma(160.6, 8.8, 18.25) where 160.6 is the mean value and 8.8 and 18.25 are the alpha and beta parameters respectively. Microsoft Excel is utilized to simulate this distribution 10 times to observe what happens to the average expected maximum value, μ_{Yn}, within each sample of size n. Table 1 shows the result of the 10th simulation for each sample of size $n = 1$ to 4, and the behavior of Y_n treated as a random variable across the 10 simulations.

Figure 1 extends the example and plots the distribution of Y_n for samples of size $n = 1$, 5, 100, and 500 successively.

Although simple, the above example illustrates some points that will be very important in its application to bridge monitoring. First, the process can be simulated and can be observed though signal peak picking with minimal computational effort. Second, each sample of size n occupies a district location for μ_{Yn} as shown in Figure 1. Third, μ_{Y2} being larger than μ_{Y3} in Table 1

conflicts with the increasing trend of μ_{Yn} as the sample size n is increased. This suggests that the process must be observed enough times to accurately capture the behavior of Y_n. In this case, 10 realizations of the random variable X were not adequate. Lastly, the underlying process rapidly approaches an invariant form after which only the mean value shifts. Although this example shows the transformation of a Gamma distribution, the same holds true for all distributions and can be generalized as (Ang & Tang, 1984)

$$F_{Y_n}(y) = [F_X(x)]^n \tag{3}$$

$$f_{Y_n}(y) = n[F_X(x)]^{n-1} f_X(x) \tag{4}$$

which is to say that the final distribution is a function only of the initial distribution and the sample of size n. Equations (3) and (4) refer to the probability distribution function (CDF) and probability density function (PDF) of Y_n, respectively.

3 INITIAL TRUCK DISTRIBUTION

A recent published study analyzed 10 years of Weigh in Motion (WIM) data in the state of New Jersey across 33 site locations forming an extensive database of truck traffic (Gindy & Nassif, 2006). Although the statistical descriptors vary somewhat from site to site and over time, the population averages provide a reasonable representation of a current day truck distribution. In this study, the population mean truck weight is 204 kN with a 95th percentile truck weight of 360 kN. A large and increasing number of extremely heavy trucks are cited as a concern. For this reason, both a Gumbel and a Gamma distribution are considered because of their negative skew and characteristic large upper tail. Both distributions are similar in shape, as shown in Figure 2a, and both result in a coefficient of variation of .44 (standard deviation = 85.5 kN) when fit to the Gindy and Nassif study.

In this paper, the Gumbel distribution is selected with the final parameters of $\alpha = .015$, $\mu_n = 156$ kN and a resulting expected value of $\mu_X = 194.4$ kN. The Gumbel distribution is selected to take advantage of the fact that the transformation shown in (4) for a Gumbel distribution results in another Gumbel distribution with an increased mean but of the same shape. Hence the transformed distribution is completely specified by (Ang & Tang, 1984)

$$\mu_{Yn} = \mu_X + \frac{\ln(n)}{\alpha} \tag{5}$$

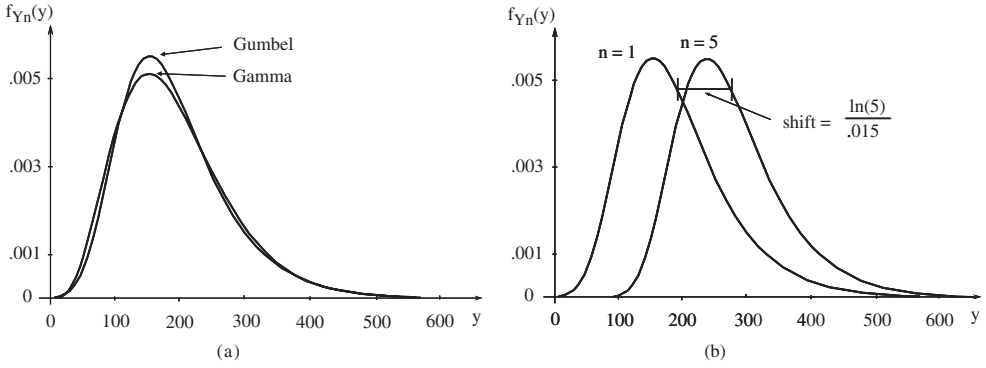

Figure 2. Modeling of the initial truck distribution based off New Jersey Department of Transportation WIM Data and qualitative shift of a Gumbel PDF for a given number of observations n.

where μ_{Yn} is the mean of the largest value, μ_X is the mean of the original distribution, n is the number of trucks observed in a specified time interval, and α is an inverse measure of dispersion. Since α is invariant when mapping or transforming the Gumbel distribution, the above equation simply results in the shift depicted in Figure 2b.

4 NUMERICAL EXAMPLES

4.1 *Concept validation and determination of required observation time*

It is first desired to confirm that a distribution can be "seen" or determined only by "peak picking" and to identify how many observations are required to reasonably characterize its parameters. To do this, the above Gumbel distribution is simulated in Excel for samples of size $n = 300$ which is intended to represent a daily truck volume of 300 trucks. Using (5), the exact solution for the average maximum expected truck live load is

$$\mu_{Yn} = 194.4\ kN + \frac{\ln(300)}{.015} = 574.7\ kN \tag{6}$$

where α is determined from fitting the Gumbel distribution as previously described. It is important to emphasize that the "peak picking" process only records maximum values of the observed event and has no visibility on the prior distribution or the number of trucks being observed. Each "day" in the simulation, 300 trucks are randomly generated from the above distribution and the maximum truck is recorded. After successive intervals ranging from 30 days to 5 years, the maximum values are averaged and their standard deviations are calculated. Hence, a "shifted" distribution is observed such as shown in Figure 2b. Within this space, the dispersion α_n can be calculated as (Menun, 2003)

$$\alpha_n = \frac{\pi}{\sqrt{6}\sigma_{Yn}} \tag{7}$$

In this simulation it is decided not to take advantage of the fact that $\alpha_n = \alpha$ for a Gumbel distribution but rather to observe it. The simulation is repeated 60 times so that each parameter can be treated as a random variable to investigate its dispersion with respect to the varying timeframes. Table 2 shows the results of the simulation. Once again, theoretical values are 574.7 kN, 85.5 kN, and .015 for μ_{Yn}, σ_{Yn}, and α_n respectively. The standard deviation and coefficient of variation are not reported for α_n as they are identical to those of σ_{Yn}.

It is shown that the mean value can be observed with confidence rather quickly whereas the characteristics of variability take longer. It should also be noted that a longer time interval may not always provide better results. For example, in a case where the live load changes over time, one may desire a model that is responsive to this change, instead of a model where incoming information is averaged with all prior data. This is a topic left for future discussion. However, it is concluded here

Table 2. Simulation results.

Time	μ_{Yn} (kN)	Std Dev of μ_{Yn} (kN)	Coef of Var of μ_{Yn} (kN)	σ_{Yn} (kN)	Std Dev of of σ_{Yn} (kN)	Coef of Var of σ_{Yn} (kN)	α_n
30 days	575.36	15.54	0.027	84.23	15.41	0.185	0.0157
90 days	573.72	9.06	0.016	84.72	8.98	0.111	0.0153
180 days	574.69	7.04	0.012	85.55	7.19	0.084	0.0151
1 yr	575.21	4.55	0.008	86.66	4.68	0.054	0.0148
2 yrs	574.77	2.81	0.005	85.21	3.47	0.041	0.0151
5 yrs	574.93	1.82	0.003	85.96	2.33	0.027	0.0149

that peak picking can observe a distribution's underlying characteristics in a fairly short time period with an acceptable level of confidence. Additionally, if the volume of daily traffic *n* is known, then the initial mean value truck μ_X can be determined, and vice versa, using (5).

4.2 *Updating a distribution through observed information*

This simulation addresses the scenario described in Section 1.2 where it is desired to update an initial conservative estimate of the average truck weight and volume of traffic using data obtained via SHM. To create the experiment, the design parameters are assumed to be 500 trucks per day with a mean value $\mu_X = 225$ kN and standard deviation $\sigma_x = 100$ kN. The simulated distribution remains as indicated previously with a PDF $f(x, \mu_n, \alpha) =$ Gumbel(156, .015) having an expected value of 194.4 kN. Simulated truck volume is 300 trucks per day. As such, there is a disparity in both the weight of the average truck and volume of traffic between the assumed and observed data.

Updating occurs every 30 days for a period of two years. Microsoft Excel is again utilized to randomly select 300 trucks per day from the Gumbel distribution. The simulation is run one time for two years producing a record of *300 trucks/day for 730 days = 266,450 trucks*. The maximum daily truck weight is selected each day from the 300 recorded and then the average and standard deviation of the maximum daily weights are computed for increasing time intervals.

After 30 days, $\mu_{Yn} = 576$ kN and, $\sigma_{Yn} = 86.5$kN. α_n is calculated using (6) as $\alpha_n = .0148$. To compute the estimated number of trucks in the observed monitoring space, one must assume that the initial mean μ_X is correct. Rearranging (5) and solving for *n* results in

$$n = \exp[(u_{Y_n} - u_X) \times \alpha] = \exp[(576 - 225) \times .0148] = 182 \; trucks \tag{8}$$

The fact that *n* is not 300 indicates disparity between the observed and assumed distributions and that updating is required. Combining data must occur in the same observation space. As such, the observed data can be mapped back to an initial distribution or the original distribution can be mapped to the assumed observed space. Here the latter is chosen. Hence, the theoretical μ_{Yn} for 300 trucks again using (5) is

$$\mu_{Y_n} = 225 + \frac{\ln(300)}{.015} = 639.3 \; kN \tag{9}$$

Because both the theoretical and observed values of μ_{Yn} are probabilistic, Bayesian updating is an appropriate method to combine the distributions. The Bayesian approach provides a weighted average of two values based upon their respective variances (Casella & Berger, 2002)

$$E(\theta \mid x) = \frac{\lambda^2}{\lambda^2 + \sigma^2} x + \frac{\sigma^2}{\sigma^2 + \lambda^2} \mu \tag{10}$$

where θ represents the random variable of interest, μ its theoretical mean, λ^2 the theoretical variance, *x* the monitoring-based mean and σ^2 the monitoring-based variance. As such, updating μ_{Yn} yields

$$\mu_{Y_n} = \frac{(100)^2}{(100)^2 + (86.5)^2}(576) + \frac{(86.5)^2}{(86.5)^2 + (100)^2}(639.3) = 649.9 \; kN \tag{11}$$

The same updating process is applied to the theoretical number of trucks *n*, the standard deviation σ_X and the shape parameter α. With these parameters, the distribution can be mapped back to the original space at $n = 0$ using the updated number of trucks as

$$\mu_X = \mu_{Y_n} - \frac{\ln(n)}{\alpha} = 649.9 - \frac{\ln(363.7)}{.0149} = 207.4 \; kN \tag{12}$$

Table 3. Updating an initial (incorrect) distribution using monitoring data.

Parameters	Avg expected truck load demand (kN) μ_x	Number of trucks	Std dev of avg expected truck (kN) σ_x
Design parameters	225	500	100
Simulated parameters	194.4	300	85.5
Updated parameters			
6 mo.	205.2	267.0	83.9
12 mo.	203.7	307.0	83.3
18 mo.	198.2	305.7	84.9
24 mo.	196.4	299.2	85.9

to determine the updated mean value of the original distribution.

This process is repeated every 30 days for 12 months resulting in $\mu_X = 203.67$ kN and $n = 307$ trucks. After some number of updates, the observed space will converge to a solution where the theoretical and observed values of μ_{Yn} and n will be equal in the observed (mapped) space. However, this will not lead to the solution of the correct initial distribution as different combinations of μ_X and n can produce the same value for μ_{Yn} in the transformed space. To address this, the data and system of equations must be observed in a different space (number of trucks). By selecting the maximum value Y_n from the observed data every two days (600 trucks in this case), μ_{Yn} maps to a separate and distinct shift of the original distribution. In this simulation, observing the maximum two-day value for 12 months results in $\mu_{Yn} = 617.7$ kN and $n = 642.3$ trucks. This information is utilized to perturb μ_X as follows

$$\mu_X = 617.7kN - \frac{\ln(642.3)}{.015405} = 198.1\,kN \tag{13}$$

and the Bayesian updating loop is again repeated using daily information for an additional 6 months. During this time, the shape parameter, standard deviation, and number of trucks become well defined in the space of 600 trucks, and then the system is perturbed again as in (13) using either $n = 300$ trucks or $n = 900$ trucks. Although more research is required to determine optimal perturbation times and the benefit of using larger and larger timeframes of data, in this scenario 6 months perturbations worked well. Perturbations were conducted within either two day or three day observation windows. Table 3 shows the result of this process over a two year period.

At the end of the two year period the results converge to within 1% of the simulated distribution. If this was the case on an actual bridge of interest, this updated distribution would represent actual on-site conditions. This information could then be considered in the calculation of the initial reliability index β_o and ensuing live load effects utilized to create the profile of the reliability index over a 75 year time horizon.

5 SUMMARY AND CONCLUSIONS

In this paper, the idea of utilizing the statistics of extremes to analyze SHM data is explored with the intent of efficiently obtaining site-specific load distribution data for incorporation into a life-cycle reliability analysis. From simulating and observing a known distribution, it is determined that a reasonable estimate of an underlying distribution can be obtained rather quickly (3–6 months) with additional improvement obtained through longer observation periods. It is then shown that it is possible to modify an initial (incorrect) assumption for the maximum expected truck weight and volume of traffic by utilizing Bayesian updating to combine assumed and observed information over time.

Although specific to an initial Gumbel distribution, the idea is transferable to other distributions and will be the subject of future study. Additional research is still needed to investigate how to best combine assumed and observed information and the sensitivity of the transformations from the original to the extreme space. However, the method shows an almost surprising potential to obtain good results using little information, low computational cost, and moderate monitoring effort.

ACKNOWLEDGMENTS

The support of the National Science Foundation through grants CMS-0217290 and CMS-0509772 to the University of Colorado, Boulder, and grants CMS-0638728 and CMS-0639428 to Lehigh University are gratefully acknowledged. Also, the support provided by the Collaborative Research Center SFB 477 "Monitoring of Structures" funded at the Technical University of Braunschweig by the German Research Foundation (DFG) is appreciated. The opinions and conclusions presented in this paper are those of the authors and do not necessarily reflect the views of the sponsoring organizations.

REFERENCES

AASHTO 1994. *AASHTO LRFD Bridge Design Specifications*, American Association of State Highway and Transportation Officials, First Edition, Washington DC.

Ang, A.H. and Tang, W.H. 1984. Probability Concepts in Engineering Planning and Design Volume II, Wiley, New York.

Casella, G. and Berger, R. L. 2002. Statistical inference. Duxbury, Thompson Learning, Pacific Grove USA.

Cohen, H., Fu, G., Dekelbab, W., and Moses, F., 2003. Predicting truck load spectra under weight limit changes and its application to steel bridge fatigue assessment. *Journal of Bridge Engineering*, 8(5), 312–322.

Frangopol, D.M. 1998. A Probabilistic Model Based on Eight Random Variables for Preventive Maintenance of Bridges, Presented at the Progress Meeting "Optimum Maintenance strategies for Different Bridge Types," London, Highways Agency, UK.

Frangopol, D.M., Kong, J.S. and Gharaibeh, E.S. 2001. Reliability-based life-cycle management of highway bridges, *Journal of Computing in Civil Engineering*, ASCE, **15**(1), 27–34.

Gindy, M. and Nassif, H. 2006. Effect of bridge live load based on 10 years of WIM data, Proceedings of the Third International Conference on Bridge Maintenance and Safety, Porto, Potugal, July 16–19, 2006, IABMAS'06, Taylor & Francis, 9 pages on CD-ROM.

Kong, J.S. and Frangopol, D.M. 2005. Sensitivity Analysis in Reliability-Based Lifetime Performance Prediction Using Simulation, *Journal of Materials in Civil Engineering*, ASCE **17**(3), 296–306.

Menun, C. 2003. CEE203 Probability Models in Civil Engineering, Course Notes, Stanford University, CA, pp.102–119.

Messervey, T. B. and Frangopol, D.M. 2006. A Framework to Incorporate Structural Health Monitoring into Reliablity-Based Life-Cycle Bridge Management Models, Proceedings of the Fifth International Conference on Computational Stochastic Mechanics, Rhodes, Greece, June 21–23, 2006.

Nowak, A.S. 1993. Live load model for highway bridges. *Structural Safety*, Elsevier, 13, 53–66.

van Noortwijk, J.M. and Frangopol, D.M. (2004). "Two probabilistic life-cycle maintenance models for deteriorating civil infrastructures," *Probabilistic Engineering Mechanics*, Elsevier, **19**(4), 345–359.

Reliability and Optimization of Structural Systems: Assessment, Design and Life-Cycle Performance – Frangopol, Kawatani & Kim (eds)

Non-Gaussianity of structural resistance in the directional simulation in load space

M.R. Moarefzadeh
Department of Civil Engineering, The University of Imam Hussein, Tehran, Iran

ABSTRACT: Directional simulation in the load space, due to considerable advantage of working in the space of lower dimension, is of remarkable importance. In this space, however, the variability of structural resistance parameters (which are normally taken to be time-independent random variables) leads the location of the involving limit states to be not constant. These locations therefore have to be assumed to be random variables. In the earlier works (e.g. Melchers 1992, Moarefzadeh, 1996), Gaussian distribution was proposed for this variability and then only two first moments were employed to describe the variability. In the paper presented by the writer earlier (i.e. Moarefzadeh, 2005), by assuming the structural resistance parameters to be independent, and by taking the other two moments(i.e. third and fourth moments) in addition to two first moments and employing "Hermite Moment Model" , it was shown that the assumption of Gaussianity may not be led to accurate results. In this paper, this investigation is extended for the cases in which the structural resistance parameters are not assumed independent any longer. In these cases, it is also shown that departure from Gaussian assumption may result in the considerable different outcomes.

Keywords: Non-Gassianity, Directional simulation, Structural resistance, Hermite Model

1 INTRODUCTION

Among varieties of techniques to estimate structural reliability, directional simulation is well developed. This technique was first proposed to be utilized in the standard Gaussian space (Ditlevsen et al. 1988). Then the technique was extended using a space in which all variables/processes are involved but in their original forms which are not necessarily Gaussian (Ditlevsen et al. 1990 and Melchers 1990). Furthermore, Melchers (1992) proposed this technique to be utilized in the load space rather than the space of all loads and structural resistances. This idea made it possible to work in a considerably lower dimensional space which in turn made the calculations more efficient. As expected, however, in this space the location of the relevant limit states, due to structural resistance variability, is not constant. In order to take this variability into account different approaches were discussed (see Melchers 1992). One approach was that for differentiable limit states, invoking the central limit theorem, a simple normal distribution is assumed to model the limit states location variability along each direction simulated. This requires only two first moments of the relevant direction variable to be found. It is, however, of interest to examine the accuracy of the results obtained by making the foregoing assumption relaxed. To achieve this objective, Moarefzadeh (2005) attempted to carry out the above examination in which the involving random variables (which in particular, contribute to set up the distribution of radial random variable along any simulated direction) were assumed to be independent. This significantly simplified the required expressions used to estimate the third and fourth required moments. This examination concluded a set of results which showed non-Gaussianity assumption could considerably affect the outcomes of the structural reliability analysis. In this paper, the same procedure proposed already

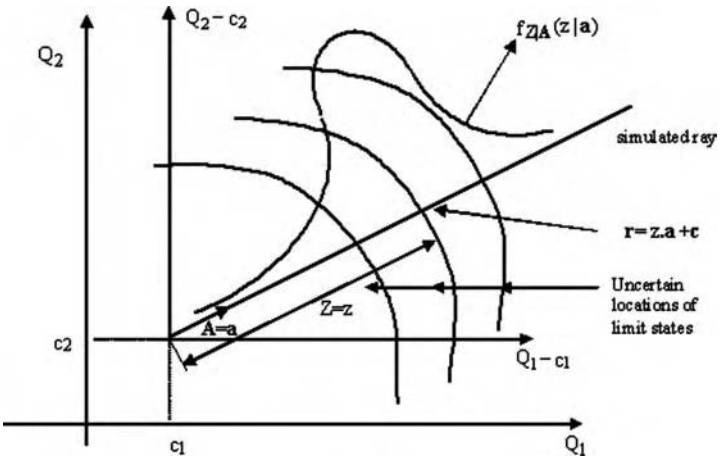

Figure 1. Directional sampling in load space.

(Moarefzadeh, 2005) is followd, however, this time independency assumption between the said variables is not made any longer. Again, in order to probabilistically describe the radial random variable, the Hermite Moment Model (Winterstein, 1988) using the first four moments is used.

In what follows, a brief description of the directional sampling technique in load space will be presented first. Then, a probabilistic description of a non-Gaussian space by the use of Hermite Moment Model is illustrated. This will be followed by a proposal for the non-Gaussian description of a directional variable in load space. Finally an example is presented to indicate typical results achieved.

2 DIRECTIONAL SAMPLING IN LOAD SPACE

Directional Simulation in load space used in this paper is basically adopted from Melchers (1992) and some elaborations made by Moarefzadeh (1995). Let the system be described by m time-independent random variables (commonly the structural characteristics) and n time-dependent continues stationary load processes which are components of two vectors **Y** and **Q** respectively. Also let system failure be considered to occur when one or more limit state(s) $G_i[\mathbf{Y},\mathbf{Q}] = 0$ ($i = 1,2,\ldots,k$) $i = 1,2,\ldots,k$ with k being the number of limit states) is violated within the period under consideration.

The directional simulation method requires formulation in the (hyper-) polar system, so that it is convenient to let:

$$\mathbf{Q} = E\mathbf{A} + \mathbf{C} \tag{1}$$

in which E is the radius variable describing the distance from the origin **C** (which may be selected as any arbitrary point) to any point in (E, **A**) space and **A** is a random directional unit vector having the probability density function (pdf) $f_{\mathbf{A}}(\mathbf{a})$.

To take the uncertainty of the relevant limit state(s) in load space into account, let a probability density function $f_{Z|\mathbf{A}}()$ be considered in which Z is the distance between origin and the limit state surface. Z is generally dependent on the direction $\mathbf{A} = \mathbf{a}$ (see Fig. 1). Since points on the limit state surface represent structural resistance R, expression (1) can be reduced to:

$$\mathbf{R} = Z\mathbf{A} + \mathbf{C} \tag{2}$$

for these points.

To estimate the probability of failure (i.e. violence of one or more limit state functions) during an assumed time duration T, the following well-known approximation may be used (e.g. Melchers 1992, Moarefzadeh and Melchers 1996):

$$p_f \leq p_{f_0} + (1 - p_{f_0})[1 - \exp(-\upsilon_D^+ . T)] \tag{3}$$

in which p_{f_0} and υ_D^+ are the initial probability of failure and the mean outcrossing rate during the time interval T and may be estimated as follows utilizing directional simulation in load space (Moarefzadeh 1995):

$$p_{f_0} = E_A\left[\int_{e=0}^{\infty} F_{Z|A}(e\,|\,\mathbf{a})\, f_Q(e\mathbf{a} + \mathbf{c}) \frac{|J_Q|}{f_A(\mathbf{a})} de\right] \tag{4}$$

$$\upsilon_D^+ = E_A\left[\int_{e=0}^{\infty} f_{Z|A}(e\,|\,\mathbf{a}) E[\mathbf{n}(\mathbf{a}).\dot{\mathbf{Q}}(t)]^+ f_Q(e\mathbf{a} + \mathbf{c}) \frac{|J_Q|}{f_A(\mathbf{a})} \frac{1}{\mathbf{a}^T.\mathbf{n}(\mathbf{a})} de\right] \tag{5}$$

in which $E_A[\ ]$ is the expectation operator in respect of the vector $\mathbf{A}$, $F_{Z|A}(\ )$ is the cumulative distribution function (cdf) of Z given $A = a$, $f_Q(\ )$ is the joint probability density function of the components of $\mathbf{Q}$, $E[\ ]+$ is the expectation operator with $E[\ ]+ = 0$ if $E[\ ]$ is negative, $\mathbf{n}(\mathbf{a})$ is the unit outward vector normal to the limit state at the interception point defined by the ray $\mathbf{A} = \mathbf{a}$ and the limit state surface, $\dot{\mathbf{Q}}(t)$ is the time derivative of $\mathbf{Q}(t)$ and $|\mathbf{J_Q}|$ is the determinant of the Jacobian matrix which establishes the relationship between elemental surface areas (or elemental volume) in spaces $\mathbf{Q}$ and (E, $\mathbf{A}$). Procedures to evaluate the terms $E[\ ]+$ and $\frac{|\mathbf{J_Q}|}{f_A(\mathbf{a})}$ may be found elsewhere (Ditlevsen et al. 1990; Moarefzadeh 1995) and are beyond of the scope of this paper.

In Equations (4) and (5) the functions $f_{Z|A}(\ )$ and $f_{Z|A}(\ )$ are required to be known. Some different approaches have been suggested in Melchers (1992) for derivation of these functions. In one of these approaches, it is assumed that the dimension of vector $\mathbf{Y}$ (i.e. which defines the structural characteristics) is a high value, so that, reasonably, the central limit theorem may be applied. Thus the Gaussian distribution has been suggested for the density function $f_{Z|A}(\ )$. It is noted that all of this is feasible provided the limit state functions are differentiable. For non-differentiable limit state functions suggestions have also been made. Assuming $f_{Z|A}(\ )$ to be Gaussian, its mean and standard deviation are required. Derivation of these values which are functions of the structural resistance variables Y_i is described in Melchers, 1992. The same reference could also be consulted where in general the problem involves more than one limit state and therefore a set of functions $f_{Z|A}()$ and $f_{Z|A}()$ should be taken into account.

3 REPRESENTATION OF NON-GAUSSIAN RANDOM VARIABLES

Let $\mathbf{X}$ be a vector whose components are a number of non-Gaussian random variables. In order to describe probabilistic properties of these variables, it is the usual practice to use their auto/joint moments. Regarding this, different methods are available in the literature (for details, see Grigoriu 1995). One approximation method is to use the so-called Hermite moment models (Winterstein 1988). Because of some advantages to be useful here (see below), this method is employed in the present work. In this method a non-Gaussian variable X_i can be related to a standard Gaussian variable U_i through the function $X_i = \sum_{n=0}^{N} \zeta_n H_{e_n}(U_i)$ where the ζ_n are constants obtained using moments of X_i. Also, $H_{e_n}(\ )$ is the Hermite function of order n. Assuming only the first four moments to represent non-Gaussianity (i.e. $N = 4$), use of this expression leads to the following relationship between X_i and U_i (Winterstein 1988):

$$X_i = H(U_i) = \mu_{X_i} + (\kappa_i \sigma_{X_i})\left[U_i + h_{3_i}(U_i^2 - 1) + h_{4_i}(U_i^3 - 3U_i)\right] \tag{6}$$

Where $h_{3i} = \gamma_{3i}/(4 + 2\sqrt{1 + 1.5(\gamma_{4_i} - 3)})$, $h_{4_i} = (\sqrt{1 + 1.5(\gamma_{4i} - 3)} - 1)/18$ with $\gamma_{ni} = E[((X_i - \mu_{Xi})/\sigma_{Xi})^n]$ and $\kappa_i = (1 + 2h_{3_i}^2 + 6h_{4_i}^2)^{-1/2}$ where strongly non-Gaussian variables could be accounted for (Winterstein 1988). It should be noted that the above formulation is valid for non-Gaussian variables X_i which posses softening behavior (i.e. their probability density functions have tails extending further out than those of the Gaussian distribution so that $\gamma_{4i} \geq 3$). Using Equation (6), the cross-covariance function $cov(X_i, X_j)$ (i.e. $= E[X_i X_j] - \mu_{X_i}\mu_{X_j}$) may be represented as (Moarefzadeh and Melchers, 2004):

$$cov(X_i, X_j) = \kappa_i \kappa_j \sigma_{X_i} \sigma_{X_j} \left\{ cov(U_i, U_j) + 2 h_{3_i} h_{3_j} cov(U_i, U_j)^2 + 6 h_{4_i} h_{4_j} cov(U_i, U_j)^3 \right\} \quad (7)$$

in which $cov(U_i, U_j)$ is the cross-covariance function of the standard Gaussian processes U_i and U_j.

4 NON-GAUSSIAN REPRESENTATION OF DIRECTIONAL VARIABLE Z

As already described (Moarefzadeh, 2005), non-Gaussianity of the variable Z is indicated using the Hermite Moment Models in which the first four moments of Z are required. Again, these four moments were shown to be of the forms to be given below. Let us assume that linear limit states be governed on the problem. These may be shown as follows:

$$G_i[\mathbf{Y}, \mathbf{Q}] = \sum_{j=1}^{m} k_j y_j - \sum_{j=1}^{n} l_j Q_j = 0 \quad (8)$$

In which $k_j (j = 1, \ldots, k_m)$ are constants (m is the number of involving material resistance variables) and l_j ($j = 1,\ldots,n$) are also constants (n is the number of loads involved), and Y_j, Q_j are respectively the jth components of material resistances and loads.

The first four moment-related-parameters may be indicated as follows for the simulated direction $\mathbf{A} = \mathbf{a} = \mathbf{a}\ [\alpha_1, \alpha_2, \ldots, \alpha_n]$:

1. mean of Z:

$$\mu_z = E[Z] = \frac{1}{\sum_{j=1}^{n} l_j \alpha_j} \left[\sum_{j=1}^{m} k_j \mu_{y_j} - \sum_{j=1}^{n} l_j \mu_{Q_j} \right] \quad (9)$$

2. the variance of Z:

$$\sigma_z^2 = E[z^2] - \mu_z^2 = \frac{1}{\left(\sum_{j=1}^{n} l_j \alpha_j \right)^2} \sum_{j}^{m} \sum_{t}^{m} k_j k_t cov(y_j, y_t) \quad (10)$$

in which $cov(y_j, y_t)$ is the (i, j)th component of the variance matrix $\mathbf{C_Y}$.

3. the skewness of Z:

$$\gamma_{3z} = \frac{E\left[(z - \mu_z)^3\right]}{\sigma_z^3} = \frac{\sum_{i}^{m} \sum_{j}^{m} \sum_{t}^{m} k_i k_j k_t E\left\{ (y_i - \mu_{y_i})(y_j - \mu_{y_j})(y_t - \mu_{y_t}) \right\}}{\left[\sum_{j}^{m} \sum_{t}^{m} k_j k_t cov(y_j, y_t) \right]^{3/2}} \quad (11)$$

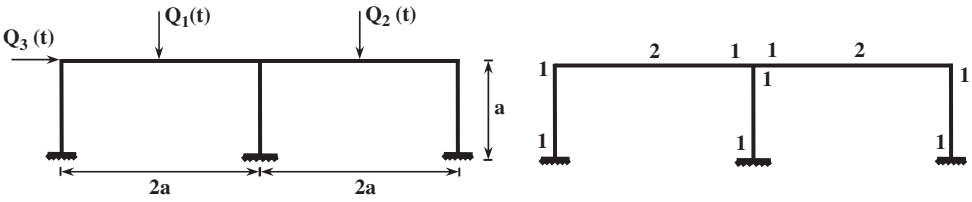

Figure 2. Defined frame in example.

4. the kurtosis of Z:

$$\gamma_{4z}=\frac{E\left[(z-\mu_z)^4\right]}{\sigma_z^4}=\frac{\sum_{i}^{m}\sum_{j}^{m}\sum_{t}^{m}\sum_{s}^{m}k_i k_j k_t k_s E\left\{(y_i-\mu_{y_i})(y_j-\mu_{y_j})(y_t-\mu_{y_t})(y_s-\mu_{y_s})\right\}}{\left[\sum_{j}^{m}\sum_{t}^{m}k_j k_t \operatorname{cov}(y_j,y_t)\right]^2} \tag{12}$$

Having γ_{3z} and γ_{4z} and then h_{3i} and h_{4i} in expression (6) known, two required functions $f_{Z|\mathbf{A}}(\,)$ and $F_{Z|\mathbf{A}}(\,)$ may be evaluated as follows. Using the relationship between Z and U (i.e. $Z=H(U)$ according to the equation(6)), by the known $Z=z^*$, $U=U^*$ may be calculated. The above two functions will then be:

$$F_{Z|\mathbf{A}}(z^*|\boldsymbol{\alpha})=\Phi(U^*) \tag{13}$$

$$f_{Z|\mathbf{A}}(z^*|\boldsymbol{\alpha})=\frac{1}{|H'(U^*)|}\phi(U^*) \tag{14}$$

in which:

$$H'(U)=\kappa[1+2h_3U+3h_4(U^2-1)]\cdot\sigma_z$$
$$\kappa=(1+2h_3^2+6h_4^2)^{-1/2}$$

Where $\Phi(U)$ and $\phi(U)$ are the probability density function and cumulative distribution function of standard normal random variable U.

5 EXAMPLE

Here in this paper, again the same rigid-plastic frame used already in Moarefzadeh, 2005, and shown in Figure 2 is examined, however, in this time two structural strength (of plastic hinges) random variables Y_1, Y_2 (corresponding to the locations shown in Fig. 2) which are not necessarily independent are used.

Four collapse modes (limit state functions) may be identified as follows:

$$G_1[\mathbf{Y},\mathbf{Q}]=2Y_1+2Y_2-Q_1(t)=0.0$$
$$G_2[\mathbf{Y},\mathbf{Q}]=2Y_1+2Y_2-Q_2(t)=0.0$$
$$G_3[\mathbf{Y},\mathbf{Q}]=6Y_1-Q_3(t)=0.0$$
$$G_4[\mathbf{Y},\mathbf{Q}]=6Y_1+2Y_2-Q_1(t)-Q_3(t)=0.0$$

Having these limit state functions, the required first four moment-related values μ_{Z_i}, σ_{Z_i}, γ_{3Z_i} and γ_{4Z_i} (i = 1,2,3,4) for any simulated direction $\mathbf{A} = \mathbf{a}$ could be estimated as follows:

$$\mu_{Z_1} = (1/\alpha_1)(2\mu_{Y_1} + 2\mu_{Y_2} - \mu_{Q_1})$$
$$\mu_{Z_2} = (1/\alpha_2)(2\mu_{Y_1} + 2\mu_{Y_2} - \mu_{Q_2})$$
$$\mu_{Z_3} = (1/\alpha_3)(6\mu_{Y_1} - \mu_{Q_3})$$
$$\mu_{Z_4} = (1/(\alpha_1 + \alpha_3))(6\,Y_1 + 2\,Y_2 - \mu_{Q_1} - \mu_{Q_3})$$

and:

$$\sigma^2_{Z_1} = (1/\alpha_1^2)\left[4\sigma^2_{Y_1} + 4\sigma^2_{Y_2} + 8\,\mathrm{cov}(Y_1, Y_2)\right]$$
$$\sigma^2_{Z_2} = (1/\alpha_2^2)\left[4\sigma^2_{Y_1} + 4\sigma^2_{Y_2} + 8\,\mathrm{cov}(Y_1, Y_2)\right]$$
$$\sigma^2_{Z_3} = (1/\alpha_3^2)\left[36\sigma^2_{Y_1}\right]$$
$$\sigma^2_{Z_4} = (1/[\alpha_1+\alpha_3]^2)\left[36\sigma^2_{Y_1} + 4\sigma^2_{Y_2} + 8\,\mathrm{cov}(Y_1, Y_2)\right]$$

and also γ_{3Z_i}, γ_{4Z_i} (i = 1,2,3,4) or briefly γ_{3Z} and γ_{4Z} which are independent from the simulated direction, may be shown to be as follows:

$$\gamma_{3Z} = \frac{k_1^3\mu_{30} + k_2^2\mu_{03} + 3k_1^2k_2\mu_{21} + 3k_1k_2^2\mu_{12}}{\left[\sum_i^2\sum_j^2 k_i k_j \mathrm{cov}(y_i, y_j)\right]^{3/2}}$$

$$\gamma_{4Z} = \frac{k_1^4\mu_{40} + k_2^2\mu_{04} + 4k_1^3k_2\mu_{31} + 4k_1k_2^3\mu_{13} + 6k_1^2k_2^2\mu_{22}}{\left[\sum_i^2\sum_j^2 k_i k_j \mathrm{cov}(y_i, y_j)\right]^{2}}$$

$$\text{In which } \mu_{rs} = E\left[(Y_1 - \mu_{Y_1})^r (Y_2 - \mu_{Y_2})^s\right].$$

Now, by the use of these formulas to show the first four-moment related expressions, and further by the use of relations (13) and (14) to estimate $f_{Z1\mathbf{A}}(\,)$ and $f_{Z1\mathbf{A}}(\,)$ the reliability analysis may be carried out. This analysis has been performed for different cases and the results are shown in Figures 3 to 10.

In Figures 3 and 4, p_{f0} and υ_D^+ have been indicated as functions of $\mathrm{cov}(Y_1, Y_2)$, for different values of μ_{40} and μ_{04} (which are assumed to be equal). For the case of non-Gaussinity the following values are taken for the other parameters: $\mu_{Y_1} = \mu_{Y_2} = 2$, $\sigma^2_{Y_1} = \sigma^2_{Y_2} = 1.0$, $\mu_{31} = \mu_{13} = 0.0$, $\mu_{30} = \mu_{03} = 1.0$, $\mu_{22} = 2.0$ and $\mu_{21} = \mu_{12} = 0.0$. Also, in this Figures Gaussian (Normal) case (i.e. $\gamma_{3zi} = 0$ and $\gamma_{4zi} = 3.0$) is shown for comparison. From the Figures, it is clearly observed that the results for two conditions of Gaussianity and non-Gaussianity are completely different. The differences appear in values and also in the behavior of the p_{f0} and υ_D^+ curves with different μ_{40} and μ_{04} i.e. the smaller μ_{40} and μ_{04} tend to smaller p_{f0} and υ_D^+ with the increase of $\mathrm{cov}(Y_1, Y_2)$.

In Figure 5, p_{f0} and υ_D^+ have been shown as functions of $\sigma^2_{Y_1}$ and $\sigma^2_{Y_2}$ (which are assumed to be equal) where $f_{Z1\mathbf{A}}(\,)$ is taken as non-Gaussian distribution. In addition the results for p_{f0} and υ_D^+ for Gaussian $f_{Z1\mathbf{A}}(\,)$ are also shown for comparison. Here in this case all values are as above in Figures 3 and 4 except $\mu_{40} = \mu_{04} = 5$ and $\mathrm{cov}(Y_1, Y_2) = 0.0$. Difference between the results of two cases of Gaussianity and non-Gaussianity is clear from the Figure. It is interesting to observe that in the case of non-Gaussianity p_{f0} and υ_D^+ tend to become smaller with the increase of $\sigma^2_{Y_1}$ and $\sigma^2_{Y_2}$.

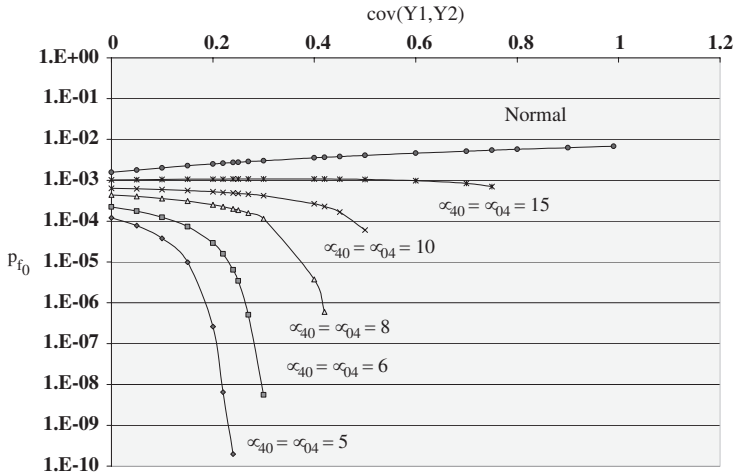

Figure 3. p_{f_0} as function of $\mathrm{cov}(Y_1, Y_2)$ for different values of μ_{40}, μ_{04}.

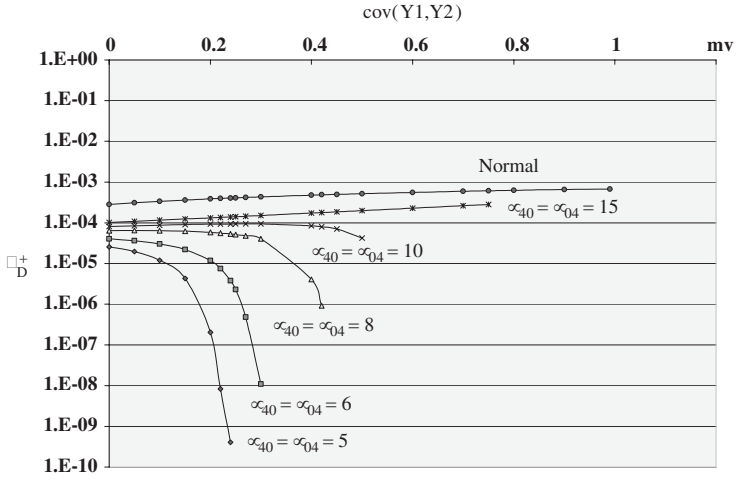

Figure 4. υ_D^+ as function of $\mathrm{cov}(Y_1, Y_2)$ for different values of μ_{40}, μ_{04}.

In Figure 6, p_{f0} and υ_D^+ are shown in terms of μ_{Y_1} and μ_{Y_2} (Note: μ_{Y_1} and μ_{Y_2} are assumed to be equal). Further, the case in which $f_{Z1A}(\ )$ is assumed to be Gaussian is also shown for comparison. Here in this case all values are as above in Figures 3 and 4 except $\mu_{40} = \mu_{04} = 5$ and $\mathrm{cov}(Y_1, Y_2) = 0.0$. As may be observed from the Figure, p_{f0} and υ_D^+ in both cases of Gaussian and non-Gaussian $f_{Z1A}(\ )$, tend to become smaller as expected, however, in the case of non-Gaussianity these values are completely different and their changes appear to be more intensive.

In Figures 7 and 8, p_{f0} and υ_D^+ are shown as functions of μ_{30} and μ_{03} (which are assumed to be equal) for different values of μ_{40} and μ_{04}. In this case, $\mathrm{cov}(Y_1, Y_2) = 0.24$ and the remaining parameters are as given in the first case above. The results are similar to those already shown for the one-dimensional case (see Moarefzadeh, 2005).

In Figures 9 and 10, p_{f0} and υ_D^+ are shown as functions of μ_{40} and μ_{04} (which are assumed to be equal) for different values of μ_{30} and μ_{03}. In this case, $\mathrm{cov}(Y_1, Y_2) = 0.2$ and the remaining parameters are as given in the first case above. Here again, the results are similar to those already given for the one-dimensional case (see Moarefzadeh, 2005).

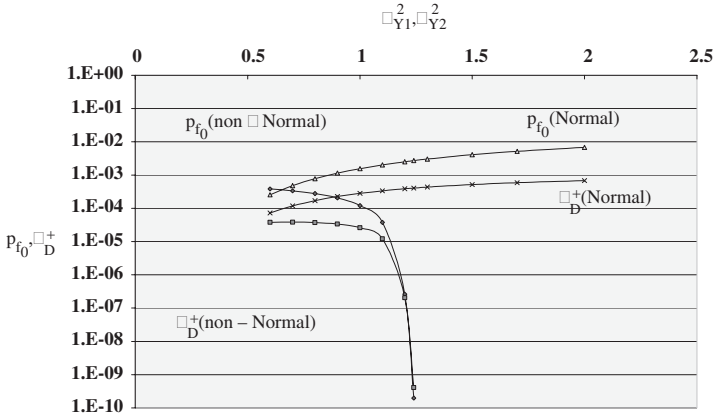

Figure 5. p_{f_0} and υ_D^+ as functions of $\sigma_{Y1}^2, \sigma_{Y2}^2$ for two cases of normality and non-normality.

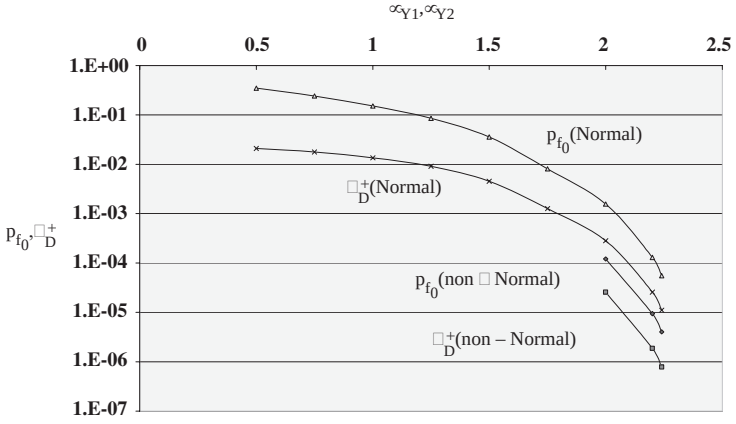

Figure 6. p_{f_0} and υ_D^+ as functions of μ_{Y1}, μ_{Y2} for two cases of normality and non-normality.

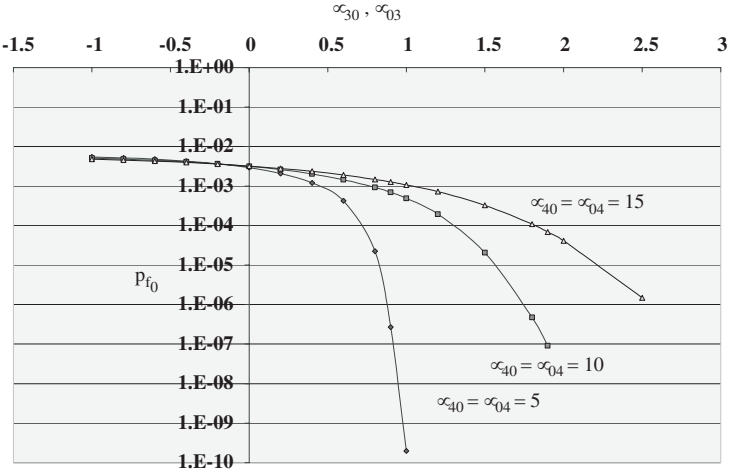

Figure 7. p_{f_0} as function of μ_{30}, μ_{03} for different values of μ_{40}, μ_{04}.

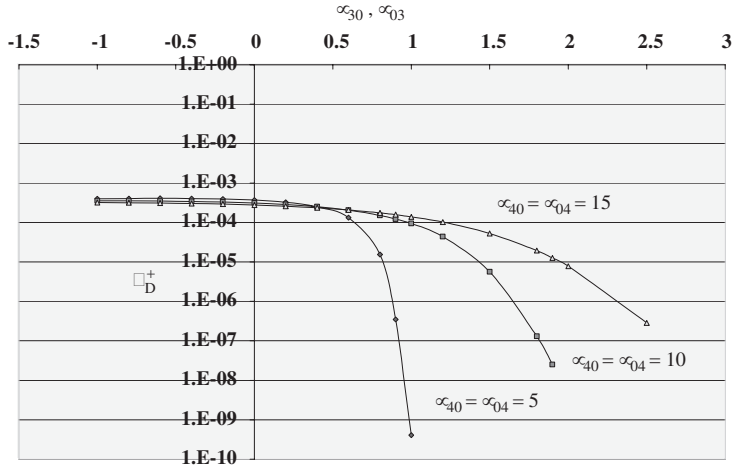

Figure 8. υ_D^+ as function of μ_{30}, μ_{03} for different values of μ_{40}, μ_{04}.

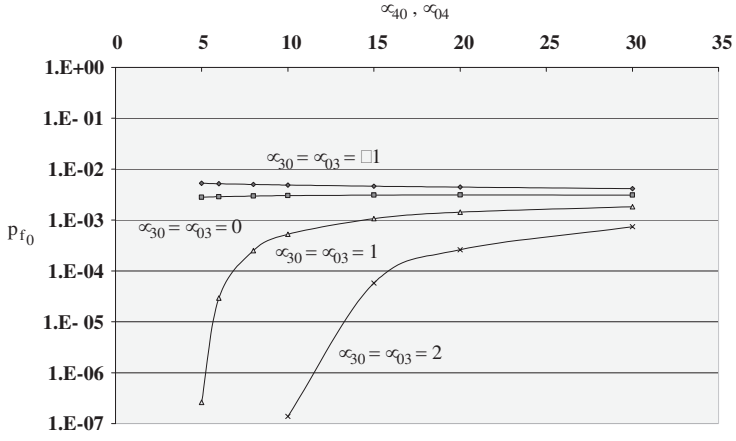

Figure 9. p_{f_0} as function of μ_{40}, μ_{04} for different values of μ_{30}, μ_{03}.

6 DISCUSSION

As is observed from the figures of the examples described already, p_{f0} and υ_D^+ are significantly dependent on the different values in which mean, covariance matrix skewness and kurtosis of the structural resistance variables Y_1 and Y_2 are of more importance. As is obvious, these parameters influence the two functions f_{Z1A} ( ) and F_{Z1A} ( ). These functions in turn, affect the results of two integrations involved in the estimation of p_{f0} and υ_D^+ (see equations (4), (5)).

An extensive discussion on the trend of p_{f0} and υ_D^+ values was made already where independency between structural resistance variable, Y_1, Y_2 is assumed (Moarefzadeh, 2005). Herein, in this paper, it is of interest to further discuss the behavior of p_{f0} and υ_D^+ with different values of dependency between Y_1, and Y_2. As is shown here, p_{f0} and υ_D^+ as functions of cov(Y_1, Y_2) is crucial where μ_{40} and μ_{04} are small and also where μ_{30} and μ_{03} are sufficiently large. From the relations to calculate γ_{3z} and γ_{4z} in this paper, it follows that with the increase of cov(Y_1, Y_2) (while μ_{30}, μ_{03}, μ_{40} and μ_{04} are constants), γ_{3z} and γ_{4z} tend to be smaller and this in turn push p_{f0} and υ_D^+ to be drastically smaller for small μ_{40} and μ_{04} as concluded already in Moarefzadeh, 2005. Obviously

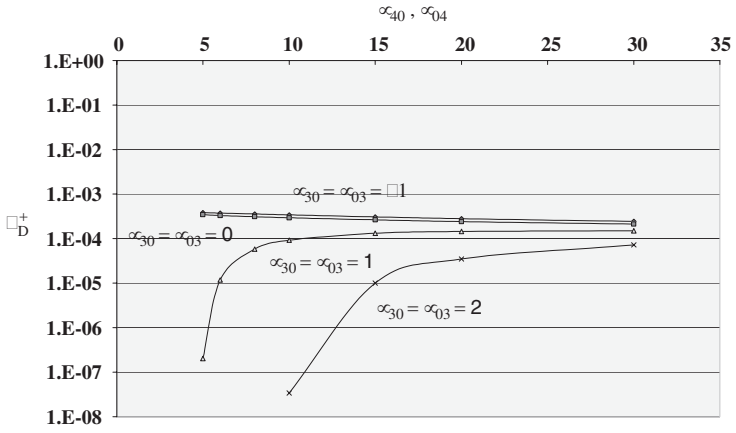

Figure 10. υ_D^+ as function of μ_{40}, μ_{04} for different values of μ_{30}, μ_{03}.

for the cases in which μ_{40} and μ_{04} are large, changes of γ_{4z} to the smaller values will be slower and therefore tendency of p_{f0} and υ_D^+ to smaller values will also be slower.

7 CONCLUSION

Directional simulation in load space was used to estimate the structural reliability. Since the location of limit states has to be considered probabilistically in this space, herein in this paper, non-Gaussianity for distribution of this location was employed. It was shown this model in which higher moments (e.g. the 3rd and 4th moments) are taken in to account is more accurate in the comparison with the models in which Gaussianity (i.e. using two first moments) is used.

In particular it was shown that dependency between the structural resistance variables could affect the initial probability of failure p_{f_0} and the out crossing rate υ_D^+ drastically in some circumstances.

REFERENCES

Ditlevsen, O., Bjerager, P., Olesen, R. and Hasofer, A.M. (1988), 'Directional Simulation in Gaussian Processes', Probabilistic Engineering Mechanics, Vol. 3, No. 4, pp. 207–217.

Ditlevsen, O., Melchers, R.E. and Gluver, H. (1990), 'General Multi-dimensional Probability Integration by Directional Simulation', Computers and Structures, Vol. 36, No. 2, pp. 355–368.

Grigoriu, A.G. (1995), 'Applied non-Gaussian Processes', Princeton Hall, Englewood, Cliffs, Newjercy, USA.

Melchers, R.E. (1990), 'Radial Importance Sampling for Structural Reliability', Journal of Engineering Mechanics, ASCE, Vol. 116, No. 1, pp. 189–203.

Melchers, R.E. (1992) 'Load-Space Formulation for Time-Dependent Structural Reliability', Journal of Engineering Mechanics, ASCE, Vol. 118, No. 5, pp. 853–870.

Moarefzadeh, M.R. (1995) 'Time-Dependent Reliability Analysis of Off-shore Structures', PhD Thesis, The University of Newcastle, NSW, Australia.

Moarefzadeh, M.R. and Melchers, R.E. (1996) 'Sample-Specific Linearization in Reliability Analysis of Off-shore Structures', Journal of Structural Safety, Vol. 18, No. 2/3, pp. 101–122.

Moarefzadeh, M.R. and Melchers, R.E. (2004), 'Nonlinear Wave Theory in Reliability Analysis of Offshore Structures', Probabilistic Engineering Mechanics, 21(2006) pp. 99–111.

Moarefzadeh, M.R. (2005), 'Structural Resistance variability in Directional Simulation in Load Space', Reliability and Optimization of structural Systems '2005, Proceedings of the 12th IFIP WG7.5 Working Conference, (Aalborg, May 2005) (Ed. J.D. Sorensen and D.M. Frangopol), pp. 143–154.

Winterstein, S.R. (1988) 'Nonlinear Vibration Models for Extremes and Fatigues', Journal of Engineering Mechanics, ASCE, Vol. 114, No. 10, pp. 1772–1790.

Reliability and Optimization of Structural Systems: Assessment, Design and Life-Cycle Performance – Frangopol, Kawatani & Kim (eds)
© 2007 Taylor & Francis Group, London, ISBN 978-0-415-40655-0

Optimal strengthening of RC bridges with degradation in safety due to chloride induced deterioration

H. Morikawa
Department of Civil Engineering of Kobe University, Kobe, Hyogo, Japan

S. Okamoto
JR-west Japan Consultants Company, Osaka, Japan

S. Kishi
Graduate School of Science and Technology of Kobe University, Kobe, Hyogo, Japan

ABSTRACT: This paper describes a method of evaluating the degradation in safety and determining the optimum time and degree of strengthening for existing concrete bridges. For optimization of strengthening, the utility function is introduced to express the objective function as the measure of effectiveness of design lifetime, safety and load carrying capacity. The genetic algorithm (GA) was applied to a searching procedure of global extreme value of the objective function. Proposed method was applied on actual existing bridge of 44 years old.

1 INTRODUCTION

Bridge evaluation, repair and rehabilitation have become to more and more important issues in the effort of maintenance of deteriorating concrete bridges. Serious deterioration of RC bridges due to chloride attack has been detected and the number of such deteriorated bridges will keep increasing in the future. That is, establishment of effective maintenance under limited budget is indispensable issue. For this purpose, the methodology for rational bridge diagnosis and effective strengthening for extending the life is need to be developed.

This paper describes a method of evaluating the degradation in safety and determining the optimum time and degree of strengthening for existing concrete bridges. For strengthening of bridges, the external cable method is used to enhance both the strength and stiffness of girders.

For optimization of strengthening, the utility function is introduced to express the objective function as the measure of effectiveness of design lifetime, safety and load carrying capacity. It is assumed that the design lifetime is given as a constraint condition and the others (i.e. safety and load carrying capacity) are the parameters of which utility is to be maximized. In this case, the multi-attribute utility function is effective. The optimization problem was considered as determination of the optimum time and degree of strengthening in order to maximize the utility function.

The genetic algorithm (GA) was applied to a searching procedure of global extreme value of the objective function. Proposed method was applied on actual existing bridge of 44 years old. The optimal strengthening for extending the life over the expected value was demonstrated and its suitability was discussed.

Table 1. Description of "Bridge Z" and conditions for analysis of safety evaluations.

Year of construction	1959
Span (m)	11.1
Distance from coast line (m)	50
Cover (mm)	80(bottom)/50(line)
Chloride ion content on the concrete surface (kg/m^3)	6.5(girder A), 5.5(girder B), 4.5(girder C)
Strength of concrete (N/mm^2)	35.7
Modulus of elasticity of concrete (kN/mm^2)	21.3
Water-cement ratio (%)	40.3
Yield strength of reinforcement (N/mm^2)	294
Cross section area of main reinforcement (mm^2)	6158
Cross section area of stirrup(mm^2)	127.2
Interval of stirrup (mm)	300

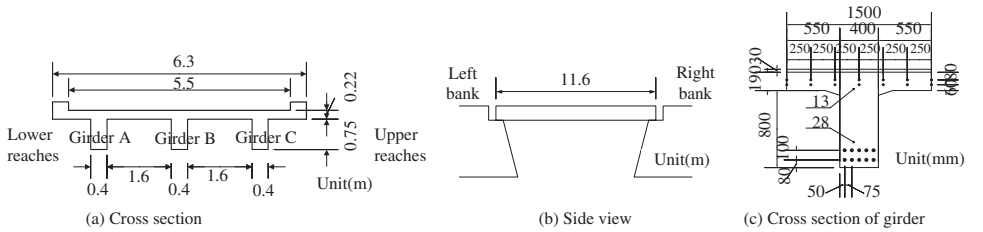

(a) Cross section (b) Side view (c) Cross section of girder

Figure 1. Outline of "Bridge Z".

2 GENERAL INSTRUCTIONS

2.1 *Outline of target bridges*

This paper focuses on the RC-T beams bridge exposed to chloride attack. An actual bridge named "Bridge Z" as shown in Table 1 and Fig. 1, was selected for evaluation. Through the visual inspection at 44 years old, many cracks due to corrosion of rebars were recognized entirely, and peeling and spalling of cover concrete were detected partially on girders A and B.

2.2 *Safety evaluation*

The safety evaluation procedure is shown in Fig. 2. The Monte Carlo simulation was applied on the prediction of deterioration, structural analysis to evaluate bending moment for each girder, analysis of load carrying capacity, in consideration of various uncertainties associated with the process of safety evaluation, and then the safety index β was calculated. The structural analysis model for evaluation of bending moment is performed by using the lattice model constituted by FEM beam elements as shown in Fig. 3. Fig. 4 shows the safety evaluation result on "Bridge *Z*" with $\beta = 4.3$ (for high consequences of failure) and 2.3 (for very low consequences of failure) as the target reliability index for ultimate limit state prescribed in ISO 13822 and $\beta = 2.08$ for limit value for actual maintenance in the Hyogo prefectural government evaluated by Morikawa. Degradation status in safety is different for each girder, and becomes complicated due to redistribution of bending moment.

2.3 *Evaluation of RC bridge strengthened by external prestressing*

In this paper, the external prestressing method was considered as the strengthening method to enhance both the strength and stiffness of girders for strengthening of RC bridge with chloride induced deterioration. Fig. 5 shows the relationship between the prestressing force *P* and the

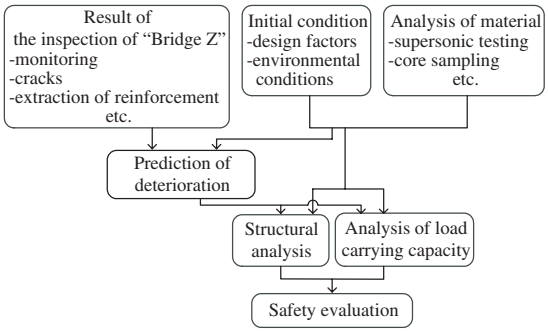

Figure 2. Flow of safety evaluation.

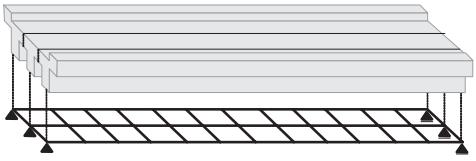

Figure 3. Structural analysis model for safety evaluation.

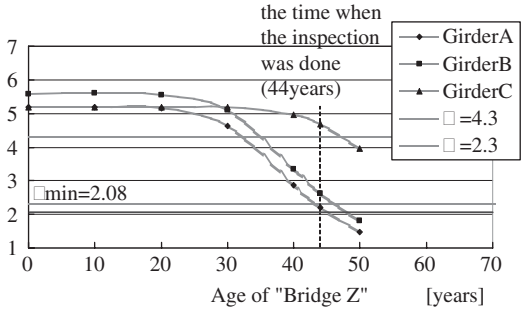

Figure 4. Result of safety evaluation of "Bridge Z".

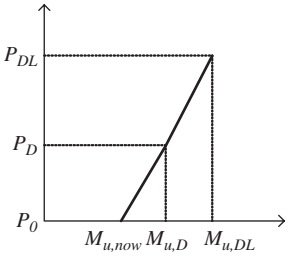

Figure 5. Relationship between P and M_u (External prestressing method).

load carrying capacity after strengthening. P_D is prestressing force against dead load, and P_{DL} is prestressing force against both dead and live loads. In this case, prestressing force P is expressed by

$$P = \frac{P_D}{R_{M_{u,D}}} \times R_{M_u} \qquad (M_{u,now} \le M_u < M_{u,D}) \tag{1}$$

$$P = P_D + \frac{(P_{DL} - P_D)}{(1.0 - R_{M_{u,D}})} \times (R_{M_u} - R_{M_{u,D}}) \qquad (M_{u,D} \le M_u < M_{u,DL}) \tag{2}$$

$$R_{M_u} = \frac{M_u - M_{u,now}}{M_{u,DL} - M_{u,now}} \tag{3}$$

$$R_{M_{u,D}} = \frac{M_{u,D} - M_{u,now}}{M_{u,DL} - M_{u,now}} \tag{4}$$

For evaluation of the load carrying capacity of girder before strengthening, FEM analysis is necessary for exact evaluation considering degradation in bond due to corrosion of rebars. For

Table 2. Evaluation of the influencing coefficient if axial force (Girder A, 44 years).

	Girder A P_A	Girder B P_B	Girder C P_C
Axial force (Girder A): $N_{act,A}$	0.874	0.215	−0.052
Axial force (Girder B): $N_{act,B}$	0.178	0.571	0.178
Axial force (Girder C): $N_{act,C}$	−0.052	0.215	0.874

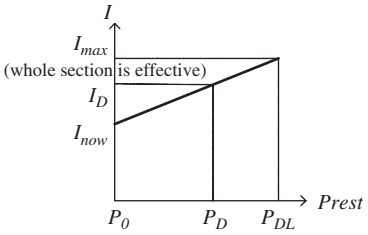

Figure 6. Assumption of the relationship between *P*and *I* (External prestressing method).

evaluation of the load carrying capacity after strengthening $M_{u,D}$, $M_{u,DL}$, the equation proposed by Mutsuyoshi was applied under the condition that the bond of corroded rebars can be restored by patch repair works for chloride induced deterioration.

In general, for the multi-beams girder bridge, bending moment is redistributed. In this case, prestressing force introduced by external cable is also redistributed. To take this effect into consideration, the axial force introduced on girder *i* is calculated by using the following equation.

$$N_{act,i} = \sum_j S_{i,j} P_j \qquad (i, j = A, B, C) \tag{5}$$

where, $S_{i,j}$: influencing coefficient for axial force, that is, ratio of the redistributed prestressing force on girder *i* to the original prestressing force introduced on girder *j*, P_j: original prestressing force introduced on girder *j*.

However, when the external cable is not set on girder *i* though the other girders are prestressed, the redistributed axial force on girder *i* does not contribute on the load carrying capacity. Therefore, the introduced prestressing force as a result of redistribution is expressed by

$$P_{act,i} = N_{act,i} \qquad \text{when} \quad P_i \neq 0 \tag{6}$$

$$P_{act,i} = 0 \qquad \text{when} \quad P_i = 0 \tag{7}$$

Table 2. shows the result of evaluation of the influencing coefficient of axial force for "Bridge *Z*".

On the other hand, the moment of inertia is assumed to be restored to the maximum value corresponding to the condition that whole section is effective, when P_{DL} is introduced. And the moment of inertia is defined as the following equation and Fig. 6.

$$I = I_{now} + \frac{I_{\max} - I_{now}}{P_{DL} - P_0} \times P \tag{8}$$

where, I_{now}: current moment of inertia, $I_{\max}$: maximum moment of inertia.

3 BASIC CONCEPT AND METHODOLOGY OF OPTIMAL MAINTENANCE

3.1 *Basic concept*

In this paper, the optimal strengthening is defined as improving the safety balance of the whole structure and extending the life over the design lifetime by minimum strengthening. That is, the objectives of the optimization were defined as follows:

① To maintain the target safety during the planned service period.
② To minimize the prestressing force for strengthening.
③ To improve or maintain the stiffness balance among consisted girders
④ To minimize the number of girders for strengthening.

However, the objective ③ was set to be an option, corresponding to the case that optimization is considered by minimizing the prestressing without consideration of stiffness balance. And repair works such as patching was also considered in order to prevent re-deterioration after strengthening.

3.2 *Multi-attribute utility approach*

Optimal strengthening might be affected by various factors such as safety, strength, residual life, cost and others. Therefore, a unified measure is needed for decision-making concerning optimization considering these factors. In this paper, the utility theory is introduced and the utility of the factors by using the convex utility function is expressed as:

$$u(x) = a + be^{-\gamma x} \qquad \gamma \geq 0 \tag{9}$$

where, γ: measure of degree of risk-aversion, a, b: normalization constants.

The expected utility for a countermeasure (strengthening) can be expressed by:

$$E(U_i) = \int_{-\infty}^{\infty} u(x) f_X^i(x) dx \tag{10}$$

where, $u(x)$: utility function for result X of a countermeasure a_i, $f_X^i(x)$: probability density function.

This computation of the expected utility can be generalized to decision analysis in which the effectiveness is measured by several attributes. The corresponding utility function and the associated probability density function will, therefore, be multi-dimensional. Hence,

$$E(U_i) = \int_{x_1} \cdots \int_{x_n} u(x_1, \cdots, x_n) f^i_{X_1, \cdots, X_n}(x_1, \cdots, x_n) dx_1 \cdots dx_n \tag{11}$$

where, $X_1, \ldots, X_n$: random variables describing values of the n respective attributes associated with each alternative, $u(x_1, \ldots x_n)$: the joint utility, $f^i_{X_1,\ldots,X_n}(x_1, \ldots, x_n)$: the joint density function.

For simplification of computation of Eq.(11) and its practical use, some assumptions can be made, as follows:

① Statistical independence
② Preferential independence
③ Utility independence

By using assumption ①, Eq. (11) can be transformed to:

$$E(U_i) = u(x_1, \cdots, x_n) \tag{12}$$

By using assumptions ② and ③, the joint utility can be expressed by:

$$u(x_1, \cdots, x_n) = \frac{1}{k}\left(\prod_{i=1}^{n}[1 + kk_i u_i(x_i)] - 1\right) \tag{13}$$

where, k and $k_i (i = 1, \ldots.., n)$ are constants to be evaluated.

Table 3. Atrributes (External prestressing method).

①	X_1	Safety margin (Girder A)
	X_2	Safety margin (Girder B)
	X_3	Safety margin (Girder C)
②	X_4	Strengthening ratio (Girder A)
	X_5	Strengthening ratio (Girder B)
	X_6	Strengthening ratio (Girder C)
③	X_7	Stiffness balance ratio (Girder A)
	X_8	Stiffness balance ratio (Girder B)
	X_9	Stiffness balance ratio (Girder C)
④	X_{10}	Number of girders for strengthening

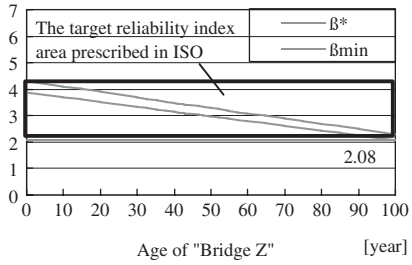

Figure 7. Target reliability.

3.3 *Formulation of attributes*

In this study, ten attributes as shown in Table 3., are defined. Those attributes were formulated as follows.

① Safety margin $X_1 \sim X_3$

Target reliability was defined a linear function changing from 4.3 to 2.3 prescribed in ISO 13822 during the planned service period, as shown in Fig. 7. And then, the lower limit for target reliability $\beta_{\min}$ was defined by shifting the above mentioned target reliability line until $\beta_{\min} = 2.08$ at the end of planned service period. Fig. 7 shows an example of target reliability in the case that the planned service period is 100 years. It is defined that $X_i = 0.0$ (finest) when safety index β' after strengthening exceed the target reliability β^*, and $X_i = 1.0$ (worst) when safety index β' after strengthening does not exceed β^*. And β^* was defined a quadratic function with the range from 0.0 to 1.0.

$$X_i = 0.0 \qquad (\beta'(t) \geq \beta^*(t)) \tag{14}$$

$$X_i = \frac{1.0}{(\beta_{\min}(t) - \beta^*(t))^2} \cdot (\beta'(t) - \beta^*(t))^2 \qquad (\beta_{\min}(t) \leq \beta'(t) < \beta^*(t)) \tag{15}$$

$$X_i = 1.0 \qquad (\beta'(t) < \beta^*_{\min}(t)) \tag{16}$$

where t: age at strengthening $\beta'(t)$: safety index after strengthening $\beta^*(t)$: target reliability at t, $\beta_{\min}(t)$: lower limit of target reliability at t.

② Strengthening ratio $X_4 \sim X_6$

$$X_i = r_j = \frac{M_{u,j} - M_{u,now,j}}{M_{u,\max,j} - M_{u,now,j}} \qquad (j = A, B, C) \tag{17}$$

where, $r_j (0 \leq r_j \leq 1.0)$: Load carrying capacity ratio of girder j, $M_{u,j}$: Load carrying capacity of girder j after strengthening, $M_{u,\max,j}$: Maximum load carrying capacity of girder j after strengthening, $M_{u,\text{now},}$: Load carrying capacity of girder j before strengthening.

For external prestressing method, strengthening ratio can be expressed as follows.

$$X_i = r_j = \frac{P_j}{P_{DL,j}} \qquad (j = A, B, C) \tag{18}$$

where, $r_j (0 \leq r_j \leq 1.0)$: prestressing ratio of girder j, P_j prestressing force of girder j, $P_{dl,j}$: limit prestressing without tensile stress for both dead and live loads

③ Stiffness balance ratio $X_7 \sim X_9$

$$X_i = \left| 1 - \frac{(EI)_m}{(EI)_n} \right| \qquad (m, n = A, B, C) \tag{19}$$

where, $(EI)_m$, $(EI)_n$: stiffness of girder m, n

④ Number of girders for strengthening X_{10}

For optimization of strengthening by external prestressing, not only minimizing the total prestressing force but also minimizing the number of girders for strengthening is considered under the condition that tensile stress does not occur at the other girders which are not strengthened by introducing external prestressing.

3.4 *Optimization scheme*

The optimization scheme can be formulated as maximizing the joint utility expressed by Eq.(13). In general, it should be noted that the solution frequently falls into the local solution in the case of multi-objective optimization. For stable convergence to the global optimal solution, the optimization scheme is divided into two steps as follows,

Step 1: at the time for strengthening t_i, calculate the optimum prestressing force $P_{j,opt}^{t_i}$ for each girder $j(j = \text{A, B, C})$ and the joint utility $u^{t_i}(x_i)$.

Step 2: determine the optimum time for strengthening as $u^{t_i}(x_i) \rightarrow \max$.

The final judgment of strengthening is usually related to the cost, social factors and so on. Therefore, the proposed two steps of optimization scheme is practical for the rational entire maintenance and management framework.

For the step 1 of optimization, the objective function and the constraint are expressed as follows.

$$u(x_1, \cdots, x_{10}) = \frac{1}{k}\left(\prod_{i=1}^{10} [1 + k k_i u_i(x_i)] - 1 \right) \rightarrow \max \tag{20}$$

subject to

$$X_i < 1.0 \qquad (i = 1 \sim 3) \tag{21}$$

The genetic algorithm (GA) was applied to a searching procedure of global extreme value of the objective function. For coding genes for the degree of strengthening of each girder, the binary scale is used for simplification.

4 APPLICATION TO AN EXISTING BRIDGE

4.1 *Optimization*

The multi-attribute utility function at 44 years old of "Bridge *Z*" was obtained as follows by using data in Table 3.

$$u(x_1, \cdots, x_{10}) = \frac{1}{0.0005233}\left(\prod_{i=1}^{10} [1 + 0.0005233\, u_i(x_i)] - 1 \right) \tag{22}$$

For application of GA, it is assumed that the crossover rate is 0.3 and mutation rate is 0.01. Fig. 8 shows the convergency of GA optimization regarding the parameter of population, that is, iteration number. It is found that a population of 100 seems to be enough for convergency. Fig. 9 shows the results of optimization of strengthening of "Bridge *Z*". For 40 years old, a combination of strengthening of girder A and B is obtained for optimum solution. On the contrary, for 44 and 50 years old, a combination of strengthening of all three girders is obtained. Through the comparison

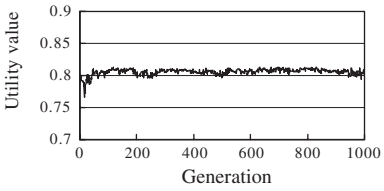

Figure 8. Convergency of GA optimization.

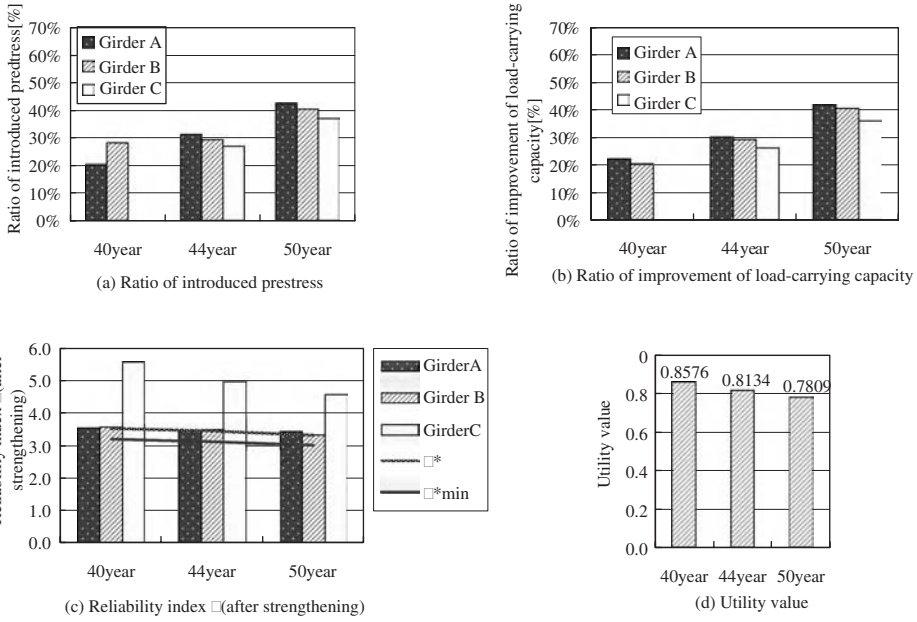

Figure 9. Result of optimization of strengthening (with consideration of stiffness balance ratio).

of total utility value, the value for 40 years old is higher than the others. Therefore, strengthening at 40 years old is desirable compared with the case of 44 and 50 years old.

4.2 *Effect of stiffness balance ratio*

In order to investigate the effect of stiffness balance ratio, optimization without consideration of the ratio was carried out. Fig. 10 shows the optimization results. For all the case of the age for strengthening, optimum solution was obtained as the same pattern, that is, a combination of strengthening of girders A and B, so that, strengthening of girder C is not necessary in this case. In the case of this bridge, the stiffness balance ratio was not significantly changed due to deterioration, therefore, the stiffness balance ratio is moved toward worse by strengthening of only girders A and B. And total prestressing force in the case without consideration of stiffness balance ratio is reduced. However, it should be noted that the bridge without well-balanced girder stiffness may cause unbalanced and sophisticated deterioration after strengthening. In order to keep well-balanced condition of girders, the consideration of stiffness balance ratio for optimal strengthening is indispensable.

5 CONCLUSIONS

This paper discussed the method of determining optimum time and degree of strengthening for existing concrete bridges with chloride induced deterioration. For strengthening of bridges, the

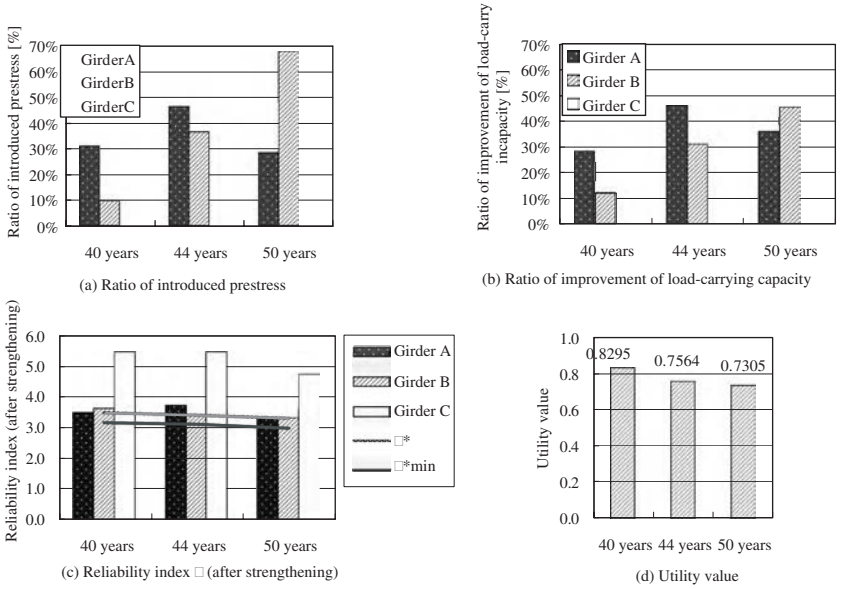

Figure 10. Result of optimization of strengthening (without consideration of stiffness balance ratio).

external prestressing method was used to enhance both the strength and stiffness of girders. For basic concept of optimal strengthening, the optimal strengthening was defined as improving the safety balance of the whole structure and extending the life over the design lifetime by minimum strengthening. To optimize strengthening, a multi-attribute utility function was introduced to express a multiple objective function as the measure of effectiveness of design lifetime, safety and load carrying capacity. The optimization problem was considered to be one of determining the optimum time and degree of strengthening in order to maximize the utility function. A genetic algorithm was applied to the procedure of searching global extreme values of the objective function. Proposed method was applied to an actual bridge of 44 years old. The optimal strengthening for extending the life over the expected value was demonstrated and its suitability was discussed.

ACKNOWLEDGEMENTS

The authors would like to extend their sincere appreciation to the Hyogo Prefectural Government for field testing of an existing bridge.

REFERENCES

Ang, A. H-S. & Tang, W. H. 1984. *Probability Concepts in Engineering Planning and Design*. Wiley.

ISO. 2001.12. *INTERNATIONAL STANDARD, Bases for Design of Structures–Assessment of Existing Structures*. ISO 13822. First edition.

Morikawa, H., Miyamoto, A. & Takeuchi, K. 1996.12. *Structural Safety Evaluation and Remaining Life Prediction of Concrete Bridges Based on Statistical Analysis*. Concrete Library International of JSCE. No. 28. pp. 51–64.

Morikawa, H., Oyama, S., Katayama, K. & Miyamoto, A. 1997.11. *Optimal Maintenance of Existing Concrete Bridges Based on Multi-attribute Utility Approach*. Proceedings of 7th International Conference on Structural Safety and Reliability. Vol. 1. pp. 451–458.

Mutsuyoshi, H., Tsuchida, K., Matupayont, S. & Machida, A. 1995.2. *Flexural Behavior and Proposal of Design Equation for Flexural Strength of Externally PC members*. Journal of Materials, Concrete structures and Pavements. No.508/V-26. pp. 67–77.

Reliability and Optimization of Structural Systems: Assessment, Design and Life-Cycle Performance – Frangopol, Kawatani & Kim (eds)
© 2007 Taylor & Francis Group, London, ISBN 978-0-415-40655-0

Evaluation of seismic performance of highway bridge system by Multi-State System approach

H. Morisaki
Pacific Consultants Co.,Ltd., Oosaka, Japan

W. Shiraki
Kagawa University, Kagawa, Japan

M. Dogaki
Kansai University, Oosaka, Japan

H. Inomo
Kagawa University, Kagawa, Japan

N. Ito
CAE Inc., Tottori, Japan

K. Yasuda
Newjec Inc., Tokyo, Japan

ABSTRACT: In this research, the "Multi State System(MSS)" theory adopted with the electric power distribution system as a seismic performance evaluation technique of the elevated highway bridge so far was applied. That is, it proposed the performance design method of the bridge system that had to capture, to evaluate the seismic performance level of each structural element of the bridge and the entire system in this conception that was not conventional as a structural system, and to aim at the elevated road bridge in the performance design system.

1 INTRODUCTION

Recently, "Performance design" is remarkable in an earthquake-proof design domestically. In this background, the enormous damage from the earthquake which attacked large cities such as Loma Prieta earthquake in 1989, North Ridge Earthquake in 1994, Hyogo-ken Nanbu Earthquake in 1995, etc. is mentioned.

"Performance design" is a design method that starts achieving this target performance after the target performance is clarified. Therefore, it is necessary to systematize the check item and the check method to the performance and this that has been openly and secretly demanded from the structure clearly so far. However, it becomes without passing specifications for highway bridges revised in March, 2002 in showing the directivity of the conversion to the performance design system, while the frame of the conventional decision theory design system was maintained.

Future directivity of seismic design system of our country asks whether it clarifies the possibility (damage and collapse probability) that it damages the structure as possibility (probability), the result results which the load over the design load affects and collapses and whether that possibility is appropriate, and it is necessary to attempt the consensus building by the clarification of the performance necessary for the structure. On designing of seismic performance for highway bridges,

each structural element of the bridge are designed individually to seismic performance which is required by each element. Based on this consideration, it is assumed that the seismic performance level of whole structural system is adequate if each element performs enough seismic performance to the estimated earthquake level. However, influence of each element to the entire structural system of seismic performance is different. It is possible that some structural elements perform enough seismic performance while others perform less because of the different influence to the entire system so that there maybe an unbalanced seismic resistance level as an entire structural system.

In this study, an elevated single span highway bridge is considered as a structural system consisted of five structural elements i.e., simple girder, bridge bearing, cable for falling prevention of bridge, pier, and foundation, and the Multi State System (MSS) approach which is usually used for designing of distribution systems such as water and power supply is proposed evaluate the seismic resistance performance of the entire bridge system. And in a conception that was not conventional, the seismic performance level of each structural element of the bridge and the entire system is evaluated. And, it proposes the performance design method of the bridge system that should be aimed in the performance design system.

2 THE BASIC CONCEPT OF MULTI STATE SYSTEM (MSS)

MSS is an idea that starts searching out the combination of a suitable state amount variable for demonstrating of the system the best performance comparatively by the reliability evaluation technique of the system of the new paradigm for a certain kind of performance for the system that has a lot of state amount variables.

2.1 *Definition and characteristic of MSS*

All technical systems are designed to perform their intended tasks in a given environment.

Some systems can perform their tasks with various distinguished levels of efficiency usually referred to as performance rates. A system that can have a finite number of performance rates is called a multi-state system (MSS).

Usually MSS is composed of elements that in their turn can be multi-state An element is an entity in a system, which is not further sub-divided. This does not imply that an element cannot be made of parts, but means only that, in a given reliability study, it is regarded as a self-contained unit and is not analyzed in terms of the reliability performances of its constituents.

The performance rates of the elements can range from perfect functioning up to complete failure. The failures that lead to the decrease in the element performance are called partial failures. After partial failure, elements continue to operate at reduced performance rates, and after complete failure the elements are totally unable to perform their tasks.

In a word, there is the state between completely out of order because of partial state of the breakdown states when seeing as the entire system. That is, a partial breakdown as the entire system exists.

2.2 *Performance display rate of the general MSS model*

Any system element j can have *kj* different states corresponding to the performance rates, represented by the set

$$g_j = \{g_{j1}, g_{j2}, \cdots, g_{jk_j}\} \tag{1}$$

where *gji* is the performance rate of element *j* in the state *i*, $i \in \{1, 2, \ldots kj\}$.

The performance rate *Gj(t)* of element *j* at any instant $t \geqq 0$ is a random variable that takes its values from *gj: Gj(t)* $\in$*gj*. Therefore, for the time interval *[0,T]*, where *T* is the MSS operation period, the performance rate of element *j* is defined as a stochastic process.

The probabilities associated with the different states (performance rates) of the system element j at any instant t can be represented by the set

$$\begin{aligned} p_j(t) &= \Pr\{G_j(t) = g_{ji}\} \\ &= \{p_{j1}(t), p_{j2}(t), \cdots, p_{jk_j}(t)\} \end{aligned} \tag{2}$$

Note that since the element states compose the complete group of mutually exclusive events (meaning that the element can always be in one and only in one k of kj States)

$$\sum_{i=1}^{kj} p_{ji}(t) = 1, \text{ for any } t: 0 < t < T \tag{3}$$

When the MSS consists of n elements, its performance rates are unambiguously determined by the performance rates of these elements. When the number of states of performance demonstrating rates of the entire system is assumed to be k, the performance demonstrating rate at time t becomes random variable $G(t)$ that takes the value of set $\{g_1, \cdots, g_k\}$.

The value of this random variable $G(t)$ can be defined by the system structural function ϕ, and can be shown by expression (4) and (5) for a basic system of the series and the parallel.

「The series system」

$$\begin{aligned} G(t) &= \phi(G_1(t), \cdots, G_n(t)) \\ &= \min\{G_1(t), \cdots, G_n(t)\} \end{aligned} \tag{4}$$

「The parallel system」

$$\begin{aligned} G(t) &= \phi(G_1(t), \cdots, G_n(t)) \\ &= G_1(t) + \cdots + G_n(t) \end{aligned} \tag{5}$$

However,

$$g_j(t),\ p_j(t),\ 1 \le j \le n \tag{6}$$

2.3 *The index to the reliability of the MSS*

It thinks about the following three as an index of the reliability of MSS.

1. Availability
2. Steady state expected performance rate
3. Steady state performance deficiency

When availability and steady state performance deficiency are calculated, the regulated performance demonstrating rate is necessary. The regulated performance demonstrating rate usually shows by w, and is a value of 1.0 or less.

(1) *Availability*

Availability can be shown as follows when the number of states is k regulations performance demonstrating rates w at the probability of securing of the system regulated performance demonstrating rate w or more and operating.

$$A(w) = \sum_{k=1}^{K} P_k 1(g_k \ge w) = \sum_{g_k \ge w} p_k \tag{7}$$

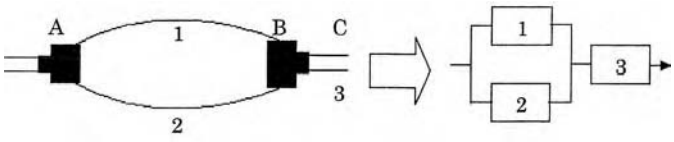

Figure 1. Fluid pipe system.

where $p_k = \lim_{t\to\infty} p_k(t)$ is the steady state probability of the MSS state k with the corresponding output performance rate g_k.

(2) *Steady state expected performance rate*
Steady state expected performance rate is an expected value of the demonstrating performance in the stationary state. The expected value of the performance demonstrating rate at time t of MSS is as follows.

$$E_t = E[G(t)] = \frac{1}{T}\sum_{t=1}^{T} G(t)$$

If the long-run probabilities $p_k = \lim_{t\to\infty} p_k(t)$ exist, the *steady-state expected performance takes the form:*

$$E_\infty = \sum_{k=1}^{K} p_k g_k \tag{8}$$

(3) *Steady state performance deficiency*
Steady state performance deficiency is the one that how performance shortage was seen from the regulated performance demonstrating rate was shown by the expected value. When MSS is a stationary state, steady state performance deficiency is as follows.

$$D_\infty(w) = \sum_{k=1}^{K} p_k \max(w - g_k, 0) \tag{9}$$

3 EXAMPLE OF EVALUATING PERFORMANCE OF MSS BY FLUID PIPE SYSTEM

It explains fluid pipe system shown in Figure 1 as an example about $G(t)$ that is the performance demonstrating rate of the entire system.

The fluid is transmitted from point A to point C. The pipes performance is measured by their transmission capacity (ton per minute).

3.1 *Performance rate of the fluid pipe system*

Elements 1 and 2 are binary. A state of total failure for both elements corresponds to a transmission capacity of 0 and the operational state corresponds to the capacities of the elements 1.5 and 2 ton per minute respectively so that $G_1(t) = \{0,1.5\}, G_2(t) = \{0,2\}$. Element 3 can be in one of three states: a state of total failure corresponding to a capacity of 0, a state of partial failure corresponding to a capacity of 1.8 tons per minute and a fully operational state with a capacity of 4 tons per minute so that $G_3(t) = \{0,1.8,4\}$. The system output performance rate is defined as the maximum flow that can be transmitted from A to C. The total flow between points A and B through the parallel pipes 1 and 2 is equal to the sum of the flows through each of these pipes. The flow from point B to point C is limited by the transmitting capacity of element 3. On the other hand, this flow

Table 1. Performance table of the fluid pipe system.

$G_1(t)$	$G_2(t)$	$G_3(t)$	$\phi(G_1(t),G_2(t),G_3(t))$	$G_1(t)$	$G_2(t)$	$G_3(t)$	$\phi(G_1(t),G_2(t),G_3(t))$
0	0	0	0	1.5	0	0	0
0	0	1.8	0	1.5	0	1.8	1.5
0	0	4	0	1.5	0	4	1.5
0	2	0	0	1.5	2	0	0
0	2	1.8	1.8	1.5	2	1.8	1.8
0	2	4	2	1.5	2	4	3.5

cannot be greater than the flow between points A and B. Therefore, the flow between points A and C (the system performance) is $G(t) = \phi(G_1(t),G_2(t),G_3(t)) = min\{G_1(t) + G_2(t),G3(t)\}$. The values of the system structure function $G(t) = \phi(G_1(t),G_2(t),G_3(t))$ for all the possible system states are presented in Table 1. The performance demonstrating rate of the entire system of this system is as follows.

$$G(t) = \{0\ ,\ 1.5\ ,\ 1.8\ ,\ 2\ ,\ 3.5\}$$

Even if it is the same performance demonstrating rate, the state of each element can be called this system MSS as the result because of the existence of a different case that has the performance demonstrating rate in 12 states.

3.2 *Reliability index of the fluid pipe system*

The state probability corresponding to each performance demonstrating rate of three Pipes elements in the above-mentioned fluid pipe system is assumed to be as follows.

$$P_1(t)=\{0.1\ ,\ 0.9\}\ ,\ P_2(t)=\{0.1\ ,\ 0.9\}\ ,\ P_3(t)=\{0.1\ ,0.2\ ,\ 0.7\}$$

Then, the probability of entering the state of 12 shown in Table 1 reaches the following values in each order.

$$0.001\ ,\ 0.002\ ,\ 0.007\ ,\ 0.009\ ,\ 0.018\ ,\ 0.063\ ,\ 0.009\ ,\ 0.018\ ,\ 0.063\ ,\ 0.081\ ,\ 0.162\ ,\ 0.567$$

Therefore, state probability $P(t)$ corresponding to performance demonstrating rate $G(t) = \{0\ ,\ 1.5\ ,\ 1.8\ ,\ 2\ ,\ 3.5\}$ of the entire system reaches the following values.

$$P(t)=\{0.109\ ,\ 0.081\ ,\ 0.180\ ,\ 0.063\ ,\ 0.567\}$$

Therefore, the index of the reliability of MSS is appreciable as follows by the use of the performance distribution of this system ($G(t)$, $P(t)$).

(1) *Availability*
As follows calculably from expression (7) when the regulated performance demonstrating rate is assumed to be $w = 1.9$.

$$A(w) = A(1.9)= 0.063 + 0.567 = 0.630$$

(2) *Steady state expected performance rate*
Steady state expected performance rate calculates from expression (8) as follows.

$$E_\infty = 0\times0.109 + 1.5\times0.081 + 1.8\times0.180 + 2\times0.063 + 3.5\times0.567 = 2.556$$

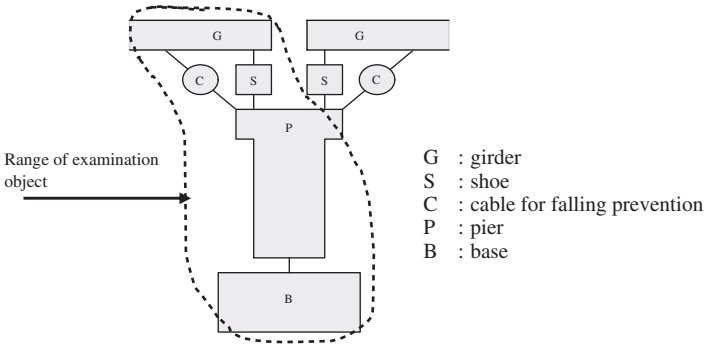

Figure 2. An elevated bridge structural system model.

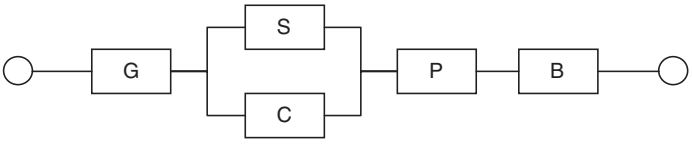

Figure 3. The structured system model.

(3) *Steady state performance deficiency*

As follows calculably from Steady state performance deficiency type (9) when the regulated performance demonstrating rate is assumed to be $w = 1.9$.

$$D_{\infty}(w) = D_{\infty}(1.9) = 0.109\times1.9 + 0.081\times0.4 + 0.180\times0.1 = 0.2575$$

4 SEISMIC PERFORMANCE EVALUATION OF HIGHWAY BRIDGE BASED ON MSS

4.1 *Modeling of bridge system*

Figure 2 shows the concept chart of the structural system that the examination targeted.

This structural system is a series system composed of the combination of two or more structural elements. Then, this structural system is modeled by combining a simple series system and the parallel system shown in Figure 3. And, seismic resistance of the entire system based on MSS is evaluated.

4.2 *Performance demonstrating rate of system and trial calculation of state probability*

(1) *Performance demonstrating rate and state probability of each structural element*

The performance demonstrating rate and the state probability of each structural element assume the value indicated in Table 2.

A basic idea of the performance demonstrating rate of each structural element is as follows.

A partial breakdown was not assumed because a past earthquake damage case was considered to the performance demonstrating rate of the girder and the base, and two states were assumed.

A performance demonstrating rate that was bigger than the performance demonstrating rate at which the part of shoe broke down was assumed to cable for falling prevention between shoe and cable for falling prevention in consideration of the weight putting on the function.

When the pier collapses, the function of the bridge is lost even if cable for falling prevention functions. Therefore, the performance demonstrating rate of pier assumed a performance

Table 2. Performance demonstrating rate and State probability.

Structural element	G(t)	P(t)
Girder	$G_G(t) = \{0, 1\}$	$P_G(t) = \{0.01, 0.99\}$
Shoe	$G_S(t) = \{0, 0.5, 1\}$	$P_S(t) = \{0.1, 0.5, 0.4\}$
Cable for falling prevention	$G_C(t) = \{0, 0.8, 1\}$	$P_C(t) = \{0.1, 0.5, 0.4\}$
Pier	$G_P(t) = \{0, 0.9, 1\}$	$P_P(t) = \{0.01, 0.05, 0.94\}$
Base	$G_B(t) = \{0, 1\}$	$P_B(t) = \{0.01, 0.99\}$

Table 3. Performance table of the shoe and cable for falling prevention.

Gs(t)	Gc(t)	ϕ (Gs(t), Gc(t))	P(t)
0	0	0	0.01
0	0.8	0.8	0.05
0	1	1	0.04
0.5	0	0.5	0.05
0.5	0.8	1.3	0.25
0.5	1	1.5	0.20
1	0	1	0.04
1	0.8	1.8	0.20
1	1	2	0.16

demonstrating rate that was larger than the performance demonstrating rate at which the part of cable for falling prevention broke down.

The state probability corresponding to the performance demonstrating rate of each structural element is assumed as follows. It explains the meaning of the state probability as an example of the case of shoe. The generation probability in the state that shoe doesn't function completely assumes and the generation probability of 0.1 and breaking down the part assumes that the generation probability in 0.5 and the state that functions completely is 0.4. Therefore, the generation probability in the state that doesn't function completely in the girder and the base means the idea as almost 0.

(2) *Performance demonstrating rate and state probability of shoe and cable for falling prevention (parallel system)*

The performance demonstrating rate and the state probability of the parallel system composed of shoe and cable for falling prevention become it as shown in Table 3.

The performance demonstrating rate and the state probability of the entire this system are as follows.

Performance demonstrating rate : $G(t)=\{0,\ 0.5,\ 0.8,\ 1.0,\ 1.3,\ 1.5,\ 1.8,\ 2.0\}$
State probability : $P(t)=\{0.01,\ 0.05,\ 0.05,\ 0.08,\ 0.25,\ 0.20,\ 0.20,\ 0.16\}$

(3) *Performance demonstrating rate and state probability of the entire structural system (series system)*

The performance demonstrating rate concerning all states that can be the combinations it becomes becoming of each structural element as shown in Table 4.The performance demonstrating rate and the state probability of the entire this system are as follows.

Performance demonstrating rate : $G(t)=\{0,\ 0.5,\ 0.8,\ 0.9,\ 1.0\}$
State probability : $P(t)=\{0.039,\ 0.049,\ 0.049,\ 0.044,\ 0.820\}$

Table 4. Performance table of the entire structural system.

G_G(t)	G_{SC}(t)	G_P(t)	G_B(t)	ϕ (G, SC,P,B) = min(G,SC,P,B)	p(G,SC,P,B)	G_G(t)	G_{SC}(t)	G_P(t)	G_B(t)	ϕ (G, SC,P,B) = min(G,SC,P,B)	p(G,SC,P,B)
0	0	0	0	0	1.00E−08	1	0	0	0	0	9.90E−07
0	0	0	1	0	9.90E−07	1	0	0	1	0	9.80E−05
0	0	0.9	0	0	5.00E−08	1	0	0.9	0	0	4.95E−06
0	0	0.9	1	0	4.95E−06	1	0	0.9	1	0	4.90E−04
0	0	1	0	0	9.40E−07	1	0	1	0	0	9.31E−05
0	0	1	1	0	9.31E−05	1	0	1	1	0	9.21E−03
0	0.5	0	0	0	5.00E−08	1	0.5	0	0	0	4.95E−06
0	0.5	0	1	0	4.95E−06	1	0.5	0	1	0	4.90E−04
0	0.5	0.9	0	0	2.50E−07	1	0.5	0.9	0	0	2.48E−05
0	0.5	0.9	1	0	2.48E−05	1	0.5	0.9	1	0.5	2.45E−03
0	0.5	1	0	0	4.70E−06	1	0.5	1	0	0	4.65E−04
0	0.5	1	1	0	4.65E−04	1	0.5	1	1	0.5	4.61E−02
0	0.8	0	0	0	5.00E−08	1	0.8	0	0	0	4.95E−06
0	0.8	0	1	0	4.95E−06	1	0.8	0	1	0	4.90E−04
0	0.8	0.9	0	0	2.50E−07	1	0.8	0.9	0	0	2.48E−05
0	0.8	0.9	1	0	2.48E−05	1	0.8	0.9	1	0.8	2.45E−03
0	0.8	1	0	0	4.70E−06	1	0.8	1	0	0	4.65E−04
0	0.8	1	1	0	4.65E−04	1	0.8	1	1	0.8	4.61E−02
0	1	0	0	0	8.00E−08	1	1	0	0	0	7.92E−06
0	1	0	1	0	7.92E−06	1	1	0	1	0	7.84E−04
0	1	0.9	0	0	4.00E−07	1	1	0.9	0	0	3.96E−05
0	1	0.9	1	0	3.96E−05	1	1	0.9	1	0.9	3.92E−03
0	1	1	0	0	7.52E−06	1	1	1	0	0	7.44E−04
0	1	1	1	0	7.44E−04	1	1	1	1	1	7.37E−02
0	1.3	0	0	0	2.50E−07	1	1.3	0	0	0	2.48E−05
0	1.3	0	1	0	2.48E−05	1	1.3	0	1	0	2.45E−03
0	1.3	0.9	0	0	1.25E−06	1	1.3	0.9	0	0	1.24E−04
0	1.3	0.9	1	0	1.24E−04	1	1.3	0.9	1	0.9	1.23E−02
0	1.3	1	0	0	2.35E−05	1	1.3	1	0	0	2.33E−03
0	1.3	1	1	0	2.33E−03	1	1.3	1	1	1	2.30E−01
0	1.5	0	0	0	2.00E−07	1	1.5	0	0	0	1.98E−05
0	1.5	0	1	0	1.98E−05	1	1.5	0	1	0	1.96E−03
0	1.5	0.9	0	0	1.00E−06	1	1.5	0.9	0	0	9.90E−05
0	1.5	0.9	1	0	9.90E−05	1	1.5	0.9	1	0.9	9.80E−03
0	1.5	1	0	0	1.88E−05	1	1.5	1	0	0	1.86E−03
0	1.5	1	1	0	1.86E−03	1	1.5	1	1	1	1.84E−01
0	1.8	0	0	0	2.00E−07	1	1.8	0	0	0	1.98E−05
0	1.8	0	1	0	1.98E−05	1	1.8	0	1	0	1.96E−03
0	1.8	0.9	0	0	1.00E−06	1	1.8	0.9	0	0	9.90E−05
0	1.8	0.9	1	0	9.90E−05	1	1.8	0.9	1	0.9	9.80E−03
0	1.8	1	0	0	1.88E−05	1	1.8	1	0	0	1.86E−03
0	1.8	1	1	0	1.86E−03	1	1.8	1	1	1	1.84E−01
0	2	0	0	0	1.60E−07	1	2	0	0	0	1.58E−05
0	2	0	1	0	1.58E−05	1	2	0	1	0	1.57E−03
0	2	0.9	0	0	8.00E−07	1	2	0.9	0	0	7.92E−05
0	2	0.9	1	0	7.92E−05	1	2	0.9	1	0.9	7.84E−03
0	2	1	0	0	1.50E−05	1	2	1	0	0	1.49E−03
0	2	1	1	0	1.49E−03	1	2	1	1	1	1.47E−01

The point to have to pay attention here is that the state to exceed 1.0 doesn't exist at the performance demonstrating rate of the entire structural system. Even if the performance of an individual element is high, this means the performance cannot be demonstrated enough for the entire system.

Table 5. Performance demonstrating rate and State probability.

Structural element	G(t)	P(t)
Girder	$G_G(t) = \{0, 1\}$	$P_G(t) = \{0.01, 0.99\}$
Shoe	$G_S(t) = \{0, 1\}$	$P_S(t) = \{0.1, 0.9\}$
Cable for falling prevention	$G_C(t) = \{0, 1\}$	$P_C(t) = \{0.1, 0.9\}$
Pier	$G_P(t) = \{0, 1\}$	$P_P(t) = \{0.01, 0.99\}$
Base	$G_B(t) = \{0, 1\}$	$P_B(t) = \{0.01, 0.99\}$

Table 6. Comparison of system performance indices.

	MSS	Binary system
A(0.5)	0.962	–
A(0.8)	0.913	–
A(0.9)	0.864	–
A(1.0)	0.820	0.961
E_∞	0.922	0.961
$D_\infty(0.5)$	0.0197	0.0197
$D_\infty(0.8)$	0.0461	0.0315
$D_\infty(0.9)$	0.0597	0.0355
$D_\infty(1.0)$	0.0777	0.0394

4.3 *Reliability index of the entire structural system*

(1) *Availability*

When the regulated performance demonstrating rate of the entire system is assumed to be w = 0.5, 0.8, and 0.9, Availability:

$$A(w) = A(0.5) = 0.049 + 0.049 + 0.044 + 0.820 = 0.962$$
$$A(w) = A(0.8) = 0.049 + 0.044 + 0.820 = 0.913$$
$$A(w) = A(0.9) = 0.044 + 0.820 = 0.864$$

(2) *Steady state expected performance rate*

$$E_\infty = 0 \times 0.039 + 0.5 \times 0.049 + 0.8 \times 0.049 + 0.9 \times 0.044 + 1.0 \times 0.820 = 0.922$$

(3) *Steady state performance deficiency*

When the regulated performance demonstrating rate of the entire system is assumed to be $w = 0.5$, 0.8, and 0.9, Steady state performance deficiency:

$$D_\infty(w) = D_\infty(0.5) = 0.039 \times 0.5 + 0.049 \times 0 + 0.049 \times 0 + 0.044 \times 0 + 0.820 \times 0 = 0.0195$$
$$D_\infty(w) = D_\infty(0.8) = 0.039 \times 0.8 + 0.049 \times 0.3 + 0.049 \times 0 + 0.044 \times 0 + 0.820 \times 0 = 0.0459$$
$$D_\infty(w) = D_\infty(0.9) = 0.039 \times 0.9 + 0.049 \times 0.4 + 0.049 \times 0.1 + 0.044 \times 0 + 0.820 \times 0 = 0.0596$$

(4) *System reliability of binary system*

A structural system collectively shows the system reliability when it is a case of the binary system and MSS in Table 6. The performance demonstrating rate and the state probability of each structural element in the binary system were risked as shown in Table 5.

The regulated performance demonstrating rate in MSS understands utilization rates in the state that the binary system functions completely from Table 6 and it is understood that it is almost equal at the time of $w = 0.5$.Moreover, steady state expected performance rate of

the binary system comes to evaluate it more excessive than MSS. On the other hand, steady state performance deficiency of the binary system comes to evaluate it more underestimating than MSS.

MSS showed the possibility to be able to become a new evaluation technique for having both the rationality and the explanation more than past system reliability in evaluating a seismic performance of a structural system.

5 CONCLUSION AND FUTURE PROBLEM

The conclusion of this study is as follows.

1. The MSS concept is introduced into the evaluation of seismic performance of entire system of bridge structure.
2. The degree of damage is modeled by a new measure such as a performance rate with a state probability, and the seismic performance level of the entire system of bridge structure consisted of girder, shoe, cable for falling prevention, pier and base is evaluated.

MSS suggests becoming an effective method as a new performance evaluation technique in the performance design in the future. On the other hand, the point that should be stuffed has been left in the weight putting between a numerical value and structural element concreting etc. a lot. Especially, the arrangement of the relation between the cost balance and the weight putting is matters of weight that cannot steer around, and in the future, problem. In addition, to discuss it with generality or more continuously in the future about "Optimization of the damage distribution", I want to advance the examination.

REFERENCES

CEN. (1999). Draft EN 1990 Euro code 0 Basis of design.

ISO. (1998). International Standard ISO/DIN 2394, General principles on reliability for structures.

Japan Road Association. (2002). Specifications for highway bridge part V; Seismic design.

Lisnianski, A. and Levitin G. (2003). Multi-state System Reliability – Assessment, Optimization and Applications -, *World Scientific*.

Shouji, M. Fujino, Y. and Abe, M. (1997.4.). Attempt of optimization of damage distribution at earthquake of elevated highway bridge system, *Japan Society of Civil Engineers Thesis collection*, No.563/I-39, pp. 79–94.

Japan Association for Earthquake Engineering. (2006.6). Performance regulations seismic designs, pp. 6–10.

Kawashima, K. (1998). Seismic design and performance criteria of bridge, *Japan Society of Civil Engineers,The 10th Japanese earthquake engineering symposium panel discussion material collection*, pp. 159–162.

Japan Society of Civil Engineers Kansai branch, (2001.7). Surveillance study on buffer type falling prevention of bridge system, Course text, pp. 4–18.

Japan Road Association. (2002). Road earthquake measures handbook (Chapter of earthquake disaster reconstruction), pp. 86–113.

Reliability and Optimization of Structural Systems: Assessment, Design and Life-Cycle Performance – Frangopol, Kawatani & Kim (eds)
© 2007 Taylor & Francis Group, London, ISBN 978-0-415-40655-0

Optimal condition control of systems comprised of multiple homogenous components

K. Nishijima & M.H. Faber
Institute of Structural Engineering, ETH Zurich, Switzerland

ABSTRACT: The optimization of the condition control of engineering systems which are comprised of a large number of homogenous components is considered. Since it is not feasible to inspect all components in such systems, the decisions for maintenance activities must be based on inspection results of a limited number of components. In this connection the decision criteria in regard to how much information is sufficient and in regard to which maintenance activities to pursue, are of particular interest. In the present paper, a Bayesian approach is proposed for identifying a criterion for how much information is sufficient and optimal to support decision making in regard to maintenance activities, employing the theory of sequential decision making. Two examples are given to illustrate how the proposed approach may be implemented into practical applications.

1 INTRODUCTION

Maintenance of engineered systems comprised of a large number of components constitutes a significant challenge in regard to optimal inspection planning. Such systems are e.g. fasteners in facade systems, anchors of retaining walls, rivets in riveted connections, riser attachments of offshore platform and railroad supports in railway systems. Since condition control of such systems often are associated with significant efforts in terms of costs and possible undesirable interruptions of operation, the decisions for maintenance activities, such as repair, exchange or replacement should be optimized, i.e. it would be desirable to identify a strategy for the assessment of the inspection and maintenance activities fulfilling given requirements to safety or risks. A general framework for the solution of such problems may be found in risk based inspection planning (RBI). Following this framework the expected total costs including inspection costs, possible maintenance costs and possible future failure costs are minimized by appropriate selection of e.g. inspection method, inspection frequency, inspection coverage and repair strategies. In the context of the inspection and maintenance planning for engineered systems containing a large number of components, the optimization by RBI aims to identify also the locations and the number of components to be inspected. Whereas the temporal aspects of the inspection planning, e.g., inspection frequency, has been investigated at depth, so far only a few studies have focused on the spatial aspects of the inspection, e.g. the location and the number of the components to be inspected, see e.g. Faber et al. (1992), Faber and Sørensen (2002), Straub and Faber (2005) and Faber et al. (2006). Presently the spatial aspects of inspection planning are approached rather differently in different application areas, and a general and consistent approach has not yet been identified. In Nishijima and Faber (2006) the special problem of optimal proof load testing for condition assessment of engineered systems comprised of a large number of components is considered, although the proposed approach can be extended to other type of inspection methods. The approach taken there is to apply Bayesian updating of common uncertainties, i.e. uncertainties which affect all components in the considered system. Separating the uncertainties which relate only to each individual component from the common uncertainties, the information in regard to the condition states of inspected components can be utilized to update the common uncertainty and thereby to (re-)assess the condition state of the entire system.

The problem discussed in the present paper is similar to that of Nishijima and Faber (2006), however, it differs in the sense that the inspection result of one component is attempted utilized to make a decision on whether additional inspections should be made. In Nishijima and Faber (2006) it is assumed that the inspections of a planned number of components are made "simultaneously" thus the results of inspections which in practice are obtained in a sequence are not utilized to decide if the results of the already performed inspections are sufficient as a basis for accepting the systems as it is or for the implementation of repair and/or maintenance activities. This assumption is reasonable in the situation where e.g. the samples taken from the components must be analyzed at a different place, e.g. laboratory. In principle, however, whenever the inspection results of already inspected components are available in the condition assessment, these results can and should be utilized to support decision making in regard to whether additional inspections are needed. The approach in the present paper is advantageous especially in the case where the marginal inspection costs are relatively high. In general, by considering the inspection results of already inspected components it is anticipated that the (expected) inspection cost is smaller than otherwise.

In the following first the problem framework is provided clearly specifying the information which must be available in regard to the quality of inspection methods in order to facilitate the optimization of inspection and maintenance activities. Appreciating the generic nature of the approach, the proposed approach allows also for comparing the efficiency of different inspection methods in a consistent way. The theory adopted in the present paper takes its roots in the field of statistical decision making known as sequential decision making, see e.g. Arrow et al. (1949) and DeGroot (1970). Bayesian statistics and Bayesian updating are utilized in a sequential manner which may in fact be considered as an application of pre-posterior analysis, see Raiffa and Schlaifer (1961). Secondly the general solution of sequential decision problems which is necessary for the optimal planning of inspections for the considered type of engineered systems is outlined and finally two illustrative examples are given to show how the proposed approach can be implemented into practical situations.

2 CONDITION ASSESSMENT

2.1 *Problem setting*

The aim of the condition assessment of engineered systems comprised of a large number of semi-identical components is to facilitate the quantification of the reliability of all the individual components of the system based on inspection results of only a selected number of the components. This in turn provides a basis for decision making in regard to repair, exchange and future maintenance activities for the overall system. The uncertainty associated with the state of each component is assumed to consist of individual uncertainties, i.e. uncertainties which are only associated with the individual components, and common uncertainties, i.e. uncertainties which are common for all components of the system. The individual uncertainties may correspond to uncertainties associated with e.g. the material properties and the geometrical characteristics of the individual components and may be assumed to be statistically independent from component to component. The common uncertainties may be associated with e.g. modeling uncertainties due to idealizations in the representation of limit state functions or statistical uncertainties due to lack of information. Updating of the common uncertainties based on inspection of selected individual components provides a basis for updating the reliability of non-inspected components and this is the perspective taken in the following. The role of inspection in this context is to collect enough information on the states of components to support optimal decision making in regard to the necessity for further inspections and maintenance activities for the overall system, such that total expected costs are minimized, or more generally an appropriately selected objective function is maximized. Whereas it is not possible to reduce, by inspection, the risk associated with aleatory uncertainty, e.g. future exposure and deterioration, it is, in principle, possible to reduce the risk associated with epistemic uncertainty. In fact, if the states of all components in an engineered system were perfectly known

(no epistemic uncertainty), the best maintenance activity could be properly chosen in accordance with the minimization of the expected total costs which is associated only with aleatory uncertainty. However, since there exists epistemic uncertainty in practical situations, additional costs, or a "penalty due to the possible incorrect assumption", must be taken into account in the optimization of inspection planning and maintenance activities. Seen in this light, an inspection is worthwhile to undertake only if the expected reduction of the "penalty" compensates the cost of an inspection. Thus, the decision maker needs to reconsider, every time a new inspection result is obtained, (1) if an additional inspection is beneficial, and (2) if it is not, the sequence of inspections is terminated and the best action must be chosen from a set of possible maintenance actions. The mathematical formulation of this decision framework is given in the subsequent section.

2.2 *Formulation*

The state of each component in an engineered system is assumed to be characterized by a random parameter, or a random vector, Θ which affects all the components of the system. The probability density function of the components of Θ is denoted by $\xi(\theta)$ or ξ. In the present paper it is assumed that all random variables are continuous unless otherwise mentioned, however, it is possible to apply the general methodology also for discrete variables with minor modifications.

The present approach requires the following information is available:

- Decision space: $D = \{d_0\} \cup D'$
- Parameter space: Ω
- Space of possible inspection results: Ξ
- Likelihood function: $p(z \mid \theta)$
- Inspection cost per component: c
- Loss function: $L(\theta, d)$

The decision space D here consists of the option that an additional inspection is made (d_0), and the options on repair and maintenance ($d \in D'$, where D' is the decision set which are relevant in case it is decided not to inspect further). The parameter space Ω is the space in which θ can take a value. The space of the possible inspection results Ξ depends on the inspection method used. The likelihood function $p(z \mid \theta)$, i.e. the conditional probability density function of the inspection result $z \in \Xi$ for a given parameter $\theta \in \Omega$ must also be given. The likelihood function quantitatively specifies the quality of the inspection method. The cost per inspection c also depends on the inspection method. It is assumed that the inspection cost per component is constant, and that the inspection results z at each inspection are conditionally independent given the parameter θ. The loss function $L(\theta, d)$ specifies the loss derived from the decision $d \in D'$ and the parameter θ given that an additional inspection is not made.

In order to identify the optimal decision at any given phase i.e. between any given two inspections, all possible future observations by inspections and the following optimal decisions must be taken into account. However, it turns out that the optimal decision $d^* \in D$ is identified as a function only of ξ, regardless of the number of inspections already made in the condition assessment. Namely,

$$d^* = \delta(\xi) \tag{1}$$

where $\delta(\cdot)$ is a decision rule which specifies the optimal decision from the decision space D. Whereas the probability density function of θ at a future inspection is updated with the corresponding inspection results, and is no more identical to the initial one, the optimal decision can still be made in accordance with the same decision rule (Equation (1)), since it provides the optimal decision for all possible cases of ξ. In this way, all future optimal decisions are already taken into account in the decision rule $\delta(\cdot)$. Thus, the problem is reduced to identify the decision rule $\delta(\cdot)$ as a function of ξ. The procedure to identify the decision rule $\delta(\cdot)$ is given in the next section in accordance with the sequential decision theory, see e.g. DeGroot (1970).

2.3 *Solution*

Let $\rho^*(\xi)$ be the minimized expected total cost, including the expected future inspection cost and the expected loss, which corresponds to the optimal decision d^* under the situation where the probability density function is ξ. Let $\xi(\cdot \mid Z)$ be the posterior probability density function conditional of the inspection result Z, which is calculated for each given realization z as:

$$\xi''(\theta \mid z) \propto p(z \mid \theta)\xi'(\theta) \tag{2}$$

where $\xi'(\cdot)$ and $\xi''(\cdot)$ represent the prior and posterior density functions of Θ respectively. Since the optimal decision should correspond to the smallest of either (1) the expected total cost when an additional inspection is made, or (2) the expected loss when no more inspections are made, the minimized expected cost $\rho^*(\xi)$ must satisfy the following equation:

$$\rho^*(\xi) = \min\left\{E[\rho^*(\xi(\cdot \mid Z))] + c,\ r(\xi)\right\} \tag{3}$$

where $r(\xi)$ is the minimized expected cost given that no further inspections are performed, i.e.,

$$r(\xi) = \min_{d \in D'} \int L(\theta, d)\xi(\theta)d\theta \tag{4}$$

The expectation in Equation (3) is made with respect to the prior probability density function of Θ and Z:

$$E[\rho^*(\xi(\cdot \mid Z))] = \int \rho^*(\xi(z)) \int p(z \mid \theta)\xi(\theta)d\theta dz \tag{5}$$

Equation (3) may be solved approximately by the following recursive formulation:

$$\gamma_{n+1}(\xi) = \min\left\{E[\gamma_n(\xi(\cdot \mid Z))] + c,\ r(\xi)\right\} \tag{6}$$

and

$$\lim_{n \to \infty} \gamma_n(\xi) = \rho^*(\xi) \tag{7}$$

under the conditions discussed in DeGroot (1970). These conditions are interpreted in the application of inspection planning as; given enough inspection results, a best decision can be chosen such that the expected loss is equal to zero. Finally, the decision rule $\delta(\cdot)$ is identified as:

$$\delta(\xi) = \begin{cases} d_0, & \left\{\xi \mid \rho^*(\xi) \neq r(\xi)\right\} \\ \arg\min_{d \in D'} \int L(\theta, d)\xi(\theta)d\theta, & \left\{\xi \mid \rho^*(\xi) = r(\xi)\right\} \end{cases} \tag{8}$$

where the operator "arg min" returns the variable which minimizes the objective function.

3 EXAMPLES

3.1 *Example 1*

The first example considers a hypothetical condition assessment with the purpose to illustrate the application of the proposed approach. It is assumed that two inspection methods (method *A* and *B*) are available, which are characterized by different inspection costs c_A and c_B, and different likelihood functions $p_A(z \mid \theta)$ and $p_B(z \mid \theta)$ respectively, see Table 1. The decision in regard to possible repair actions must be made in correspondence with the possibilities represented by the decision

Table 1. Characteristics of two inspection methods.

Inspection method	Inspection cost c	Possible inspection results Ξ	Likelihood function $p(z \mid \theta)$		
A	$c_A = 1$	$\Xi^A = \{z_1^A, z_2^A\}$		θ_1	θ_2
			z_1^A	0.8	0.3
			z_2^A	0.2	0.7
B	$c_B = 2$	$\Xi^B = \{z_1^B, z_2^B\}$		θ_1	θ_2
			z_1^B	0.9	0.2
			z_2^B	0.1	0.8

set $D' = \{d_1, d_2\}$. The state of the considered engineered system is represented by the parameters $\theta \in \Omega = \{\theta_1, \theta_2\}$, characterized by the probability mass function ξ: $\xi(\theta_1) = \pi$ and $\xi(\theta_2) = 1 - \pi$, $(0 \le \pi \le 1)$, where π is the probability or the degree of belief that θ_1 is true. Prior to the decision making in regard to repair actions, the decision maker can make an additional inspection (d_0) to reduce the uncertainty of the parameters $\theta \in \Omega = \{\theta_1, \theta_2\}$. The loss function is assumed to be given as:

$$L(\theta, d) = \begin{cases} 0, & (\theta, d) = (\theta_1, d_1), (\theta_2, d_2) \\ 10, & (\theta, d) = (\theta_1, d_2) \\ 20, & (\theta, d) = (\theta_2, d_1) \end{cases} \tag{9}$$

For the present example Equations (2)–(5) may be written as:

$$\pi(z) = \frac{p_{X}(z \mid \theta_1)\pi}{p_{X}(z \mid \theta_1)\pi + p_{X}(z \mid \theta_2)(1-\pi)}, \ (z \in \Xi^{X}) \tag{10}$$

$$\rho^{X^*}(\pi) = \min\left\{E[\rho^{X^*}(\pi(Z))] + c_{X},\ r(\pi)\right\} \tag{11}$$

$$r(\pi) = \min\left\{10(1-\pi),\ 20\pi\right\}, \quad (0 \le \pi \le 1) \tag{12}$$

$$\begin{aligned} E[\rho^{X^*}(\pi(Z))] = {} & \rho^{X^*}(\pi(z_1^{X})) \cdot \left[p_{X}(z_1^{X} \mid \theta_1)\pi + p_{X}(z_1^{X} \mid \theta_2)(1-\pi) \right] \\ & + \rho^{X^*}(\pi(z_2^{X})) \cdot \left[p_{X}(z_2^{X} \mid \theta_1)\pi + p_{X}(z_2^{X} \mid \theta_2)(1-\pi) \right] \end{aligned} \tag{13}$$

where X stands for A and B.

The approximate solutions of Equation (11) for $\rho^{A^*}(\pi)$ and $\rho^{B^*}(\pi)$ are obtained in accordance with Equation (6) and (7), and the results are shown in Figure 1. From Figure 1 (left) it is seen that in the case of inspection A, an inspection should be made if and only if π is between 0.392 and 0.843. Whenever π falls in the interval of $[0, 0.392]$, the inspection should be terminated and the decision d_2 should be made. This is because the expected loss when d_2 is chosen is smaller than the expected loss when d_1 is chosen, i.e. $20\pi < 10(1-\pi)$. On the other hand, whenever π falls in the interval of $(0.843, 1]$, the sequence of inspections should be terminated and the decision d_1 should be made. This can be interpreted as the stopping rule for the sequence of inspections in the condition assessment. For instance, if the prior probability of π is 0.5, then at least one inspection should be made. π is updated based on the outcome of the inspection in accordance with Equation (10). Inspections should be continued until π falls outside of the interval of $(0.392, 0.843]$. Comparing the expected total costs associated with inspection A and B, the decision rule for the choice of the inspection method prior to condition assessment is identified as:

- If $0 \le \pi \le 0.392$, then the decision d_2 should be made without any inspection.
- If $0.392 < \pi \le 0.577$ or $0.773 < \pi \le 0.843$, then inspection method A should be adopted.

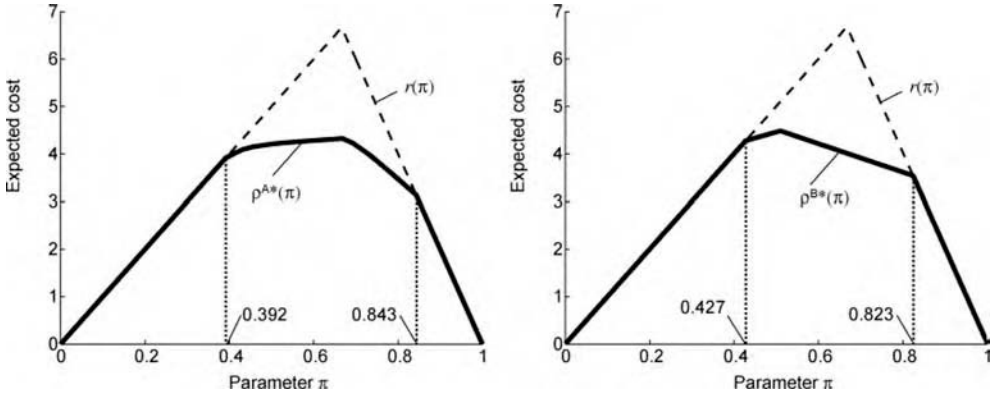

Figure 1. Minimized total costs $\rho^{A^*}(\pi)$ and $\rho^{B^*}(\pi)$ for inspection method A (left) and B (right).

- If $0.577 < \pi \leq 0.773$, then inspection method B should be adopted.
- If $0.843 < \pi \leq 1$, then the decision d_1 should be made without any inspection.

It should be mentioned that in the present consideration once the inspection method is chosen the method is assumed not to be changed in the condition assessment.

3.2 *Example 2*

The components in an engineered system are suspected not to fulfill the desired reliability. In order to facilitate the decision making for repair action, the condition assessment is to be planned. The resistances R_i of components ($i = 1, 2, 3, \ldots$) are assumed to be modeled by normally distributed random variables with a mean value equal to Θ and standard deviations equal to one:

$$R_i \overset{d}{\sim} N(\Theta, 1^2) \tag{14}$$

where the parameter Θ represents the common uncertainty. The parameter space is assumed to be equal to the entire real space, i.e. $\Omega = \Re$. The resistance R_i of a component is measured by inspection. The space of possible inspection result is identical to that of the resistance R_i, i.e. $\Xi = \Re$. The likelihood function of the parameter θ given the inspection result r is written as:

$$p(r \mid \theta) = \frac{1}{\sqrt{2\pi}} \exp\left[-\frac{(r-\theta)^2}{2}\right] \tag{15}$$

It is assumed that the parameter Θ prior to the condition assessment follows the normal distribution with the mean μ_0 and the standard deviation σ_0, i.e.:

$$\xi(\theta) = \frac{1}{\sqrt{2\pi}\sigma_0} \exp\left[-\frac{(\theta-\mu_0)^2}{2\sigma_0^{\,2}}\right] \tag{16}$$

The updating of the parameter Θ with the mean μ' and the standard deviation σ' in accordance with Equation (2) implies that the updated parameter with the observation r follows the normal distribution with mean μ'' and standard deviation σ'', where:

$$\mu'' = \frac{\mu' + r\sigma'^2}{1+\sigma'^2} \quad \text{and} \quad \sigma'' = \frac{\sigma'}{\sqrt{1+\sigma'^2}} \tag{17}$$

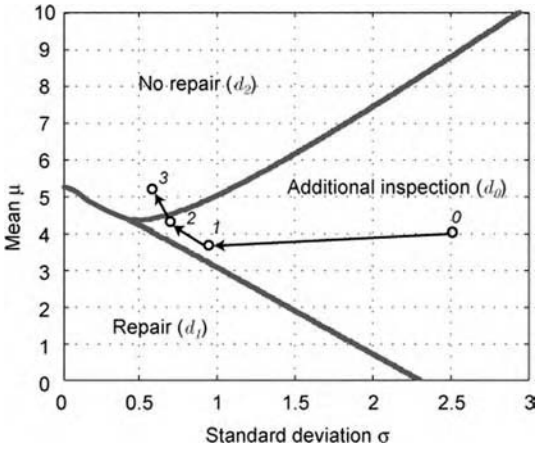

Figure 2. Decision rule for additional inspection (d_0), repair (d_1) and no repair (d_2).

Therefore, the decision rule can be specified as a function of the mean μ and the standard deviation σ of the parameter Θ. In regard to the exposure to the components it is, for illustrational purpose, assumed that the annual maximum load S follows a normal distribution with the mean of zero and unit variance. The set of repair actions, D', is composed of "repair" (d_1) and "no repair" (d_2). The loss function is assumed as:

$$L(\theta,d)=\begin{cases}0, & \{(\theta,d_1)\,|\,p_F(\theta)>p_{acc}\}\cup\{(\theta,d_2)\,|\,p_F(\theta)\le p_{acc}\}\\ c_R, & \{(\theta,d_1)\,|\,p_F(\theta)\le p_{acc}\}\\ \kappa(p_F(\theta)-p_{acc}), & \{(\theta,d_2)\,|\,p_F(\theta)>p_{acc}\}\end{cases} \tag{18}$$

where c_R is the repair cost of the engineered system, and equal to 2000, κ is the cost coefficient and equal to 1000, p_{acc} is the acceptable annual failure probability, here assumed equal to 10^{-4}, and $p_F(\theta)$ is the annual failure probability given θ, written as:

$$p_F(\theta)=P[R_i-S<0\,|\,\theta]=\Phi\left(-\theta/\sqrt{2}\right) \tag{19}$$

The inspection cost per component is assumed to be unity.

Following the procedure presented in Section 2.3, the decision rule $\delta(\sigma, \mu)$ is obtained as is shown in Figure 2. The figure provides the optimal decision depending on the uncertainty of the parameter Θ. For instance, in the case of $(\sigma_0, \mu_0) = (2.5, 4)$ prior to a condition assessment (indexed by 0) the optimal decision is to make an additional inspection since the point belongs to the domain of d_0. If the results of the inspections up to and including the third are 3.5, 5.0 and 7.1 respectively, the mean and the standard deviation of the parameter Θ are updated as shown in Figure 2 (indexed by 1, 2 and 3). It is seen from the figure that additional inspections should be made up to the third time, since the point (σ, μ) falls in the domain of d_0. However, after the third inspection the point (σ, μ) falls in the domain of d_2, therefore, inspections should be terminated and repairs performed according to d_2.

4 DISCUSSIONS

Whereas in the present examples the common uncertainty Θ is characterized by either one or two parameters, in general the characteristics of the probability density function $\xi(\theta)$ cannot be

represented by a few parameters. In these situations, it is not easy to solve the functional Equation (3). The possible strategies are 1) to discretize the parameter space Ω and the probability density function $\xi(\theta)$, 2) to apply the natural conjugate distributions for the likelihood function $p(z \mid \theta)$ and the probability density function $\xi(\theta)$, and 3) to approximate the prior and the posterior density function by the normal probability density function, or by non-normal density functions which are characterized by non-linear transformations from the normal random variables on the basis of information on the statistical moments.

In the present formulation of the approach it is assumed that the correlation between the components in an engineered system is considered though the common parameter Θ. Thus, in the case where the correlation due to e.g. geometry between components is of relevance the present approach cannot be applied. The extension of the approach in this direction is a future task.

It should be mentioned that the inspection method used in a condition assessment can be also interpreted, in the context of the present approach, as a combination of the several inspections. The present approach can be applied also for such inspection methods whenever the inspection result z and the state of the component θ are related though the likelihood function $p(z \mid \theta)$. In cases where the interruption of the operation of the structural system due to the inspection is significant, inspection cost should include the loss associated with the reduced functionality of the structural system due to the inspection.

5 CONCLUSIONS

The optimization of the condition assessment of large-scale engineered systems is considered. In the context of sequential inspections in condition assessment, the optimization problem is reduced to identify the optimal decision rule for stopping the sequence of inspections. The general formulation and procedure to identify the decision rule are presented in accordance with the sequential decision theory. The present approach is generic so that the approach is consistently applicable whenever the necessary information is available. Appreciating the generic nature, the approach can be applied for different inspection methods in a consistent way, which is especially useful when a decision maker has to choose one of several possible inspection methods suitable in a given situation.

Two examples are given to illustrate how the presented approach is implemented. In the first example the procedure to establish the decision rule as well as to compare the efficiencies of two inspection methods are explained. In the second example, it is shown how the obtained decision rule which is represented by a map – the partitions in the parameter space – is utilized in practical situations, emphasizing the advantage of the present approach.

REFERENCES

Arrow, K.J., Blackwell, D. & Girshick, M.A. 1949. Bayes and Minimax Solutions of Sequential Decision Problems. *Econometrica* 17: 213–244.

DeGroot, H. 1970. *Optimal Statistical Decisions*: John Wiley&Sons, Inc.

Faber, M.H. & Sørensen, J.D. 2002. Indicators for Inspection and Maintenance Planning of Concrete Structures. *Structural Safety* 24: 377–396.

Faber, M.H., Sorensen, J.D. & Kroon, I.B. 1992. Optimal inspection strategies for offshore structural systems; *Proceedings of the 11th offshore mechanics and arctic engineering conference, Calgary*.

Faber, M.H., Straub, D. & Maes, M.A. 2006. A Computational Framework for Risk Assessment of RC Structures Using Indicators. *Computer-Aided Civil and Infrastructure Engineering* 21(3): 216–230.

Nishijima, K. & Faber, M.H. 2006. Optimal proof load testing of large quasi-identical component systems; *Second Forum on Engineering Decision Making, IFED, Lake Louise, Canada*, 26–29 April, 2006.

Raiffa, H. & Schlaifer, R. 1961. *Applied Statistical Decision Theory*, Cambridge: Cambridge University Press.

Straub, D. & Faber, M.H. 2005. Risk Based Inspection Planning for Structural Systems. *Structural Safety* 27(4): 335–355.

Reliability and Optimization of Structural Systems: Assessment, Design and Life-Cycle Performance – Frangopol, Kawatani & Kim (eds)
© 2007 Taylor & Francis Group, London, ISBN 978-0-415-40655-0

An investigation on story failure modes of frame structures

Wu-Chuan Pu & Yan-Gang Zhao
Nagoya Institute of Technology, Nagoya, Japan

ABSTRACT: Story failure mode is a structural failure pattern that should be avoided during earthquake excitations. In structural reliability analysis, the story failure mode with the highest occurrence probability is the most significant for its influence on the overall probability of structural failure. The object of this study is to search for the most likely undesirable story failure mode in a probabilistic way. The story failure modes are defined by three patterns: upper story failure pattern, middle story failure pattern and lower story failure pattern. The failure probabilities of story failure modes of multi-story frame structures designed with different column over-design factors are evaluated by FORM, and the comparison of these probabilities is conducted. It is found that for an n-story frame structure there are n story failure modes have likelihood to be the dominant story failure mode, and they are the upper failure mode with $n-1$ failure stories and all the $n-1$ lower story failure modes.

1 INTRODUCTION

As is widely accepted, the entire beam-hinging failure mode, as shown in Figure 1, is the preferable failure pattern of frame structure. Story failure mechanism, in which the plastic hinges develop in the beams and columns of one or a few stories, is a kind of failure pattern that should be avoided to form in structure under earthquake excitations, but inevitably, many cases of story mechanisms can be observed in almost every major earthquake. In deterministic design of frame structures, some preferred failure modes are often selected and the strength of structural members are designed according to the strength requirements of these selected failure modes. In reality, however, the well-designed structure may fail unexpectedly to some undesirable failure modes, such as story mechanisms, due to the uncertainties in member strength and external load (Kuwamura et al. 1989). Since it is impossible to absolutely ensure the structure fail according to the designed failure mode in deterministic meaning, it is essential to identify the likely failure modes and understand the order in which they are likely to occur.

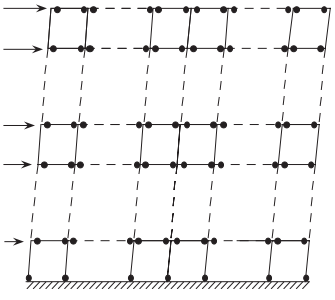

Figure 1. The entire beam-hinging failure mode.

Many methods have been developed by researchers on search of dominant failure mechanisms of frame structures, and basically three main procedures have been made popular for the generation of failure modes: exhaustive enumeration, repeated structural analysis, and optimization (Simoes 1990). Some studies have also been focused on the story failure modes or the damage distribution along the height of frame, for example the study by Ogawa (1983), in which it was indicated that with the increase of the column over-design factor the plastic hinges tend to form in the more stories from the first floor, and to ensure an entire beam-hinging pattern, a quite high column over-design factor is required. In the present paper, the story failure modes are investigated in terms of probabilistic way. The probabilistic orders of story failure modes of frame structure designed under a certain reliability level are investigated through computing and comparing their failure probabilities. The likely story failure modes that are considered dominant for structural reliability and structure design are identified.

2 ANALYSIS ASSUMPTIONS

For the ductile frame structures studied in this paper, all the computations are carried based on the following commonly used assumptions:

(1) Frame structures are with elastic-plastic behavior. The failure of a section means the imposition of a hinge and an artificial moment at this section.
(2) The only structural uncertainty considered is the uncertainty of member strength, the other structural parameters are assumed to be deterministic for a specific structure. The coefficient of variation of moment strength of member is 0.1 (AIJ 1990).
(3) All of the beams and columns are designed to make the structure have the same value of the column over-design factor at each beam-column node. It means there is only one value of column over-design factor for a specific structure.
(4) The external loads are considered to consist of only the static lateral earthquake load, which are assumed to be concentrated forces triangularly distributed along the height of the structures. This assumption is often used in simple seismic design. The coefficient of variation of earthquake load suggested by AIJ (1993) and used in this study is 0.8.
(5) Plastic moment capacities of sections are statistically independent of the applied loads and independent of each other. The entire random variables are lognormal distributed.

3 DEFINITIONS OF STORY FAILURE PATTERNS

Because of the large quantity of the potential story failure modes of a specific multi-story frame, the story failure modes are defined and classified before the probabilistic evaluation so that the investigation can be carried on in each single type. In this study, the definitions of story failure modes are made according to the distribution of the failure stories along the height of frame. Essentially, the story failure mode may develop by one of the three patterns: upper story failure pattern, middle story failure pattern and lower story failure pattern. In upper failure pattern, the plastic hinges form in the columns and beams of one floor and all the beams above this floor; middle story failure pattern features one or several continuous failure stories in the middle of frame, and the top floor and ground floor keep unbroken; lower story failure pattern features one or several continuous failure stories from the ground floor. Figure 2 shows the common form of each story failure pattern, where n_c is the number of the failure stories, n_b is the number of unbroken stories of middle story failure pattern at the bottom of frame.

The performance functions for the three story failure patterns, which will be used in the reliability analysis followed, can be obtained according to the principle of virtual work as:

$$G_U(\mathbf{X}) = 2\sum_{i=1}^{m} M_{bni} + 2\sum_{j=n-n_c+1}^{n-1}\sum_{i=1}^{m} M_{bij} + \sum_{l=1}^{2} M_{csl} + \sum_{l=1}^{m-1} M_{cl} - \sum_{j=n-n_c+1}^{n}(j+n_c-n)hP_j \qquad (1)$$

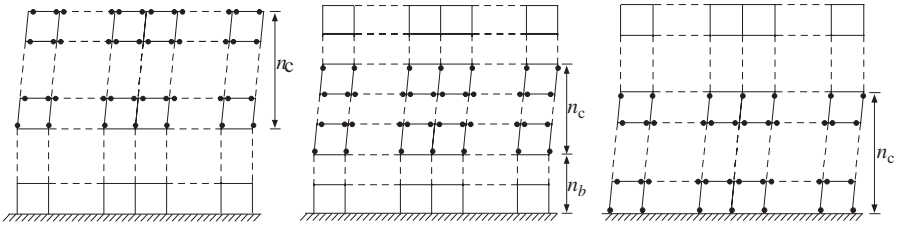

(a) Upper story failure pattern (b) Middle story failure pattern (c) Lower story failure pattern

Figure 2. Story failure patterns.

$$G_M(\mathbf{X}) = 2\sum_{j=1}^{n_c-1}\sum_{i=1}^{m} M_{bij} + \sum_{l=1}^{4} M_{csl} + \sum_{l=1}^{2m-2} M_{cl} - \sum_{j=n_b+1}^{n_b+n_c}(j-n_b)hP_j - \sum_{j=n_b+n_c+1}^{n} n_c hP_j \tag{2}$$

$$G_L(\mathbf{X}) = 2\sum_{j=1}^{n-1}\sum_{i=1}^{m} M_{bij} + \sum_{l=1}^{4} M_{csl} + \sum_{l=1}^{2m-2} M_{cl} - \sum_{j=1}^{n_c} jhP_j - \sum_{j=n_c+1}^{n-n_b} n_c hP_j \tag{3}$$

where G_U, G_M and G_L are the performance functions of upper story failure pattern, middle story failure pattern and lower story failure pattern, respectively; n = the number of stories; m = the number of bays; h = the floor height; M_{bij} = the plastic moment strength of the beam of ith bay, jth story; M_{csl} = the plastic moment strength of exterior column; M_{cl} = the plastic moment strength of interior column; and P_j = the earthquake load acting on the jth story.

It should be noted that the lower story failure pattern defined in this study can be considered as a special case of middle story failure pattern when $n_b = 0$. Let $n_b = 0$, Eq. (2) becomes equivalent to Eq. (3). Comparing the entire beam-hinging pattern shown in Figure 1 to the upper story failure pattern shown in Figure 2(a), one can find that upper story failure pattern will transform into the entire beam-hinging failure pattern if $n_c = n$, so the performance function for entire beam-hinging failure pattern can be obtained from Eq. (1) by assuming $n_c = n$ as:

$$G_T(\mathbf{X}) = 2\sum_{i=1}^{m} M_{bni} + 2\sum_{j=1}^{n-1}\sum_{i=1}^{m} M_{bij} + \sum_{l=1}^{2} M_{csl} + \sum_{l=1}^{m-1} M_{cl} - \sum_{j=1}^{n} jhP_j \tag{4}$$

where G_T is the performance function of the entire beam-hinging failure mode.

4 EVALUATION METHOD

In general, the frame structures are designed to fail according to the entire beam-hinging failure pattern in a certain reliability level. To ensure a meaningful comparison of failure probabilities of story failure modes, the same load condition is required for the probability evaluation. In this study, the mean value of the load leading to a certain reliability index of entire beam-hinging failure pattern $\beta_T = 2.0$ is computed backward by the first-order reliability method (FORM) (Ang & Tang 1984) firstly, then the obtained load is applied to compute the failure probability of each story failure mode. By comparing the failure probabilities of story failure modes, their relative probabilistic relationships can be understood.

The structures used for analysis are the 2-bay, multi-story steel frames designed with different column over-design factors ranging from 1.0 to 3.0. All the frames are with the floor height of 4 m and span length of 8 m, and the moment strength of top beam of 104.1 $kN \cdot m$. All the story failure modes of 2-span, 7-story frame are depicted in Figure 3.

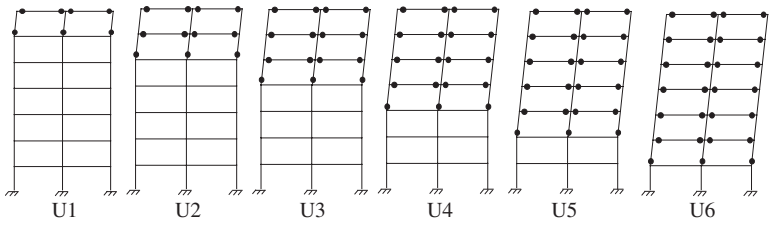

(a) Upper story failure modes

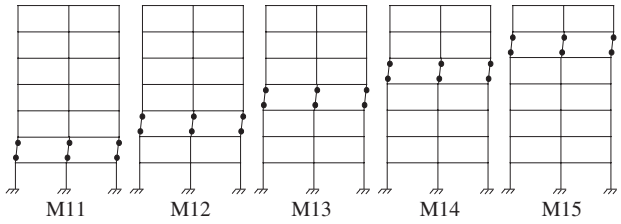

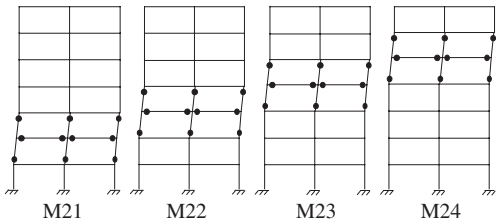

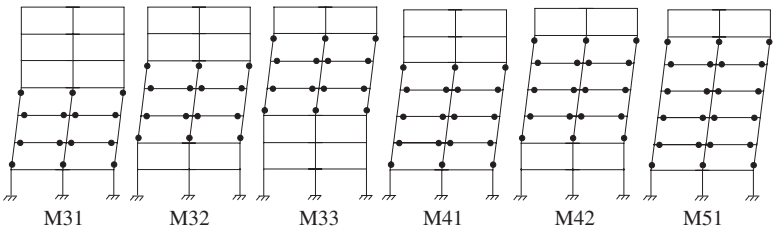

(b) Middle story failure modes

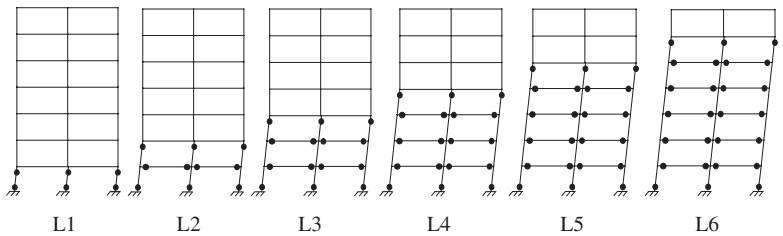

(c) Lower story failure modes

Figure 3. Story failure modes of 7-story frame.

5 EVALUATION RESULTS

5.1 *Upper story failure pattern*

Figure 3(a) shows the 6 upper story failure modes of 7-story frame. Figure 4(a) shows their failure probabilities for frames designed with column over-design factor of 1.0, 1.4, 1.8, 2.4 and 2.8,

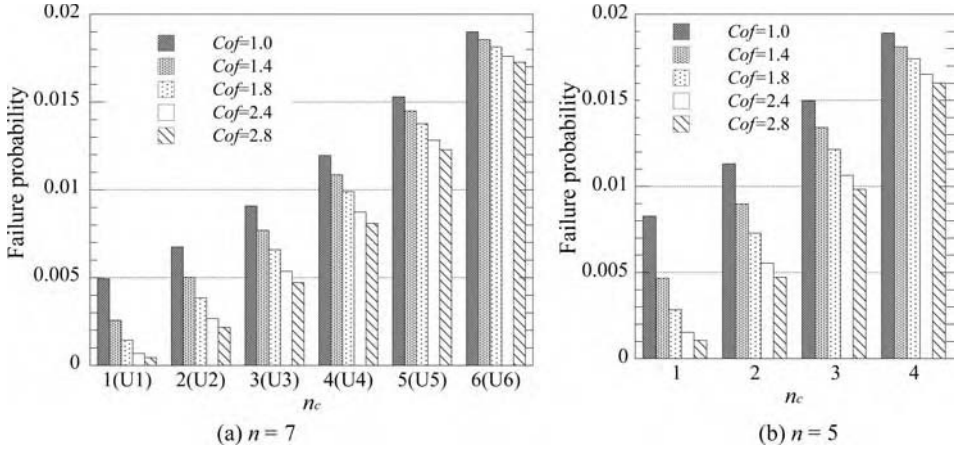

Figure 4. Failure probabilities of upper story failure modes.

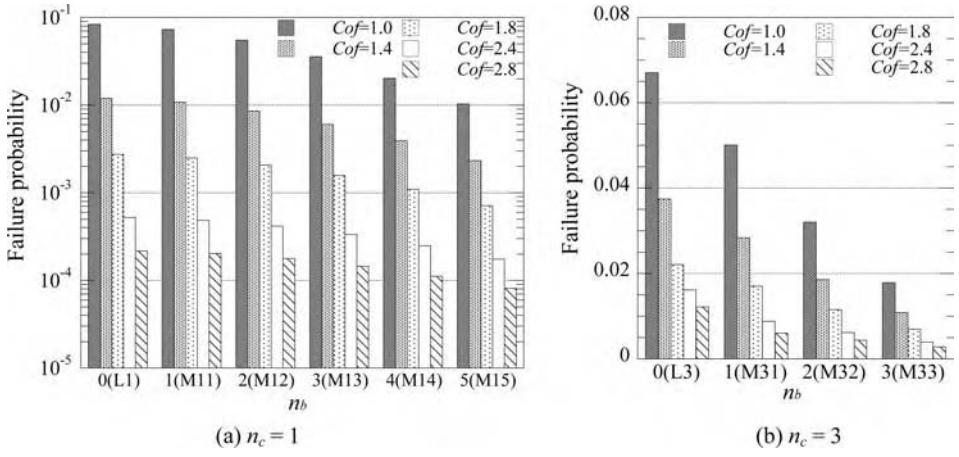

Figure 5. Failure probabilities of middle story failure modes.

respectively. From Figure 4(a) it can found that for a specific frame the failure probabilities of upper story failure modes increase with the increase of n_c, namely for upper story failure pattern, the plastic hinges tend to develop in more stories to form the story failure mode close to the entire beam-hinging failure pattern. Figure 4(b) shows the probabilities of upper story failure modes of 5-story frames, from which the same tendency can be found, and the same is true for other multi-story frames. As described previously, the entire beam-hinging failure pattern can be unified into the upper story failure pattern, so one can know that the failure probabilities of upper story failure modes will not exceed that of the entire beam-hinging failure pattern.

5.2 *Middle story failure pattern*

Figure 3(b) shows all the middle story failure modes of the 7-story frame. To understand the relationships of the failure probabilities of middle story failure modes, the computed failure probabilities for $n_c = 1$ are shown in Figure 5(a). From Figure 5(a) one can see that the probability scales of middle story failure modes are much different for differently column over-designed frames, and the probabilities of middle story failure modes of frame with large column over-design factor are

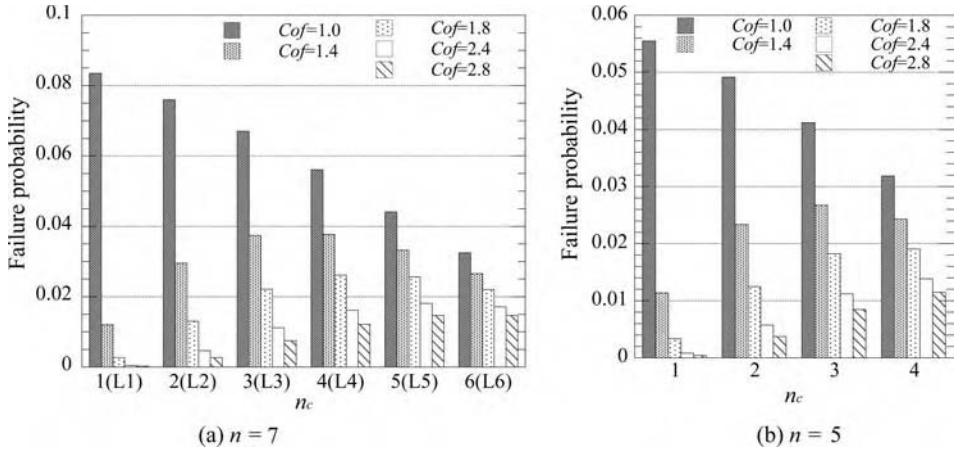

Figure 6. Failure probabilities of lower story failure modes.

quite small. For the middle story failure modes with the same n_c, the failure probabilities decreases with the increase of n_b. As described before, the lower story failure pattern can be considered as a special case of middle story failure pattern, and the lower story failure mode is comparable with middle story failure modes. In Figure 5, the lower story failure mode is corresponding to $n_b = 0$. One can see that for a specific frame the lower story failure mode is more likely to form than the middle story failure modes with the same number of failure stories. Figure 5(b) shows the results for case of $n_c = 3$, from which the same tendency can be found.

5.3 *Lower story failure pattern*

Figure 3(c) shows the 6 lower story failure modes of the 7-story frame. Figure 6(a) shows the failure probabilities of lower story failure modes for 5 cases of column over-design factor. One can see that for a specific frame no obvious monotony can be found between the probabilities and the number of failure stories n_c. For the frame designed with column over-design factor of 1.0, mode L1 is the most likely lower story failure mode; for the frame with column over-design factor of 1.4 and 1.8, mode L3 is the most likely one; and for the frame designed with column over-design factor of 2.4 and 2.8, the most likely lower story failure mode turn to be mode L5 and L6, respectively. The order of the failure probabilities of lower story failure modes is affected by the column over-design factor of frame. For the low column over-designed frame, the plastic hinges tend to form in a few stories; for the highly column over-designed frame, the plastic hinges tend to form in more stories.

5.4 *The probabilistic order of the most likely story failure modes*

The three story failure patterns have been investigated separately, and from the discussion above it can be summarized that the most likely story failure modes are the lower story failure modes and the upper story failure mode with the most failure stories. To get a better understanding on the probabilistic order of these modes, it is meaningful to have a comparison between the upper story failure mode and the lower story failure modes. Figure 7 compares the probabilities of the entire beam-hinging failure mode, the lower story failure modes and the upper story failure mode with the most failure stories for 7-story frames. One can see that when the frame is designed with relatively low column over-design factor, the lower story failure modes are with higher probabilities than the probability of entire beam-hinging failure mode. For the frames designed with relatively high column over-design factor, the probability of entire beam-hinging failure mode will exceed

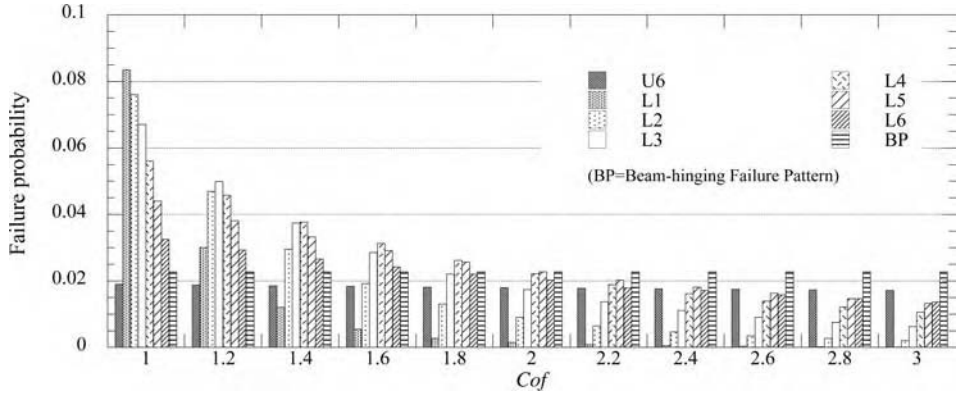

Figure 7. The probabilistic order of story failure modes for frames with different column over-design factors.

the probabilities of lower story failure modes. The column over-design factor corresponding to the point where the probability of entire beam-hinging failure mode exceeds that of lower story failure modes is generally considered as the low limit to avoid the story failure modes of frame structure. For the frame designed with high column over-design factors, the upper failure mode with the most failure stories will take place of the lower story failure modes to be the most likely story failure mode.

6 CONCLUSIONS

The story failure modes of frame structures are classified into three patterns: upper story failure pattern, middle story failure pattern and lower story failure pattern. The failure probabilities of each pattern were investigated. It was obtained that:

(1) Regardless of the column over-design factor of frame, the failure probabilities of upper story failure modes will get a growth with the increase of the number of the failure stories.
(2) For the middle story failure modes with the same number of failure stories, the probabilities decrease with the increase of the number of unbroken stories at bottom. Consider the lower story failure mode as a special case of middle story failure pattern where the number of the unbroken stories at bottom is 0, the lower story failure mode is more likely to form than the middle story failure modes with the same number of the failure stories.
(3) The probabilistic orders of lower story failure modes are affected by the column over-design factor of frame. For a relatively highly column over-designed frame, the lower story failure mode with more failure stories tend to form during earthquake more likely.
(4) In general, for the relatively low column over-designed frame, the lower story failure modes are more likely to form than the preferable entire beam-hinging failure pattern, for the frame designed with a column over-design factor larger than a specific value, the probability of entire beam-hinging failure pattern is larger than the probabilities of all the story failure modes. This specific column over-design factor is the low limit to avoid the story failure modes of frame probabilistically.

REFERENCES

Ang A. H-S. & Tang W. 1984. *Probability concepts in engineering planning and design*. Vol.II-Decision, Risk and Reliability. J. Wiley & Sons, New York.
Architecture Institute of Japan. 1990. *Ultimate strength and deformation capacity of building in seismic design*.

Architecture Institute of Japan. 1993. *Recommendations for loads on buildings*.
Kuwamura H., Sasaki M., Kato B. 1989. Mechanism-based seismic design considering random yield strength. *Journal of Structural and Construction Engineering* No.401: 151–162.
Ogawa K. 1983. On the optimum elastic limit strength distribution of structural members in steel frames (Part 1: Dynamic collapse mechanism and energy absorbing capacity). *Journal of Structural and Construction Engineering* No.323. 13–22.
Ogawa K. 1983. On the optimum elastic limit strength distribution of structural members in steel frames (Part 2: Numerical examples). *Journal of Structural and Construction Engineering* No.328: 18–25.
Simoes L.M.C. 1990. Stochastically dominant modes of frames by mathematical programming. *Journal of Structural Engineering*, ASCE, 116(4), pp.1040–1059.

Reliability and Optimization of Structural Systems: Assessment, Design and Life-Cycle Performance – Frangopol, Kawatani & Kim (eds)
© 2007 Taylor & Francis Group, London, ISBN 978-0-415-40655-0

Elasto-plastic response of steel bridge pier base joint under seismic loading

Masahiro Sakano
Department of Civil & Environmental Engineering, Kansai University, Osaka, Japan

Yuji Nishigaki
Graduate School of Engineering, Kansai University, Osaka, Japan

Yoriko Kawakami
Hanshin Expressway Corporation, Osaka, Japan

ABSTRACT: In this study, the elasto-plastic response of a whole structure, including both superstructures and substructures, was estimated by means of dynamic elasto-plastic finite element analysis, and the elasto-plastic strain history at the top end of triangular ribs was estimated by means of static elasto-plastic finite element analysis using the results obtained by dynamic elasto-plastic finite element analysis. As a result, displacement response of the steel bridge pier can be estimated by means of dynamic elasto-plastic finite element analysis. The maximum displacement response $\delta_{\max}$ is 207 mm and the minimum displacement response $\delta_{\min}$ is -291 mm at the top of column in the case of a 0.03 damping coefficient. By means of static elasto-plastic finite element analysis, it was shown that there was a possibility that the maximum strain range ($\Delta\varepsilon_{y\max}$) can exceed 20% at the top end of triangular ribs.

1 INTRODUCTION

In the 1995 Hyogoken-Nanbu Earthquake, a rigid steel frame bridge pier was fractured at its base joint, as shown in Fig. 1. Cracks were developed at the top of triangular ribs between column and base plate, and connected one another. Eventually, more than a half section of the column failed[1].

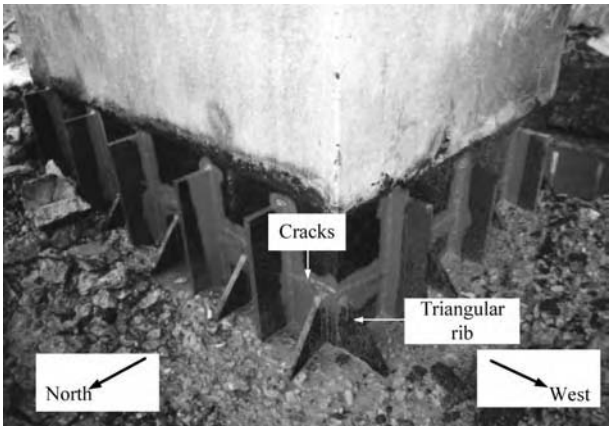

Figure 1. Cracks connecting the top ends of triangular ribs.

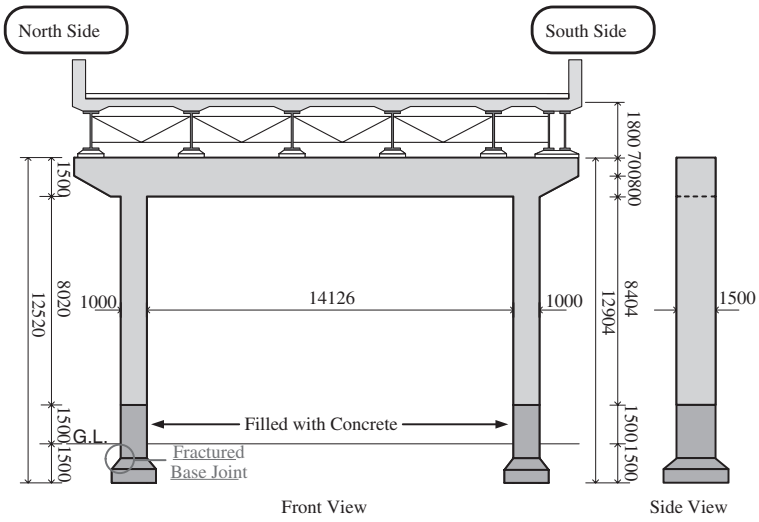

Figure 2. Analyzed steel bridge pier and superstructures.

These cracks are presumed to have been initiated at the fillet weld toe on the column side near the top end of the triangular ribs, and propagated from the northwest corner to the northeast and southwest corners connecting each other. There is a possibility that extremely low cycle fatigue cracks could be developed by excessive cyclic loading during the earthquake. In this study, the elasto-plastic response of the whole structure, including both superstructures and substructures, was estimated by means of dynamic elasto-plastic finite element analysis, and the elasto-plastic strain history at the top end of triangular ribs was estimated by means of static elasto-plastic finite element analysis using the results obtained through dynamic elasto-plastic finite element analysis.

2 ELASTO-PLASTIC RESPONSE OF A WHOLE STEEL PIER

2.1 *Analytical method*

Figure 2 shows the analyzed steel bridge pier and superstructures. Figure 3 shows its analytical model. Dynamic elasto-plastic finite element analysis was conducted using a three-dimensional beam element. The large-mass method was applied in order to shake the ground directly using the seismic acceleration record (N-S direction) measured at the Osaka Gas Fukiai Plant during the Hyogoken-Nanbu Earthquake (see Fig. 4). The beam element was supposed to be a uniform box section, neglecting longitudinal and transverse stiffeners and filled concrete. Material properties were supposed as follows;

Young's modulus: 200 GPa
Poisson's ratio: 0.3
Unit mass of steel: 7850 t/m^3
Yield stress: 235 MPa
The damping coefficient: 0.03 and 0.05

2.2 *Analytical results*

Figure 5 shows displacement response at the top of the north column. The horizontal axis represents time t (s), and vertical axis represents relative displacement of the north column top to the north

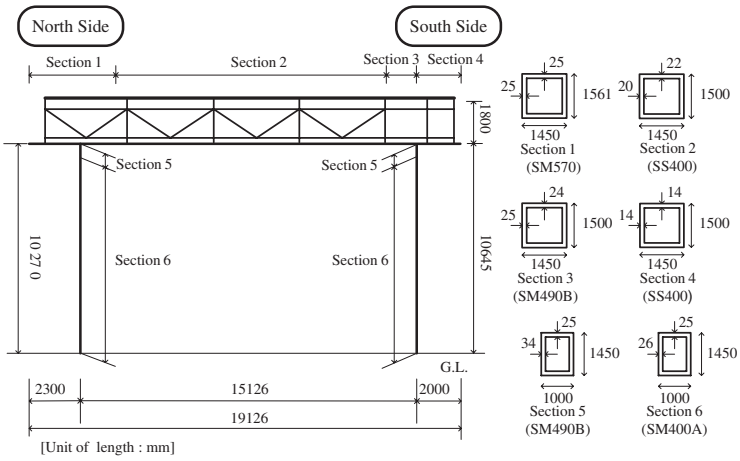

Figure 3. Analytical model of the steel pier and superstructures.

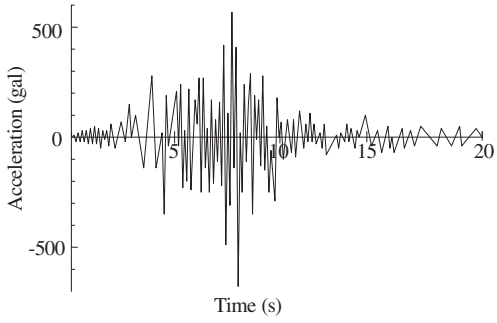

Figure 4. Seismic acceleration record of N-S direction at the Osaka Gas Fukiai Plant.

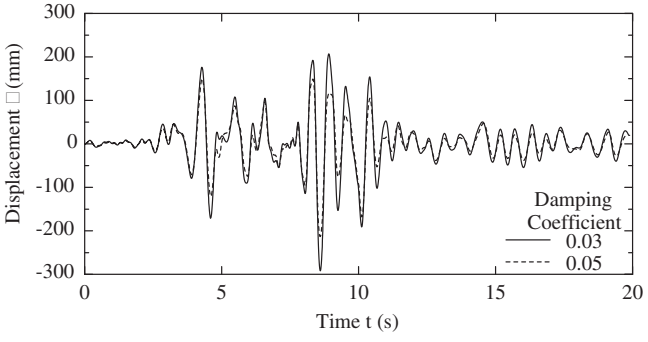

Figure 5. Displacement response at the top of the north column.

column bottom. Solid and broken lines show the displacement response in cases of damping coefficients 0.03 and 0.05, respectively. The maximum displacement response $\delta_{\max}$ is 207 mm and the minimum displacement response $\delta_{\min}$ is -291 mm in the case of a 0.03 damping coefficient, while $\delta_{\max}$ is 155 mm and $\delta_{\min}$ is -233 mm in the case of a 0.05 damping coefficient.

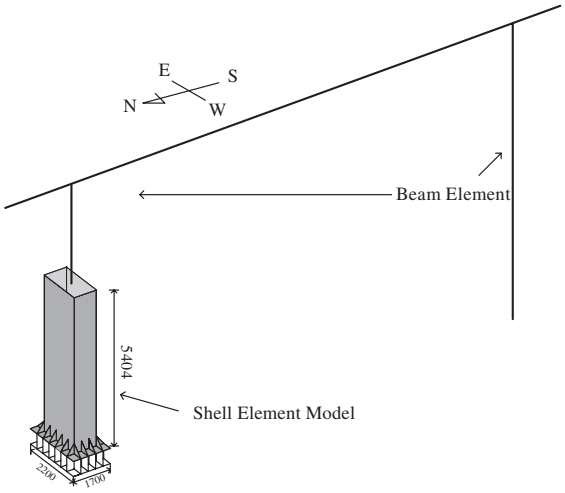

Figure 6. Analytical model for static elasto-plastic finite element analysis.

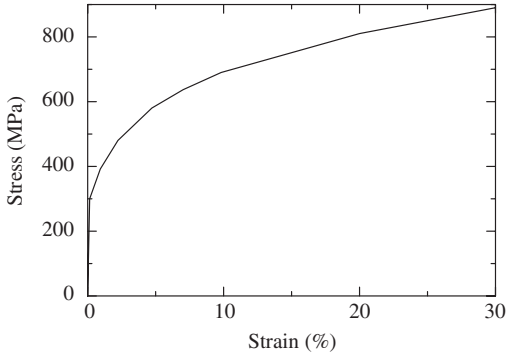

Figure 7. Cyclic stress-strain curve used in the static elasto-plastic analysis.

3 STRAIN HISTORY OF STEEL PIER BASE JOINT WITH TRIANGULAR RIBS

3.1 *Analytical method*

Figure 6 shows an analytical model for the static analysis. Static elasto-plastic finite element analysis was conducted using three-dimensional shell elements for the north column where cracks were detected, and three-dimensional beam elements for the other beam and column members. Figure 7 shows the cyclic stress-strain curve[2] used in the static analysis. The base plate at the bottom end of the column was completely restrained. The displacement obtained in the dynamic elasto-plastic analysis was applied to the top of the column, and then elasto-plastic strain history at the top end of the triangular ribs was estimated.

3.2 *Analytical results*

Figure 8 shows a longitudinal strain distribution near the top of the northwest triangular ribs. Remarkable strain concentration is observed at the top end of the triangular ribs, as shown in Fig. 8. Figure 9 shows strain history at the top of the triangular ribs in the northwest corner. The maximum value of tensile strain is 21.6% and the minimum value of compressive strain is -14.3% in the case of a 0.03 damping coefficient.

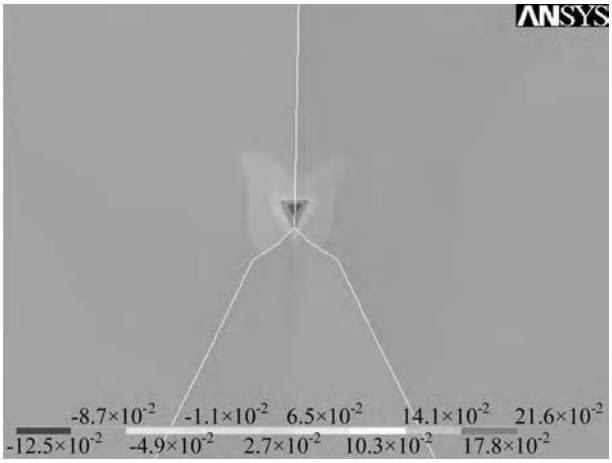

Figure 8. Longitudinal strain distribution near the top end of triangular ribs.

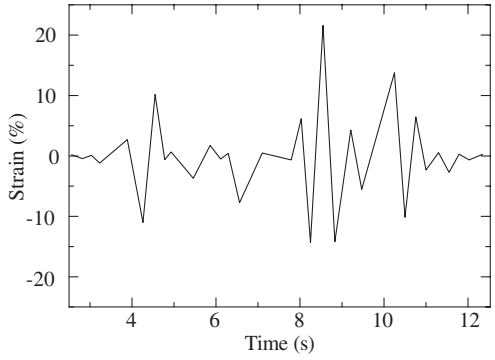

Figure 9. Strain history at the top of the northwest triangular rib.

4 CONCLUSIONS

The principal results obtained through this study are as follows

(1) Displacement response of the steel bridge pier can be estimated by means of dynamic elasto-plastic finite element analysis. The maximum displacement response $\delta_{\max}$ is 207 mm and the minimum displacement response $\delta_{\min}$ is -291 mm at the top of column in the case of a 0.03 damping coefficient.
(2) By means of static elasto-plastic finite element analysis, it was shown that there was a possibility that the maximum strain range ($\Delta\varepsilon_{y\max}$) can exceed 20% at the top end of the triangular ribs.

REFERENCES

Hanshin Expressway Maintenance Technology Center: Research Report on the Plastic Deformation Capacity of Steel Piers, (1995, in Japanese)

Nishimura, T. and Miki, C., Strain-controlled Low Cycle Fatigue Behavior of Structural Steels, *Proc. of JSCE*, **279**, 29 (1978, in Japanese)

Reliability and Optimization of Structural Systems: Assessment, Design and Life-Cycle Performance – Frangopol, Kawatani & Kim (eds)
© 2007 Taylor & Francis Group, London, ISBN 978-0-415-40655-0

Modelling the loss of steel-concrete bonds in corroded reinforced concrete beams

P. Thoft-Christensen
Aalborg University, Aalborg, Denmark

ABSTRACT: The existing stochastic models for deterioration of reinforced concrete structures is extended by adding modelling of "loss of bond" due to corrosion between the reinforcement bars and the surrounding concrete.

1 INTRODUCTION

Life-cycle assessment of the structural reliability of a reinforced concrete structure is based on modelling of the deterioration of the concrete. The most serious deterioration is often corrosion of the reinforcement due to chloride penetration of the concrete. A fully satisfactory modelling of the corrosion of the reinforcement has not yet been established. Modelling of the corrosion initiation is often based on Fick's law of diffusion; see e.g. Thoft-Christensen (1998). After initiation of corrosion in the reinforcement it is often assumed that the cross-section of the reinforcement decreases with time. By this modelling it is simple to perform a deterministic or stochastic estimate of the so-called reliability profile that is the capacity or reliability as functions of time; see e.g. Thoft-Christensen (1998).

The reliability profile consists of six parts:

1. Chloride penetration;
2. Corrosion initiation;
3. Corrosion evolution;
4. Initial cracking;
5. Crack propagation; and
6. Spalling.

Deterioration steps 1–3 are well understood, and are presented in numerous papers, but steps 4, 5 and 6 have only recently been investigated in this connection; see e.g. Thoft-Christensen et al. (2005), (2007).

In this paper the effect of deterioration on steel-concrete bond in reinforced concrete structures is studied. A lot of experimental research in this area has been published; see e.g. FIB (2000). The drawback of this research is that the results are highly dependent on the specific structures considered. In a paper by Lundgren (2002) a more general approach based on a modelling of the corrosion layer between the steel and the concrete is taken. The results of this approach, and similar approaches used by other researchers, are in this paper used to formulate the bases for a stochastic model for loss of bond due to corrosion of the reinforcement. The above mentioned six parts of the reliability profile outlined above will hereby be increased with one more important subject of significance for several of the six parts of the reliability profile.

2 THE PHYSICAL EFFECTS OF CORROSION

Only chloride induced corrosion of the reinforcement is considered is paper. If the rate of chloride penetration into the concrete is modelled by Fick's law of diffusion, then the time to initiation

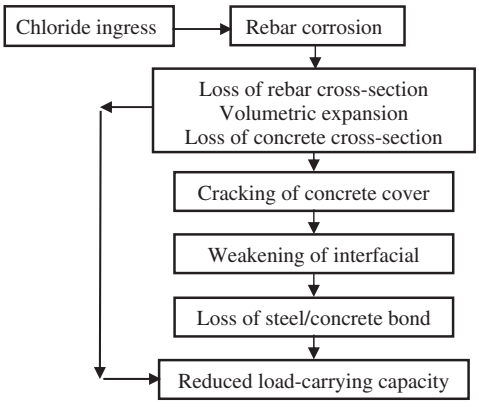

Figure 1. The physical effect of corrosion.

of reinforcement corrosion may be evaluated. The result will depend on several factors namely the concrete cover, the diffusion coefficient, the critical chloride concentration at the site of the corrosion, the equilibrium chloride concentration on the concrete surface, and the initial chloride concentration in the concrete. All these parameters are modelled by stochastic variables or stochastic processes. The distribution of the corrosion initiation time may then be estimated using Monte-Carlo simulation.

With increasing corrosion the tensile stresses in the concrete will reach a critical value and cracks will be developed. During this process the volume of the corrosion products at initial cracking of the concrete will occupy three volumes, namely the porous zone near the reinforcement, the expansion of the concrete due to rust pressure, and the space of the corroded steel. With this modelling and some minor simplifications the time from corrosion imitation to crack initiation may be estimated. The controlling parameters are the diameter of the reinforcement bar, the annual mean corrosion rate, the density of the steel, and the density of the rust products. All these parameters are modelled by stochastic variables or stochastic processes. The distribution of the crack initiation time may then be estimated using Monte-Carlo simulation.

After formation of the initial crack the rebar cross-section is further reduced due to the continued corrosion, and the crack width w_{crack} is increased. Several researchers have investigated the evolution of corrosion cracks in reinforced concrete beams experimentally. In the experiments an impressed current are normally used to artificially corrode the beams.

The corrosion process and its effect on a reinforced concrete structure are schematic illustrated in figure 1. The final result will be a reduced load-carrying capacity of the structure primarily due to the reduced steel bar cross-section and the loss of bond between the steel bar and the surrounding concrete.

3 THE BOND STRESS

In figure 2 is shown the interfacing zone between the steel bar and the surrounding concrete. The spitting stress component perpendicular to the rebar is due to the volume increase of the corrosion product. The bond stress parallel to the rebar is due to the effect of the corrosion on the friction between the reinforcement and the concrete.

Initially the chemical bond between the steel reinforcement and the surrounding concrete is weak. Therefore the weak bond is broken at a very low stress and only friction between the steel and the concrete contribute to the bond stress. For a plain round rebar friction is the main component to the bond stress. For ribbed bars the mechanical interlock between the ribs and the concrete plays a major role although the concrete between the ribs easily breaks.

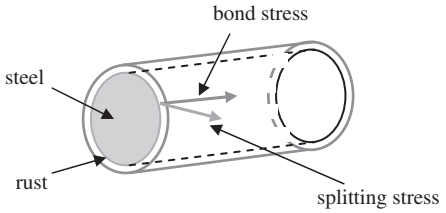

Figure 2. Definition of bond and splitting stresses.

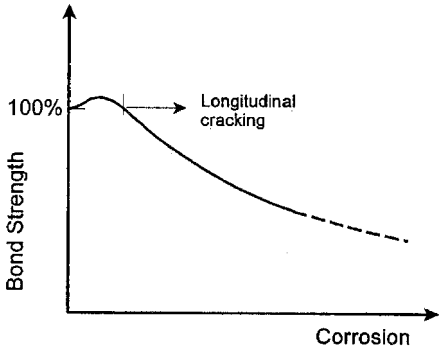

Figure 3. Schematic illustration of the variation in bond strength with corrosion (taken from FIB (2000)).

In figure 3 is shown the variation in the bond strength with corrosion. The bond stress is increased a little in the time period from corrosion initiation to longitudinal cracking is established due to the increased pressure between the reinforcement and the surrounding concrete. Rust is enclosed between the steel and the concrete and only a minor part of the rust may disappear into small cracks and voids in the concrete. When cracks are opened from the rebars to the surface of he concrete then the rust will to some extend be able to disappear into these open cracks and the pressure between the rebars and the surrounding concrete will decrease. The friction between the rebars will therefore also decrease and so will the bond stress.

4 CORROSION INDICES

In this section three important corrosion indices will be introduced, namely

- The crack /corrosion index γ equal to the increase of the surface crack width divided with the corresponding decrease of the rebar diameter
- The bond /corrosion index λ equal to the reduction of bond strength divided with the corresponding decrease of the rebar diameter.
- The bond /crack index η equal to the reduction in bond strength divided with the corresponding increase of surface crack

These 3 indices and will be discussed in more detail in the next chapters.

5 THE CRACK/CORROSION INDEX γ

Several researchers have investigated the evolution of corrosion cracks in reinforced concrete beams experimentally, e.g. Andrade et al. (1993). To reduce the duration of testing, artificial corrosion by electrical current is a common experimental approach. During the test, the loss of rebar cross-section is monitored and the corresponding crack evolution is measured by strain gauges attached to the surface of the specimen. In the study by Andrade et al. (1993), four simple test specimens were investigated. The specimens are small reinforced concrete beams with only a single rebar with a 20 or 30 mm concrete cover. In figure 4, the results from this experimental study are shown.

After formation of the initial crack, the rebar cross-section is further reduced due to the continued corrosion, and the width of the crack is increased as shown in figure 2. In all four experiments by Andrade et al. (1993), proportionality between the reduction of the rebar diameter ΔD_{bar} and the

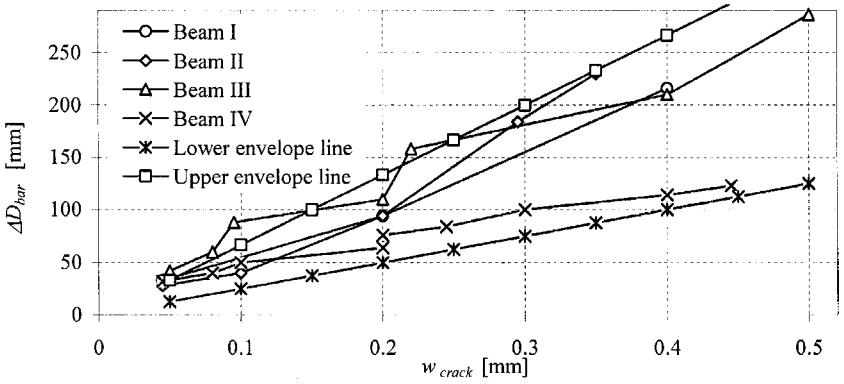

Figure 4. Reduction of rebar diameter ΔD_{bar} versus the crack width w_{crack}, based on data in Andrade et al. (1993).

maximum crack Δw_{crack} width measured at the surface of the concrete specimen is found

$$\Delta w_{crack} = \gamma \Delta D_{bar} \tag{1}$$

where the crack-corrosion index γ is the proportionality constant. From the experiments shown in figure 4, the upper and lower bound for γ is determined as being of the order 1.5 to 5.

6 THE BOND/CORROSION INDEX η

In the literature there are a vast number of experimental tests on the relationship between the residual bond strength f_{bond} and the corrosion penetration. Empirical expressions for this relationship based on laboratory testing as been publisher by e.g. Rodriguez et al. (1994a), (1994b), (1996), Coronell & Gambarova (2004), Fang et al. (2004), and Söylev & Francois (2005).

The relationship has also been numerically studied by several researchers (using FEM analysis) such as Lundgren (2000), (2002) (2005a,b), Lundgren & Gylltoft (2000), and Berra et al. (2003).

The behaviour of reinforced concrete beams with loss of bond has also been studied by several researchers: see e.g. Jeppsson & Theladersson (2003), Harajli (2004), Toongoenthong & Maekawa (2000) & Darwin (2005).

Figure 5 (taken from FIB (2000)) shows a linear relationship between the residual bond strength f_{bond} and the corrosion penetration based on Rodriguez et al. (1994a), (1994b), and (1996). The linear relation shown in figure 5 between the reduction of the bond strength $\Delta \tau_{bond}$ (%) and the decrease the rebar diameter ΔD_{bar} may be written

$$\Delta \tau_{bond} = \eta \Delta D_{bar} \tag{2}$$

where the bond/corrosion index η is equal to 50%/mm.

7 THE BOND/CRACK INDEX λ

By combining (1) and (2) a linear relation between the reduction of the bond strength $\Delta \tau_{bond}$ (%) and the increase in crack width Δw_{crack} (mm) is obtained

$$\Delta \tau_{bond} = \frac{\eta}{\gamma} \Delta w_{crack} = \lambda \Delta w_{crack} \tag{3}$$

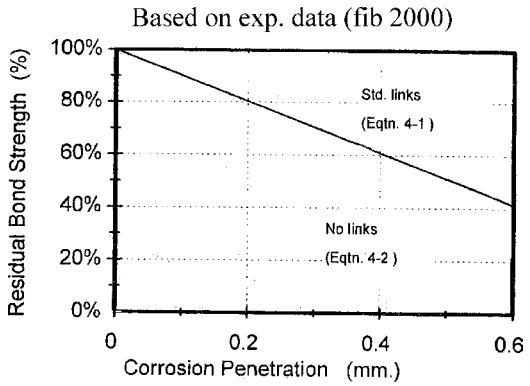

Figure 5. Relationship between residual bond strength f_{bond} and the corrosion penetration (taken from FIB (2000)).

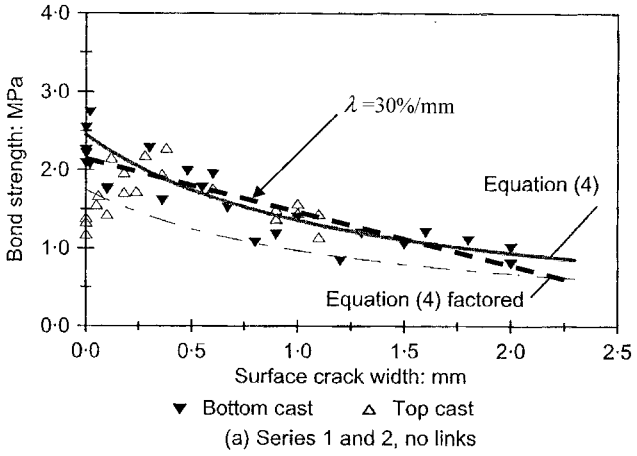

Figure 6. Relationship between bond strength f_{bond} and longitudinal crack width w_{crack} (from the top part of Fig. 8 in Cairns, Du & Law (2006)).

where the bond/crack index $\lambda = \gamma/\eta$ is of the order 10–60%/mm depending of the beam cross-section.

In the paper by Cairns, Du & Law (2006) it is suggested that corroded plain bars the surface crack width Δw_{crack} may provide a better parameter than the corrosion penetration ($0.5\,\Delta D_{bar}$) in assessing the residual bond strength.

In figure 6 is shown some test data obtained by Cairns, Du & Law (2006). In the figure is the relationship between the bond strength and the surface crack width for bottom and top castings. Using non-linear curve fitting the obtained the following relation between the residual bond strength f_{bond} and the crack width w_{crack}

$$f_{bond} = \frac{1}{(1+0.8w_{crack})} f_0 \tag{4}$$

where f_0 is the design bond strength. If instead a linear curve fitting is used (the straight dotted line) one obtain approximately

$$f_{bond} = (1-0.30w_{crack}) f_0 \tag{5}$$

and the bond/crack index $\lambda = 30\%/\text{mm}$. This is in good agreement with the estimations indicated above.

8 DISCUSSION

The final outcome of the deterioration due to corrosion of the reinforcement of a reinforced concrete beam is a reduced load-carrying capacity of the structure. This is primarily due to

- The reduced steel bar cross-section, and
- The loss of bond between the steel bar and the surrounding concrete.

In estimation of the load-carrying capacity, it is therefore of great value to be able to estimate the reduced steel bar cross-section (the corrosion of the rebar) and the loss of bond. In the paper is presented a new linear model by which the corrosion degree as well as the loss of bond may be evaluated by simple measurement of the concrete crack width at the surface of the structure.

The corrosion is estimated by the crack-corrosion index γ. γ may be estimated experimentally or numerical using two or three dimensional FEM techniques. The value of γ is typical in the interval 1.5–5. Due to the uncertainties involved in the estimation of the crack-corrosion index γ will normally be modelled as a stochastic variable.

The loss of bond is estimated by the bond/crack index $\lambda = \gamma/\eta$, where bond/corrosion index η may be estimated using the methods described in section 6. It is also possible to estimate λ directly by testing. η and λ are modelled as stochastic variables.

Using these linear models, it is possible estimate the load-capacity reduction. Like the above mentioned indices the load capacity will be modelled as a stochastic variable.

9 CONCLUSIONS

In the paper are derived two linear equations by which the amount of corrosion of the reinforcement as well as the loss of bond may be estimated by observing the width of cracks at the surface of the reinforced concrete element.

REFERENCES

Andrade, C., C. Alonso & F.J. Molina. 1993. Cover Cracking as a Function of Bar Corrosion: Part 1–Experimental Test.*Materials and Structures*, Vol. 26, pp. 453–464.

Berra M., A. Castellani, D. Coronelli, S. Zanni & G. Zhang. (2003). Steel-Concrete Bond Deterioration due to Corrosion: Finite-Element Analysis for different Confinement Levels. *Magazine of Concrete Research*. Vol. 55, pp. 237–247.

Cairns, J., Y. Du & D. Law (2006). Residual Bond Strength of Corroded Plain Round Bars. *Magazine of Concrete Research*. Vol. 58, pp. 221–231.

Coronell, D. & P. Gambarova. 2004. Structural Assessment of Corroded Concrete Beams: Modelling Guidelines. *Journal of Structural Engineering*, Vol. 130, pp. 1214–1224.

Darwin, D. 2005. Tension Development Length and Lap Splice Design for Reinforced Concrete Members. *Prog. Structural Engineering Materials*. Vol. 7, pp. 210–225.

Fang, C., K. Lundgren, L. Chen & C. Zhu. 2004. Corrosion Influence on Bond in Reinforced Concrete. *Cement and Concrete Research*, Vol. 34, pp. 2159–2167.

FIB. 2000. Bond of reinforcement in concrete. State-of-the art report. Task Group Bond Models. FIB bulletin 10, Lausanne 2000.

Harajli, M.H. 2005. Comparison of Bond Strength of Steel Bars in Normal- and High-Strength Concrete. *Journal of Materials in Civil Engineering*. Vol. 16, pp. 365–374.

Jeppsson, J. & S. Thelandersson. 2003. Behavior of Reinforced Concrete Beams with Loss of Bond at Longitudinal Reinforcement. *Journal of Structural Engineering*, Vol. 129, pp. 1376–1383.

Lundgren, K. & K. Gylltoft 2000. A Model for the Bond between Concrete and Reinforcement. *Magazine of Concrete Research*, Vol. 52, pp. 53–63.

Lundgren, K. 2001. Bond between Corroded Reinforcement and Concrete. Department of Structural Engineering, Chalmers University of Technology, Sweden. Report No. 00:3, 2001.

Lundgren, K. 2002. Modelling the Effect of Corrosion on Bond in Reinforced Concrete. *Magazine of Concrete Research*, Vol. 54, pp. 165–173.

Lundgren, K. 2005a. Bond between Ribbed Bars and Concrete. Part 1: Modified Model. *Magazine of Concrete Research*, Vol. 57, pp. 371–382 .

Lundgren, K. 2005b. Bond between Ribbed Bars and Concrete. Part 2: The Effect of Corrosion. *Magazine of Concrete Research*, Vol. 57, pp. 383–395.

Rodriguez, J., L.M. Ortega & A.M. Garcia. 1994a. Assessment of Structural Elements with Corroded Reinforcement. *Corrosion and Corrosion Protection of Steel in Concrete,* Academic Press, 1994, pp. 171–185.

Rodriguez, J., L.M. Ortega & J. Casal. 1994b. Corrosion of Reinforcing Bars and Service Life of Reinforced Concrete Structures. International Conference on "Concrete across Borders", Odense, Denmark Vol. II, 1994, pp. 315–326.

Rodriguez, J., L.M. Ortega, J. Casal & J.M. Diez. 1996. Assessing Structural Conditions of Concrete Structures with Corroded Reinforcement. International Congress on "Concrete in Service Mankind", Dundee, UK. 1996.

Söylev, T.A. & R. Francois. 2005. Corrosion of Reinforcement in Relation to Presence of Defects at the Interface between Steel and Concrete. *Journal of Materials in Civil Engineering*. Vol. 17, pp. 447–455.

Thoft-Christensen, P. 1998. Assessment of the Reliability Profiles for Concrete Bridges. *Engineering Structures*, Vol. 20, pp. 1004–1009.

Thoft-Christensen, P. 2000. Modelling of the Deterioration of Reinforced Concrete Structures. *Proc. IFIP WG7.5 Conference on "Optimization and Reliability of Structural Systems", Ann Arbor, MI, USA*, September 25–27, pp. 15–26.

Thoft-Christensen, P., S. Svensson & H.L. Frandsen. 2005. 3D-modelling of Corrosion Crack Opening. Proc. IFIP WG 7.5 Conference, Aalborg, Denmark, May 22–25.

Thoft-Christensen, P., H.L. Frandsen & S. Svensson. 2007. Numerical Study of Corrosion Crack Opening. Accepted for publication in *Structures and Infrastructure*, 2007.

Toongoenthong, K. & K. Maekawa. 2005. Multi-Mechanical Approach to Structural Performance Assessment of Corroded RC Members in Shear. *Journal of Advanced Concrete Technology*. Vol. 3, February 2005, pp. 107–122.

Reliability and Optimization of Structural Systems: Assessment, Design and Life-Cycle Performance – Frangopol, Kawatani & Kim (eds)
© 2007 Taylor & Francis Group, London, ISBN 978-0-415-40655-0

Random vibrations and peak response of a shear beam under high frequency seismic effects

Z. Zembaty
Opole University of Technology, Opole, Poland

ABSTRACT: In present paper selected results of a study of non-stationary random vibrations of a shear beam excited by time segments of band limited white noise are presented. The root mean square (*rms*) and peak response of the shear beam is studied for two characteristic frequency bands: the conventional 1–4 Hz and higher frequency 4–16 Hz, characteristic for rockburst ground motion. The "switching off" fundamental modes for high frequency excitations results in characteristic overshoot of the stationary response level by the non-stationary *rms* response and an amplification of the response in the upper part of the shear beam.

1 INTRODUCTION

Typical seismic effects which can affect civil engineering structures derive from earthquakes which dominate in the frequency band 0–5 Hz and decay to zero at about 10 Hz (see e.g. acceleration records from European database by Ambressays et al. 1999). In some situations e.g. of a shallow focus and near-field record, particular site geology or for vertical seismic components this upper limit can be extended, sometime even up to 20 Hz.

The structural foundations can however be subjected to kinematic motions also from artificial or semi-artificial seismic effects like:

- rockbursts,
- nuclear underground explosions,
- distant conventional explosions (e.g. from surface mining, quarries),
- close (to structure) explosions of underground ammunition storages
- pile hammering,
- traffic ground motion etc.

These sources of seismic vibrations, differ primarily in the energy released. Depending on the source-to-site distance ranging from tens of meters to tens of kilometres, the actual, generated ground motion may substantially differ because various frequency bands attenuate differently in the ground. Though excitations deriving from these artificial sources of seismic excitations result usually in low level vibrations and (with few exceptions) causing only minor structural damage, most of these effects occur much more frequently than natural earthquakes and often generate human discomfort as well as induce strong equipment response. And since they differ qualitatively from natural seismic vibrations they are worth further detailed studies. Indeed, as the frequency content of excitations increases, the resulting structural motion departs more and more from classic seismic vibrations. Thus some conclusions based on classic seismic engineering may even be misleading. These problems with respect to the description of rockburst induced ground motions were studied in detail by Zembaty (2004).

In what follows structural response problems are analyzed in terms of non-stationary random vibrations and peak response of a uniform shear beam to band limited seismic excitations.

2 SHEAR BEAM AS A SIMPLIFIED TALL-BUILDING MODEL UNDER HIGH FREQUENCY SEISMIC EXCITATIONS

The natural frequencies of the first vibration mode of typical civil engineering structures, particularly multistory buildings, usually stay below 5 Hz. The shift of dominating frequency band from 1–5 Hz typical for natural earthquakes to about 5–20 Hz characteristic for rockbursts or even to 50–100 Hz characteristic for blasts leads then to excitations of higher natural modes of the structure. The unique features of such structural response derive not only from exciting these higher vibration modes but rather from the lack of the fundamental mode(s) in the overall seismic vibrations. To capture only the essential effects differing higher frequency vibrations from the conventional ones, the simplest possible model should be applied. In this study a shear beam was chosen for this purpose. Unlike single-degree-of-freedom-system the shear beam may vibrate in several natural modes and represents a simplified model of very important structural system: a tall building, capturing some specific effects occurring during high frequency seismic excitations.

Consider a shear beam shown schematically on the left side of Fig. 1. The equation of motion of such cantilever shear beam under horizontal seismic excitations $u(t)$ takes following form:

$$\frac{\partial^2 q}{\partial t^2} + \frac{c_1}{m}\frac{\partial q}{\partial t} - c_S^2 \frac{\partial^2 q}{\partial z^2} = -\ddot{u}(t) \tag{1}$$

in which $c_S = k/m$ represents velocity of shear waves propagating along the beam, k stands for its shear stiffness, m it is mass per unit length and c_1 represents damping effects.

For the cantilever shear beam the natural frequencies ω_j and modes ψ_j equal:

$$\omega_j = (2j-1)\frac{\pi c_S}{2H}, \qquad \psi_j(z) = \sin\left(\frac{\omega_j z}{c_S}\right) \tag{2,3}$$

where H stands for the height of the shear beam from Fig. 1.

Although the shear beam is rather simple structural model its seismic response is in good agreement with complicated finite element analyses of buildings making it a very convenient structural model as it captures specific dynamic properties of high buildings while it is still relatively simple in numerical analyses.

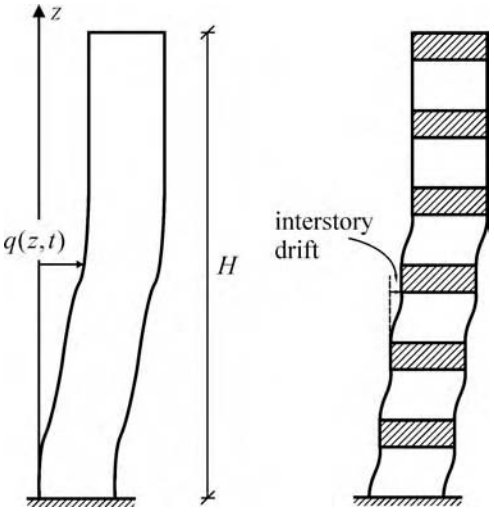

Figure 1. Shear beam model of a multi story building.

3 STOCHASTIC PROCESS REPRESENTING HIGH FREQUENCY SEISMIC EFFECTS

The stochastic process which can effectively model high frequency, seismic effects should take into account two particular features of the modeled ground motion, i.e. specific spectral content usually shifted into higher frequency band and short duration of excitations.

Consider a stationary pulse of band-limited white noise with spectral intensity S_0. The non-stationary structural response to such excitations properly reflects the strongest non-stationarity possible to be present in seismic vibrations. The white noise excitations are switched on at $t = 0$ and off after t_0 seconds. Thus the structural response builds up until $t = t_0$ and then decays to zero in free vibrations. To compare structural vibrations with excitations from different frequency bands and still keep approximately the same intensity level, the constant PGV criterion is usually applied (e.g. Dowding 1996, Lu et al 2002). When analyzing rockburst seismic effects the variations in the frequency band are not as substantial as for the blast effects (see e.g. Zembaty 2004, Lu et al. 2002) and the constant intensity criterion can be applied by keeping constant rms velocity of excitations. Under this assumption the frequency band from ω_a to ω_b can be changed only if the respective *rms* excitation velocity is kept constant, which for assumed, excitation stationary random processes means:

$$\int_{\omega_a}^{\omega_b} S_V d\omega = \int_{\omega_a}^{\omega_b} \frac{S_{\ddot{U}}}{\omega^2} d\omega = \int_{\omega_a}^{\omega_b} \frac{S_0}{\omega^2} d\omega = S_0 \left[\frac{1}{\omega_a} - \frac{1}{\omega_b} \right] = const \tag{4}$$

where S_V stands for spectral density of excitation velocity. The unique features of the high frequency seismic excitations of structures appear then in switching on and off various natural modes of Eqs. (3, 4) while changing frequency band (ω_a ; ω_b), and keeping constant intensity.

4 NONSTATIONARY RANDOM VIBRATIONS OF A SHEAR BEAM

Application of the familiar modal expansion yields, after some algebra, the solution of eq.2

$$q(z,t) = -\sum_{j=1}^{\infty} \psi_j(z) a_j \int_0^t \ddot{u}(t-\tau) h_j(\tau) d\tau \tag{5}$$

in terms of modal impulse response functions $h_j(t)$ and modal participation factors a_j.

Assume now that the horizontal accelerations are modeled by a non-stationary random process with zero mean and spectral representation in format of following Stieltjes-Fourier representation (Priestley 1966):

$$\ddot{u}(t) = \int_{-\infty}^{\infty} A(t,\omega) e^{i\omega t} d\hat{\ddot{u}}(\omega) \tag{6}$$

in which $A(t,\omega)$ it is a deterministic modulating function and symbol ˆ stands for random function with orthogonal increments i.e.:

$$\left\langle d\hat{\ddot{u}}(\omega_1) d\hat{\ddot{u}}^*(\omega_2) \right\rangle = \begin{cases} \left\langle \left| d\hat{\ddot{u}}(\omega) \right|^2 \right\rangle = S_{\ddot{u}}(\omega) \mathrm{d}\omega & \text{for} \quad \omega_1 = \omega_2 = \omega \\ 0 \quad \text{for} \quad \omega_1 \neq \omega_2 \end{cases} \tag{7}$$

Substituting spectral representation (6) into the eigen series solution (5) gives

$$q(t,z) = \int_{-\infty}^{\infty} M(z,t,\omega) e^{i\omega t} d\hat{\ddot{u}}(\omega) \tag{8}$$

in terms of response modulating function:

$$M(z,t.\omega)=\sum_{j=1}^{\infty}a_j\psi_j(z)\int_0^t h_j(\tau)A(t-\tau,\omega)e^{-i\omega\tau}d\tau \tag{9}$$

When one considers the excitations as stationary process switching "on" and "off", as was already assumed in the previous section, the modulating function $A(t,\omega)$ simplifies to a "box-car" form $A(t)=1$ for $0<t<t_0$ and zero elsewhere. In this case the integral (9) can be calculated in closed form and equals:

$$M_j(z,t,\omega)=\begin{cases}0 & \text{for} \quad t<0\\ \mathrm{H}_j(\omega)[1-P_j(t,\omega)] & \text{for} \quad 0<t<t_0\\ \mathrm{H}_j(\omega)[P_j(t-t_0,\omega)-P_j(t,\omega)] & \text{for} \quad t>t_0\end{cases} \tag{10}$$

where $H_j(\omega)=[\omega_j^2-\omega^2+2i\xi_j\omega_j\omega]^2$ stands for modal frequency response function and

$$P_j(t,\omega)=\frac{1}{\omega_{jd}}e^{-\xi_j\omega_j t}\left(\cos\omega t-i\sin\omega t\right)\left[(\xi_j\omega_j+i\omega)\sin\omega_{jd}t+\omega_{jd}\cos\omega_{jd}t\right] \tag{11}$$

Equation (8) together with the orthogonal property (7) and simple definition of shear force for the shear beam $F(z)=K\partial q/\partial z$ can now be used to calculate any response statistics of the response process. For example the mean square displacements and shears along the height of the shear beam equals:

$$\sigma(z,t)=\int_{-\infty}^{\infty}M(z,t,\omega)M^*(z,t,\omega)S_{\bar{u}\bar{u}}(\omega)d\omega \tag{12}$$

with

$$M(z,t.\omega)=\begin{cases}M_q(z,t,\omega)=\sum_{j=1}^{\infty}a_j\psi_j(z)\int_0^t h_j(\tau)A(t-\tau,\omega)e^{-i\omega\tau}d\tau & \text{for displacements}\\ M_F(z,t,\omega)=K\sum_{j=1}^{\infty}a_j\dfrac{\partial\psi_j(z)}{\partial z}\int_0^t h_j(\tau)A(t-\tau,\omega)e^{-i\omega\tau}d\tau & \text{for shear forces}\end{cases} \tag{13}$$

5 PEAK STRUCTURAL RESPONSE

To properly asses the structural response one needs to know estimations of peak response rather than only mean square response derived in the previous section. For stationary random vibrations the classic peak factors of Davenport (1964) or Vanmacke (1975) can be applied. This assumption in seismic engineering is true for most of the structures ($T_1<5$ s) and typical earthquakes (strong motion duration >10 to 15s). This is however clearly not the case for the vibrations of ordinary buildings ($0.5\text{ s}<T_1<5$ s) under short, 1–2 s high frequency excitation pulses analysed here. In this case the peak response can be obtained only by using numerical estimations from the formulae proposed as early as in 1972 by Yang who proposed to calculate the first excursion probability of double, symmetric barrier $\pm\lambda$

$$P(\lambda)=1-\exp\left[-\int_0^{\infty}\nu(\tau,\lambda)d\tau\right] \tag{14}$$

as a function of time dependent failure rate $\nu(t, \lambda)$:

$$\nu(t,\lambda) = 2\nu_+(t,\lambda)\frac{1-\exp[-\nu_e(t,\lambda)/(2\nu_+(t,\lambda))]}{1-\nu_+(t,\lambda)/\nu_+(t,0)} \tag{15}$$

in which $\nu_+(t, \lambda)$ stands for mean number of up-crossing level λ by the response process, while $\nu_e(t, \lambda)$ represents respective mean number of crossing level λ by the envelope of the response process. The mean number of crossing level λ with positive slope by the response process $q(t)$ can be obtained using the familiar Rice formula, after integrating the joint (gaussian) probability density of the process $q(t)$ and its derivative $\dot{q}(t)$. The detailed, lengthy formulae for mean upcrossing rates of the process and the envelope can be found in the paper by Yang (1972) or Zembaty (1988).

The peak value of the response can be defined as λ corresponding to respective probability of excursion. For example the median peak value $\lambda_{0.5}$ corresponds to probability of outcrossing domain $\pm\lambda$ with probability 0.5, which leads to following algebraic equation

$$0.5 = \exp\left[-\int_0^\infty \nu(\tau, \lambda_{0.5})d\tau\right] \tag{16}$$

in which the unknown median peak value is in the integrand. This equation can only be solved numerically. In an analogy to Vanmarcke's peak factor one can define the median peak factor as the ratio of median peak value to the maximum rms response i.e.: $r_{0.5} = \lambda_{0.5}/\max\sigma(t)$.

6 NUMERICAL EXAMPLE

Consider the shear beam from Fig. 1, with height $H = 35$ m. The main parameter which accounts for both elastic and inertial properties of the shear beam it is the value of velocity of shear waves propagating along their height, c_S. The values of c_S ranging from 100 m/s to 200 m/s are commonly met in the literature (Todorovska and Trifunac 1989, Todorovska and Lee 1989, Safak, 1999). In this paper the value of $c_S = 170$ m/s has been applied. The cantilever beam with such parameters can roughly represent a 10 story, prefabricated building usually build with the same cross-section along its height. The first eight natural frequencies were calculated for these values of H and c_S using Eq. 3 equal $f_i = 1.21$, 3.64, 6.07, 8.50, 10.93, 13.36, 15.79 and 18.21 Hz. In the following calculations the value of damping ratio $\xi = 0.05$, the same for all the modes of analysed beam is applied.

To model the characteristic effect of frequency shift in excitations as described earlier two frequency bands are considered:

(a) from 1 to 4 Hz (dominating spectrum of earthquakes or rockbursts type II)
(b) from 4 to 16 Hz (high-frequency effects of rockbursts type I)

The cut-off frequencies of band-limited white noise can be obtained just by multiplying them by a single "scale" factor $s = 1$ or 4 as required in formula 5. When looking at the natural frequencies of the beam (displayed above) it can be seen that in the first case only the first two natural modes will be excited while for the second case only modes 3–7 will contribute in the vibrations.

Consider now the non-stationary response of the shear beam under band limited short time, white noise excitations. The duration of excitations was chosen to be 1.5s, typical for the type I rockbursts (Zembaty 2004) and comparable with the first natural period of the analysed shear beam. In Fig. 2 the *rms* shear response is shown for base shear force (b, d) and for $z = 31.5$ m (a, c). Figures 2a, b show the response for the frequency band 1–4 Hz while Figs. 2c, d show the *rms* shear response for frequency band 4–16 Hz. In all analysed cases the response gradually increases until $t = 1.5$ s and then slowly decreases, with some oscillations reflecting the fundamental period of the structure. For the low frequency band (a,b) and such short duration of excitations (1.5 s)

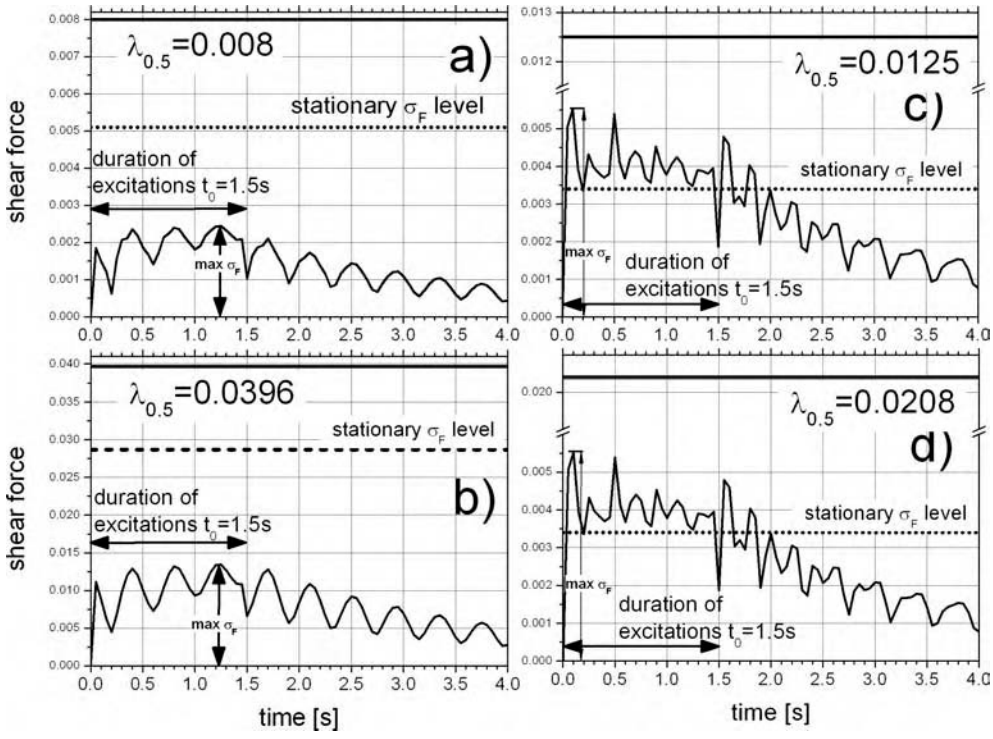

Figure 2. Rms shear as a function of time for $z = 0$ (base shear - b,d) and $z = 31.5$ m (a,c), low frequency excitations, bandwidth 1–4 Hz - scale factor s = 1 - (a,b), high frequency excitations, bandwidth 4–16 Hz - scale factor s = 4 - (c,d).

the *rms* response starts to decay well below the stationary response level. However for the high frequency excitations the non-stationary response reaches its maximum already at the beginning of excitations, substantially overshooting the stationary response level. The median peak factors (Eq.39) are higher for the high frequency excitations: $r_{0.5} = 3.75$ for $z = 31.5$ m and 3.77 for $z = 0$. For low frequency excitations these values equal 3.25 and 2.94 respectively. This means that the distribution of peaks is practically the same for base shears and $z = 31.5$ m and generally much wider for the high frequency excitations. In Fig.3 the maxima of rms non-stationary responses and respective median peak values are shown as functions of z. The stationary rms response level is shown for comparison too. For the assumed criterion of constant peak velocity the high-frequency excitations result in smaller response (Fig. 3b) than for the low frequency effects (Fig. 3a).

7 CONCLUSIONS

Short duration, high frequency seismic effects on structures represent specific type of excitations in civil engineering. Critical contribution to the overall seismic structural response is contributed by the frequency band below 5Hz. A shift in the ground motion Fourier spectrum to higher frequencies results in excitations of higher eigenmodes of the structure. If at the same moment, the excitation spectrum lacks the low frequency band (<5 Hz) then the structural response may substantially be changed. The deterministic analysis of a wide range of problems regarding this type of structural dynamics was dealt with in the paper by Lu et al. (2002), particularly for very high frequency shifts. Present paper aimed at intermediate shift of excitation frequencies (4–16 Hz) and at analysing non-stationary random vibrations of a shear beam modeling multi story buildings.

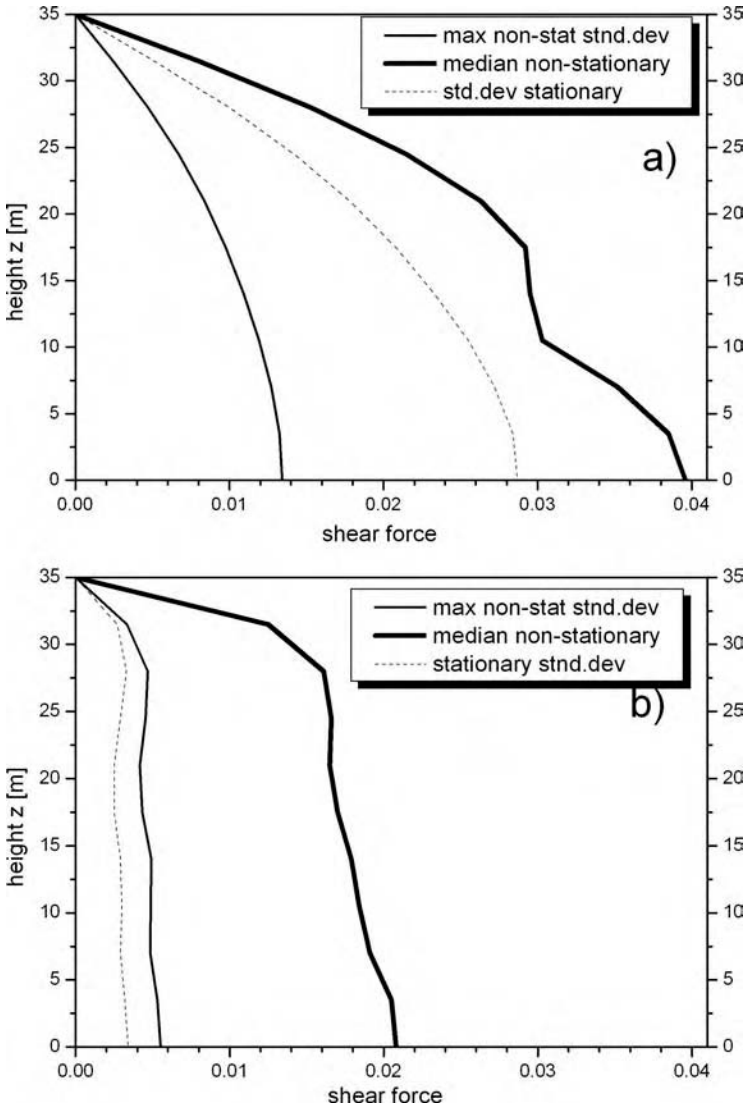

Figure 3. Max rms shear, median peak value and stationary rms shear as functions of height for scale factor s = 1 - spectral bandwidth 1–4 Hz (a,b) scale factor s = 4 - spectral bandwidth 4–16 Hz (c,d).

Unlike for the conventional random vibrations (which slowly build up) and for short excitations their *rms* values may never reach the respective stationary level before the excitations are seized (Fig. 2a,b), the high frequency effects cause the *rms* response to almost instantly cross the stationary level, resulting in characteristic over-shoot phenomena (Fig. 2c,d). When comparing the low frequency vibrations with the high frequency ones (with the same excitation velocities) the conventional seismic excitations result in higher response, but the dominating contribution of higher modes of vibration results in specific increase of the high frequency response in the upper part of the shear beam (Fig. 3b).

Most of the high frequency excitations, met in practice, do not cause substantial structural damages but evidently affect comfort of people living in the nearby buildings. In addition these high frequency vibrations transmitted from the soil may cause particular response and damages to

the equipment inside of the buildings. For very deep mines generating rockbursts from 2 km below the ground, their local Richter magnitude m_L may reach a value up to 5 and cause multimillion dollar losses on the ground and in some cases endanger the life of people, particularly for the mine crews working underground. Another important field of application of these extended non-stationary random vibration analyses covers the safety of buildings threaten by strong nearby underground explosions.

REFERENCES

Ambraseys N., Smit P., Berardi R., Rinaldis D., Cotton F., Berge-Thierry C., *Dissemination of European Strong- Motion Data*. CD-ROM collection. European Council, Environment and Climate Research Programme, 1999.

Davenport A.G., Note on the distribution of the largest value of a random function with application to gust loading, *Proceedings of the Institution of Civil Engineers*, vol. 28, 1964, pp. 187–196.

Dowding C.H., *Construction vibrations*, Prentice Hall, London 1996.

Lu Y., Hao H., Ma G., Zhou Y., Local-mode resonance and its structural effects under horizontal ground shock excitations, *Journal of Sound & Vibration*, vol. 254, no. 1, 2002, pp. 51–68.

Priestley M.B., Power spectral analysis of nonstationary random processes, *Journal of Sound & Vibration*, vol. 6, 1967, 86–97.

Safak E., Wave-propagation formulation of seismic response of multistory buildings, *Journal of Structural Engineering, ASCE*, vol. 125, no. 4, 1999, pp. 426–437.

Todorovska M.I. and Lee V.W., Seismic waves in buildings with shear walls or central core, *Journal of Engineering Mechanics, ASCE*, vol. 115, no. 12, 1989, pp. 2669–2686.

Todorovska M.I. and Trifunac M.D., Antiplane earthquake waves in long structures, *Journal of Engineering Mechanics, ASCE*, vol. 115, no. 12, 1989, pp. 2687–2708.

Vanmarcke E.H., On the distribution of the first passage time for normal stationary random processes, *Journal of Applied Mechanics, ASME*, vol. 42, 1975, 215–220.

Yang J.-N., Nonstationary envelope process and first excursion probability, *Journal of Structural Mechanics*, vol. 1, 1972, 231–248.

Zembaty Z., A note on non-stationary stochastic response and strong motion duration, *Earthquake Engineering & Structural Dynamics*, vol.16, 1988, 1189–1200.

Zembaty Z., Rockburst induced ground motion – a comparative study, *Soil Dynamics & Earthquake Engineering*, vol.24, no.1, January 2004, pp. 11–23.

Reliability and Optimization of Structural Systems: Assessment, Design and Life-Cycle Performance – Frangopol, Kawatani & Kim (eds)
© 2007 Taylor & Francis Group, London, ISBN 978-0-415-40655-0

Case studies on determination of load and resistance factors by method of moments

Yan-Gang Zhao, Zhao-Hui Lu
Department of Architecture, Nagoya Institute of Technology, Nagoya, Japan

Alfredo H-S. Ang
Department of Civil & Environmental Engineering, University of California, Irvine, USA

Yuefeng Geng
Department of Architecture, Nagoya Institute of Technology, Nagoya, Japan

ABSTRACT: In this paper, the basic principle of the load and resistance factor format for structural design is reviewed, and the principle for the determination of load and resistance factors using method of moments are described. Some case studies are conducted and it is found that although the load and resistance factors obtained using the method of moments are different from those obtained through the first order reliability method, the required structural resistances under a specific design condition are almost the same. Since the present formula is based on the first few moments of the load and resistances, the LRFs can be determined even when the distributions of the random variables are unknown.

1 INTRODUCTION

As the insurance of the performance of a structure must be accomplished under conditions of uncertainty, probabilistic analysis will generally be necessary for reliability-based structural designs. However, the reliability-based structural design may also be developed without a complete probabilistic analysis. If the required safety factors are predetermined on the basis of specified probability-based requirement, reliability-based design may be accomplished through the adoption of appropriate deterministic design criteria, e.g., the use of traditional safety factors.

For obvious reasons, design criteria should be as simple as possible; moreover, they should be developed in a form that is familiar to the practical engineers. This can be accomplished through the use of load amplification factors and resistance reduction factors, known as the LRFD format (Ang & Tang, 1984, Ellingwood et al., 1982). That is the nominal design loads are amplified by appropriate load factors and the nominal resistances are reduced by corresponding resistance factors, and safety is assured if the factored resistance is at least equal to the factored loads. The appropriate load and resistance factors must be developed in order to obtain designs that achieve a prescribed level of reliability.

The load and resistance factors are generally determined using the first order reliability method (FORM), in which the "design point" must be determined and derivative-based iteration has to be used. In this paper, the basic principle of the load and resistance factor format for structural design is reviewed, and the principle for the determination of load and resistance factors using method of moments is described. From the investigation of the present paper, it is found that although the load and resistance factors obtained using the method of moments are different from those obtained through the first order reliability method, the required structural resistances under a specific design condition are almost the same.

2 REVIEW ON DETERMINING LOAD AND RESISTANCE FACTORS

The LRFD format may be expressed as the follows.

$$\phi R_n \geq \Sigma \gamma_i S_{ni} \tag{1}$$

where ϕ = the resistance factor; γ_i = the partial load factor to be applied to load S_i; R_n = the nominal value of the resistance; S_{ni} = the nominal value of load S_i.

In reliability-based structural design, the resistance factor ϕ and the load factor γ_i should be determined on the basis of achieving a specified reliability. That is, the design format, Eq. 1, should be equivalent to the following equations in probability terms.

$$G(X) = R - \Sigma S_i \tag{2}$$

$$P_f \leq P_{fT} \quad \text{or} \quad \beta \geq \beta_T \tag{3}$$

where R and S_i are the random variables representing the uncertainty included in resistance and load effects. P_f and β are the probability of failure and reliability index corresponding to the performance function Eq. 2. P_{fT} and β_T are the target probability of failure and target reliability index, respectively.

If R and S_i are mutually independent normal random variables, the second moment method is correct and the design formula becomes

$$\beta_{2M} \geq \beta_T \tag{4}$$

where

$$\beta_{2M} = \frac{\mu_G}{\sigma_G}, \quad \mu_G = \mu_R - \Sigma \mu_{Si}, \quad \sigma_G = \sqrt{\sigma_R^2 + \Sigma \sigma_{Si}^2} \tag{5}$$

where β_{2M} is the second moment reliability index; μ_G and σ_G are the mean value and standard deviation of the performance function G, respectively; μ_R and σ_R are the mean value and standard deviation of R, respectively; μ_{Si} and σ_{Si} are the mean value and standard deviation of S_i, respectively.

Substituting Eq. 5 in Eq. 4, produces,

$$\mu_R(1 - \alpha_R V_R \beta_T) \geq \Sigma \mu_{Si}(1 + \alpha_{Si} V_{Si} \beta_T) \tag{6}$$

Comparing Eq. 6 with Eq. 1, the load and resistance factors may be expressed as,

$$\phi = (1 - \alpha_R V_R \beta_T)\frac{\mu_R}{R_n} \qquad \gamma_i = (1 + \alpha_{Si} V_{Si} \beta_T)\frac{\mu_{Si}}{S_{ni}} \tag{7}$$

When R and S_i are non-normal random variables, the reliability index expressed in Eq. 5 is not correct. The reliability index corresponding to the performance function Eq. 2 is generally obtained by the first order reliability method (FORM). The design format can be expressed as

$$R^* \geq \Sigma S_i^* \tag{8}$$

And the load and resistance factors can be obtained as (Ellingwood et al., 1982, Galambos et al., 1982).

$$\phi = \frac{R^*}{R_n}, \quad \gamma_i = \frac{S_i^*}{S_{ni}} \tag{9}$$

where R^* and S_i^* are the values, respectively, of variable R and S_i at the design point of FORM. Since R^* and S_i^* are obtained using derivative-based iteration, explicit expressions of R^* and S_i^* are not available. Some simplifications are proposed in order to avoid iterative computation (Mori, 2002, Mori & Maruyama 2005, Ugata 2000).

In the present paper, the reliability index in Eq. 3 will be obtained using the method of moments. Since the central moments of the performance function, as described in Eq. 2, can be obtained quite easily, the probability of failure, which is defined as Prob[$G(\mathbf{X}) < 0$] can be expressed as a function of the central moments. Since no derivative-based iteration is necessary in the proposed method, the determination of the required load and resistance factors should be simpler accomplished.

3 LOAD AND RESISTANCE FACTORS BY METHODS OF MOMENT

3.1 *Determination of load and resistance factors using third moment method*

Consider the performance function in Eq. 2, without loss of generality, standardize the performance function $G(\mathbf{X})$ using the following standardized variable

$$z_u = \frac{G - \mu_G}{\sigma_G} \tag{10}$$

Then the probability of failure corresponding to the performance function Eq. 2 can be expressed as the following equation according to its definition.

$$\begin{aligned} P_f &= Prob[G \le 0] = Prob[z_u \sigma_G + \mu_G \le 0] \\ &= Prob[z_u \le -\frac{\mu_G}{\sigma_G}] = Prob[z_u \le -\beta_{2M}] \end{aligned} \tag{11}$$

where β_{2M} is the second-moment reliability index expressed in Eq. 5a.

The relationship between the standardized variable z_u and the standard normal variable can be expressed as (Zhao & Ono, 2000)

$$u = \frac{1}{2\lambda}(\sqrt{1 + 2\lambda^2 + 4\lambda z_u} - \sqrt{1 - 2\lambda^2}) \tag{12}$$

where λ is simplified by the following equation (error is less than 2% for $-1 < \alpha_{3G} < 1$) (Zhao & Ono 2001).

$$\lambda = \alpha_{3G}/6 \tag{13}$$

where α_{3G} is the 3rd dimensionless central moment, i.e., the skewness of $G(\mathbf{X})$. α_{3G} is given as

$$\alpha_{3G} = (\alpha_{3R}\sigma_R^3 - \Sigma\alpha_{3i}\sigma_{Si}^3)/\sigma_G^3 \tag{14}$$

Substituting Eq. 14 in Eq. 12, the result for Eq. 12 can be simplified as

$$u = \frac{1}{\alpha_{3G}}(\sqrt{9 + \alpha_{3G}^2 + 6\alpha_{3G} z_u} - 3) \tag{15}$$

Let the CDF of z_u be F, then we have

$$F(z_u) = \Phi(u) = \Phi\left[\frac{1}{\alpha_{3G}}(\sqrt{9 + \alpha_{3G}^2 + 6\alpha_{3G} z_u} - 3)\right] \tag{16}$$

Then, Eq. 11 can be expressed as

$$P_f = F(-\beta_{2M}) = \Phi\left[\frac{1}{\alpha_{3G}}\left(\sqrt{9+\alpha_{3G}^2-6\alpha_{3G}\beta_{2M}}-3\right)\right] \tag{17}$$

Therefore, the reliability index can be given as

$$\beta_{3M} = \frac{1}{\alpha_{3G}}\left(3-\sqrt{9+\alpha_{3G}^2-6\alpha_{3G}\beta_{2M}}\right) \tag{18}$$

Note, here, the CDF of z_u is only used to deduce the Eq. 18, no F is used in the calculation of β. Since the first three moments of $G(\mathbf{X})$ is used in the Eq. 18, β_{3M} in Eq. 18 is a third moment reliability index.
Substituting Eq. 18 in the design format described in Eq. 3, yields,

$$\frac{1}{\alpha_{3G}}\left(3-\sqrt{9+\alpha_{3G}^2-6\alpha_{3G}\beta_{2M}}\right) \geq \beta_T \tag{19}$$

After some arrangements, we have

$$\beta_{2M} \geq \beta_T - \frac{1}{6}\alpha_{3G}\left(\beta_T^2-1\right) \tag{20}$$

Denoting the right side of Eq. 20 as β_{2T}, one obtains

$$\beta_{2M} \geq \beta_{2T} \tag{21a}$$

$$\beta_{2T} = \beta_T - \frac{1}{6}\alpha_{3G}\left(\beta_T^2-1\right) \tag{21b}$$

Equation 21a is as same as Eq. 3. It means that if the second moment reliability index β_{2M} is at least equal to β_{2T}, the reliability index β will be at least equal to the target reliability index β_T, and the required reliability is satisfied. Therefore, β_{2T} can be considered to be a target value of β_{2M}, and is denoted as the target second moment reliability index hereafter.

Substituting Eq. 5 in Eq. 21a, yields,

$$\mu_R(1-\alpha_R V_R \beta_{2T}) \geq \Sigma\mu_{Si}(1+\alpha_{Si}V_{Si}\beta_{2T}) \tag{22}$$

Comparing Eq. 22 with Eq. 1, the load and resistance factors may be expressed as,

$$\phi = (1-\alpha_R V_R \beta_{2T})\frac{\mu_R}{R_n} \qquad \gamma_i = (1+\alpha_{Si}V_{Si}\beta_{2T})\frac{\mu_{Si}}{S_{ni}} \tag{23}$$

where V_R and V_{Si} are the coefficient of variation, respectively, of R and S_i, and α_R and α_{Si} are the direction cosines, respectively, for R and S_i, which are the same as Eq. 8.

Comparing Eq. 23 with Eq. 7, one may understand that after replacing β_T in Eq. 7 by β_{2T} in Eq. 23, the determination of load and resistance factors using the third moment method is essentially the same as that by the second moment method.

3.2 *Determination of load and resistance factors using fourth moment method*

The standardized variable z_u can be expressed as a polynomial function of the standard normal variable u as the following equation, which was suggested by Fleishman (1978)

$$z_u = a_1 + a_2 u + a_3 u^2 + a_4 u^3 \tag{24}$$

where a_1, a_2, a_3 and a_4 are the polynomial coefficients that can be obtained by making the first four moments of the left side of Eq. 24 equal to those of the right side.

Eq. 24 is simple if the coefficients a_1, a_2, a_3, and a_4 are known. However, the determination of the four coefficients is not easy, since the solution of nonlinear equations has to be found when using Eq. 24. An alternative way may be the first two polynomials of the Cornish-Fisher expansion (Stuart & Ord 1987).

$$z_u = S(u) = u + \frac{1}{6}\alpha_{3G}(u^2 - 1) + \frac{1}{24}(\alpha_{4G} - 3)(u^3 - 3u) \tag{25}$$

where α_{4G} = the 4th dimensionless central moment, i.e., the kurtosis of $G(\mathbf{X})$, which is calculated from

$$\alpha_{4G} = \frac{1}{\sigma_G^4}(\alpha_{4R}\sigma_R^4 + 6\sigma_R^2\sum_{i=1}^{n}\sigma_{Si}^2 + \sum_{i=1}^{n}\alpha_{4Si}\sigma_{Si}^4 + 6\sum_{i=1}^{n-1}\sum_{j>i}^{n}\sigma_{Si}^2\sigma_{Sj}^2) \tag{26}$$

One can see that Eq. 25 is in close form and is quite easily to be used, however, since the first four moments of the right side of Eq. 25 are not equal to those of the left side, the transformation generates relatively large errors.

In order to improve the Cornish-Fisher expansion, Winterstein (1988) developed an expansion expressed as

$$z_u = -\tilde{k}\tilde{h}_3 + \tilde{k}(1 - 3\tilde{h}_4)u + \tilde{k}\tilde{h}_3 u^2 + \tilde{k}\tilde{h}_4 u^3 \tag{27a}$$

in which

$$\tilde{h}_3 = \frac{\alpha_{3G}}{4 + 2\sqrt{1 + 1.5(\alpha_{4G} - 3)}}, \tilde{h}_4 = \frac{\sqrt{1 + 1.5(\alpha_{4G} - 3)} - 1}{18} \tag{27b}$$

$$\tilde{k} = \frac{1}{\sqrt{1 + 2\tilde{h}_3^2 + 6\tilde{h}_4^2}} \tag{27c}$$

Denote Eq. 27a as

$$z_u = S(u) \tag{28}$$

And suppose the inverse function of S is

$$u = S^{-1}(z_u) \tag{29}$$

Let the CDF of z_u be F, then we have

$$F(z_u) = \Phi(u) = \Phi[S^{-1}(z_u)] \tag{30}$$

According to Eq. 11, the reliability index is expressed as

$$\beta = -\Phi^{-1}(P_f) = -S^{-1}(-\beta_{2M}) \tag{31}$$

Substituting Eq. 31 in the design format described in Eq. 3, yields,

$$\beta = -S^{-1}(-\beta_{2M}) \geq \beta_T \tag{32}$$

From which,

$$\beta_{2M} \geq -S(-\beta_T) = \tilde{k}\tilde{h}_3 + \tilde{k}(1 - 3\tilde{h}_4)\beta_T - \tilde{k}\tilde{h}_3\beta_T^2 + \tilde{k}\tilde{h}_4\beta_T^3 \tag{33}$$

Denoting the right side of Eq. 33 as β_{2T}, one obtains

$$\beta_{2M} \geq \beta_{2T} \tag{34a}$$

$$\beta_{2T} = \tilde{k}\tilde{h}_3 + \tilde{k}(1-3\tilde{h}_4)\beta_T - \tilde{k}\tilde{h}_3\beta_T^2 + \tilde{k}\tilde{h}_4\beta_T^3 \tag{34b}$$

As described in the previous section, Equation 34a is as same as Eq. 3. It means that if the second moment reliability index β_{2M} is at least equal to β_{2T}, the reliability index β will be at least equal to the target reliability index β_T, and the required reliability is satisfied. Therefore, β_{2T} is the target second moment reliability index.

Since Eq. 34a is the same as Eq. 4 except that the right side is β_{2T}, the load and resistance factors corresponding to Eq. 34a can be easily obtained by substituting β_T in the right side of Eq. 4 with β_{2T}. The design formula is essentially the same as Eq. 22 and the load and resistance factors are essentially the same as Eq. 23.

When $\alpha_{4G} = 3$ and $\alpha_{3G} = 0$, Eq. 35 becomes $\beta_{2T} = \beta_T$, which is exactly the same as Eq. 4, and the load and resistance factors can be determined using Eqs. 7 & 8.

Since the formula above is based on the first four moments of the load and resistances, the LRFs can be determined even when the distributions of the random variables are unknown.

The variations of the target second moment reliability index β_{2T} with respect to the target reliability index β_T are shown in Fig. 1a in the case of $\alpha_{3G} = 0$, in Figs. 1b, 1c, and 1d in the cases of $\alpha_{4G} = 2.8$, $\alpha_{4G} = 3.0$, and $\alpha_{4G} = 3.2$, respectively. From these figures, one can see that β_{2T} is generally larger than β_T for negative α_{3G} and smaller than β_T for positive α_{3G}. One can also see that β_{2T} is generally larger than β_T for $\alpha_{4G} > 3.0$ and smaller than β_T for positive $\alpha_{4G} < 3.0$.

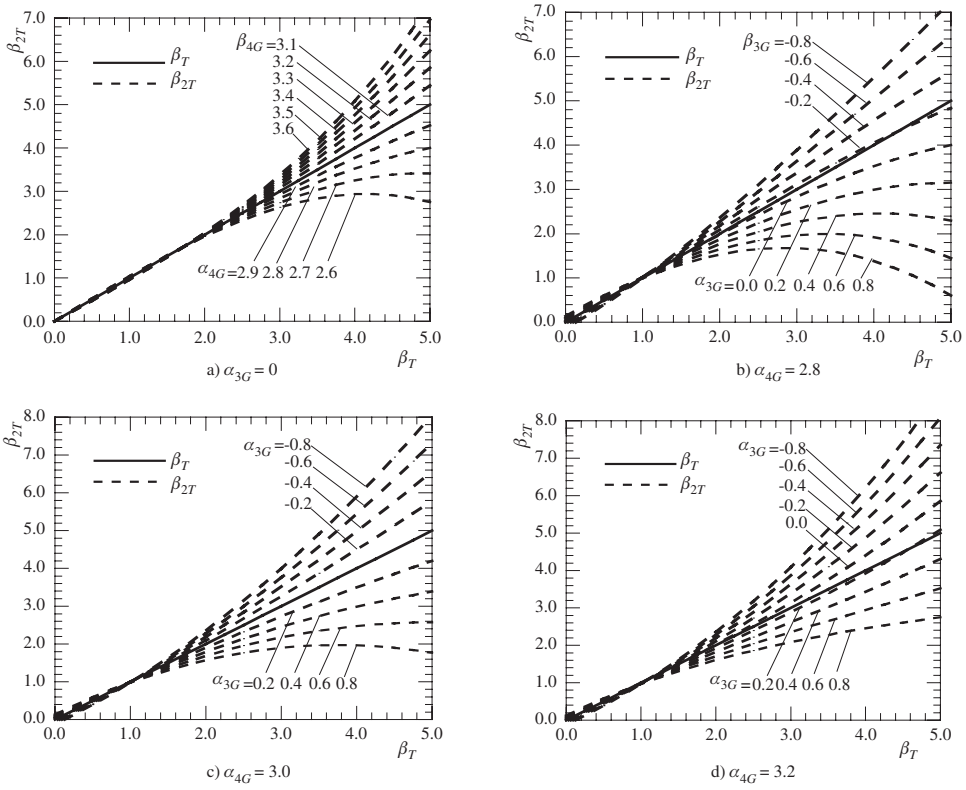

Figure 1. Variations of target 2 M reliability index with respect to α_{3G} and α_{4G}.

3.3 *Determination of the mean value of resistance*

Since the load and resistance factors are determined when the reliability index is equal to the target reliability index, the mean value of the resistance should be determined under this condition (hereafter referred to as the target mean resistance). In this study, the target mean resistance is computed using the following approximate equation.

$$\mu_{RT} = \mu'_R + (1 + \frac{1}{2}\alpha'_{3G})(\beta_T - \beta'_M)\sigma'_G \tag{35}$$

where

$$\mu'_R = \Sigma\mu_{Si} + \beta_T\sqrt{\Sigma\sigma_{Si}^2} \tag{36}$$

where μ_{RT} = the target mean resistance; σ'_G and α'_{3G} = the standard deviation and skewness of G obtained using μ'_R; β'_M = third or fourth moment reliability index obtained using μ'_R.

4 NUMERICAL EXAMPLES

Example 1

Consider the following performance function,

$$G(X) = R - (D + L) \tag{37}$$

where R = resistance, a lognormal variable with $\mu_R/R_n = 1.1$, $V_R = 0.15$,

D = dead load, a normal variable with $\mu_D/D_n = 1.0$, $V_D = 0.1$, and

L = live load, a Weibull variable with $\mu_L/L_n = 0.45$, $V_L = 0.4$.

The skewness for R, D, and L are 0.453, 0, and 0.2768, respectively, and the kurtosis for R, D, and L are 3.368, 3, and 2.78, respectively.

The load and resistance factors obtained using the proposed method of moments are illustrated in Figs. 2a and 2b for $\beta_T = 2$ and $\beta_T = 3$, respectively, compared with the corresponding factors obtained using FORM. The target mean resistances obtained using the proposed method and those obtained by FORM are illustrated in Figs. 3a and 3b for $\beta_T = 2$ and $\beta_T = 3$, respectively. From Figs. 2 and 3, one can see that although the load and resistance factors obtained by the present method are different from those obtained by FORM, the target mean resistances obtained by the present methods are essentially the same as those obtained by FORM. That is, the same design

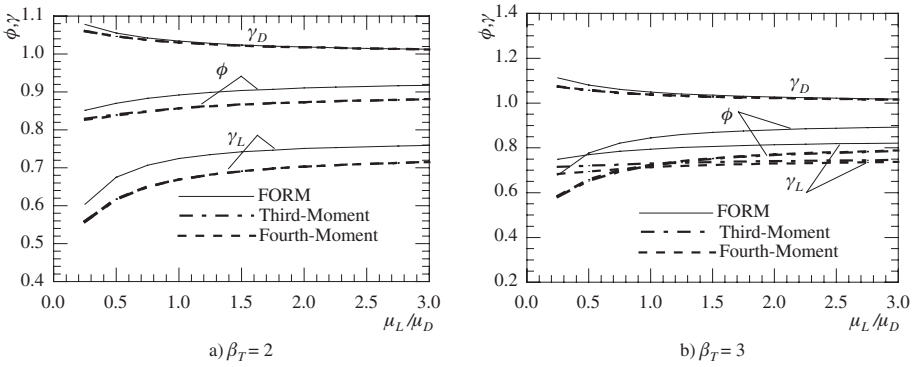

Figure 2. Load and resistance factors for Example 1.

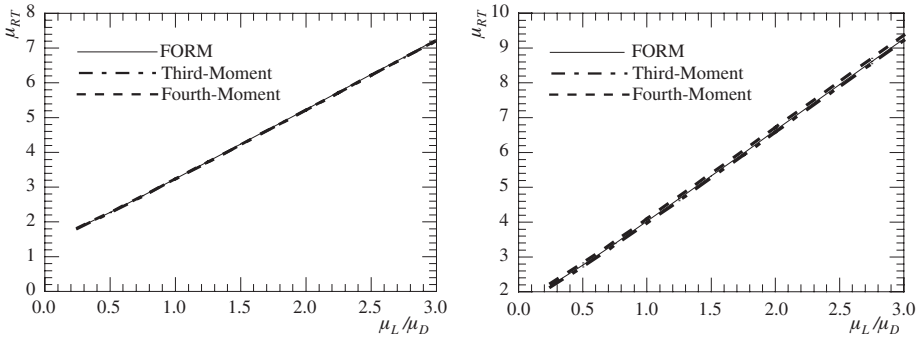

Figure 3. Target mean resistance for Example 1.

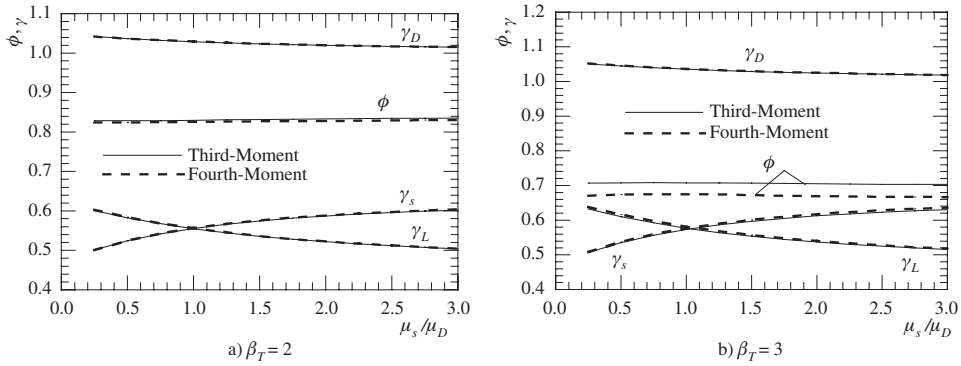

Figure 4. Load and resistance factors for Example 2.

results will be obtained by the FORM and moment method even though the load and resistance factors of the methods are different.

Example 2

Consider the following performance function,

$$G(X) = R - (D + L + S) \tag{38}$$

where R = resistance with unknown CDF, the known information are $\mu_R/R_n = 1.1$, $V_R = 0.15$, $\alpha_{3R} = 0.453$, and $\alpha_{4R} = 3.368$,

D = dead load, a normal variable with $\mu_D/D_n = 1.0$, $V_D = 0.1$, $\alpha_{3D} = 0$, and $\alpha_{4D} = 3$,

L = live load with unknown CDF, the known information are $\mu_L/L_n = 0.45$, $\mu_L/\mu_D = 0.5$, $V_L = 0.4$, $\alpha_{3L} = 1.264$, and $\alpha_{4L} = 5.969$, and

S = snow load which is the main load, a Gumbel variable with $\mu_S/S_n = 0.45$, $V_S = 0.4$, $\alpha_{3S} = 1.14$, and $\alpha_{4S} = 5.4$.

Since the CDFs of R and L are unknown, the FORM is impossible. Here, the LRFs are obtained using the proposed method.

The load and resistance factors obtained using the proposed methods of moments are illustrated in Figs. 4a and 4b for $\beta_T = 2$ and $\beta_T = 3$, respectively. The target mean resistances obtained using the proposed method are illustrated in Figs. 5a and 5b for $\beta_T = 2$ and $\beta_T = 3$, respectively. From Figs. 4a and 5a, one can see both the results of the load and resistance factors and the target mean resistances obtained by the third and fourth moment methods have good agreements.

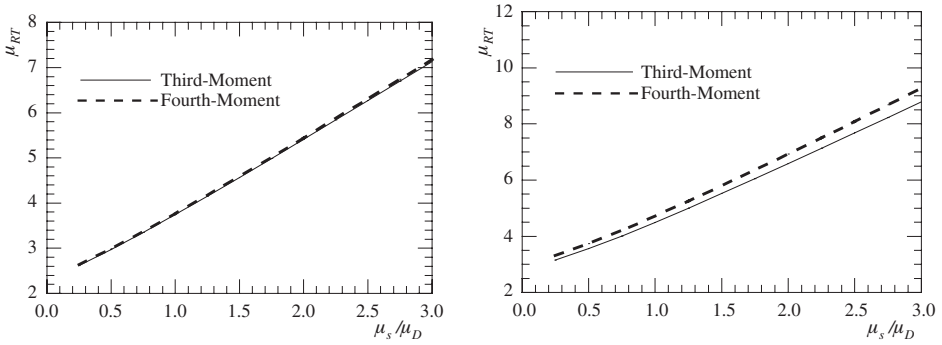

Figure 5. Target mean resistance for Example 2.

From Fig. 4b, one can see that all results of the load factors obtained by the third and fourth moment methods have good agreements but the resistance factors obtained by the two methods have visible differences. From Fig. 5b, one can see the target mean resistances obtained by the third and fourth moment methods have visible differences. This is because the third moment method in the later case produces relatively larger error since only the first three moments of the performance function are used. The application ranges of third moment method in terms of skewness are given by the following equation (Zhao et al., 2006).

$$-120r/\beta_{2M} \le \alpha_{3G} \le 40r/\beta_{2M} \tag{39}$$

where r is the allowable error.

From the equation, one can understand that the skewnesses of the performance function for $\beta_T = 2$ are within the application of 3M with $r = 1\%$ while that for $\beta_T = 3$ are beyond the application with $r = 1\%$. This can explain why there are visible differences between the target mean resistance obtained by the third and fourth moment methods.

5 CONCLUSIONS

(1) Determination of load and resistance factors using the method of moments is proposed. Derivative-based iteration, which is necessary in FORM, is not required in the proposed method. For this reason, the proposed method is simpler to apply.
(2) Although the load and resistance factors obtained by the present method are different from those obtained by FORM, the target mean resistances obtained by both methods are essentially the same.
(3) Since the present formula is based on the first few moments of the load and resistances, the LRFs can be determined even when the distributions of the random variables are unknown.

REFERENCES

Ang, A. H-S. and Tang, W. Probability Concepts in Engineering Planning and Design, Vol II – Decision, Risk, and Reliability. New York, J. Wiley & Sons; 1984.

Ellingwood, B., MacGregor, G., Galambos, T.V. and Cornell, C. A. Probability based load criteria: Load factor and load combinations. *J. Struct. Div, ASCE* 1982; 108(5): 978–997.

Fleishman, A.L. "A method for simulating non-normal distributions." *Psychometrika* 1978; 43(4): 521–532.

Galambos, T.V., Ellingwood, B. MacGregor, G. and Cornell, C.A. Probability based load criteria: Assessment of current design practice. *J. Struct. Div, ASCE* 1982; 108(5), 959–977.

Mori, Y. Practical method for load and resistance factors for use in limit state design (in Japanese). *J. Struct. Constr. Eng.*, AIJ 2002; No. 559: 39–46.
Mori, Y. and Maruyama, Y. Simplified method for load and resistance factors and accuracy of sensitivity factors (in Japanese). *J. Struct. Constr. Eng.*, AIJ 2005; No. 589: 67–72.
Stuart, A. and Ord, J.K. Kendall's Advanced Theory of Statistics, Vol. 1, Distribution Theory. Fifth edition, London: Charles Griffin; 1987.
Ugata, T. Reliability analysis considering skewness of distribution-Simple evaluation of load and resistance factors (in Japanese). *J. Struct. Constr. Eng.*, AIJ 2000; No. 529: 43–50.
Winterstein, S.R. Nonlinear vibration models for extremes and fatigue. *J. Engrg. Mech.*, ASCE 1988; 114(10): 1772–1790.
Zhao, Y.G. and Ono, T. Third-moment standardization for structural reliability analysis. *J. Struct. Engrg, ASCE* 2000; 126(6): 724–732.
Zhao, Y.G., Ono, T., Idota, H. and Hirano, T. A three-parameter distribution used for structural reliability evaluation. *J. Struct. Constr. Eng.*, AIJ 2001; No. 546: 31–38.
Zhao, Y.G., Lu, Z.H. and Ono, T. A Simple Third-Moment Method for Structural Reliability. *J. of Asian Architecture and Building Engineering* 2006; 5(1): 129–136.

Reliability and Optimization of Structural Systems: Assessment, Design and Life-Cycle Performance – Frangopol, Kawatani & Kim (eds)
© 2007 Taylor & Francis Group, London, ISBN 978-0-415-40655-0

A method for computing reliability bound of series structural systems

Wei-Qiu Zhong
Department of Civil Engineering, Dalian University of Technology, Dalian, China

Yan-Gang Zhao
Department of Architecture, Nagoya Institute of Technology, Nagoya, Japan

Alfredo H-S. Ang
Department of Civil & Environmental Engineering, University of California, Irvine, USA

ABSTRACT: In the present paper, in order to improve the accuracy of the narrow bound estimation method, a computationally effective point estimation method for calculating the joint probability of every pair of failure modes is introduced and examined for series systems. Based on the computational results of several illustrative examples, it can be seen that the results by the present method are in good agreements with those obtained through integration.

1 INTRODUCTION

The evaluation of system reliability for structures has been an active area of research for over three decades. According to the logical relationship of the failure modes of structures, structural systems can be divided into three types; namely, series systems, parallel systems and hybrid structural systems. Of interest here is the reliability assessment of series systems which is encountered most frequently in practical design and analysis.

The failure probability of a series structural system theoretically involves multi-dimensional integration which is usually difficult to evaluate especially for structures of practical significance. The search for efficient computational procedures for estimating system reliability has resulted in several approaches including bounding techniques and efficient Monte-Carlo simulations (MCS).

The bounding methods include the wide bound estimation method and the narrow bound estimation method. For the narrow bound method, the joint failure probability of every pair of failure modes needs to be calculated. In this study, in order to improve the accuracy of the narrow bound estimation method, a point estimation of the joint failure probability of series structural systems is proposed and examined.

2 REVIEW OF SYSTEM RELIABILITY OF SERIES SYSTEMS

Consider a series structural system with k possible failure modes and let the performance function for failure mode i be given by

$$g_i(\mathbf{X}) = g_i(x_1, x_2, \cdots, x_n), \qquad i = 1,2,\cdots,k \tag{1}$$

where $x_1, x_2, \ldots, x_n$ are the basic random variables, and $g_i(\cdot)$ is the performance function.

Define the failure event for failure mode i as

$$E_i = [g_i(\mathbf{X}) \le 0] \tag{2}$$

Since the occurrence of any failure event E_i will cause the failure of the structure, the failure event E of the structure is the union of all the possible failure modes, which can be expressed as

$$E = E_1 \cup E_2 \cup \cdots \cup E_k \tag{3}$$

In structural reliability theory, the failure probability P_f of a series structural system corresponding to the occurrence of the event E of Eq.(3) theoretically involves the following integration

$$P_f = \int\cdots\int_{(E_1 \cup E_2 \cup \cdots \cup E_k)} f_{x_1 x_2 \cdots x_n}(x_1, x_2, \cdots, x_n)\mathrm{d}x_1\mathrm{d}x_2\cdots\mathrm{d}x_n \tag{4}$$

where $f(\cdot)$ is the pertinent joint probability density function.

The evaluation of the above multi-dimensional integration is often difficult, especially for structures of practical dimensions. For this reason, approximate methods have been proposed and developed. These include the following "wide" bound technique for the failure probability of series structural systems (e.g., Cornell, 1967)

$$\max_{1 \le i \le k}(P_{fi}) \le P_f \le 1 - \prod_{i=1}^{k}(1 - P_{fi}) \tag{5}$$

where P_{fi} is the failure probability of the ith failure mode.

Since only the failure probability of a single failure mode is considered, and the correlation of the failure modes is neglected, the above wide bound estimation method is simple to evaluate; however, the bounds can be very wide especially for a complex system.

A "narrow" bound estimation method for the failure probability of series systems is also available (Ditlevsen, 1979)

$$P_{f1} + \sum_{i=2}^{k}\max(P_{fi} - \sum_{j=1}^{i-1}P_{fij}, 0) \le P_f \le \sum_{i=1}^{k}P_{fi} - \sum_{i=2}^{k}\max_{j<i}(P_{fij}) \tag{6}$$

where P_{fij} is the joint probability of the simultaneous occurrences of the ith and jth failure modes. The left and right hand sides of Eq. (6) are, respectively, the lower bound and upper bound of the failure probability of a series structural system with k potential failure modes. Observe that because the joint probability of simultaneous failures of every pair of failure modes must be evaluated, the resulting bounds of Eq. (6) is narrower than those of Eq. (5).

As is well known, P_{fij} can be expressed by (Ang and Tang, 1984)

$$P_{fij} = \Phi_2(-\beta_i, -\beta_j, \rho_{ij}) = \int_{-\infty}^{-\beta_i}\int_{-\infty}^{-\beta_j}\phi_2(x_i, x_j, \rho_{ij})\mathrm{d}x_i\mathrm{d}x_j \tag{7}$$

where

$$\phi_2(x_i, x_j, \rho_{ij}) = \frac{1}{2\pi\sqrt{1-\rho_{ij}^2}}\exp\left(-\frac{1}{2}\cdot\frac{x_i^2 + x_j^2 - 2\rho_{ij}x_i x_j}{1-\rho_{ij}^2}\right) \tag{8}$$

β_i and β_j are the reliability indices corresponding to the ith and jth failure modes, respectively; ρ_{ij} is the correlation coefficient between the ith and jth failure modes. $\phi_2(\cdot)$ and $\Phi_2(\cdot)$ are the probability density function and cumulative distribution function, respectively, of the two-dimensional standard normal distribution.

Equation (7) is an accurate expression for P_{fij}. To obtain the results, however, numerical integrations would be needed. To avoid such numerical integrations, further approximations are often adopted (involving further bounds for P_{fij}). Specific formulas for evaluating the lower and upper bounds of the joint failure probability P_{fij} were proposed by Ditlevsen (1979) as follows

$$\left.\begin{array}{ll} \max[\mathrm{P(A)},\mathrm{P(B)}] \le P_{fij} \le \mathrm{P(A)}+\mathrm{P(B)} & \rho_{ij} \ge 0 \\ 0 \le P_{fij} \le \min[\mathrm{P(A)},\mathrm{P(B)}] & \rho_{ij} < 0 \end{array}\right\} \tag{9}$$

where

$$\begin{aligned} \mathrm{P(A)} &= \Phi(-\beta_i)\Phi\left(-\frac{\beta_j-\rho_{ij}\beta_i}{\sqrt{1-\rho_{ij}^2}}\right) \\ \mathrm{P(B)} &= \Phi(-\beta_j)\Phi\left(-\frac{\beta_i-\rho_{ij}\beta_j}{\sqrt{1-\rho_{ij}^2}}\right) \end{aligned} \tag{10}$$

Since Eq.(9) is a bound rather than a specific value, it is not convenient to use in Eq.(6).

Feng (1989) gave a point estimate for the joint failure probability P_{fij} as

$$P_{fij} = [\mathrm{P(A)}+\mathrm{P(B)}][1-\arccos(\rho_{ij})/\pi] \tag{11}$$

where the definitions of P(A) and P(B) are the same as those in Eq.(9) and can be also calculated by Eq.(10). Since Eq.(11) is a specific value rather than a bound, it is convenient and considered to have high accuracy to be used in Eq.(6) for obtaining the narrow bounds of the system reliability (Wu and Burnside 1990; Song 1992; Penmesta and Grandhi 2002; Adduri et al., 2004). As described by Feng (1989), when the correlation coefficient $\rho_{ij} = 0$ or 1, Eq.(11) gives accurate solutions; whereas when $0 < \rho_{ij} < 1$, the calculational accuracy is reasonably high, especially when $\rho_{ij} \le 0.6$. However, as will be shown later, the lower bound obtained with Eq.(11) can sometimes be lower than the lower bound given by Eq. (9).

Introduced in the present paper, is an alternate method for estimating the joint failure probability, P_{fij}.(Zhao, Zhong and Ang, 2007)

3 A POINT ESTIMATE OF THE JOINT FAILURE PROBABILITY

To express the formulas more conveniently, β_1 and β_2 are used to represent β_i and β_j, respectively. And ρ is used to represent ρ_{ij}. Without loss of generality, assume $0 < \beta_1 \le \beta_2$.

Let Z_1 and Z_2 be the limit state functions in standard normal space corresponding to β_1 and β_2; then, the geometrical relationship between $Z_1 = 0$ and $Z_2 = 0$ can be depicted in Fig.1(a) when $\beta_1/\beta_2 \ge \rho$ and in Fig.1(b) when $\beta_1/\beta_2 < \rho$.

Let the angle between OB (β_1) and OC (β_2) be v, then

$$v = \arccos(\rho) \tag{12}$$

In Fig.1, the crossing point of $Z_1 = 0$ and $Z_2 = 0$ is point A. Define the length of the line segment OA as crossing index β_0, and denote the angle between OA and OB as v_1, and the angle between OA and OC as v_2; then v_1 and $v_2$can be expressed as

$$v_1 = \arccos(\beta_1/\beta_0), \quad v_2 = \arccos(\beta_2/\beta_0) \tag{13}$$

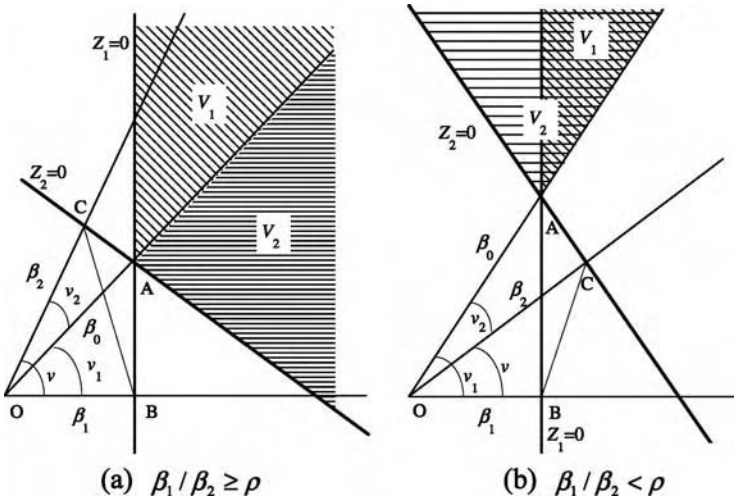

Figure 1. Probability calculation of P_{f12} in standard normal space.

With the aid of the geometrical relationships of β_0, β_1 and β_2, β_0 can be given as

$$\beta_0 = \sqrt{\frac{\beta_1^2 - 2\rho\beta_1\beta_2 + \beta_2^2}{1-\rho^2}} \tag{14}$$

Let V_1 denote the area of the failure zone between ray OA and $Z_1 = 0$, and V_2 denote the area of the failure zone between OA and $Z_2 = 0$, shown as the respective shaded zones in Fig. 1. The angle $\angle$OAB is equal to $\pi/2 - \nu_1$ and the angle $\angle$OAC is equal to $\pi/2 - \nu_2$. Since the joint failure probability P_{f12} is the area of the failure zone between $Z_1 = 0$ and $Z_2 = 0$, P_{f12} can be given as the following equation according to the geometrical relations in Fig. 1.

$$P_{f12} = \begin{cases} V_1 + V_2 & \beta_1/\beta_2 \geq \rho \\ P_{f2} + V_1 - V_2 & \beta_1/\beta_2 < \rho \end{cases} \tag{15}$$

In particular, when $\beta_1/\beta_2 = \rho$, $\beta_0 = \beta_2$. Then one can see that $V_2 = \frac{1}{2}P_{f2}$ from both Fig.1(a) and Fig.1(b), which means that both the formulas in Eq. (15) give the same results for $\beta_1/\beta_2 = \rho$.

When $\nu_m \geq \pi/4$ (where $m = 1, 2$), V_m of Eq. (15) can be obtained by constructing two perpendicular lines DD′ and EE′ through point A, the crossing point of $Z_1 = 0$ and $Z_2 = 0$. Let the angle $\angle$DAO $= \angle$EAO $= \pi/4$, as shown in Fig. 2.

Obviously, if EE′ and DD*prime* are considered to be limit state lines, both of their corresponding reliability indices would be $\beta_0/\sqrt{2}$. Since EE′ and DD′ are perpendicular, the probability associated with the area enclosed by $\angle$E′AD′ (gray area in Fig. 2) can be obtained as $\Phi^2(-\beta_0/\sqrt{2})$. Since the angle between OA and $Z_m = 0$ (the shaded zone in Fig. 2) that corresponds to V_m is $\pi/2 - \nu_m$, we have

$$\frac{\frac{\pi}{2}}{\Phi^2(-\beta_0/\sqrt{2})} \approx \frac{\frac{\pi}{2} - \nu_m}{V_m} \tag{16}$$

Hence, V_m can be given as

$$V_m \approx \Phi^2(-\beta_0/\sqrt{2})(1 - \frac{2\nu_m}{\pi}) \qquad \nu_m \geq \pi/4, \text{ where } m = 1, 2 \tag{17}$$

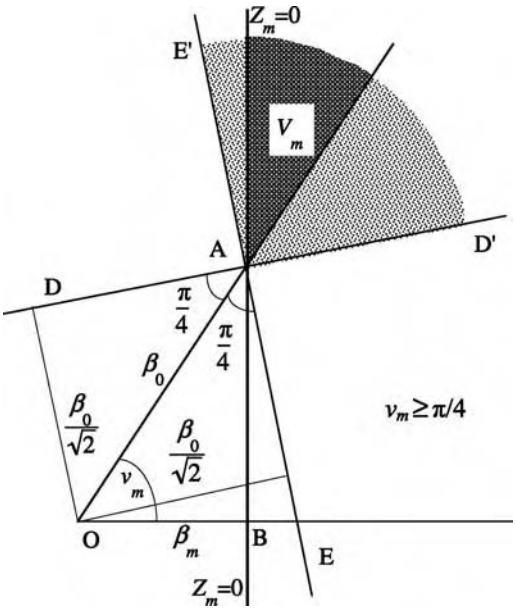

Figure 2. Geometrical relations for $v_m \geq \pi/4$.

Similarly, when $v_m < \pi/4$ (where $m = 1, 2$), V_m can be given as

$$V_m \approx \Phi(-\beta_m)\Phi(-\sqrt{\beta_0^2 - \beta_m^2}) - \Phi^2(-\beta_0/\sqrt{2})\frac{2v_m}{\pi} \qquad v_m < \pi/4, \text{ where } m = 1, 2 \tag{18}$$

Write

$$P_m = \Phi(-\beta_m)\Phi(-\sqrt{\beta_0^2 - \beta_m^2}) \tag{19}$$
$$P_0 = \Phi^2(-\beta_0/\sqrt{2})$$

Then Eqs. (17) and (18) can be written as

$$V_m = \begin{cases} P_0(1 - \dfrac{2v_m}{\pi}) & v_m \geq \dfrac{\pi}{4} \\ P_m - P_0\dfrac{2v_m}{\pi} & v_m < \dfrac{\pi}{4} \end{cases} \qquad \text{where } m = 1, 2 \tag{20}$$

Eqs. (15) and (20) are the proposed formulas for estimating the joint failure probability P_{f12}.

When $v_m = \frac{\pi}{4}$, according to Eq.(13), $\beta_0 = \sqrt{2}\beta_m$, then $P_m = P_0 = \Phi^2(-\beta_m)$. In this case, the two formulas in Eq. (20) give the same results.

In particular, when $\rho = 0$, it can be seen that $v = \arccos(0) = \frac{\pi}{2}$ and $\beta_0 = \sqrt{\beta_1^2 + \beta_2^2}$, then

$$P_1 = P_2 = \Phi(-\beta_1)\Phi(-\beta_2)$$

Since $v_1 + v_2 = v = \frac{\pi}{2}$, and $v_1 \geq v_2$, one can see that $v_1 \geq \frac{\pi}{4}$. Then P_{f12} is given by

$$P_{f12} = \Phi(-\beta_1)\Phi(-\beta_2) \qquad \rho = 0 \tag{21}$$

Another special case is when $\rho = 1$. Obviously, P_{f12} can not be directly given by the equations given above since β_0 is not defined when $\rho = 1$. In this case, when $\rho \to 1$, we have

$$\lim_{\rho \to 1} P_{f12} = P_{f2} \tag{22}$$

4 EXAMINATION AND EXAMPLES

In order to evaluate the advantage or superiority of the proposed method, a number of series structural systems are examined.

Example 1

Consider first a series structural system with only two failure modes. Several cases are examined to compare the results by different methods as follows.

When the reliability indices of the two failure modes are the same, the results for P_{f12} are presented in Figs. 3a through 3c with $\beta_1 = \beta_2 = 2$; $\beta_1 = \beta_2 = 3$; and $\beta_1 = \beta_2 = 4$, respectively, and for various correlation coefficient ρ. Figs. 4a–4c show the solutions obtained by integration, the Ditlevsen's bounds, Feng's point estimation, and the point estimation proposed here. From the figures, it can be seen that (1) Ditlevsen's bounds correctly bound the integration results, (2) the results by Feng's method are quite close to the integration results, and (3) the results given by the present method have a better agreement with the integration method than those by Feng's method.

When the reliability indices for the two failure modes are different, the variations of the joint failure probability P_{f12} with respect to the correlation coefficient ρ are depicted in Figs. 3d through 3f, respectively, for $\beta_1 = 2.5$, $\beta_2 = 3.5$; $\beta_1 = 2$, $\beta_2 = 4$; and for $\beta_1 = 1$, $\beta_2 = 5$. From these figures, it can be seen that the integration results are always located between the narrow bound solutions. Both the results by Feng's method and the present method have good agreements with the integration method when $\rho = 0$ and $\rho = 1$. However, whereas the results by the present method have a good agreement with those by integration for all the three cases, the results given by Feng's method tend to be lower than the lower bound solution especially for large ρ and this discrepancy becomes very large for significant differences in the two reliability indices (as can be seen in Fig. 3f).

Example 2

Consider a one-story one-bay elastoplastic frame shown in Fig. 4 (after Ono, et al., 1990). The loads M_i and member strengths S_i are independent log-normal random variables with mean values of $\mu_{M1} = \mu_{M2} = 500$ ft kip, $\mu_{M3} = 667$ ft kip, $\mu_{S1} = 50$ kip, $\mu_{S2} = 100$ kip and standard deviations of $\sigma_{M1} = \sigma_{M2} = 75$ ft kip, $\sigma_{M3} = 100$ ft kip, $\sigma_{S1} = 15$ kip, $\sigma_{S2} = 10$ kip. The performance functions that correspond to the six most likely failure modes obtained from stochastic limit analysis are listed below with the FORM reliability index for each mode given in parentheses to show the relative dominance of the different modes

$$g_1 = 2M_1 + 2M_2 - 15S_1 \quad (\beta_F = 3.247) \tag{23a}$$

$$g_2 = M_1 + 3M_2 + 2M_3 - 15S_1 - 10S_2 \quad (\beta_F = 3.551) \tag{23b}$$

$$g_3 = 2M_1 + M_2 + M_3 - 15S_1 \quad (\beta_F = 3.562) \tag{23c}$$

$$g_4 = M_1 + 2M_2 + M_3 - 15S_1 \quad (\beta_F = 3.562) \tag{23d}$$

$$g_5 = M_1 + M_2 + 2M_3 - 15S_1 \quad (\beta_F = 3.784) \tag{23e}$$

$$g_6 = M_1 + M_2 + 4M_3 - 15S_1 - 10S_2 \quad (\beta_F = 3.848) \tag{23f}$$

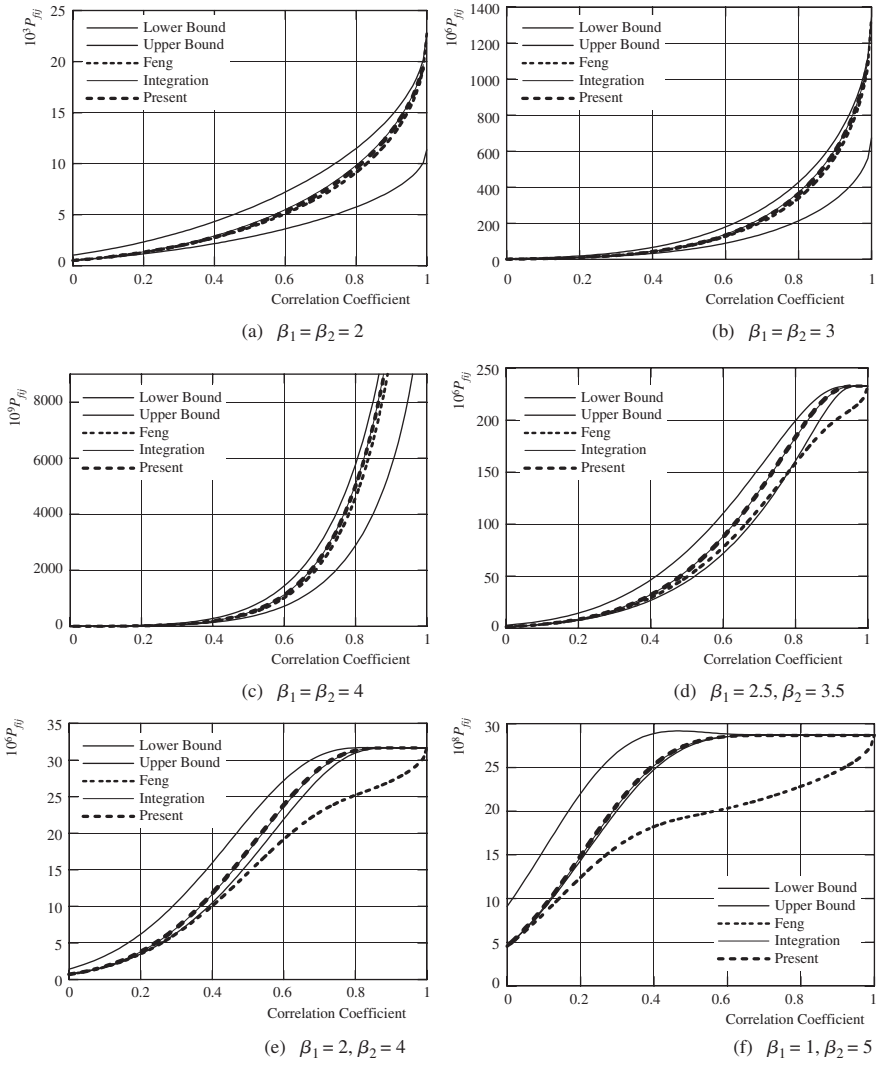

Figure 3. Variations of the joint failure probability, P_{f12}, with respect to correlation coefficient.

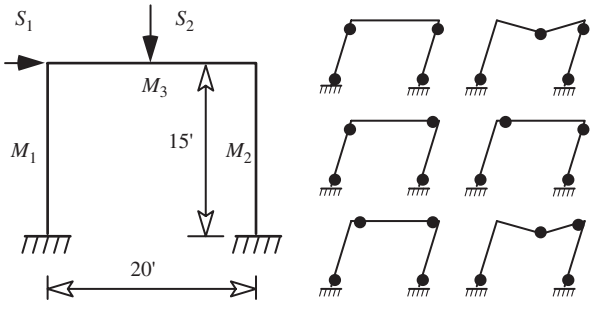

Figure 4. 1-story 1-bay frame of example 3.

Using the performance functions listed in Eq. (23) the correlation matrix is as follows

$$[C]=\begin{bmatrix} 1 & 0.810 & 0.942 & 0.875 & 0.753 & 0.499 \\ 0.810 & 1 & 0.932 & 0.837 & 0.895 & 0.855 \\ 0.942 & 0.932 & 1 & 0.937 & 0.920 & 0.749 \\ 0.875 & 0.837 & 0.937 & 1 & 0.920 & 0.749 \\ 0.753 & 0.895 & 0.920 & 0.920 & 1 & 0.923 \\ 0.499 & 0.855 & 0.749 & 0.749 & 0.923 & 1 \end{bmatrix}$$

and the joint failure probability for each pair of failure modes are given as

$$[P_{fij}]=10^{-6}\begin{bmatrix} 582.8 & 72.81 & 147.1 & 101.4 & 28.14 & 4.778 \\ 72.81 & 191.8 & 88.45 & 47.40 & 40.39 & 26.43 \\ 147.1 & 88.45 & 183.9 & 89.31 & 46.88 & 13.27 \\ 101.4 & 47.40 & 89.31 & 183.9 & 46.88 & 13.27 \\ 28.14 & 40.39 & 46.88 & 46.88 & 77.14 & 27.83 \\ 4.778 & 26.43 & 13.27 & 13.27 & 27.83 & 59.50 \end{bmatrix}$$

From the matrix above the lower and upper bounds of the system failure probability are obtained, respectively, as $7.017*10^{-4}$ and $9.331*10^{-4}$. The corresponding MCS solution using a 10 million sample size is $6.147*10^{-4}$ with a c.o.v. of 1.275%. One can see that the MCS result is outside the indicated bounds. This is because the FORM reliability indices used in calculating the above bounds are not accurate for each performance function. Using the 4M approach (Zhao and Ang, 2003), the reliability indices are more accurately obtained as 3.293, 3.623, 3.629, 3.629, 3.871, 3.957 corresponding to the six respective performance functions of Eq. (27). With these latter reliability indices, the joint failure probability for each pair of failure modes are then obtained as follows

$$[P_{fij}]=10^{-6}\begin{bmatrix} 495.1 & 56.0 & 115.4 & 79.51 & 20.28 & 3.080 \\ 56.0 & 145.2 & 66.66 & 35.14 & 28.49 & 17.28 \\ 115.4 & 66.66 & 142.3 & 68.13 & 33.46 & 8.628 \\ 79.51 & 35.15 & 68.13 & 142.3 & 33.46 & 8.628 \\ 20.28 & 28.49 & 33.46 & 33.46 & 54.23 & 18.06 \\ 3.080 & 17.28 & 8.628 & 8.628 & 18.06 & 37.86 \end{bmatrix}$$

The bounds of the system failure probability become $5.844*10^{-4}$ and $7.147*10^{-4}$. Then, we can observe that the MCS solution for the system failure probability of $6.147*10^{-4}$ is clearly bounded by the narrow bounds.

5 CONCLUSIONS

In order to improve the narrow bounds of the failure probability of a series structural system, a point estimation method is introduced for calculating the joint probability of every pair of failure modes of the system. Based on the computational results of the illustrative examples, the following conclusions can be observed:

(1) With the point estimation of the failure probability for each pair of failure modes in a series structural system, the results of the narrow bound method can be improved.

(2) When the correlation coefficient, $\rho = 0$, or $\rho = 1$, the present method gives accurate solutions; whereas when $0 < \rho < 1$, the present method yields results that are quite close to those obtained by numerical integration and are consistently located between the lower and upper bound solutions.
(3) Sometimes accurate estimates of the reliability indices of the individual failure modes is necessary for determining the correct narrow bounds of the system failure probability. This is illustrated in Example 3.
(4) The method by Feng gives good results when the reliability indices for the pair of failure modes are the same; however, when the reliability indices of the two failure modes are different, Feng's method generally gives results that are below the lower bound for relatively large correlation coefficient. Moreover, this error increases for larger difference in the two reliability indices.

REFERENCES

Adduri, R.P., Penmestsa, R., and Grandhi, R. (2004). "Estimation of structural system reliability using fast Fourier transforms." *10th AIAA/ISSMO Multidisciplinary Analysis and Optimization Conference*, Albany, New York.

Ang, A. H-S., and Tang, W. (1984). *Probability Concepts in Engineering Planning and Design, Vol II – Decision, Risk, and Reliability,* J. Wiley & Sons, New York.

Cornell, C.A. (1967). "Bounds on the reliability of structural systems." *J. Struct. Div., ASCE*, 93(1), 171–200.

Ditlevsen, O. (1979). "Narrow reliability bounds for structural systems." *J. Struct. Mech*., 7(4), 453–72.

Feng Y.S. (1989). "A method for computing structural system reliability with high accuracy." *Computers & Structures*, 33 (1), 1–5.

Ono, T., Idota, H., and Dozuka, A. (1990). "Reliability evaluation of structural systems using higher-order moment standardization technique." *J. of Struct. Constr. Engng., AIJ, No*. 418, 71–79 (In Japanese).

Penmestsa, R., and Grandhi, R. (2002). "Structural system reliability quantification using multipoint function." *AIAA Journal*, 40(12), 2526–2531.

Song, B.F. (1992). "A numerical Integration method in affine space and a method with high accuracy for computing structural system reliability." *Computers & Structures*, 42(2), 255–262.

Wu, Y.T., and Burnside, O.H. (1990). "Computational methods for probability of instability calculations." *AIAA/ASME/ASCE/AHS/ASC 31th Structures, Structural Dynamics and Materials Conference*, A90-29283 11–39.

Zhao, Y.G., and Ang, A. H-S. (2003). "System reliability assessment by method of moments." *J. Struct. Eng., ASCE*, 129(10), 1341–1349.

Zhao, Y.G., Zhong, W.Q. and Ang, A. H-S. (2007). "Estimating Joint Failure Probability of Series Structural Systems." *J. Eng. Mech., ASCE*, (In publication).

Reliability and Optimization of Structural Systems: Assessment, Design and Life-Cycle Performance – Frangopol, Kawatani & Kim (eds)
© 2007 Taylor & Francis Group, London, ISBN 978-0-415-40655-0

Author index